THREE APPLICATIONS OF GREEN CHEMISTRY IN ENGINEERING:

(1) SILYLAMINES AS REVERSIBLE IONIC LIQUIDS FOR CARBON DIOXIDE CAPTURE

(2) CARBON DIOXIDE AS A PROTECTING GROUP IN CHEMICAL SYNTHESES

(3) MITIGATING THE THERMAL DEGRADATION OF POLYVINYL CHLORIDE

A Thesis
Presented to
The Academic Faculty

By

Jackson R. Switzer

In Partial Fulfillment
Of the Requirements for the Degree
Doctor of Philosophy in Chemical Engineering

Georgia Institute of Technology

August 2013

THREE APPLICATIONS OF GREEN CHEMISTRY IN ENGINEERING:

(1) SILYLAMINES AS REVERSIBLE IONIC LIQUIDS FOR CARBON DIOXIDE CAPTURE

(2) CARBON DIOXIDE AS A PROTECTING GROUP IN CHEMICAL SYNTHESES

(3) MITIGATING THE THERMAL DEGRADATION OF POLYVINYL CHLORIDE

Approved By:

Dr. Charles Eckert
School of Chemical and Biomolecular Engineering
Georgia Institute of Technology

Dr. Christopher Jones
School of Chemical and Biomolecular Engineering
Georgia Institute of Technology

Dr. Charles Liotta
School of Chemistry and Biochemistry
Georgia Institute of Technology

Dr. Krista Walton
School of Chemical and Biomolecular Engineering
Georgia Institute of Technology

Dr. William Koros
School of Chemical and Biomolecular Engineering
Georgia Institute of Technology

Date Approved: 12 June 2013

This thesis is dedicated to my family and friends, for their longtime support of my educational pursuits.

ACKNOWLEDGEMENTS

A debt of gratitude is owed to my graduate advisors, Dr. Charles Eckert and Dr. Charles Liotta. Drs. Eckert and Liotta have made a positive impact on my education that I will profit from throughout my career. Dr. Eckert gave support and assistance in expanding my undergraduate chemistry studies to include chemical engineering. I owe him thanks for helping prepare me for my qualifying exams, ensuring I had a firm grasp of engineering thermodynamics. I am honored to be his 100th doctoral chemical engineering student. Dr. Liotta greatly expanded my knowledge of physical organic chemistry, challenging me to think outside of product catalogs to formulate original molecules for syntheses. Together, they significantly improved my scientific writing and presentation ability. Dr. Eckert instilled the elegance of brevity while Dr. Liotta coached me on the importance of thoughtful and planned presentation.

Further, appreciation is due to my thesis committee. My committee has continuously provided attentive advice as well as encouraging support.

I would also like to thank Dr. Pamela Pollet. She is a critical component of the Eckert-Liotta research group and a treasured friend. Her unrivaled knowledge of practical organic chemistry was of great worth in attempting new syntheses. Her mentorship during throughout my graduate studies was invaluable.

My family and friends, to include the three mentioned above, are to who this thesis is dedicated. My family’s longtime support of my academic pursuits is under-recognized but lovingly appreciated. My friends have made my graduate study an

enjoyable time, offering both support and an outlet for activities outside of the laboratory. My graduate colleagues Kyle Flack and Amy Rohan deserve special thanks and have grown to be especially close friends. I am additionally grateful for Christine Keith, who provided daily encouragement during the thesis writing process.

TABLE OF CONTENTS

LIST OF TABLES

LIST OF FIGURES

LIST OF ABBREVIATIONS

ΔH_{rxn}	enthalpy of reaction
ACN	acetonitrile
ATR-FTIR	attenuated total reflectance Fourier-transform infrared (spectroscopy)
BTU	British thermal unit
CHO	1,2-cyclohexene oxide
CO2	carbon dioxide
COSMO-RS	conductor-like screening model for realistic solvation
Cp	heat capacity
CV	continuous vulcaizations
DBU	1,8-diazabicyclo[5.4.0]undec-7-ene
DCP	dicumyl peroxide
DEHP	bis(2-ethylhexyl) phthalate
DIDP	diisodecyl phthalate
DINP	diiosononyl phthalate
DIPEA	diisopropyl ethylamine
DLaTGS	deuterated L-alanine doped triglycene sulphate
DMESA	3-(aminopropyl)dimethylethylsilane
DMF	dimethyl formamide
DMSO	dimethyl sulfoxide
DOE	Department of Energy
DSC	differential scanning calorimetry
EH	1,2-epoxyhexane
GC-MS	gas chromatography – mass spectrometry

HPLC	high-performance liquid chromatography
LC-MS	liquid chromatography – mass spectrometry
MEA	monoethanolamine
MW	megawatt
NMR	nuclear magnetic resonance (spectroscopy)
NSF	National Science Foundation
PE	polyethylene
phr	parts per hundred resin
PID	proportional-integral-derivative (controller)
ppb	parts per billion
PTC	phase transfer catalyst
PVC	polyvinyl chloride
RevIL	reversible ionic liquid
RT	room temperature
SDMESA	N-methyl-3-(aminopropyl)dimethylethylsilane
STEtSA	N-methyl-3-(triethylsilyl)propan-1-amine
TESA	triethoxysilylpropylamine
TEtSA	3-(aminopropyl) triethylsilane
TEtSBA	4-(aminobutyl) triethylsilane
TEtSEtA	2-(aminoethyl) triethylsilane
TEtSMA	1-(aminomethyl) triethylsilane
THF	tetrahydrofuran
THSA	3-(aminopropyl) trihexylsilane
TMBG	tetramethyl-butyl guanidine
TMG	1,1,3,3-tetramethylguanidine
TMSA	trimethoxysilylpropylamine

TPSA	3-(aminopropyl) tripropylsilane
trans-TEtSA	(trans)-3-(triethylsilyl)prop-2-en-1-amine
trans-α,αDMe-TEtSA	2-methyl-4-(triethylsilyl)-butyl-2-amine
trans-α,αDMe-TPSA	2-methyl-4-(tripropylsilyl)-butyl-2-amine
TSIL	task-specific ionic liquid
UV-visible	ultraviolet-visible (spectrospcoy)
XLPE	cross-linked poyethylene
α,αDMe-TEtSA	2-methyl-4-(triethylsilyl)-butyl-2-amine
αMe-TEtSA	4-(triethylsilyl)-butyl-2-amine
βMe-TEtSA	2-methyl-3-(triethylsilyl)propylamine

SUMMARY

Green chemistry principles served as a guide for three industrially-relevant projects. In the first project, silylamines were applied as reversible ionic liquids for CO_2 capture from post-combustion flue gas streams. The effect of silylamine structure was thoroughly researched to develop a comprehensive library of silylamines and an accompanying set of structure-property relationships. The proposed solvent systems have the potential to present significant energy savings, as design has focused on their use in a non-aqueous, solvent-free environment.

The second project also dealt extensively with CO_2, as a reversible, *in-situ* protecting group for amines. Three strategies for the reversible protection of amines using CO_2 were developed and evaluated. Further, a chemoselective reaction was performed using CO_2 to protect a reactive amine and consequentially direct reactivity elsewhere within the same molecule. The CO_2-protection technology developed has significant impact in multi-step industrial syntheses, as reversible, *in-situ* protection with CO_2 could eliminate the need for separate protection and deprotection unit operations.

Lastly, a study was performed on the thermal degradation and stabilization of PVC in the presence of both plasticizers and thermal stabilizers. The study combined both model compound experiments as well as work with bulk PVC blends to gain a holistic understanding of the processes that take place during the degradation and stabilization of PVC. A bio-based plasticizer was investigated as a replacement for petroleum-based phthalate plasticizers. Additionally, two novel thermal stabilizers for PVC were presented and evaluated.

CHAPTER 1 - INTRODUCTION

1.1 Green Chemistry Principles

Green chemistry refers to the conscious design of chemical processes which make maximum use of raw materials, in a safe and energy efficient manner, with as little waste generation as possible.[1] It is considered an innovative, non-regulatory, economically driven approach towards sustainability.[2] Paul Anastas and John Warner first defined the 12 principles of green chemistry in their book *Green Chemistry: Theory and Practice*.[3] The principles have come to shape and define the fields of green and sustainable chemistry, directing researchers and industry towards design of environmentally benign processes. The 12 principles are listed in Table 1.1.[3]

Table 1.1 – 12 Principles of Green Chemistry

Twelve Principles of Green Chemistry	
1.	It's better to prevent waste than to treat or clean up waste after it is formed.
2.	Synthetic methods should be designed to maximize the incorporation of all materials used in the process into the final product.
3.	Wherever practicable, synthetic methodologies should be designed to use and generate substances that possess little or no toxicity to human health and the environment.
4.	Chemical products should be designed to preserve efficacy of function while reducing toxicity.
5.	The use of auxiliary substances (e.g. solvents, separation agents, etc.) should be made unnecessary wherever possible and, innocuous when used.
6.	Energy requirements should be recognized for their environmental and economic impacts and should be minimized. Synthetic methods should be conducted at ambient temperature and pressure.
7.	A raw material of feedstock should be renewable rather than depleting wherever technically and economically practicable.
8.	Unnecessary derivization (blocking group, protection/deprotection, and temporary modification of physical/chemical processes) should be avoided whenever possible.
9.	Catalytic reagents (as selective as possible) are superior to stochiometric reagents.

Table 1.1 – continued

10.	Chemical products should be designed so that at the end of their function they do not persist in the environment and break down into innocuous degradation products.
11.	Analytical methodologies need to be further developed to allow for real time, in-process monitoring and control prior to the formation of hazardous substances.
12.	Substances and the form of a substance used in a chemical process should be chosen so as to minimize the potential for chemical accidents, including releases, explosions, and fires.

The twelve principles of green chemistry are integral to the three research topics presented in this thesis. The first research project – Silylamines as Reversible Ionic Liquids for CO_2 Capture – details the design and development of alternate solvents for CO_2 capture, which eliminate the need for solvent (Principle 5) and are targeted at energy minimization (Principle 6). The second project – CO_2 as a Protecting Group in Chemical Syntheses – proposes the use of CO_2 as an *in-situ*, reversible protecting group for amines. The use of CO_2 in place of a traditional protecting group could eliminate the need for added unit operations typically reserved for protection and deprotection (Principle 8). Lastly, the third project – Mitigating the Thermal Degradation of Polyvinyl Chloride – investigates the effectiveness of traditional and novel stabilizers in PVC + plasticizer formulations. Plasticizers derived from renewable resources (i.e. soybean oil) were studied as replacements for petroleum-derived plasticizers (Principle 7).

To achieve the implementation of green chemistry, a second element is also needed – favorable economics. Then and only then will industry adopt the methods of green chemistry. In fact, this combination of green chemistry and viable costs is what defines a sustainable process. While much of this thesis pertains to green chemistry, an important recognition of the potential costs of the proposed processes must be maintained to ensure sustainability and thus industrial viability.

The remainder of this chapter provides a brief background for each of the three aforementioned projects and highlights the motivation for the thesis work presented in later chapters. Because the thesis work was conducted in the Eckert-Liotta multidisciplinary research group, organic chemistry and chemical engineering are intertwined throughout the thesis. This multidisciplinary approach has allowed for both fundamental design as well as applied functional studies of the topics investigated.

1.2 Reducing CO_2 Emissions

The United States faces an energy dilemma; demand for energy is at an all-time high, as is concern over rising greenhouse gas emissions – specifically carbon dioxide (CO_2) emissions. In 2011, the United States consumed 97.3 quadrillion BTUs of energy (up from 94.5 in 2009), emitting over 5.5 billion metric tons of CO_2.[4,5] Figure 1.1 shows a breakdown of energy use by sector.[4] Electric power generation is responsible for the majority of energy usage in the United States.

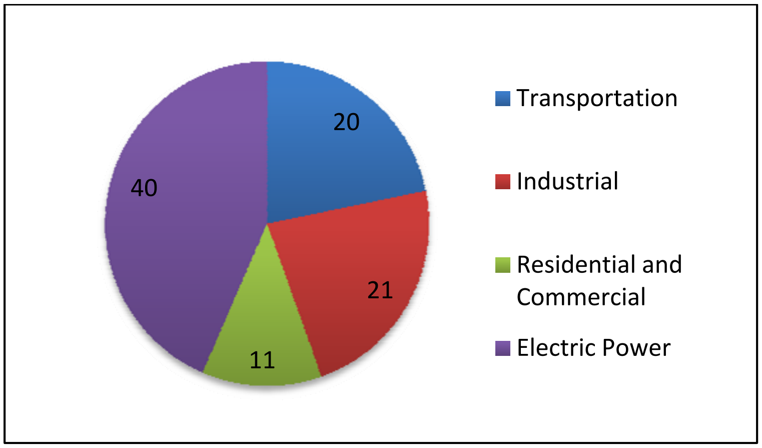

Figure 1.1 – 2011 US energy use by sector

Figure 1.2 shows 2011 electric power generation by source. Coal provided nearly half of the electricity generated, whereas renewable resources accounted for only 13% of our electricity.[4] Coal is preferred in the electricity generation industry, as it is established, cheap, and abundant.

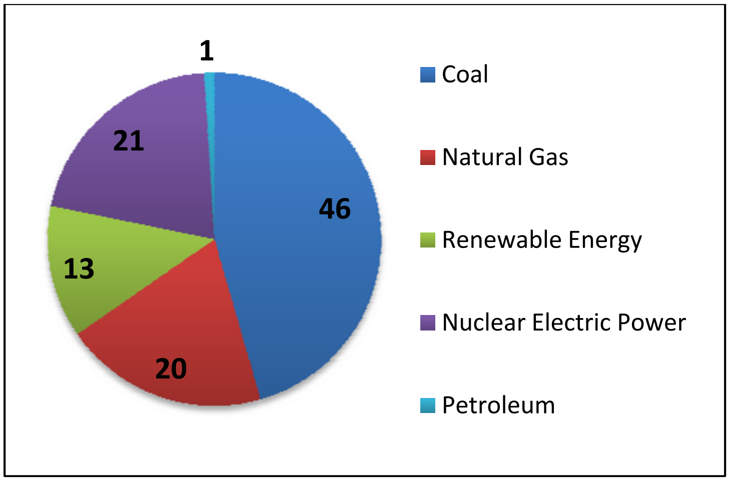

Figure 1.2 – 2011 US electric power generation by source

According to the 2011 Annual Energy Outlook published by the independent US Energy & Information Administration, coal is expected to remain the predominant source of electricity generation through 2035.[6] In 2035, coal is predicted to account for 43% of electricity generation while natural gas is predicted to increase to 25%. Though the percentage of coal use in 2035 will be nearly the same, capacity is projected to grow considerably as energy use is projected to increase annually at a rate of 0.7% through 2035.[6]

While coal is a staple in terms of electricity generation, it is the primary contributor to carbon dioxide – a staple greenhouse gas – emissions in terms of electricity generation. Electric generation from coal emits more carbon dioxide per unit energy produced than natural gas and petroleum sources.[7] Figure 1.3 shows historical CO_2

emissions from electricity generation – including coal, petroleum, and natural gas.[8]

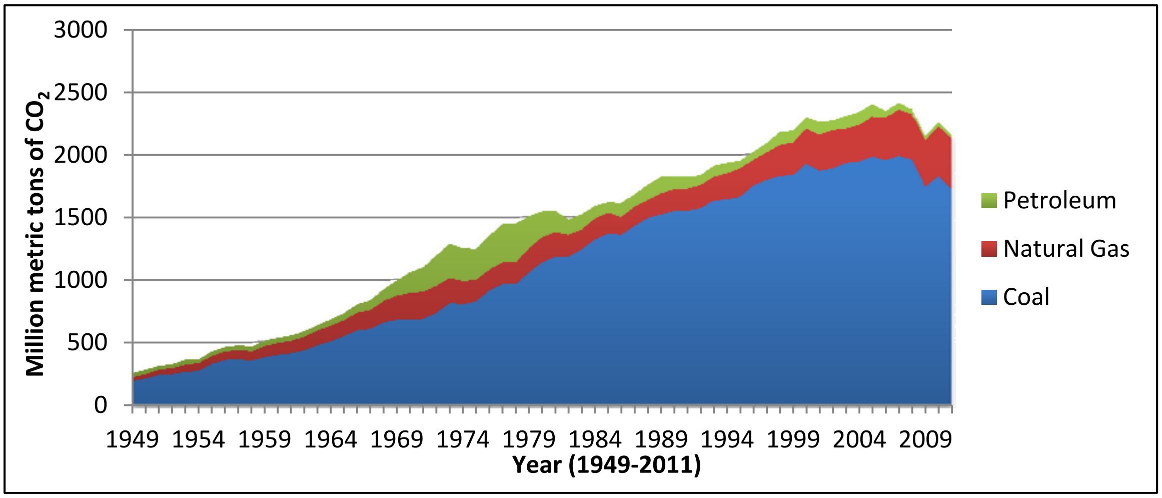

Figure 1.3 – US CO_2 emissions from electricity generation (1949-2011)

As shown in Figure 1.3, CO_2 emissions from coal power plants represent a substantial percentage (79%) of the total CO_2 emissions from the electricity generation sector.[8] Further, according to the Department of Energy, 94.5% of the CO_2 emissions from coal power plants through 2020 will result from existing coal power plants.[9] As such, existing coal power plants are and will remain a significant source of CO_2 emissions in terms of electricity generation. To mitigate CO_2 emissions from the electricity generation sector, effective CO_2 capture technologies adaptable to existing coal power plants are necessary.

There are numerous novel methods for CO_2 capture being researched.[10] They include the use of membranes, solid absorbents, and liquid solvents.[11] Membranes technologies primarily rely on size exclusion to achieve separation.[12] Solid adsorbents and liquid absorbents both utilize either chemical reaction or physical absorption to capture CO_2.[11,13] Of these, liquid absorbents are often considered the most developed.

Liquid solvents that capture CO_2 via chemical reaction are capable of recovering 75-90% of CO_2, producing a high purity CO_2 product stream.[14]

Chapter 2 presents a novel liquid solvent system for application to CO_2 capture in an absorption based process. Silylamines are used as reversible ionic liquids for the capture and release of CO_2 in a non-aqueous process. Structure-property relationships are presented based on modifications explored to the silylamine structure and the resulting effect on relevant CO_2 capture properties (i.e. energy minimization).

1.3 Increasing the Efficiency of Industrial Syntheses

The field of organic chemistry has become extremely complex as the result numerous breakthroughs in synthetic chemistry. However, control over the reactivity of functional groups in complex molecules remains elusive. To that end, protecting groups are commonly used to block reactive sites and prevent unwanted interaction and/or reaction of a particular functional group. Protecting groups are so common in organic chemistry, that there are entire textbooks on their use, nearly asserting that avoiding them is impossible.[15] Even on molecules of low complexity, protecting groups are sometimes routinely used.[16]

Ideally, protecting groups are easily removed and separated from the resulting product mixture. However, the use of a protecting group requires at minimum two additional steps to a) protect the functional group and b) to deprotect the functional group after the desired reaction has been performed. These added steps drastically lower the efficiency of the synthesis process and can also lead to unwanted side reactions.[17] To further complicate the use of a protecting group, following deprotection it must be separated and discarded, compounding overall waste production.

In his seminal paper on atom economy, Barry Trost states, “The limitations of raw materials, combined with environmental concerns, necessitate our rethinking of strategies toward complex organic synthesis. Although some of the most important industrial processes recognize the advantages of atom-economical reactions, most do not.” Trost et al. have further shown that for every kilogram of fine chemical and pharmaceutical product produced, between 5-100 times that in chemical waste is generated.[18]

The use of protecting groups greatly decreases the atom economy of a given synthesis, as it involves the use of a species which does not appear in the end product but rather is wasted. What would be ideal – assuming a protecting group is necessary – is a group that is easily reversible, recoverable for reuse, and that can be introduced *in situ*. As Hoffman states, “particularly when protections would be necessary for just a single operation, it is advisable to switch to an in situ production scheme; that is, to attain a one-pot sequence of protection, reaction, deprotection. In this situation, it is not necessary that the protection be durable.”[19]

Chapter 3 introduces an alternative to traditional protecting groups. CO_2 is employed as an *in-situ*, reversible protecting group. CO_2 is regarded as a green solvent, as it is natural, renewable, non-flammable, nontoxic, and readily evaporating. It can be rapidly separated from products and catalysts by simple depressurization and recapture. Further, its ability to be recycled eliminates the waste generation and use of it *in situ* prevents the need for added synthesis steps.

1.4 Mitigating Thermal Degradation in Polyvinyl Chloride Formulations

PVC formulations for use in electrical wire applications often contain numerous ingredients but at least include a plasticizer and often include thermal stabilizers. Plasticizers are used to increase the flexibility of PVC by shielding the polymer chains from one another; thermal stabilizers are used to prevent the thermal degradation of the polymer backbone by reaction with labile chlorine atoms or by scavenging HCl released during the degradation process.[20]

The most common plasticizers used are phthalates which include: diisodecyl phthalate (DIDP), bis(2-ethylhexyl) phthalate (DEHP), and diisononyl phthalate (DINP). These general purpose plasticizers represent 85% of the global plasticizer consumption (6 Mton/year).[21] Of note, phthalate plasticizers are 100% derived from crude oil, a nonrenewable fossil fuel, with an increasingly volatile cost. Further, low molecular weight phthalate plasticizers such as DEHP are under increased scrutiny over health concerns resulting from the migration of the plasticizer out of the polymer.[22]

In attempt to introduce long-term sustainability to the PVC market, bio-based plasticizers are being researched as replacements for phthalates derived from crude oil. Examples of bio-based plasticizers include oils of the castor plant, soybean, palm, rapeseed, sunflower, and linseed. Plasticizers originating from starch have also been studied. In terms of those derived from oils, the unsaturated double bonds in their structure are often epoxidized to increase compatibility with the PVC polymer.[23]

In addition to plasticizers, thermal stabilizers are often added to PVC formulations to increase the polymer's resistance to thermal degradation. The thermal degradation of polyvinyl chloride (PVC) presents a significant problem for maintaining polymer performance after processing. Common thermal stabilizers include metal soaps of stearates such as zinc or calcium stearate.[20,21]

While the thermal degradation and stabilization of PVC in the presence of phthalate plasticizers has been studied, the research is largely segmented and focused on model studies in reaction solvents. Further, research on the thermal degradation in stabilization of PVC in the presence of bio-based plasticizers is needed. Chapter 4 details both model and bulk PVC studies on the thermal degradation and stabilization of the polymer in the presence of stearate stabilizers as well as both phthalate and bio-based plasticizers. Further, new and novel thermal stabilizers that are derived from natural products are presented.

1.5 References

(1) Anastas, P. T.; Williamson, T. C. *Green Chemistry: Designing Chemistry for the Environment* **1996**, *626*, 1EPA, U. Washington, D.C., 2013; Vol. 2013.

(2) Manley, J. B.; Anastas, P. T.; Cue Jr., B. W. *Journal of Cleaner Production* **2008**, *16*, 743.

(3) *Green chemistry: theory and practice*; Anastas, P. T.; Warner, J. C., Eds.; Oxford University Press: Oxford, England, 1998.

(4) U.S. Energy Information Administration: Washington, 2011; Vol. 2011.

(5) Department of Energy: Washington, 2010; Vol. 2011.

(6) “Annual Energy Outlook 2011 with Projections to 2035,” U.S. Energy Information Administration, 2011.

(7) U.S. Energy Information Administration: Washington, 2010; Vol. 2011.

(8) U.S. Energy Information Administration: Washington, 2011; Vol. 2011.

(9) Ciferno, J. P.; Litynski, J. L.; Plasynski, S. I. "DOE/NETL Carbon Dioxide Capture and Storage RD&D Roadmap," National Energy Technology Laboratory, 2010.

(10) Jones, C. W. *Annual Review of Chemical and Biomolecular Engineering* **2011**, *2*, 31Han, S.; Huang, Y.; Watanabe, T.; Dai, Y.; Walton, K. S.; Nair, S.; Sholl, D. S.; Meredith, J. C. *ACS Combinatorial Science* **2012**, *14*, 263.

(11) Aaron, D.; Tsouris, C. *Separation Science and Technology* **2005**, *401*, 321.

(12) Powell, C. E.; Qiao, G. G. *Journal of Membrane Science* **2006**, *279*, 1Brunetti, A.; Scura, F.; Barbieri, G.; Drioli, E. *Journal of Membrane Science* **2010**, *359*, 115Lively, R. P.; Chance, R. R.; Kelley, B. T.; Deckman, H. W.; Drese, J. H.; Jones, C. W.; Koros, W. J. *Industrial & Engineering Chemistry Research* **2009**, *48*, 7314Zhang, X.; He, X.; Gundersen, T. *Energy & Fuels* **2013**, *Articles ASAP*, Articles ASAP.

(13) Burtch, N. C.; Jasuja, H.; Dubbeldam, D.; Walton, K. S. *Journal of the American Chemical Society* **2013**, *135*, 7172Choi, S.; Drese, J. H.; Eisenberger, P. M.; Jones, C. W. *Environmental Science and Technology* **2011**, *45*, 2420Didas, S. A.; Kulkarni, A. R.; Sholl, D. S.; Jones, C. W. *ChemSusChem* **2012**, *5*, 2058Li, F. S.; Qui, W.; Lively, R. P.; Lee, J. S.; Rownaghi, A. A.; Koros, W. J. *ChemSusChem* **2013**, Articles ASAP.

(14) Kohl, A. L.; Nielsen, R. *Gas purification*; 5th edition ed.; Gulf Publishing Company: Houston, 1997.

(15) Wuts, P. G. M. *Greene's protective groups in organic synthesis*; 4th ed. / ed.; Wiley-Interscience: Hoboken, N.J. :, 2007Kocienski, P. J. *Protecting Groups*; 3rd edition ed.; Thieme: New York, 2005.

(16) Young, I. S.; Baran, P. S. *Nature Chemistry* **2009**, *1*, 193.

(17) Sierra, M. A.; de la Torre, M. C. *Dead Ends and Detours, Direct Ways to Successful Total Synthesis*; Wiley-VCH: Weinheim, 2004.

(18) Trost, B. M. *Science* **1991**, *254*, 1471Trost, B. M.; Li, C.-J. *PNAS* **2008**, *105*, 13197Sheldon, R. A. *Green Chemistry* **2007**, *9*, 1273.

(19) Hoffmann, R. W. *Synthesis* **2006**, *21*, 3531.

(20) Minkser, K. S.; Zaikov, G. E. *Chemistry of Chlorine-Containing Polymers: Syntheses, Degradation, Stabilization*; NOVA Science Publishers: Huntington, 2000.

(21) Wilkes, C. E.; Summers, J. W.; Daniels, C. A. *PVC Handbook*; Carl Hanser Verlag, 2005.

(22) Europa Europa.eu, 2005; Vol. 2013.

(23) Matthysen, L.; Martinz, D. O.; Solvay, 2011; Vol. 2013Bouchareb, B.; Benaniba, M. T. *Journal of Applied Polymer Science* **2007**, *107*, 3442Sun, B.; Chaudhary, B. I.; Shen, C.-Y.; Mao, D.; Yuan, D.-M.; Dai, G.-C.; Li, B.; Cogen, J. M. *Polymer Engineering and Science* **2012**.

CHAPTER 2 - SILYLAMINES AS REVERSIBLE IONIC LIQUIDS FOR CO_2 CAPTURE

2.1 Abstract

Silylamines exhibit competitive CO_2 capture properties compared to traditional aqueous alkanol amine solvent systems. Moreover, silylamines have the potential to present significant energy savings as our intent has focused around their use in a non-aqueous CO_2 capture process. Whereas traditional aqueous alkanol amine solvent systems incur a sizable energy penalty during the regeneration step from heating the excess water present, our non-aqueous silylamines do not. The design of a non-aqueous solvent system is a sizable challenge; any proposed solvent must be carefully screened not only to demonstrate superior CO_2 capture, but also to meet certain processing standards that dictate the industrial viability of the solvent system. Herein, we demonstrate the importance of silylamine design on influencing both CO_2 capture and industrial processing parameters.

2.2 Introduction

2.2.1 Aqueous amines for CO_2 capture

Aqueous amine solutions are generally the standard point of reference when examining alternative solvents for absorbent-based CO_2 capture processes. The most elementary solvent is monoethanolamine as shown in Figure 2.1.[1]

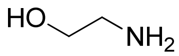

Figure 2.1 - Monoethanolamine (MEA), a traditional CO_2 capture solvent

It is commonly used in as a dilute aqueous solution (20-30 wt%) to capture CO_2; it has mainly seen use in natural gas sweetening applications. The amine functionality of monoethanolamine reacts with CO_2 to form both carbamate and ammonium ions in solution (

Figure 2.2). As it is used in water, bicarbonate is also formed. The hydroxyl tail of monoethanolamine serves to improve its water solubility. It is run dilute to limit the viscosity of the CO_2-rich monoethanolamine ionic species. In practice, monoethanolamine is run to capture CO_2 at loadings near 0.2-0.3 moles of CO_2 per mole of amine with a maximum loading near 0.5 moles of CO_2 per mole of amine.[1]

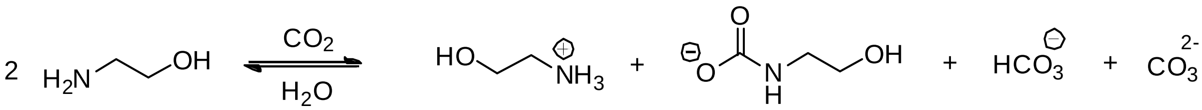

Figure 2.2 - Aqueous reaction of monoethanolamine with CO_2

While monoethanolamine is very reactive towards CO_2, it suffers from several drawbacks. The foremost drawback is the cost for regeneration incurred. Figure 2.3 shows a simplified absorber-stripper process schematic utilizing a heat exchanger between the two columns. Flue gas enters the bottom of the absorption tower near 40°C. The monoethanolamine solution is fed into the top of the absorption tower, allowed sufficient residence time to capture CO_2 and then pumped to the stripper to regenerate the solvent to release a pure CO_2 stream. Because it is a dilute aqueous solvent system, the stripper is run at temperatures upwards of 110°C to enable sufficient heating of the water and monoethanolamine to bring about CO_2 release. This solvent regeneration step is very costly and inefficient as much heat is wasted in simply heating the water of the solvent.[2,3]

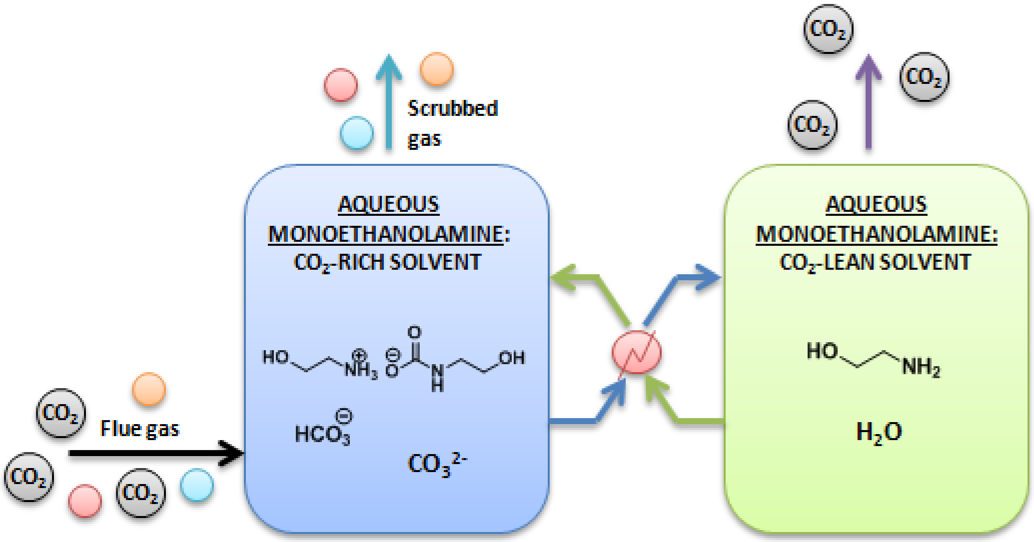

Figure 2.3 - Simplified monoethanolamine CO_2 capture process

The second drawback in using monoethanolamine relates to degradation. Monoethanolamine is subject to both thermal and oxidative degradation. Figure 2.4 shows the thermal degradation of monoethanolamine under stripper conditions as studied by Rochelle et al.[4] In the presence of CO_2 and water, monoethanolamine can form ring-closed structures like 2-oxazolidone. Once formed, 2-oxazolidone can further react with another molecule of monoethanolamine to form N,N'-di(2-hydroxyethyl)urea. This molecule can further be hydrolyzed to form the hydroxyl-diamine as shown in the second-to-last reaction of Figure 2.4. The last reaction shows an additional degradation pathway. In it, the monoethanolamine carbamate species can react with a second molecule of monoethanolamine to dehydrolize, forming the irreversible urea shown.[4]

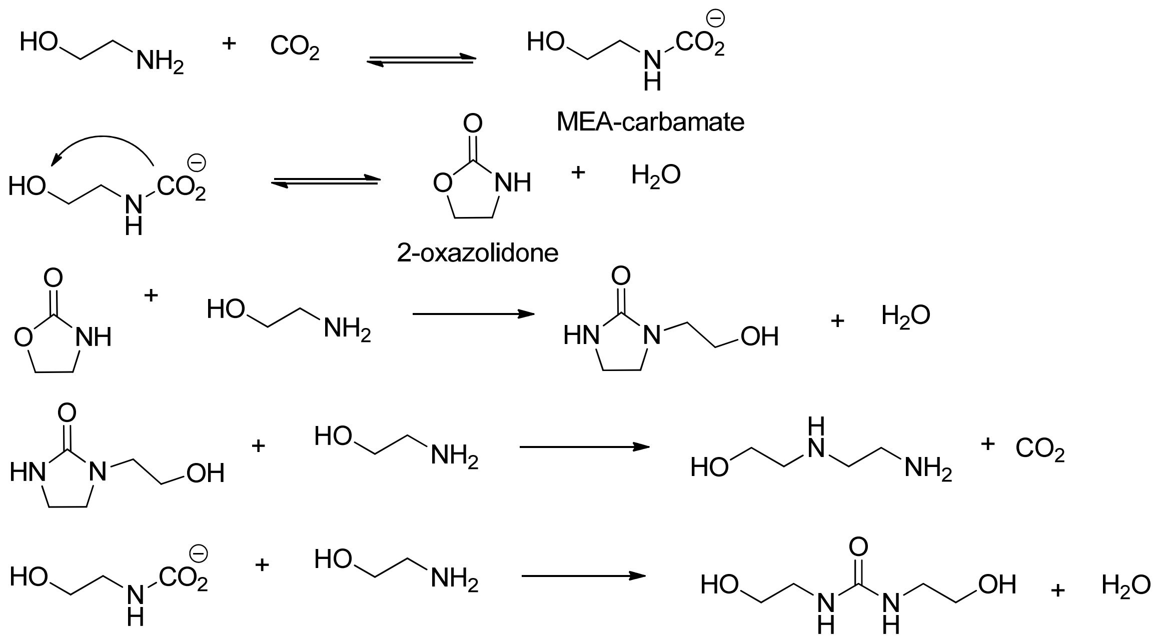

Figure 2.4 - Thermal degradation pathways of monoethanolamine

The oxidative degradation of monoethanolamine proceeds through radical formation to yield formaldehyde and ammonia – both very volatile products. The oxidative degradation of monoethanolamine is catalyzed by traces of iron, as often found in the columns and piping construction of an industrial process. A scheme for the oxidative degradation is shown in Figure 2.5.[5,6]

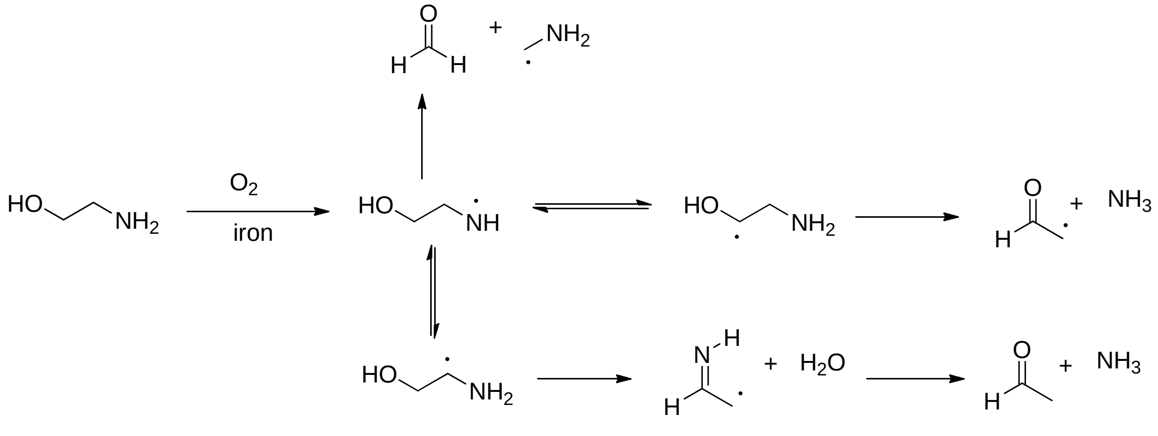

Figure 2.5 - Oxidative degradation of monoethanolamine

Lastly, monoethanolamine is corrosive. As is well know with amines, metal pitting in absorber towers and processing pipes can occur as a result of extended contact with amines. The degradation of monoethanolamine often requires use of a continual make-up stream to maintain CO_2 capture efficiencies in the process. It has been reported that this makeup stream can be as large as 3.1 kg of monoethanolamine per ton of CO_2 captured.

To mitigate these challenges, several additives have been developed. Most commercial monoethanolamine solutions involve the use of several proprietary alkanol amines as well as corrosion inhibitors. Examples include UCARSOL developed by Dow, PostCap developed by Siemens, and post-combustion CO_2 capture solutions provided by Babcock-Hitachi. Lowering the energy required for regeneration however, remains a challenge. Aside from process improvements and design schematic alterations, the use of a dilute aqueous solution for an absorption based process has largely gone unchallenged.[1]

2.2.2 Specifications for the design of alternative solvents

In attempting development of a solvent to replace the aqueous monoethanolamine system, it is valuable to define the necessary specifications to ensure the new solvent's industrial viability but also to improve upon existing solvents. Chief to solvent design is that any solvent used must be selective for CO_2. An example post-combustion flue gas stream composition is shown in Table 2.1. As shown, flue gas contains nitrogen, oxygen, water, and trace gases such as SO_2 in addition to CO_2.

Table 2.1 - Example composition of a post-combustion flue gas stream

Component	Approximate Volume Percent
CO_2	12-14
N_2	65
H_2O	18
O_2	2
SO_x / NO_x	ppm levels

Second, the solvent system must be cost-efficient. This manifests itself it two ways: 1) the energy used to capture the CO_2 must be at a minimum 2) the solvent used must cost little and be recyclable. It must be understood that the pure CO_2 stream produced is not a product of any substantial value at this time. While interest is rising on its use as a reagent feedstock in industrial reactions, the applications are by in large, fairly specific and still in development.[7,8]

2.2.3 Ionic liquids for CO_2 capture

Ionic liquids have been proposed as an alternate solvent system for CO_2 capture. Defined as molten salts with melting points below 100°C, room temperature ionic liquids were introduced by Paul Walden in 1914. Their attraction for use in CO_2 capture is their high CO_2 solubility. CO_2 held physically by weak van der Waals forces requires a low cost of regeneration as chemical bonds have not been formed that must later be broken during solvent regeneration.[9] This is attractive in natural gas applications where the CO_2 partial pressure is high in the target separation stream, as physical absorption of CO_2 by ionic liquids is most effective at elevated pressures. Figure 2.6 A shows 1-butyl-3-methylimadazolium hexafluorophosphate, a traditional ionic liquid. Figure 2.6 B shows several common cations that are used, included quaternary phosphonium cations, pyridinium cations, quaternary amine cations, and guanidinium cations. Figure 2.6 C gives examples of two additional common anions – chloride and a nitrogen anion.[10]

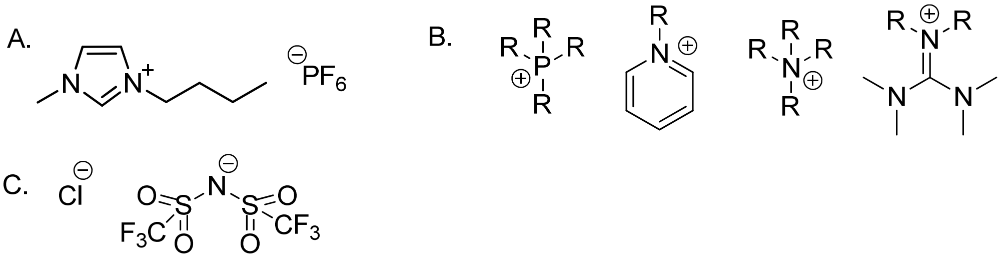

Figure 2.6 – A. A traditional ionic liquids B. Common cations used C. Common anions used

To capitalize on the physical absorption capability of ionic liquids but improve their utility towards post-combustion flue gas compositions, Brennecke et al. have developed a class of tailored ionic liquids called task-specific ionic liquids (TSILs).[10,11] They have taken traditional ionic liquids and added alkyl amine tails to both the cation and anion species. The added amine functionality enables the task-specific ionic liquid to capture CO_2 via chemical reaction to form ammonium carbamate ion pairs while maintaining its characteristic ability to physically absorb CO_2 through physical solubilization.

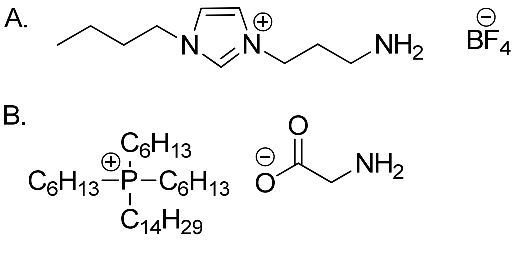

Figure 2.7 - Two examples of task-specific ionic liquids (TSILs)

A number of custom-synthesized task-specific ionic liquids have been investigated. Most recently, anion-amine-functionalized task-specific ionic liquids have been reported, showing exceptional CO_2 capacities through formation of carbamic acid.

Figure 2.8 shows an anion-amine-functionalized task-specific ionic liquid derived from glycine.[10,12] The carbamate anionic tail stabilizes the absorbed CO_2 as carbamic acid rather than allowing formation of a di-anion.

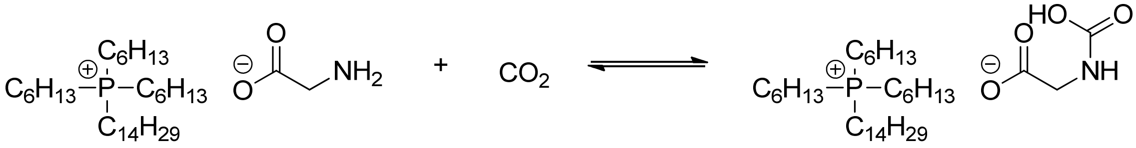

Figure 2.8 - Reaction of glycine derived task-specific ionic liquid with CO_2 to form carbamic acid

Traditional ionic liquids as well as task-specific ionic liquids face challenges in controlling viscosity. They remain viscous pre- and post-CO_2 capture unless long bulky alkyl tails are employed on the ionic liquid or cosolvents are used.[13] Adding weight to the ionic liquid quickly decreases the CO_2 capture efficiency of the solvent on a mole of CO_2 captured per kilogram of solvent used basis. Use of a cosolvent also decreases CO_2 capture efficacy, especially in terms of adding to the heating requirement necessary for regeneration of the ionic liquid.[14]

Our research group has sought to combine the idea of ionic liquids with the nature of conventional alkanol amine solvents in a switchable solvent system we call reversible ionic liquids. We have sought to increase CO_2 capture efficacy while targeting a usable ionic liquid viscosity and minimizing the energy required for regeneration.

2.2.4 Reversible ionic liquids for CO_2 capture

Defined as solvents that undergo step changes in properties upon exposure to an external stimulus, switchable solvents have been investigated for incorporation into a number of chemical process operations (i.e. reactions, extractions, and separations).[15] The Eckert-Liotta research group along with Jessop et al. have developed a class of switchable solvents deemed reversible ionic liquids that utilize CO_2 to shift from a non-ionic to ionic solvent.[16-20]

Reversible ionic liquids contain amine functionalities that react with CO_2 in non-aqueous conditions to form ammonium carbamate ion pairs (Figure 2.9). These switchable solvents are designed so that in reaction with CO_2 the ionic species formed do not salt out but rather remain liquids at room temperature. Key to the solvent systems is that upon moderate heating or sparging with an inert gas, the ionic liquid is easily reversed back to its starting amine.[21]

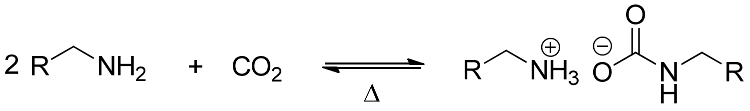

Figure 2.9 - Reaction of an amine to form an ammonium carbamate ion pair

A number of reversible ionic liquids have been developed and previously reported by our group.[21] The solvents are versatile in that small changes in the structure of the starting amine can affect large changes in the properties of the ionic form (i.e. induce a large change in the polarity of the solvent). Reversible ionic liquids were initially developed for the coupling of reactions and separations, taking advantage of the change in solvent properties induced by the CO_2 switch.[18] However recently, reversible ionic liquids have shown potential in CO_2 capture.[19,21,22]

2.2.4.1 Two component reversible ionic liquids

The first reversible ionic liquid system developed by our group in collaboration with Jessop et al. involved a strong base and an alcohol.[20] The primary two bases investigated were 1,8-diazabicyclo[5.4.0]undec-7-ene (DBU) or tetramethyl-butyl guanidine (TMBG). In the presence of an equimolar quantity of alcohol, when exposed to CO_2, the alcohol forms its corresponding carbonate anion while the base picks up the proton involved to form an ammonium cation. The reaction scheme is shown in Figure 2.10.[16,18]

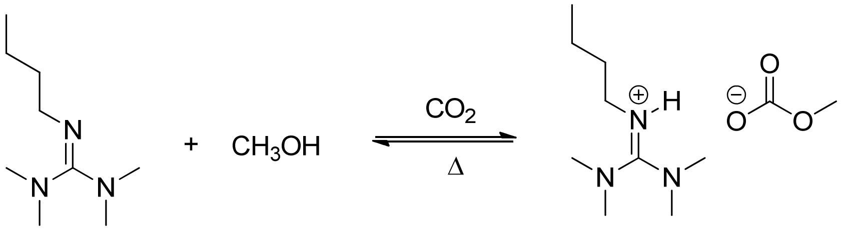

Figure 2.10 - Guanidine + methanol reversible ionic liquid system

While an effective proof of concept, two-component reversible ionic liquids have the disadvantage of requiring an equimolar amount of alcohol to reach their maximum CO_2 capture capacities. Further, the choice of an alcohol requires trade-offs. Methanol allows for the highest CO_2 capacity in a mole of CO_2 per kilogram of solvent; however it has a low boiling point (65°C). Significant losses would likely occur during regeneration as the reversible ionic liquid system requires heating to release the absorbed CO_2. Further, if a higher boiling alcohol was used, the heat capacity of the system would also increase, adding to the energy cost of regeneration. Additionally, the water solubility of light alcohols is a concern; flue gas normally contains residual water. Separation of alcohols from water on an industrial level would add to the CO_2 capture cost. A single component reversible ionic liquid would eliminate the need for alcohol.[16,18]

2.2.4.2 One component reversible ionic liquids

One component reversible ionic liquids were initially based on commercially available trialkoxysilanes coupled with allyl amine to yield 3-(aminopropyl)trialkoxysilanes as shown in Figure 2.11.[17,19]

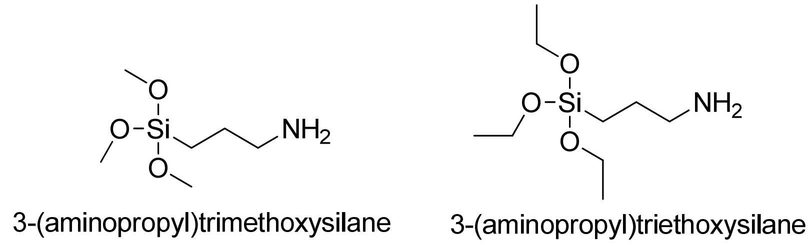

Figure 2.11 - Two siloxane-based one component reversible ionic liquids investigated

The silylamines react with CO_2 to form ammonium carbamate salts and remain ionic liquids after reaction (Figure 2.12). We attribute the ability to remain as ionic liquids and not solidify after reaction with CO_2 to the presence of the silicon atom.[17,23,24] It has been reported that incorporation of a silicon atom in conventional ionic liquids brought about significant decreases in viscosity. On a molecular level, it must be related in part to the Lewis acidity of the silicon atom when compared to a carbon atom.[23,25] Recent studies by General Electric on aminodisiloxanes for CO_2 capture have also sought to capitalize on the viscosity decrease seen with the inclusion of a silicon atom.[26]

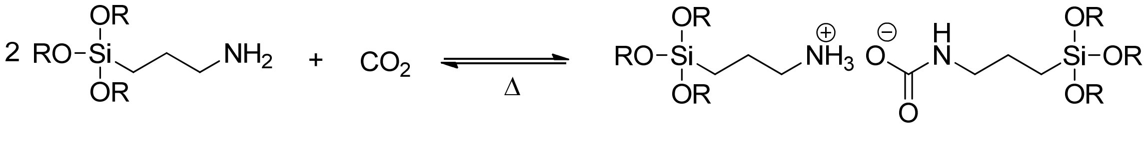

Figure 2.12 - Reaction of 3-(aminopropyl)trialkoxysilane with CO_2 to form a reversible ionic liquid

We demonstrated that the trialkoxysilylamines were reactive towards CO_2 to yield ionic liquids, and furthermore that the ionic liquids formed were thermally reversible.[16]

Due to the elevated boiling points of trialkoxysilylamines, concerns over solvent losses due to evaporation were alleviated. Further, we proposed that by changing the length of the alkyl chains tethered to the silicon atom we could affect the properties of the reversible ionic liquid.[19]

Unfortunately trialkoxysilylamines are water sensitive. In the presence of the water, the silicon-oxygen bond can be hydrolytically cleaved, leading to degradation of the solvent. Drying the water-laden flue gas stream before contacting the CO_2 capture solvent would be energy intensive and is unlikely to be economically feasible. With this in mind, we decided to transition away from siloxane-based amines in favor of silane based amines. The silicon-carbon bond is stable in water and is not subject to hydrolytic cleavage.

The basic trialkylsilylamine structure is shown in Figure 2.13.[19] From this starting structure, we investigated a large number of structural modifications and their effects on the relevant CO_2 capture properties of the corresponding reversible ionic liquid formed after reaction with CO_2.[19,22,27]

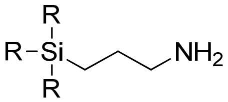

Figure 2.13 - Basic trialkylsilylamine structure

The structural modifications investigated can be grouped into five main categories. They are as follows:

1. Varying the length of the three alkyl chains attached to the silicon atom
2. Varying the length of the tether between the silicon atom and the amine

3. Investigating the effect of alkyl branching along the propyl chain backbone of the silylamine
4. Investigating the effect of unsaturation in the propyl chain tether between the silicon atom and the amine
5. Varying the order of the amine from primary to secondary by the addition of a methyl group to the amine

The silylamines prepared are listed in Table 2.2. The detailed synthesis of each is listed in Appendix A. Following Table 2.2 is a description of the utility of the reversible ionic liquid system and the experimental methods used to characterize the relevant CO_2 capture properties. A discussion then follows on the properties of the reversible ionic liquid affected by the five categories of modification; the properties include CO_2 capture capacity, reversible ionic liquid viscosity, temperature of reversal (CO_2 release), temperature of silylamine evaporation, and the enthalpy of regeneration.

Table 2.2 - Silylated amines discussed in this chapter

Silylamine structure	Abbreviation	Molecular name
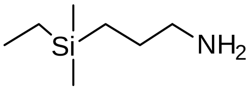	DMESA	3-(aminopropyl)dimethylethylsilane
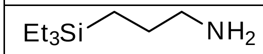	TEtSA	3-(aminopropyl) triethylsilane
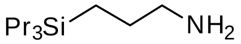	TPSA	3-(aminopropyl) tripropylsilane
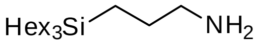	THSA	3-(aminopropyl) trihexylsilane

Table 2.2 – continued

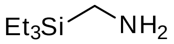	TEtSMA	1-(aminomethyl) triethylsilane
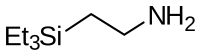	TEtSEtA	2-(aminoethyl) triethylsilane
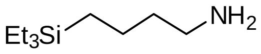	TEtSBA	4-(aminobutyl) triethylsilane
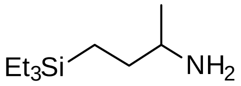	αMe-TEtSA	4-(triethylsilyl)-butyl-2-amine
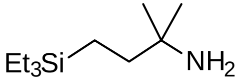	α,αDMe-TEtSA	2-methyl-4-(triethylsilyl)-butyl-2-amine
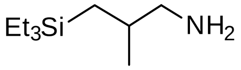	βMe-TEtSA	2-methyl-3-(triethylsilyl)propylamine
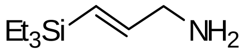	*trans*-TEtSA	(*trans*)-3-(triethylsilyl)prop-2-en-1-amine
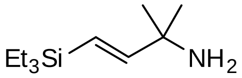	*trans*-α,αDMe-TEtSA	2-methyl-4-(triethylsilyl)-butyl-2-amine
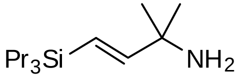	*trans*-α,αDMe-TPSA	2-methyl-4-(tripropylsilyl)-butyl-2-amine
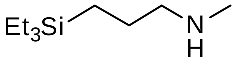	STEtSA	N-methyl-3-(triethylsilyl)propan-1-amine
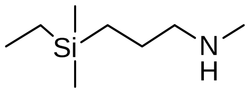	SDMESA	N-methyl-3-(aminopropyl)dimethylethylsilane

2.3 Experimental Methods

2.3.1 Measurements of CO_2 uptake

2.3.1.1 Gravimetric measurement of CO_2 uptake at 25°C

For gravimetric uptake experiments, approximately 1 milliliter of silylamine was added to an argon-purged scintillation vial at 25°C. A sand bath was used to maintain the temperature of the vial at 25°C. CO_2 at 1 bar was introduced using a diffuser tube (type C porosity) until weight uptake was determined to be constant. The majority of the CO_2 uptake occurs within the first 10 minutes, as shown in Figure 2.14. However, to ensure complete conversion to the reversible ionic liquid at equilibrium, on average, the silylated amines were allowed to react with CO_2 for 75 minutes. The increase in weight observed in going from the silylamine to the forming the reversible ionic liquid was assumed to be representative of the CO_2 uptake. Experiments were conducted in triplicate.

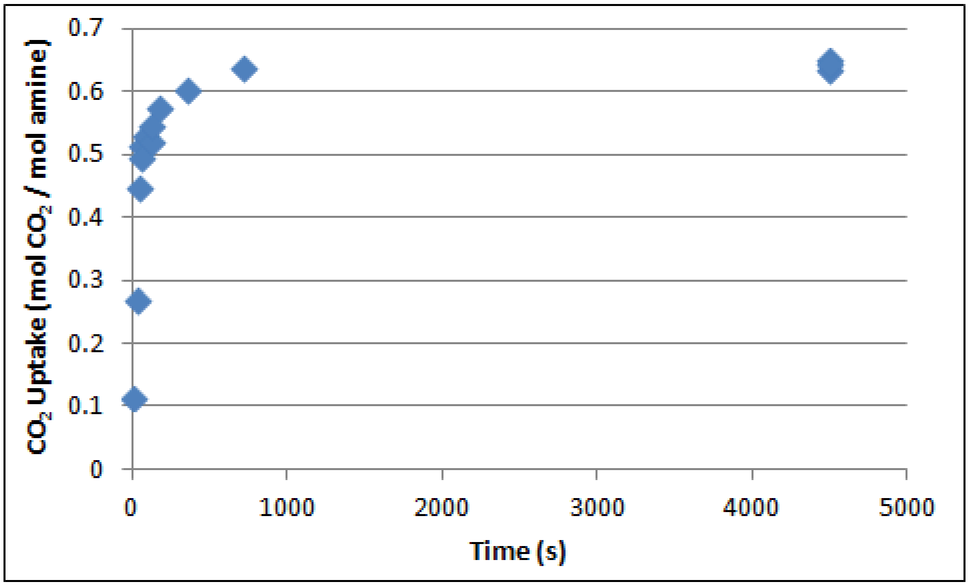

Figure 2.14 - CO_2 uptake vs. time at 25°C for 3-(aminopropyl) tripropylsilane

The elimination of water from the system was critical to the above experiments as the presence of water in the silylamine could lead to additional CO_2 uptake via formation of bicarbonate. Additionally, any water absorbed during the experiment could lead to a false attribution of the weight uptake solely to CO_2 absorbance. Karl-Fischer analysis indicated that a representative silylamine, 3-(aminopropyl) tripropylsilane, contained on average 0.12 weight % water after synthesis and distillation. This amount of water is insignificant compared to the CO_2 weight uptake observed. All of the silylamines were stored under nitrogen in a glove box until use. During the gravimetric experiments, care was taken to keep the silylamines under an atmosphere of argon until CO_2 is introduced. The CO_2 employed was SFC grade, certified to contain less than < 250 ppb H_2O with a purity of 99.9999%.[28]

2.3.1.2 Gravimetric measurement of CO_2 uptake at 40°C

Gravimetric uptake experiments at 40°C were conducted in a similar manner to the procedure described at 25°C. The sand bath used to regulate the temperature of the vial was kept at 40°C. In addition, a heated gas line was used to ensure that the temperature of the CO_2 contacting the solvent was at least 40°C. To heat the gas line, stainless steel tubing wrapped in heating tape controlled by Variac variable autotransformers was used. The temperature of the gas line was monitored by an internal thermocouple. A picture of the system is shown in Figure 2.15 and a diagram of its components is shown in Figure 2.16. Note – the system also includes a bubbler system for use in creating a humidified gas stream. For the 40°C gravimetric measurements, the bubblers were bypassed.

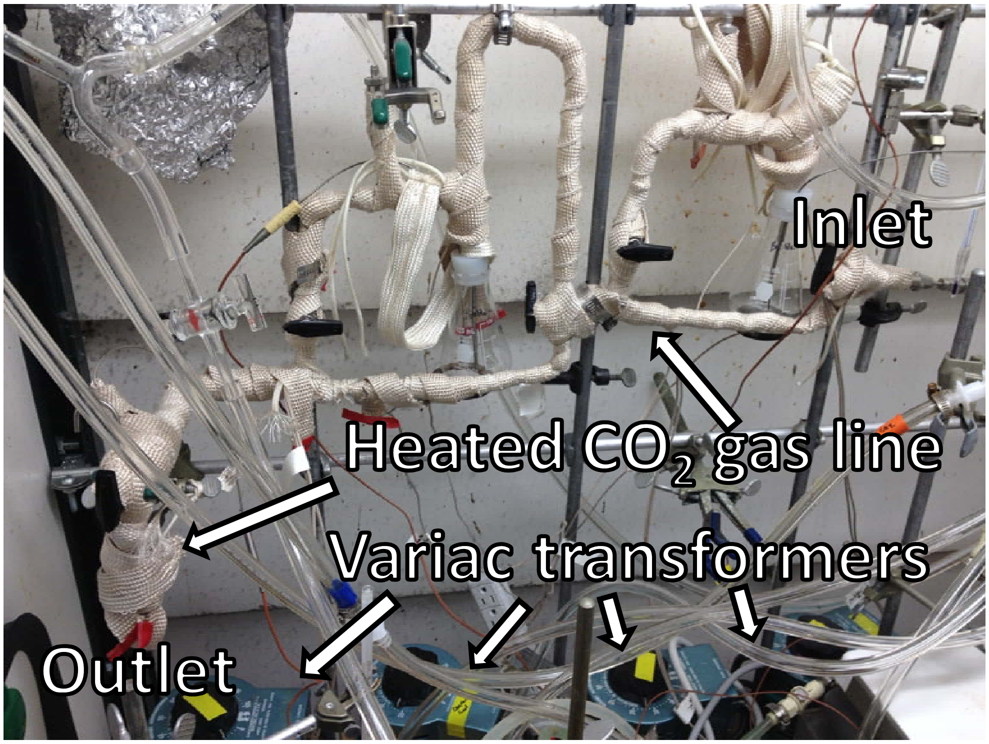

Figure 2.15 - Heated CO_2 gas line and bubbler system

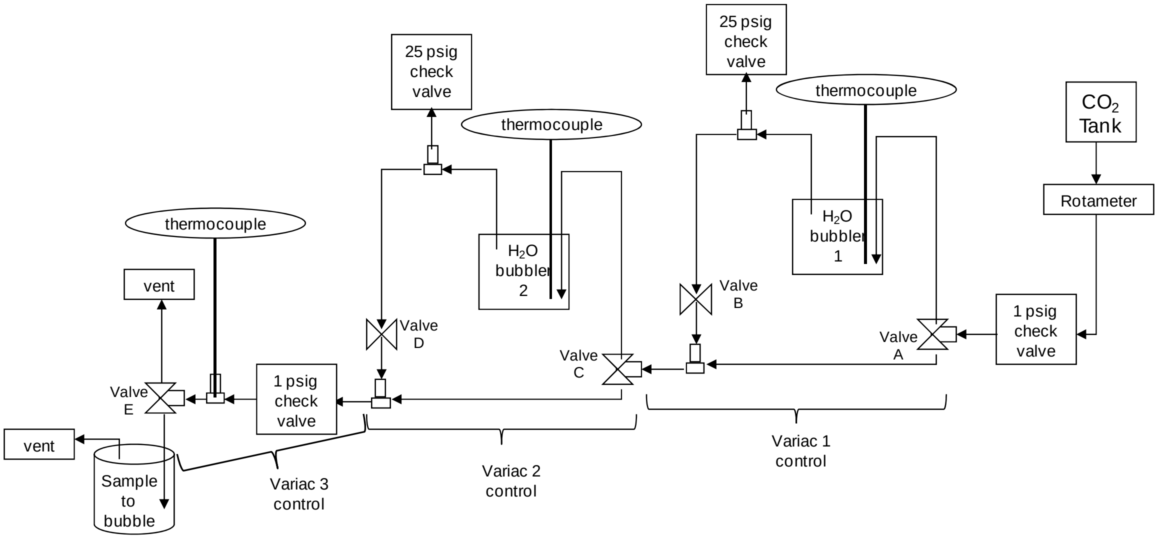

Figure 2.16 - Diagram of heated CO_2 gas line and bubbler system

2.3.1.3 Refractive index as an indicator of conversion

The refractive index of the solvent can be used to measure conversion of the silylamine to the reversible ionic liquid in its reaction with CO_2. To measure the refractive index a Reichert Arias 500 refractometer was used. Approximately 0.2 mL of sample was placed on the sample glass; measurements were taken when the sample reached thermal equilibrium at 25°C. A graph of refractive index versus conversion to the reversible ionic liquid is shown in Figure 2.17. Here conversion is arbitrarily defined as unity when the highest refractive index was achieved; however, the technique could have been combined with the gravimetric CO_2 uptake experiments to attempt quantification on a molar basis.

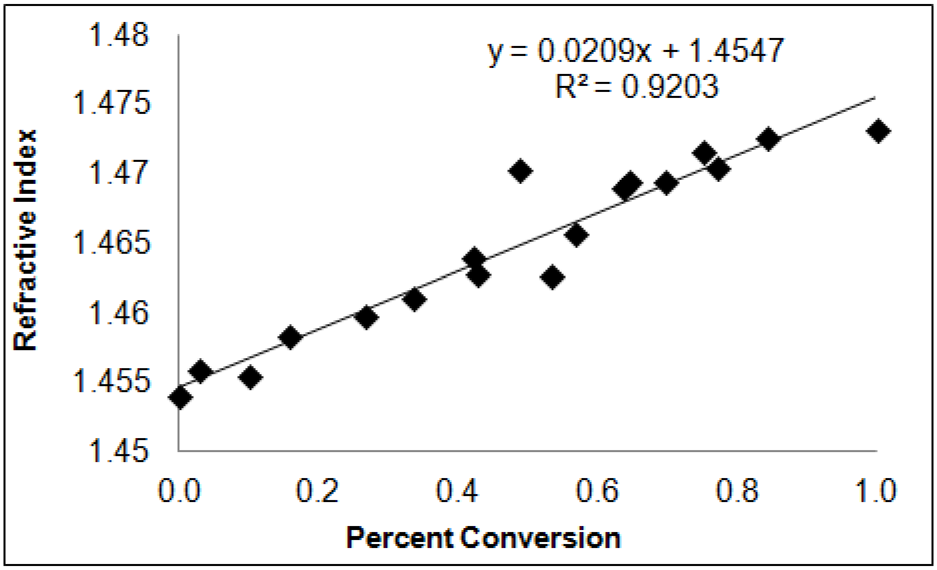

Figure 2.17 - Refractive index as a function of conversion to the reversible ionic liquid for 3-(aminopropyl) tripropylsilane

2.3.1.4 ATR-FTIR for decoupling chemical reaction and physical absorption

Infrared measurements were made using attenuated total reflectance (ATR) Fourier-transform infrared (FTIR) spectroscopy. The device used was a Shimadzu IRPrestige-21 FTIR spectrophotometer with a deuterated L-alanine doped triglycene sulphate (DLaTGS) detector. The ATR cell used was a heated Golden Gate accessory supplied by Specac Inc. A custom stainless steel reactor was used to perform the high pressure physical absorption experiments. A range of 400-4000 cm^{-1} is scanned at a resolution of 1cm^{-1} using 32 scans.

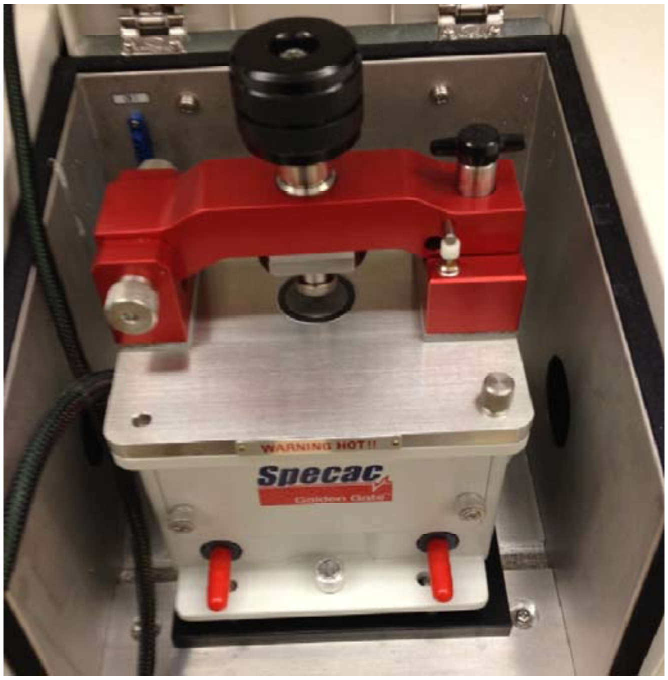

Figure 2.18 - Golden Gate ATR cell with bridge

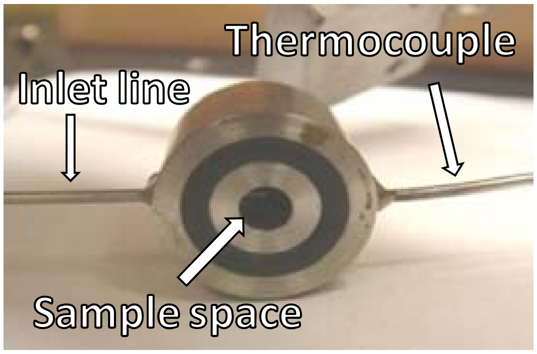

Figure 2.19 - Custom high-pressure, heated ATR reactor cell

ATR-FTIR allows quantitative differentiation between chemically reacted and physically absorbed CO_2. Chemically reacted CO_2 is represented by the N-H stretch of the ammonium cation from 2600-3100 cm^{-1}, the asymmetric CO_2^- stretch of the carbamate anion at 1575 cm^{-1}, and the carbonyl stretch of carbamic acid at 1700 cm^{-1}.

Physically absorbed CO_2 is represented by the asymmetric stretch of CO_2 at 2330 cm^{-1}. Figure 2.20 shows ATR-FTIR spectra of a model silylamine, 3-(aminopropyl)tripropylsilane, before and after reaction with 1 bar of CO_2 at 25°C.

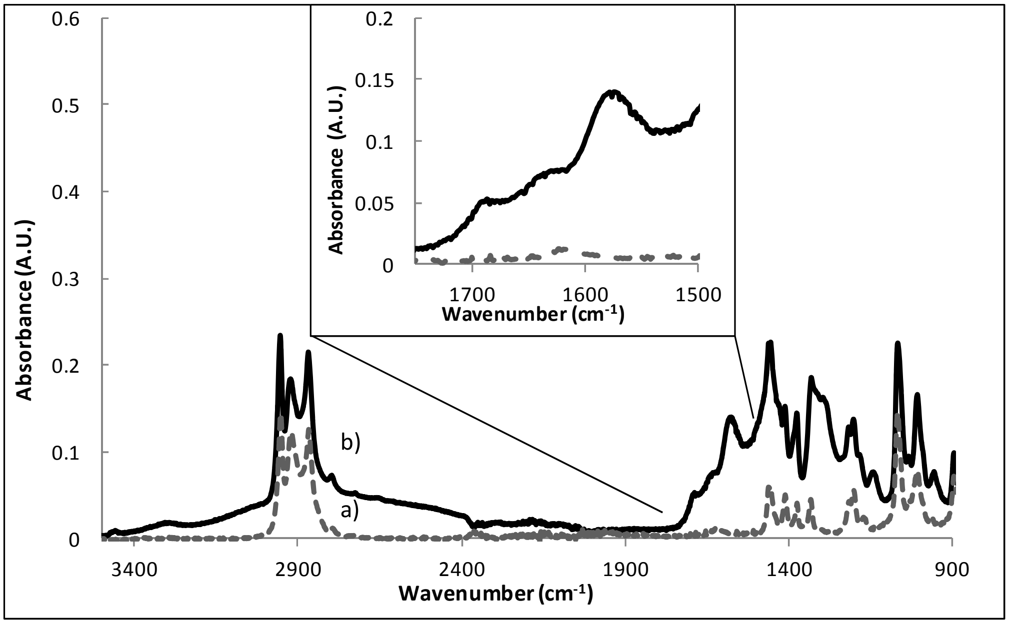

Figure 2.20 - a) 3-(aminopropyl) tripropylsilane and b) 3-(aminopropyl) tripropylsilane reversible ionic liquid after reaction with 1 bar of CO_2 at 25°C

Figure 2.21 shows the asymmetric CO_2 stretch (v_3 mode) at pressures between zero and 60 bar at 35°C for the reversible ionic liquid form of 3-(aminopropyl)tripropylsilane. As the pressure of CO_2 in equilibrium with the reversible ionic liquid increases, the absorbance of the CO_2 asymmetric stretch also increases.

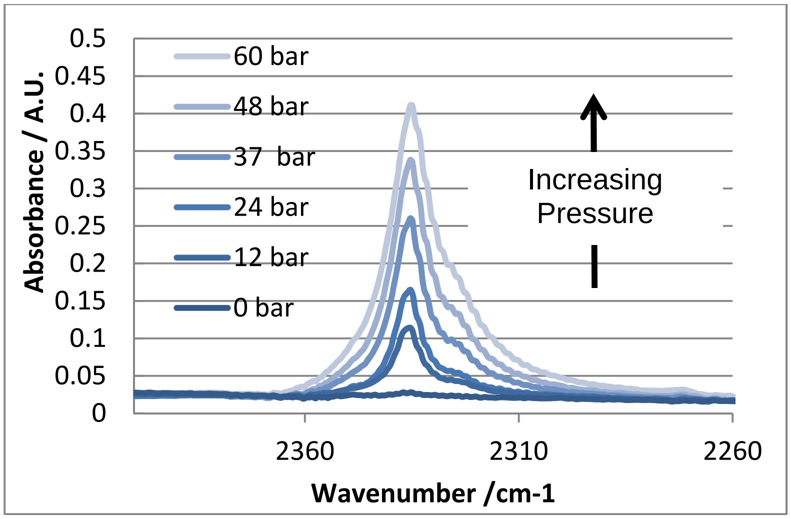

Figure 2.21 - ATR-FTIR asymmetric CO_2 stretch (0-60 bar) in 3-(aminopropyl)tripropylsilane at 35°C

Henry's Law constants ($H_{CO_2,RevIL}$) of CO_2 in the reversible ionic liquids were calculated using ATR-FTIR. Henry's Law is a limiting case of vapor-liquid equilibrium, valid for systems at sufficiently low solubility to preclude any effects of solute-solute interactions. Henry's Law states that the solubility of a gas in equilibrium with a liquid phase is directly proportional to the partial pressure of the gas in the vapor phase. Henry's law is both solute and solvent specific. If the vapor phase is assumed to be ideal, it can be written as $y_{CO_2}P = X_{CO_2}H_{CO_2,RevIL}$. We determined Henry's Law constants by a straight-line fit (through the origin) of a plot of mole fraction of CO_2 vs. CO_2 pressure using data points below 30 bars of CO_2 pressure (Figure 2.22). As a control, we first measured the Henry's constant of the conventional ionic liquid [BMIM][PF_6]. The $H_{CO_2,[BMIM][PF6]}$ was found to be 58 bar at 25°C- a result consistent with the reported value of 53.4 bar.[29]

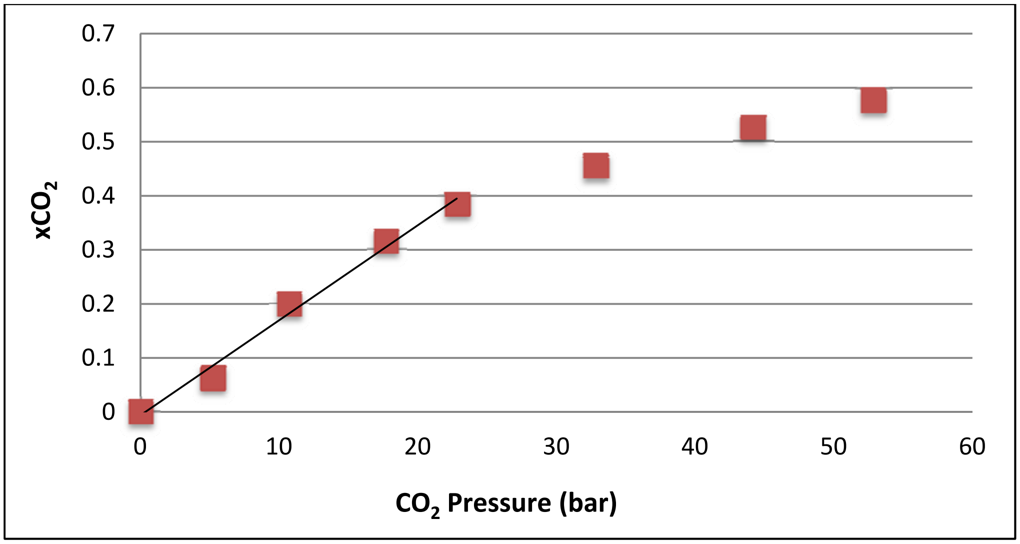

Figure 2.22 – Mole fraction of CO_2 in the reversible ionic liquid of 3-(aminopropyl)tripropylsilane as a function of CO_2 pressure at 35°C

2.3.1.5 Calculation of theoretical van der Waals volume

The van der Waals volume is the theoretical volume occupied by the molecule assuming the atoms are hard spheres. Bondi developed a group contribution method to determine van der Waals volumes.[30] This method provides a way to determine van der Waals volumes of complex molecules by summing the contributions of each individual segment. Shown in Table 2.3 are the individual van der Waals volume contributions used in the void volume calculations.

Table 2.3 - Theoretical van der Waals volume group contributions

Segment	van der Waals volume (cm^3/mol)
CH_3-	13.67
-CH_2-	10.23
>CH-	6.78
-O-	5.2
>Si<	6.82
Ion pair	38.36

Bondi did not present van der Waals volume values for ion pairs. To calculate the volume occupied by the carbamate and ammonium ion pair, volume contributions for a secondary amine, carboxylic acid and a primary amine were substituted. There is likely associated error with this assumption; however, this assumption was consistent for each reversible ionic liquid enabling a relative comparison. The van der Waals volumes of several ionic liquids calculated with the group contribution method were compared with the results of a molecular model simulation (B3LYP 6-31G*) and the values were within good agreement (< 5% difference).

2.3.1.6 ^{13}C NMR for verification of reversible ionic liquid formation

^{13}C NMR was used to verify complete formation of the reversible ionic liquid. A ^{13}C spectrum is shown in Figure 2.23 of 3-(aminopropyl)tripropylsilane before addition of CO_2. The spectrum inset shows the silylamine structure and assigns carbon atoms to the observed peaks. Figure 2.24 shows a ^{13}C spectrum of the 3-(aminopropyl)tripropylsilane reversible ionic liquid after reaction with 1 bar of CO_2 at 25°C. The ammonium-carbamate / carbamic acid structure of the reversible ionic liquid is also shown with its carbon peaks assigned on the spectrum. For the reversible ionic liquid, the NMR is taken neat with the use of a $CDCl_3$ capillary. This is done to prevent any reversal of the ionic species back to the starting silylamine. Proton (^{1}H) NMR was not used; the high viscosity of the reversible ionic liquid gives rise to broad overlapping peaks that cannot be differentiated accurately.

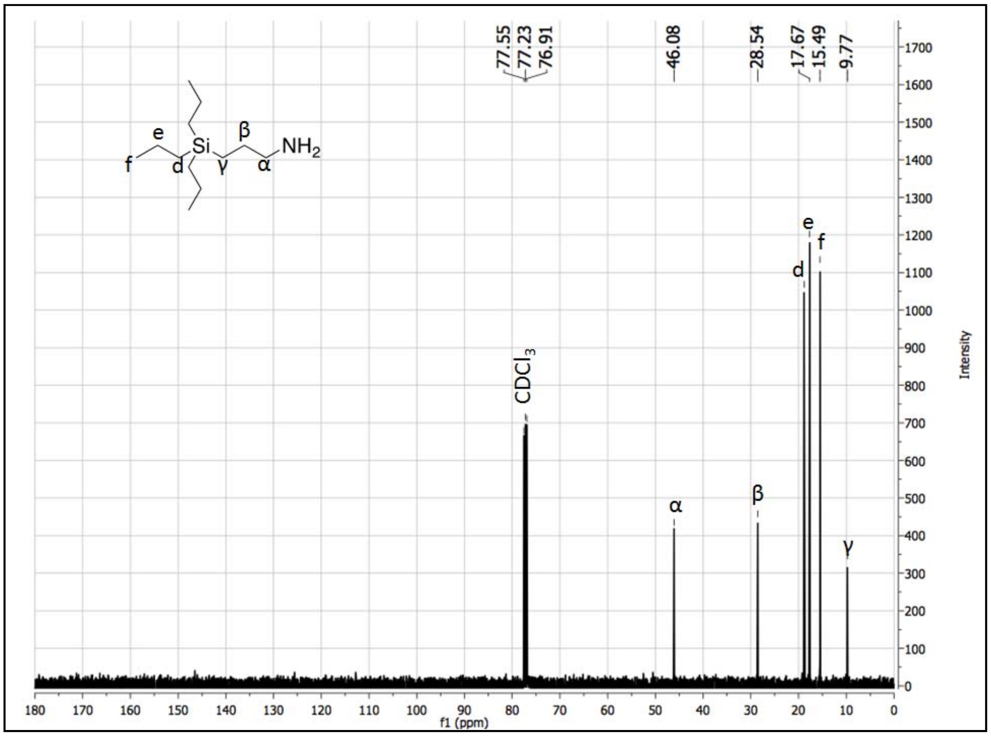

Figure 2.23 - ^{13}C NMR spectrum of 3-(aminopropyl) tripropylsilane before CO_2 addition

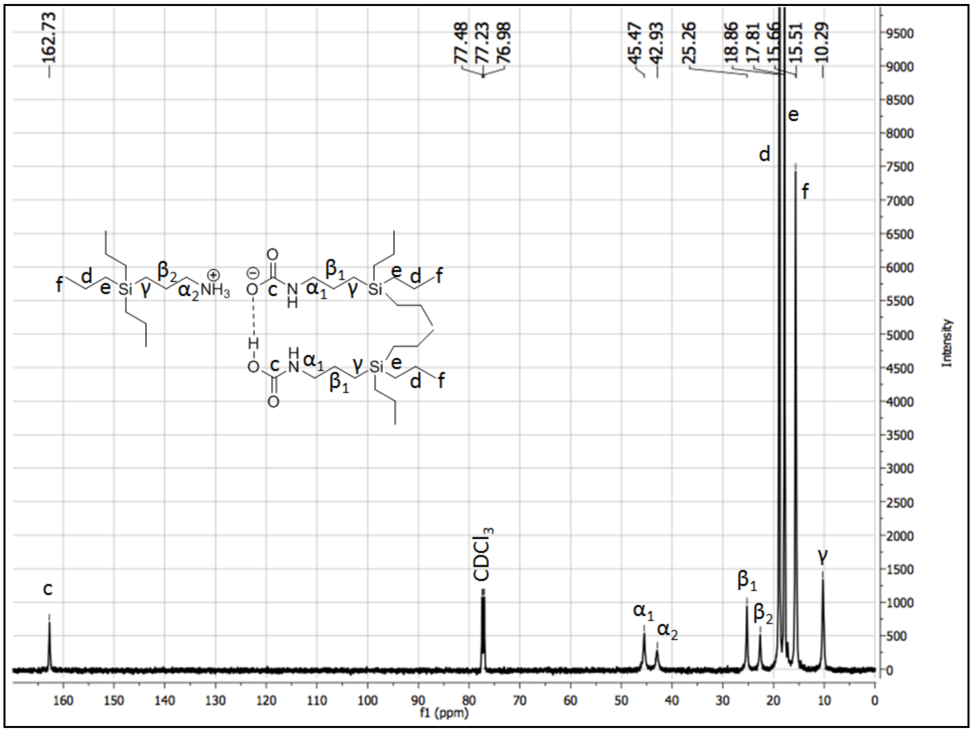

Figure 2.24 - ^{13}C NMR spectrum of 3-(aminopropyl) tripropylsilane reversible ionic liquid – after reaction with 1 bar of CO_2 at 25°C

2.3.1.7 Quantitative ^{13}C NMR for investigation of carbamic acid

For the quantitative ^{13}C experiments, the starting amine (3-(aminopropyl) tripropylsilane) was added to an argon-purged NMR tube sealed using a septum. One bar of CO_2 was then introduced for 75 minutes by sparging using a long 18-gauge stainless steel needle (a 21 gauge needle was also used to vent the system). Weight measurements were made before and after CO_2 introduction, to calculate the gravimetric CO_2 uptake. The average CO_2 capacity measured gravimetrically in the quantitative NMR experiments was 0.62±0.01 moles of CO_2 per mole of amine. It is assumed that the slightly lower CO_2 uptake observed in the NMR experiments compared to the gravimetric capacities reported in this chapter is a result of mass transfer limitations in the NMR tube.

To conduct quantitative ^{13}C NMR, three important experimental changes are needed over standard ^{13}C NMR. They include: 1) a full 90° pulse 2) extended delay time and 3) proton decoupling only during the acquisition period. The first is to ensure complete excitation of the nucleus. The second is to allow full relaxation after the pulse is applied. To determine the appropriate delay time, an inversion recovery T_1 experiment was performed. For 3-(aminopropyl) tripropylsilane in its reversible ionic liquid form, the longest T_1 time comes from the carbonyl carbon (162.73 ppm) at 4.027 seconds. It is generally recommended that the delay time used be 5 times the longest T_1 time. As such, for all of the quantitative experiments performed, a delay time of 20 seconds was used. The last experimental change (3) is done to avoid a false and disproportional signal buildup during proton decoupling as a result of the Nuclear Overhauser Effect. The protocol is named inverse gated decoupling. To increase the signal to noise ratio, 2000 scans were performed for each experiment over a period of 12 hours.

2.3.2 Viscosity measurements of the reversible ionic liquid

2.3.2.1 Viscosity measurements at 25°C

The viscosity of each ionic liquid was measured using a Rheosys Merlin II cone and plate viscometer. Samples were applied to the plate and allowed to reach thermal stability prior to data collection. Shear rates vary between 10 and 2000 s^{-1}. The average viscosity over the shear range was recorded.

Figure 2.25 - Rheosys Merlin II viscometer

2.3.2.2 Viscosity measurements at 40°C

The plate of the viscometer is controlled by a PID temperature controller. The plate was heated to 40°C and allowed to equilibrate for at least 15 minutes prior to conducting an experiment. Once equilibrated, the reversible ionic liquid was placed onto the plate; the cone was then lowered, and the sample was allowed to equilibrate for 10 minutes. The shear rate was varied between 10 and 2000 s^{-1} and the average viscosity was recorded.

2.3.3 Thermodynamic measurements of the reversible ionic liquids

Thermodynamics of the reversible ionic liquids consists of:

1. The sensible heat required to raise the temperature of the CO_2-rich solvent from the capture temperature to the reversal temperature, $Q = mC_p\ \Delta T$

2. Latent heat of the reaction between CO_2 and silylamine, ΔH_{rxn}

3. Enthalpy of mixing/demixing of physically absorbed CO_2 in the reversible ionic liquid, $\Delta H_{dissolution}$

In $Q = mC_p\,\Delta T$, m is the mass of the CO_2 rich solvent and depends on the CO_2 capture capacity. C_p is the heat capacity estimated using the group contribution method by Ruzicka and Domalski. At 40°C, the average C_p of our silylamines was found to be 2.1 J/g-K while that of our reversible ionic liquids was found to be 2.3 J/g-K. $\Delta T = T_{rev}-T_{cap}$, is the difference between the reversal and the capture temperature. In the actual absorber unit, T_{cap} will be dictated by the temperature of flue gas stream. A T_{cap} of 40°C can be used as the basis for all of our reversible ionic liquid results. The quantity that is dependent on the silylamine structure is T_{rev}. To minimize the heat input for heating the reversible ionic liquid, we would prefer lower values of $T_{rev.}$ Further, it is important that T_{rev} be sufficiently less than the silylamine evaporation temperature (T_{evap}) to avoid silylamine loss during regeneration. However, very low values of the reversal temperature would leave very small window for operating the absorber and the stripper.

Since our compounds capture CO_2 both by chemical reaction and physical absorption, two kinds of enthalpies constitute the enthalpy required for regeneration of the silylamine: $\Delta H_{regeneration} = \Delta H_{rxn} + \Delta H_{dissolution}$. ΔH_{rxn} is associated with removing the chemically reacted CO_2 and $\Delta H_{dissolution}$ accounts for removal of the physically absorbed CO_2.

Differential scanning calorimetry (DSC) is used to calculate the temperature of reversal (T_{rev}), the silylamine evaporation temperature (T_{evap}), as well as the enthalpy of regeneration ($\Delta H_{regeneration}$). DSC measurements are performed using a Q20 TA DSC

Instrument. The reversible ionic liquid is loaded into a hermetic DSC pan and sealed. Temperature is ramped from -40°C to 400°C at a rate of 5°C/min. All experiments were performed in triplicate. An example thermogram is shown in Figure 2.26.

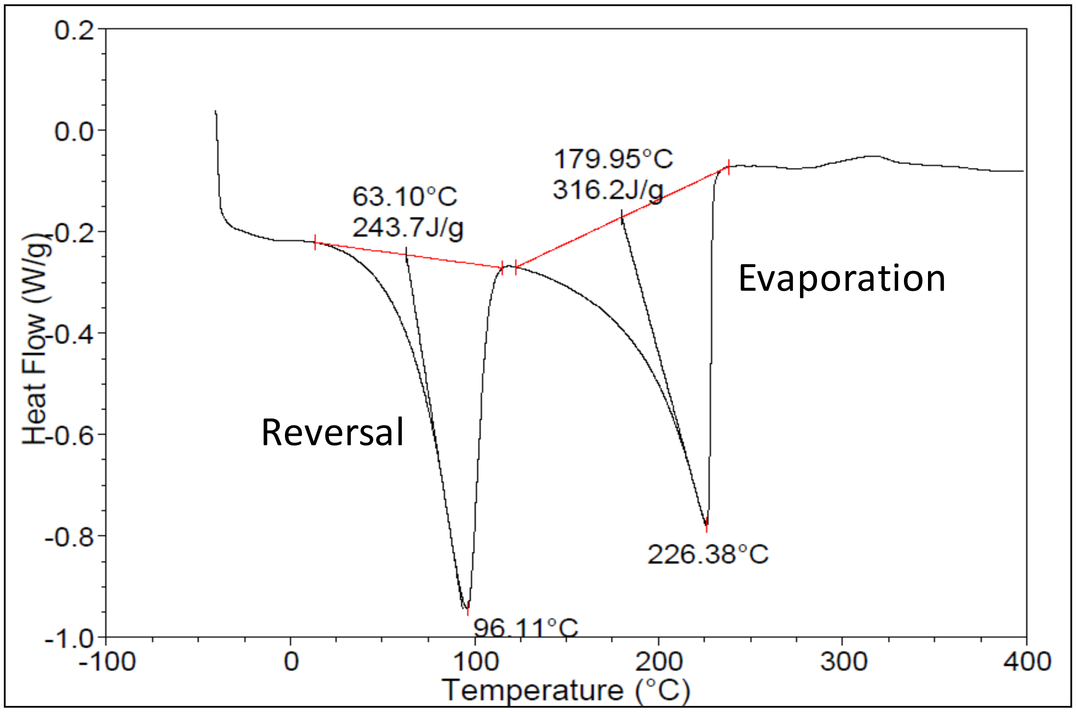

Figure 2.26 - DSC thermogram for the reversible ionic liquid of 3-(aminopropyl) tripropylsilane

2.3.3.1 Determination of melting point, reversal temperature, solvent evaporation temperature, and enthalpy of regeneration

Reversal temperature and the temperature of evaporation are determined as the intersection of two tangents drawn from the beginning and bottom of the respective endotherm events observed in the DSC. The enthalpy of regeneration is calculated by integrating the reversion endotherm with respect to time.

2.3.3.2 Estimation of heat capacity

C_p is the heat capacity estimated using the group contribution method by Ruzicka and Domalski.[31] At 40°C, the C_p of 3-(aminopropyl)tripropylsilane was found to be 2.1 J/g-K while that of the reversible ionic liquid was found to be 2.3 J/g-K.

2.3.4 Theoretical calculations

Calculations of the nitrogen exposed area and nitrogen atomic charge on several of the silylamines were performed using the Spartan® 2010 molecular modeling software package. The geometries of the silylamines were optimized using density functional theory using the B3LYP 6-31G* basis set. All silylamines were optimized to their lowest energy confirmations before calculating the nitrogen exposed area or atomic charge.

2.3.5 Scale-up analysis

An ASPEN HYSYS simulation was performed to evaluate the energy required by our reversible ionic liquids to meet a 90% CO_2 capture target. Experimental data for reaction enthalpy, reversal temperature, density, and boiling point of our solvents was integrated in the simulation. Estimates of the critical properties were calculated using the methods described in *The Properties of Gases and Liquids*.[31] The results were compared to the literature values for an aqueous monoethanolamine CO_2 capture process.[32]

2.4 Results and Discussion

2.4.1 Changing the alkyl chain length of trialkyl silylpropylamines

The first structural modification investigated to the base silylamine structure (Figure 2.27) was increasing the length of the alkyl chain around the silicon atom. The length of the alkyl chain surrounding the propyl amine was varied from dimethyl ethyl (DMESA), to ethyl (TEtSA), propyl (TPSA), and hexyl (THSA).

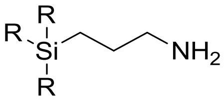

Figure 2.27 - Base silylamine structure

We hypothesized that by increasing the alkyl chain length around the silicon atom, we would be able to reduce the reversible ionic liquid viscosity. Further, while we expect a decrease in the CO_2 capacity on a mole of CO_2 capture per kilogram of amine due to the increasing molecular weights, we postulated that CO_2 uptake due to physical absorption could increase as a result of increase in void volumes in the reversible ionic liquid at longer alkyl chain lengths.

2.4.1.1 CO_2 uptake

The CO_2 uptake measured using gravimetry under 1 bar of CO_2 at 25°C is reported in Figure 2.28. DMESA exhibited a significantly lower CO_2 uptake than the other thee silylamines shown. This lower CO_2 uptake is rationalized due to mass transfer limitations. Upon reaction with CO_2, DMESA immediately forms a solid, likely trapping some unreacted silylamine from reacting with CO_2. It is seen that as the alkyl chain length around the silicon atom increases, the CO_2 uptake increases slightly on a mole of CO_2 captured per mole of amine basis.

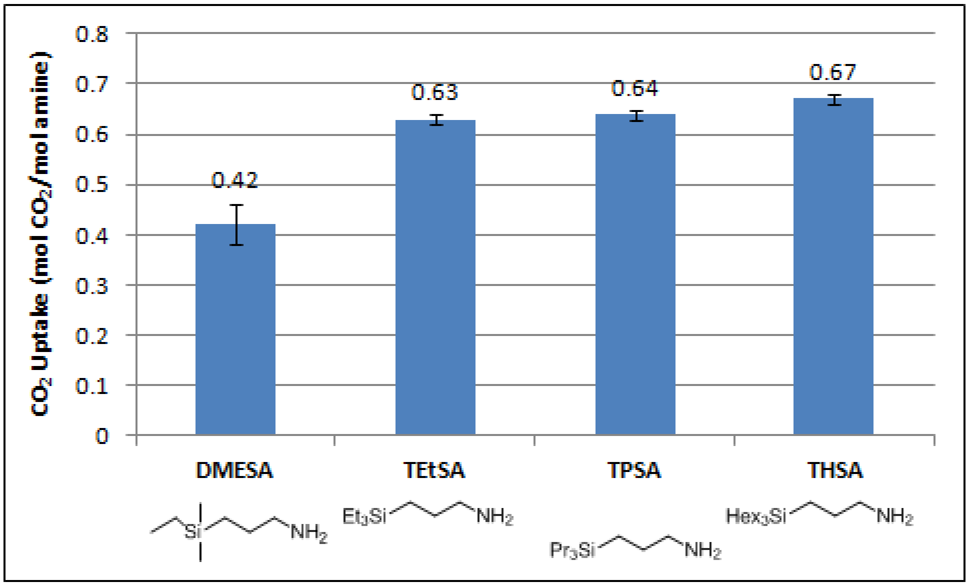

Figure 2.28 - CO_2 uptake of silylamines DMESA, TEtSA, TPSA, and THSA in a mole CO_2 per mole amine basis

The increase in CO_2 capacity with alkyl chain length is attributed to an increase in physical absorption. The Henry's constants for CO_2 solubility in the reversible ionic liquid form of TEtSA, TPSA, and THSA at 25°C are reported in

Table 2.4. Using the equation $y_{CO2}P = x_{CO2}H_{CO2,RevIL}$ and the reported Henry's constants, under 1 bar of CO_2 the expected CO_2 uptake from chemical absorption increases as the length of alkyl chain surrounding the silicon atom increases. THSA exhibits nearly 0.02 moles of CO_2 physically absorbed per mole of amine of CO_2 solubility while TEtSA just reaches 0.01 moles of CO_2 physically absorbed per mole of amine.

Table 2.4 - Henry's constant of TEtSA, TPSA, and THSA for CO_2 solubility in the reversible ionic liquid at 25°C

Reversible ionic liquid	Henry's Constant (bar, 25°C)
TEtSA	69±2
TPSA	52±2
THSA	44±3

Figure 2.29 summarizes the physically absorbed CO_2 mole fraction (x_{CO_2}), calculated from the ATR-FTIR data as a function of CO_2 pressure (bar) at 35°C for the TEtSA, TPSA, and THSA reversible ionic liquids. At one bar CO_2 pressure, the mole fraction of CO_2 in the reversible ionic liquid is between 1.3×10^{-2} and 2.0×10^{-2} depending on the silylamine structure. The reversible ionic liquid of 3-(aminopropyl)trihexylsilane exhibited the highest CO_2 solubility ($x_{CO_2}=2.0 \times 10^{-2}$), while TPSA and TEtSA have comparable but lower CO_2 physical absorptions ($x_{CO_2}=1.3 \times 10^{-2}-1.7 \times 10^{-2}$). CO_2 solubilities in traditional ionic liquids have been reported in the literature and exhibit comparable solubility values. For example, [BMIM][PF6], [EMIM][Tf_2N], and [EMIM][CF_3SO_3] exhibit comparable CO_2 solubility, ranging between 1.4×10^{-2} and 2.7×10^{-2} mole CO_2/mol ionic liquid at 30˚C.[33]

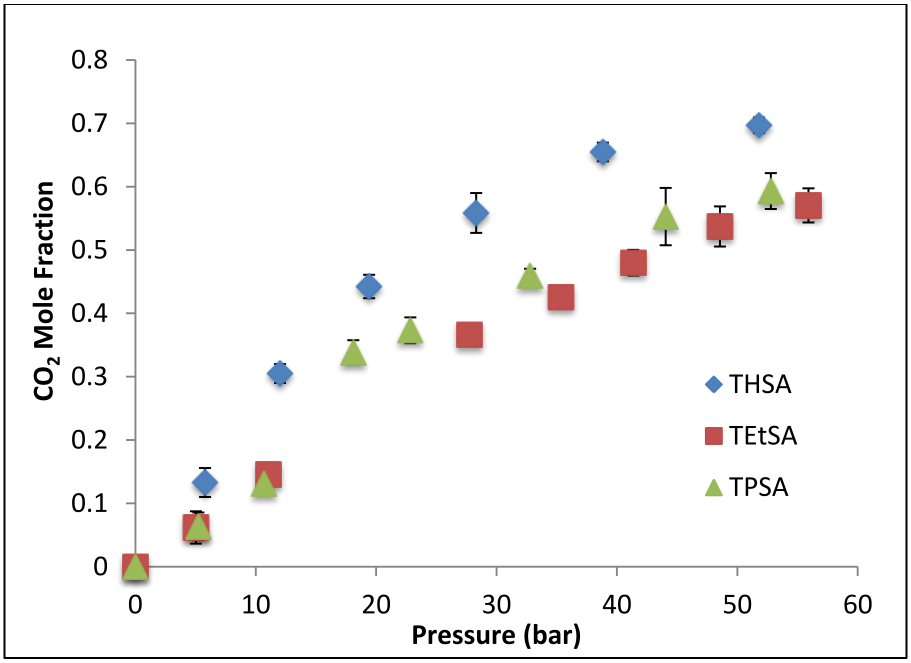

Figure 2.29 - CO_2 mole fraction as a function of pressure at 35°C for TEtSA, TPSA, and THSA

We also compared the variations between the physical absorption capacities of the reversible ionic liquids to differences in the theoretical "void volume." The void volume (V_V) of a reversible ionic liquid is the "empty" space between the molecules, and was found by subtracting the theoretical van der Waals volume (V_{vdW}) from the experimentally determined molar volume (V_M) as described in the experimental section.[30] A plot of $H_{CO_2,RevIL}$ (bar, at 35°C) versus V_V (cm^3/mol) is given in Figure 2.30. The void volume correlates roughly with the Henry's constant as expected.

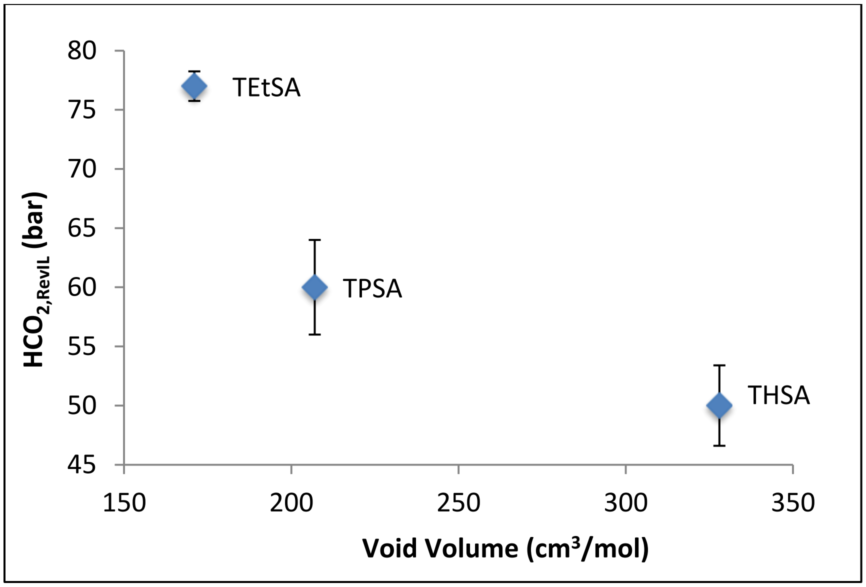

Figure 2.30 - Henry's constant of TEtSA, TPSA, and THSA at 35°C versus void volume

While presentation of the CO_2 uptake in terms of moles of CO_2 per mole of amine is useful for understanding the chemical reaction and relative physical absorption between silylamines, the importance of molecular weight should be highlighted. Industry has significant interest in learning the relative efficiency of CO_2 uptake in terms of moles of CO_2 captured per kilogram of amine solvent. The data are presented in Figure 2.31 for DMESA, TEtSA, TPSA, and THSA under 1 bar of CO_2 at 25°C. Whereas in a mole of CO_2 per mole of amine basis, THSA exhibited the highest CO_2 uptake, here THSA is the lowest performer, as a result of its high molecular weight. Thus, in designing silylamines for CO_2 capture, an awareness of the size and bulkiness of the silylamine must be maintained. While physical absorption is attractive because of the low amount of energy required for regeneration, here at least, it comes at a compromise for significant gains in the molecular weight of the silylamine solvent.

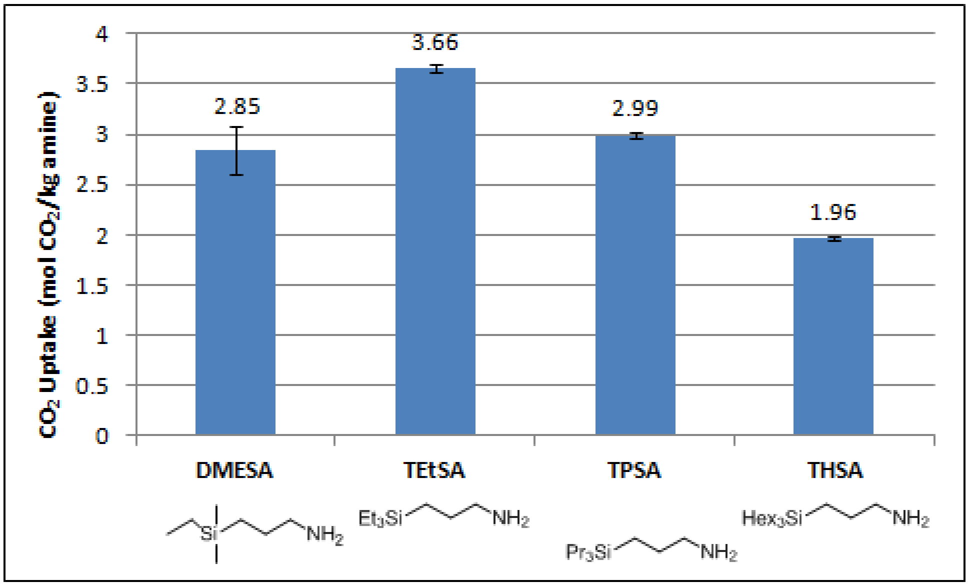

Figure 2.31 - CO$_2$ uptake of silylamines DMESA, TEtSA, TPSA, and THSA in a mole CO$_2$ per kilogram amine basis

2.4.1.2 Enhanced CO$_2$ uptake via carbamic acid formation

It is commonly presumed in literature that the equilibrium reaction of a primary amine with CO$_2$ in traditional organic solvents gives a 2:1 amine to CO$_2$ mole ratio, forming only ammonium-carbamate ion pairs.[34] The 2:1 amine to CO$_2$ stoichiometry should dictate 0.50 moles of CO$_2$ per mole of amine of theoretical CO$_2$ uptake resulting from the chemical reaction. However, as shown in Figure 2.28, the gravimetric CO$_2$ uptakes observed at 25°C are on average of 30% greater than 2:1 stoichiometry (0.65 moles of CO2 per moles of amine, excluding DMESA). This corresponds to 0.15 moles of additional CO$_2$ uptake per mole of amine not accounted for by the conventional chemical reaction.

A fraction of the 0.15 moles of additional uptake results from physical absorption of CO$_2$ into the reversible ionic liquid. As presented and calculated from the Henry's constants (

Table 2.4), physical absorption accounts for approximately 0.01 moles of CO_2 per mole of amine of CO_2 uptake at 1 bar and 25°C. Thus physical absorption of CO_2 at 1 bar along with the conventional chemical reaction, gives a theoretical CO_2 capacity limited to 0.51 moles of CO_2 per mole of amine. Still, the silylamines outperform this theoretical limit by over 25%. We suggest this enhanced CO_2 uptake is the result of the formation of carbamic acid stabilized by hydrogen bonding with a carbamate anion (Figure 2.32).[35]

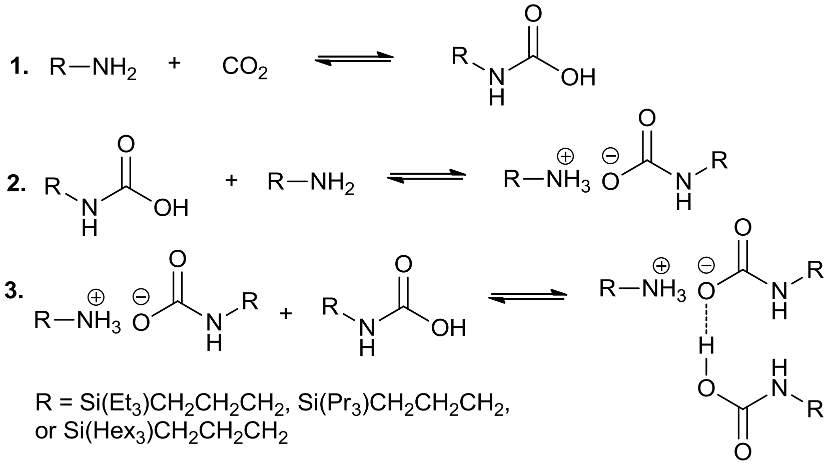

Figure 2.32 - **Equilibria proposed for the reaction of CO_2 with silylamines in solvent-free conditions**

The first equilibrium in Figure 2.32 is the reaction of a molecule of silylated amine with CO_2 to form the corresponding carbamic acid species. In the absence of added solvent, the free amine is essentially the solvent for this reaction. Given the large quantity of free amine at the early stages of reaction with CO_2, the carbamic acid is then deprotonated as shown in the second equilibrium reaction. This results in the conventional ammonium carbamate ion pair. As this ion pair concentration increases, the free amine is no longer the effective reaction solvent; it is replaced by the increasing concentration of ionic species – the reversible ionic liquid. As shown in the third equilibrium, it is proposed that when the reversible ionic liquid is acting as a solvent, carbamic acid is stabilized via hydrogen bonding with the carbamate anion.

It is important to note that the overall stoichiometry depicted in the third equilibrium reaction in Figure 2.32 is two moles of CO_2 absorbed per three moles of amine reacted. This would then give a theoretical CO_2 uptake capacity by chemical reaction of 0.67 moles of CO_2 per mole of amine. This value is in good agreement with our gravimetric results shown in Figure 2.28, as we report an average CO_2 uptake capacity of 0.65±0.02 moles of CO_2 per mole of amine.

To further investigate the complex equilibria, quantitative ^{13}C NMR experiments were carried out on the 3-(aminopropyl) tripropylsilane reversible ionic liquid. A ^{13}C NMR spectrum of the reversible ionic liquid after reaction with 1 bar of CO_2 at room temperature is presented in Figure 2.33 (CO_2 uptake measured gravimetrically at 0.62±0.01 moles CO_2 per mole amine). The carbon peak assignments are shown in Figure Figure 2.34. We observe distinct signals for the alpha and beta carbon peaks on the propyl backbone relative to the amine nitrogen. The signals result from the differing chemical environments of the ammonium cation and the carbamic acid-carbamate anion. The peaks labelled α_2 and β_2 are attributed to the ammonium cation of the reversible ionic liquid while the peaks labeled α_1 and β_1 are assigned to the hydrogen-bonded carbamic acid-carbamate anion. Differences in the environment of the carbamate anion versus the carbamic acid via ^{13}C NMR are not expected as the exchange of the acidic hydrogen between the two species is likely too rapid to be observed by NMR spectroscopy.

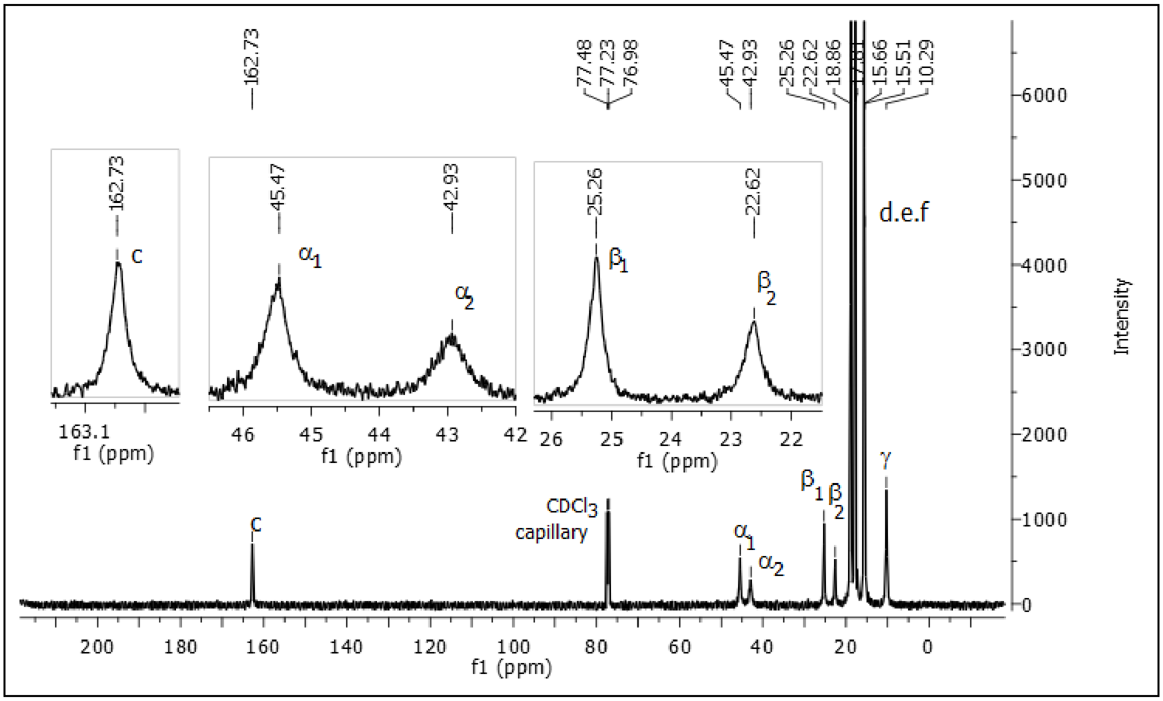

Figure 2.33 – Quantitative ^{13}C NMR spectrum of the 3-(aminopropyl)tripropylsilane reversible ionic liquid

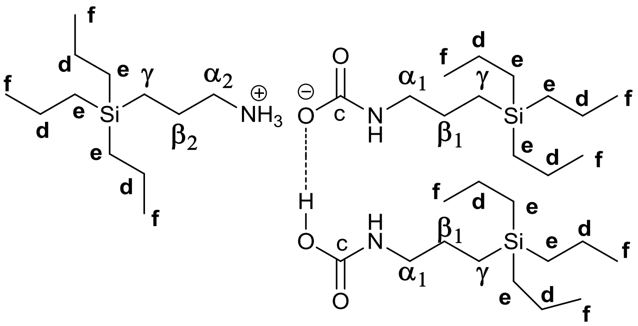

Figure 2.34 -^{13}C peak assignments for the 3-(aminopropyl)tripropylsilane reversible ionic liquid

Integration of the ^{13}C NMR peaks is consistent with the presence of carbamic acid along with the ammonium carbamate ion pair. Relative integrations of the carbonyl (c), alpha (α_1, α_2) and beta (β_1, β_2) peaks of interest are shown in Table 2.5.

Table 2.5 - Quantitative 13C NMR areas of the 3-(aminopropyl)tripropylsilane reversible ionic liquid

^{13}C peak	Relative integration
c – 162.73 ppm	1.92±0.08
α_1 – 45.47 ppm	1.69±0.08
α_2 – 42.93 ppm	1.00[a]
β_1 – 25.26 ppm	1.81±0.11
β_2 – 22.62 ppm	1.12±0.05
[a]Reference area, other areas are relative to this value	

If the conventional 2:1 amine to CO_2 stoichiometry adequately explained the equilibrium then each of the α and β peaks should integrate to the same values. However, both the α and β carbon peak integrations show that the further downfield carbon – α_1 and β_1 – integrate to comparable values – 1.69±0.08, 1.81±0.11 respectively. These integrations are approximately 65% greater than their split carbon counterpart – α_2 and β_2 – of 1.00 and 1.12±0.05 respectively. Therefore, the increased areas of the downfield α and β carbon peaks are in agreement with the hydrogen-bonded carbamic acid-carbamate anion complex. This is also supported by the carbonyl carbon peak area of 1.92±0.08, which aligns with the area of the α_1 and β_1 carbon peaks.

We considered the possibility of an additional adduct of CO_2 to one molecule of amine as proposed in literature.[8] However, the quantitative ^{13}C NMR does not support this hypothesis. If two molecules of CO_2 were attached to one amine nitrogen to form a bis-anion, then two corresponding ammonium cations would be required to counterbalance the charges. In this case the carbon peaks representing the ammonium cation (α_2, β_2) would have to be larger than the carbamate anion carbon peaks (α_1, β_1). This is the opposite of what is observed.

ATR-FTIR spectra were collected for 3-(aminopropyl) tripropylsilane and the corresponding reversible ionic liquid as a function of CO_2 pressure at 25°C (Figure 2.35). The reversible ionic liquid shows a broad absorption from 2600-3100 cm^{-1} corresponding to the N-H and C-H stretching frequencies of the ammonium cation and hydrocarbon C-H's (Figure 2.20). N-H bending is observed at 1646 cm^{-1}. The absorption at 1575 cm^{-1} is assigned to the asymmetric CO_2^- stretch of the carbamate anion. It is postulated that the absorption at 1700 cm^{-1} is the carbonyl stretch of the carbamic acid species. As pressure is increased, this carbonyl stretch increases and the asymmetric CO_2^- stretch of the carbamate anion decreases. This is consistent with an increase in concentration of carbamic acid and a decrease in concentration of carbamate. Assignments are in agreement with those in literature.[12,36]

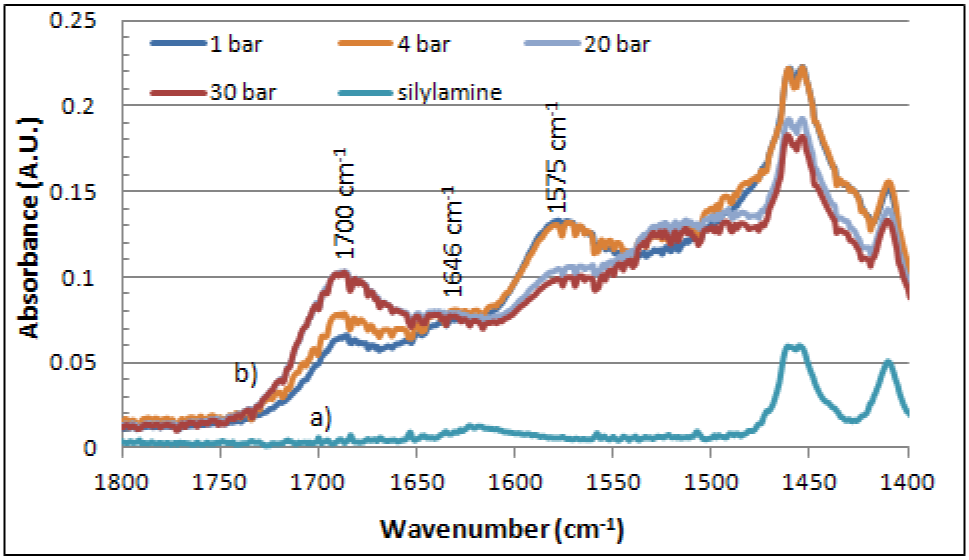

Figure 2.35 – FTIR spectrum of a) 3-(aminopropyl)tripropylsilane and b) the 3-(aminopropyl)tripropylsilane reversible ionic liquid as a function of CO_2 pressure

Experimental results are consistent with the stabilization of the carbamic acid by hydrogen bonding with the carbamate anion. The formation of this species enhances the theoretical CO_2 capacity for chemical reaction from 0.50 moles of CO_2 per mole of amine to 0.67 moles of CO_2 per mole of amine. This enhancement in CO_2 uptake is certainly desirable in furthering the reversible ionic liquids as efficient solvent systems for CO_2 capture.[35]

2.4.1.3 CO_2 uptake at 40°C

The CO_2 uptake under 1 bar of CO_2 at 40°C was measured using gravimetry with the experimental setup described in section 2.3.1.2. Compared to the CO_2 uptake observed at 25°C (Figure 2.28), a slight decrease is observed for TEtSA (0.03 moles of CO_2 per mol of amine). Similar results are seen for TPSA; at 25°C a CO_2 capacity of 0.64 moles of CO_2 per mole of amine is observed, while at 40°C a capacity of 0.57 moles of CO_2 per mole of amine is observed. THSA evidences a 38% decrease in CO_2 capacity at

40°C compared to 25°C; this decrease in CO_2 uptake is attributed to the low reversal temperature of the reversible ionic liquid (see section 2.4.1.6).

Table 2.6- CO_2 uptake at 40°C under 1 bar of CO_2 for TEtSA, TPSA, and THSA

Silylamine	CO_2 uptake @ 40°C (mol CO_2/mol amine)	CO_2 uptake @ 40°C (mol CO_2/kg amine)
TEtSA	0.603±0.002	3.48±0.01
TPSA	0.57±0.02	2.65±0.07
THSA	0.41±0.02	1.21±0.06

2.4.1.4 Reversible ionic liquid viscosity

Upon reaction of these silylamines with CO_2 to form their corresponding reversible ionic liquid, a significant increase in viscosity is observed. All of the starting silylamines presented in this thesis exhibit a viscosity <100 cP. However, the reversible ionic liquid (formed after reaction of the silylamine with CO_2) viscosity has a strong dependence on silylamine structure. Shown in Figure 2.36 is a plot of the reversible ionic liquid viscosity for DMESA, TEtSA, TPSA, and THSA at both 25 and 40°C. As mentioned, DMESA forms a solid immediately upon reaction with CO_2. The reversible ionic liquids follow the trend DMESA>TEtSA>TPSA>THSA in terms of viscosity. As the length of the alkyl chain increases around the silicon atom, viscosity decreases. The viscosity of THSA is nearly 60 percent less than TEtSA at 25°C.

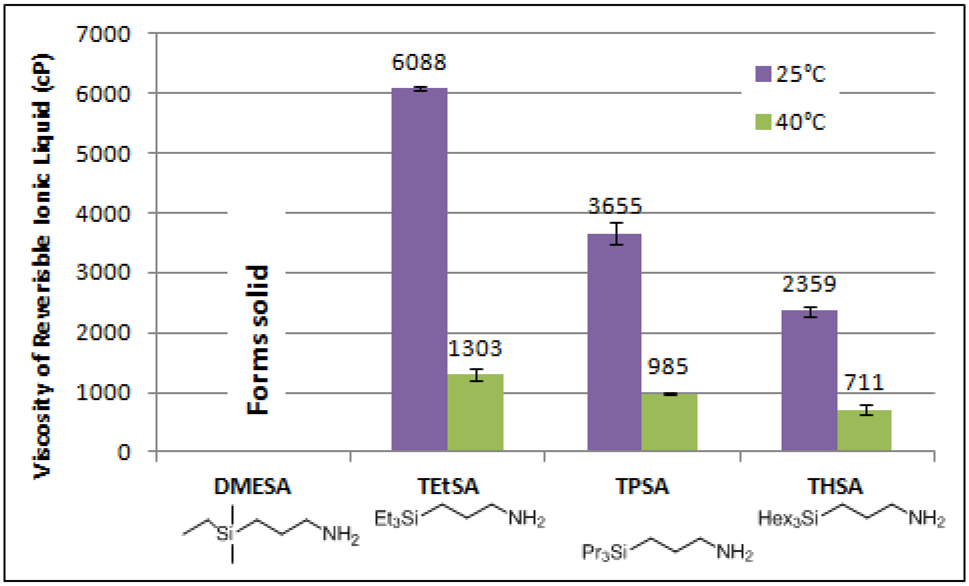

Figure 2.36 - Reversible ionic liquid viscosity of DMESA, TEtSA, TPSA, and THSA at 25 and 40 °C

The viscosities plotted in Figure 2.36 are not industrially viable. The industrial limit cited by our sponsor ConocoPhillips is near 200 cP. However, the clear structure-viscosity relationship is significant as it suggests that with cognizant design, we can tune the silylamine molecular structure to obtain a desired viscosity. Further, it is important to highlight the decrease in viscosity observed at 40°C. On average, a 74 percent decrease is seen for the reversible ionic liquid of TEtSA, TPSA, and THSA at 40°C compared to 25°C. This is also significant, as most publications suggest the average flue gas temperature from a coal-fired power plant that would be relevant to a post-combustion CO_2 capture process is near 40°C.

2.4.1.5 Lowering viscosity by controlling CO_2 uptake

A unique property of the reversible ionic liquid viscosity was observed as CO_2 uptake was varied. Figure 2.37 shows a plot of CO_2 uptake in moles of CO_2 per mole of amine (measured using gravimetry) versus reversible ionic liquid viscosity at 25°C. The viscosity follows a near S-shaped curve similar in appearance to a hockey stick. Not until a CO_2 uptake nearing 0.45 moles of CO_2 per mole of amine does the viscosity increase drastically. This finding is important because it shows that by controlling conversion to the reversible ionic liquid species we have an additional handle on limiting the viscosity rise during reaction with CO_2.

The viscosity behavior can be explained by examining the reaction equilibrium in terms of traditional solute-solvent systems. At the start of the reaction with CO_2, the silylamine is essentially the reaction solvent, which we have established has a viscosity less than 100 cP. As the reaction takes place, the concentration of ionic species increases as does the viscosity. However not until a point near a CO_2 uptake of 0.45 moles of CO_2 per mole of amine does the viscosity take a dramatic upturn. This is likely due to the dominant presence of the ionic species at higher CO_2 uptake points; it becomes the effective solvent for the reaction and as such, its viscosity then dominates the solvent system.

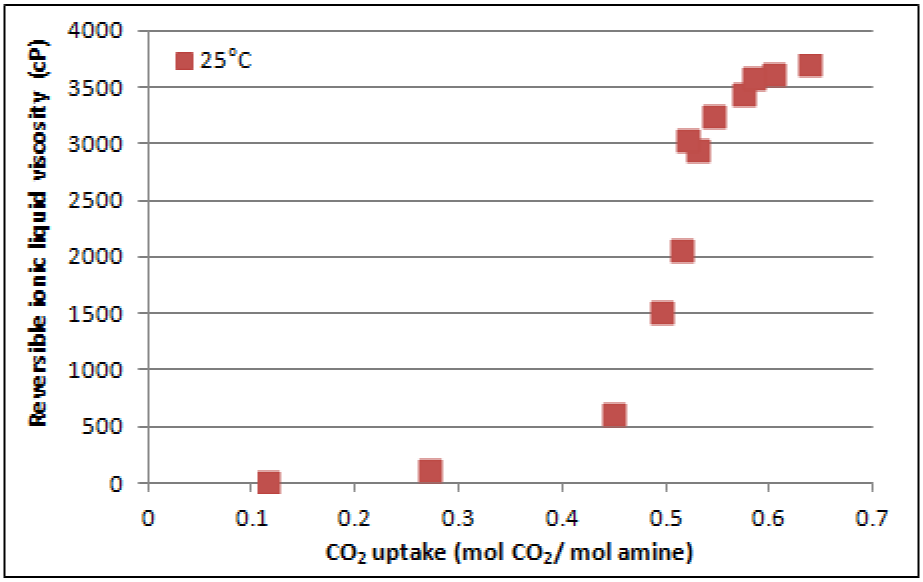

Figure 2.37 - Reversible ionic liquid viscosity of TPSA at 25°C as a function of CO_2 uptake

A plot of viscosity versus CO_2 uptake was also taken at 40°C for TPSA (Figure 2.38). What should immediately stand out when compared to the 25°C curve is that at 40°C higher CO_2 uptakes can be achieved at lower viscosities. In example, at 25°C with 0.45 moles of CO_2 per mole of amine, the viscosity of TPSA is 620 cP. When measured at 40°C, a viscosity of 620 cP is not reached until an uptake nearing 0.52 moles of CO_2 per mole of amine. Of note, at a CO_2 uptake of 0.39 moles of CO_2 per mole of amine the viscosity is only 144 cP – a reversible ionic liquid viscosity nearing industrial viability.

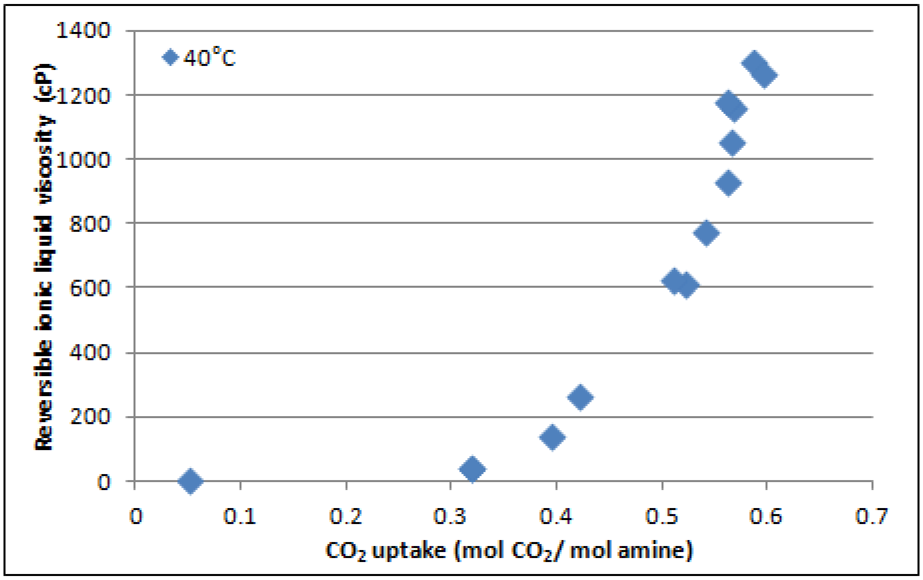

Figure 2.38 – Reversible ionic liquid viscosity of TPSA as a function of CO_2 uptake at 40°C

2.4.1.6 Thermodynamics

The relevant thermodynamic properties of the four reversible ionic liquids are shown in Table 2.7 as determined by DSC. The reversal temperature is defined as the temperature at which CO_2 is released from the reversible ionic liquid to reform the silylamine. As the length of the alkyl chain around the silicon atom increases, the reversal temperature decreases while the silylamine evaporation temperature increases. Thus the largest separation between the two temperatures exists for THSA. It is important that the silylamine evaporation temperature be sufficiently greater than the reversal temperature to avoid evaporation and loss of the silylamine during the reversal step.

Table 2.7 - Thermodynamic properties of DMESA, TEtSA, TPSA, and THSA

Reversible ionic liquid	Reversal temperature (°C)	Silylamine evaporation temperature (°C)	Enthalpy of regeneration (kJ/mol CO_2)
DMESA	80±8	138±17	130±14[a]
TEtSA	71±3	168±12	83±6
TPSA	64±2	180±11	89±3
THSA	51±1	233±1	81±3
[a]Forms solid upon reaction with CO_2, enthalpy is combined melting and reversal, melt temperature: 66±3°C			

The enthalpy of regeneration is also shown in Table 2.7. It is calculated from the DSC thermogram based on the CO_2 uptake of each of the silylamines. TEtSA, TPSA, and THSA all exhibit similar enthalpies of regeneration near 85 kilojoules per mole of CO_2.[2] For reference, the enthalpy of regeneration of a traditional aqueous MEA solvent system is reported as 96 kilojoules per mole of CO_2 (at loadings near 0.5 moles of CO_2 per mole of amine). DMESA has a higher enthalpy of regeneration of 130 kilojoules per mole of CO_2 because it encompasses both melting of the solid formed in the reaction with CO_2 as well as CO_2 release.

2.4.1.7 Structure-property notes

Varying the length of the alkyl chain around the silicon atom in silylamines has a major effect on the viscosity of the reversible ionic liquid formed as well as the temperatures of reversal and silylamine evaporation. By lengthening the alkyl chain, reversible ionic liquid viscosity was decreased by 60% from TEtSA to THSA at 25°C.

The reversal temperature dropped by nearly 30°C over the range of alkyl chains investigated while the evaporation temperature rose by almost 100°C.

Caution must be exercised however in lengthening the alkyl chain around the silicon atom, as the increased molecular weight of THSA negatively affects its CO_2 uptake capacity on a mole of CO_2 captured per kilogram of amine basis under 1 bar of CO_2. Of these four silylamines, TEtSA and TPSA exhibited the most favorable properties. Though their equilibrium viscosities are not industrially viable, an important curve was shown evidencing that usable viscosities can be achieved at operating temperatures by controlling the CO_2 uptake of the silylamine. TEtSA (Figure 2.39) will be used throughout Chapter 2 as a baseline for optimization and a benchmark for comparison.

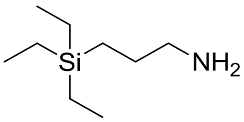

Figure 2.39 - 3-(aminopropyl)triethylsilane

2.4.1.8 Demonstration of recyclability

Reversibility of the ionic liquid formed upon reaction with CO_2 is critical for industrial applicability. To demonstrate the recyclability of the solvent, 3-(aminopropyl) tripropylsilane (TPSA) was used as a model silylamine. The refractive index was measured before CO_2 addition and then after addition of 1 bar of CO_2 for 75 minutes at 25°C. The refractive index of TPSA before CO_2 addition is 1.4540. At its equilibrium CO_2 uptake, the reversible ionic liquid form of TPSA yields a refractive index of 1.4735. Reversal was conducted at 100°C for 90 minutes. The refractive index was measured again after reversal. This process was repeated for five consecutive cycles as shown in Figure 2.40. The study shows that comparable refractive index values are obtained both after CO_2 uptake and reversal. No significant decrease in CO_2 uptake is observed after 5 cycles.

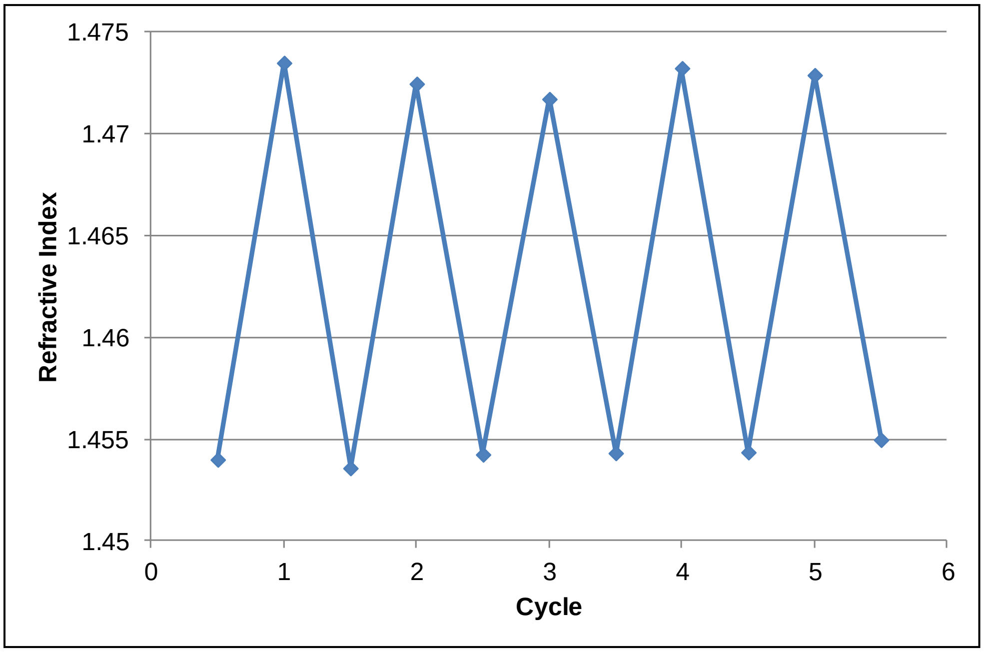

Figure 2.40 - Recyclability of 3-(aminopropyl) tripropylsilane over 5 cycles using refractive index

To further investigate the recyclability of TPSA, the study was also performed using gravimetry. Instead of using refractive index, the normalized weight uptake was recorded after each uptake and reversal cycle. Again, TPSA was reacted with 1 bar of CO_2 for 75 minutes at 25°C. Reversal was conducted by heating the ionic liquid at 100°C for 90 minutes. The results are shown in Figure 2.41. A slight mass loss is observed over the cycling, as the normalized mass begins to fall below its initial starting point and a slight decrease in overall CO_2 uptake is observed. This can be attributed to a) incomplete reversal during heating or b) evaporation of the silylamine during reversal. A ^{1}H NMR spectrum was recorded after the study; no degradation of the silylamine was evident.

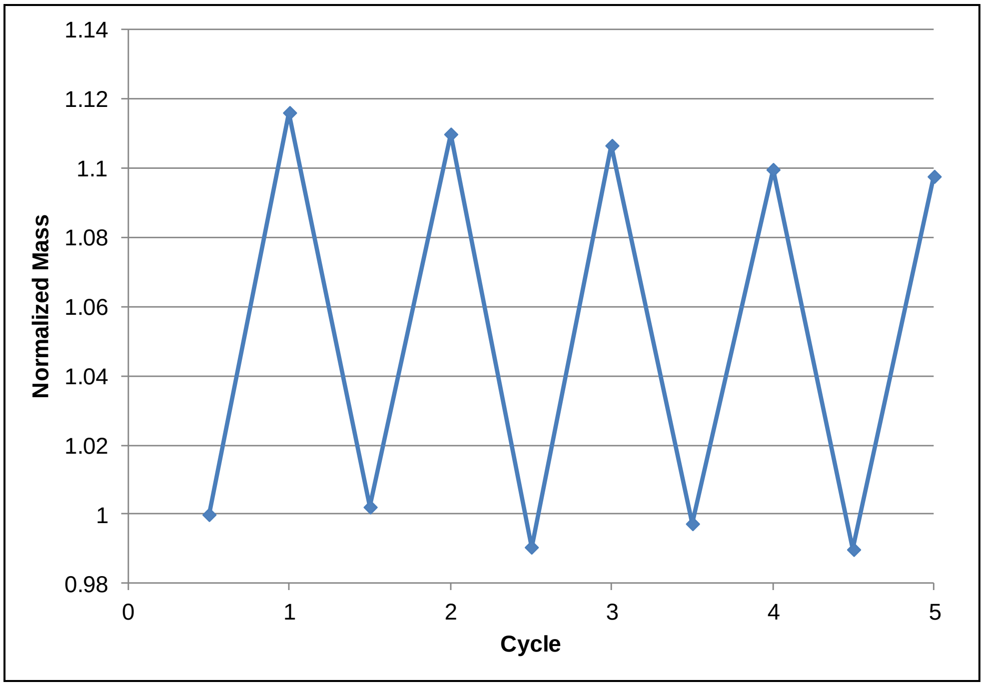

Figure 2.41 - Recyclability of 3-(aminopropyl) tripropylsilane over 5 cycles using gravimetry

While ^{1}H NMR conducted is not representative of an exhaustive degradation study, it is significant that no breakdown of the silylamine was observed. The conventional aqueous amine, monoethanolamine, is subject to both thermal and oxidative degradation – largely as a result of the proximity of the alcohol and amine functional groups.[6,37] As silylamines do not have a comparative alcohol group, we expect degradation effects to be mitigated.

2.4.2 Varying the silicon atom – amine proximity

Silicon was incorporated into the reversible ionic liquid as it proved beneficial in maintaining an ionic liquid rather than forming a solid salt after reaction with CO_2 for the amines studied. While a direct carbon amine analog (silicon-free) to the silylamines investigated is not available due to the difficulty of synthesis, we were able to determine the effect of the proximity of the silicon atom to the reactive amine on its reversible ionic liquid properties, most importantly viscosity. The distance between the silicon atom and the amine was varied to include a methylene linker (TEtSMA), ethylene linker (TEtSEtA), propylene linker (TPSA), and a butylene linker (TEtSBA).

2.4.2.1 CO_2 uptake

The equilibrium CO_2 uptake at 25°C under 1 bar of CO_2 for TEtSMA, TEtSEtA, TEtSA, and TEtSBA is shown in Figure 2.42. The first three silylamines exhibit similar CO_2 uptake capacities, while the last – TEtSBA – shows a significantly lower CO_2 capacity of 0.35 moles of CO_2 per mole of amine. This is likely due to mass transfer limitations in reaching the complete equilibrium; TEtSBA forms a solid immediately upon reaction with CO_2.

While the TEtSMA, TEtSEtA, and TEtSA all share similar CO_2 capacities on a moles of CO_2 per mole of amine basis, it is worthwhile to note the difference in molecular weights. In a mole of CO_2 per kilogram of amine solvent, TEtSMA exhibits a 12% increase in efficiency (4.09 moles of CO_2 per kilogram of amine) over TEtSA (3.66 moles of CO_2 per kilogram of amine). This highlights the importance molecular weights and hence design can have on the overall efficiency of a given CO_2 capture solvent.

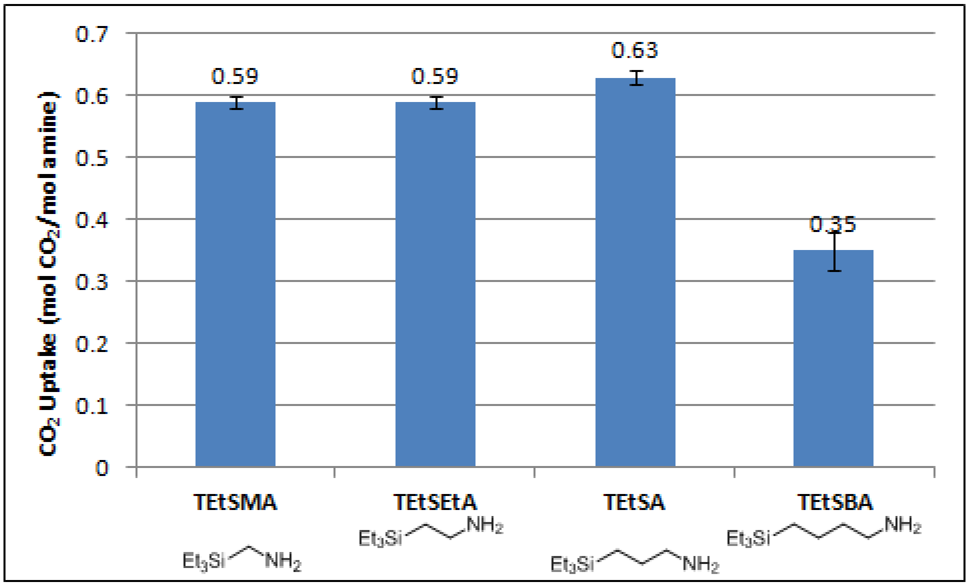

Figure 2.42 - Equilibrium CO2 uptake for TEtSMA, TEtSEtA, TEtSA, and TEtSBA at 25°C under 1 bar CO_2

2.4.2.2 Reversible ionic liquid viscosity

The viscosity of the reversible ionic liquid formed after the reaction of CO_2 with the corresponding silylamine for TEtSMA, TEtSEtA, TEtSA, and TEtSBA at 25 and 40°C is shown in Figure 2.43. Both TEtSEtA and TEtSBA form solids upon reaction with CO_2, while TEtSMA and TEtSA remain reversible ionic liquids. It was expected that the viscosity of the TEtSEtA would fall between that of TEtSMA and TEtSA; however, after continued exposure to CO_2, the reversible ionic liquid forms a solid. Excluding this anomaly (TEtSEtA) the others follow a clear trend; as the alkyl distance between the silicon atom and the amine is increased, viscosity increases drastically in the order of TEtSMA << TEtSA << TEtSBA. An approximate 75% reduction in viscosity is seen at 40°C compared to 25°C for TEtSMA and TEtSA as well.

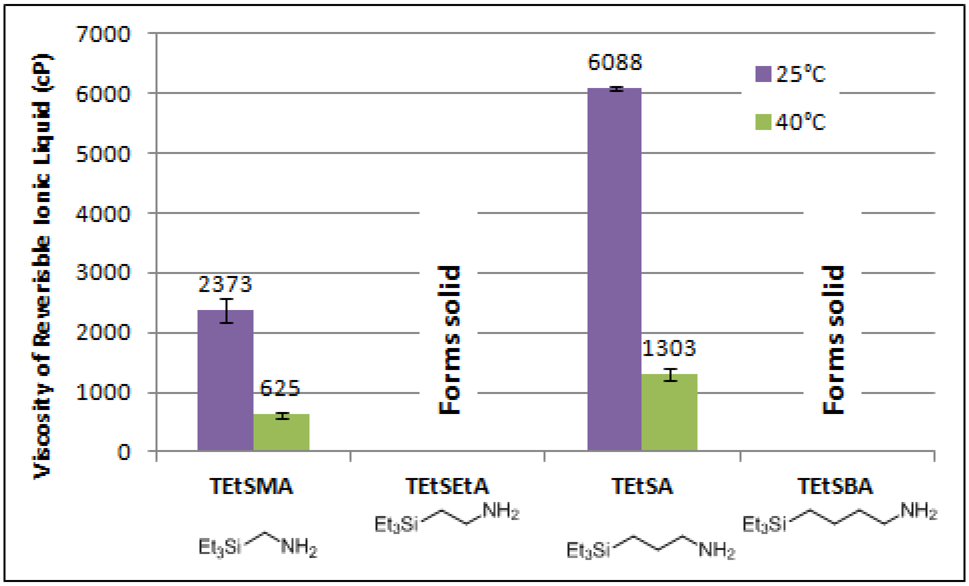

Figure 2.43 - Reversible ionic liquid viscosity for TEtSMA, TEtSEtA, TEtSA, and TEtSBA at 25 and 40°C

2.4.2.3 Thermodynamics

Table 2.8 lists the thermodynamic properties of TEtSMA, TEtSEtA, and TEtSBA. Both TEtSMA and TEtSBA form solids upon reaction with CO_2 – though it was noted that solid formation occurs much quicker in the case of TEtSBA. Excluding TEtSEtA the reversal temperature of these reversible ionic liquids were within 10°C at of each other at 78°C on average while the silylamine evaporation temperature varied between 150 and 213°C. TEtSMA exhibited a similar enthalpy of regeneration to that of TEtSA, near 80 kilojoules per mole of CO_2. This enthalpy is on par with the enthalpies reported in the prior section. The primary contributor to the enthalpy of regeneration is the reversal of the carbamate formation. Since all of the silylamines presented thus far are primary amines, a similar enthalpy for the reaction is expected.

Table 2.8 – Thermodynamic properties of TEtSMA, TEtSEtA, TEtSA, and TEtSBA

Reversible ionic liquid	Reversal temperature (°C)	Silylamine evaporation temperature (°C)	Enthalpy of regeneration (kJ/mol CO$_2$)
TEtSMA	78±5	150±18	76±7
TEtSEtA	109±3	213±14	91±16[a]
TEtSA	71±3	168±12	83±6
TEtSBA	84±4	197±23	152±19[b]
[a]Forms solid upon reaction with CO$_2$, enthalpy is combined melting and reversal, melt temperature: 50±0°C [b]Forms solid upon reaction with CO$_2$, enthalpy includes melting, melt temperature: 66±4°C			

2.4.2.4 Structure-property notes

The effect of varying the length of the alkyl chain between the silicon atom and the amine has a significant effect on viscosity. As the silicon atom is placed closer to the reactive amine, viscosity decreases. When a butyl linker is used in the case of TEtSBA, a solid is formed upon reaction with CO$_2$. However, when only a methylene linker is used the reversible ionic liquid viscosity is on the order of 2,000 cP at 25°C under 1 bar of CO$_2$. The silylamine with an ethylene linker, TEtSEtA is the exception to this trend. It remains unclear as to why it does not follow the others. CO$_2$ capture capacities and the thermodynamic valuables were comparable to the other silylamines examined, except for those which formed solids.

2.4.3 Effect of branching in trialkyl silylpropylamines

Sartori and Savage proposed in 1983 that steric hindrance and basicity control CO$_2$-amine reactions.[38] It has been shown that placement of a bulky substituent next to the amino group lowers the stability of the carbamate formed in comparison of monoethanolamine to 2-amino-2methyl-1-propanol as shown in Figure 2.44.[39]

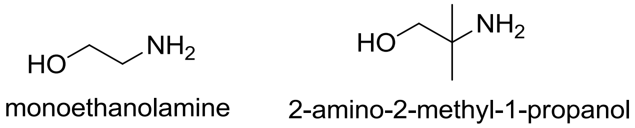

Figure 2.44 - Structures of monoethanol amine and 2-amino-2-methyl-1-propanol

By analogy, we proposed to investigate similar modifications with our silylamines to see the effect of branching on CO_2 uptake as well as the other reversible ionic liquid properties of interest.

2.4.3.1 Theoretical calculations

To begin the study on the effect of branching in trialkyl silylpropylamines, we first did a molecular modeling study to identify what effect branching near the amine site would have on the nitrogen exposed area and the nitrogen atomic charge. The area and atomic charge were calculated on the optimized geometry of the silylamine. Table 2.9 shows the predicted nitrogen exposed area and nitrogen atomic charge for several initially proposed silylamines.

Table 2.9 - Calculated nitrogen exposed area and nitrogen atomic charge for proposed branched silylamines

Branching	Nitrogen exposed area (Å^2)	Nitrogen atomic charge (Mulliken charge)	Synthesized silylamine
TEtSA (base)	8.277	-0.716	TEtSA
α-methyl	7.924	-0.721	αMe-TEtSA
α-dimethyl	7.729	-0.713	α,αDMe-TEtSA
α,β-methyl	7.452	-0.710	--
α-ethyl	8.110	-0.716	--
β-methyl	7.866	-0.717	βMe-TEtSA
β-dimethyl	7.720	-0.721	--
β-ethyl	7.013	-0.714	--

A clear trend can be seen in the effect of branching at the α position with respect to the amine in terms of the nitrogen exposed area. As branching increase (α-methyl to α-dimethyl) the exposed nitrogen area clearly decreases. In the case of an α-ethyl branch, an increase in the exposed nitrogen area is seen relative to the others; this is likely due to the increased distance of the methyl protons from the amine site. Branching on the β carbon has a milder effect than branching at the α carbon, except in the case of β-ethyl where a large decrease in the nitrogen exposed area is seen. This is likely due to the proximity of the methyl hydrogens to the amine in its lowest energy conformation.

The nitrogen atomic charge shows only mild variance in branching with methyl or ethyl groups. Methyl and ethyl alkyl groups are not strong electron withdrawing or donating substituents, thus significant changes in the nitrogen atomic charge as a result of their addition are not expected.

From the initial modeling results, three branched silylamines were synthesized: αMe-TEtSA, α,αDMe-TEtSA, and βMe-TEtSA. Their CO_2 uptake and reversible ionic liquids properties are presented below in comparison to the unbranched baseline silylamine TEtSA.

2.4.3.2 CO_2 uptake

The CO_2 uptake results are shown in Figure 2.45. Both αMe-TEtSA and βMe-TEtSA exhibit equilibrium CO_2 capacities at 25°C under 1 bar of CO_2 similar to that of TEtSA (0.63, 0.59, and 0.63 moles of CO_2 per mole of amine, respectively). The silylamine α,αDMe-TEtSA however exhibits a considerably lower CO_2 capacity of only 0.46 moles of CO_2 per mole of amine. This reduced capacity is a direct result of the steric hindrance around the amine. The steric hindrance destabilizes the carbamate formed upon reaction with CO_2, shifting the reaction equilibrium.

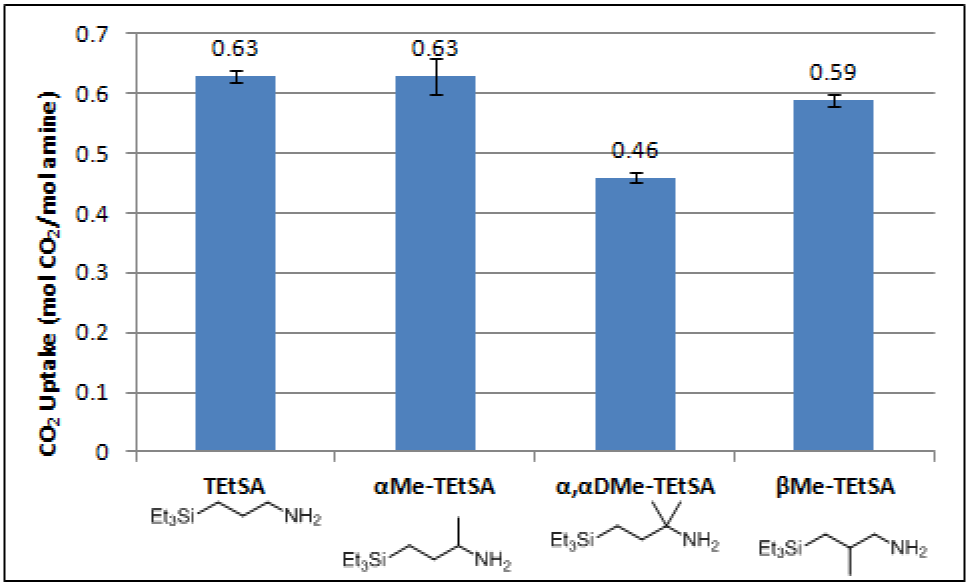

Figure 2.45 - Equilibrium CO_2 uptake values for TEtSA, αMe-TEtSA, α,αDMe-TEtSA, and βMe-TEtSA at 25°C under 1 bar of CO_2

2.4.3.3 CO_2 uptake at 40°C

The CO_2 uptake at 40°C was measured gravimetrically for two of the branched amines - βMe-TEtSA and α,αDMe-TEtSA. At 40°C, βMe-TEtSA exhibits a CO_2 uptake of 0.599±0.003 moles of CO_2 per mole of amine under 1 bar of CO_2. The same CO_2 uptake is observed at 25°C (Figure 2.45). The silylamine α,αDMe-TEtSA also shows the same capacity at 40°C (0.46±0.02) as at 25°C. The results suggest that as long as the reversal temperature of the ionic liquid is sufficiently above 40°C, the equilibrium CO_2 uptake is not significantly affected.

2.4.3.4 Reversible ionic liquid viscosity

The viscosity of the reversible ionic liquid forms of the branched amines, measured at both 25 and 40°C are shown in Figure 2.46. As seen with the CO_2 uptake capacities, αMe-TEtSA and βMe-TEtSA exhibit comparable reversible ionic liquid viscosities to TEtSA whereas α,αDMe-TEtSA has a much lower viscosity. The lower viscosity of α,αDMe-TEtSA is attributed to incomplete conversion to the reversible ionic liquid form as explained in the previous section on CO_2 uptake.

As seen with TEtSA, at 40°C an 80% decrease in viscosity is seen for βMe-TEtSA, while for αMe-TEtSA and α,αDMe-TEtSA an even greater 90% decrease is observed.

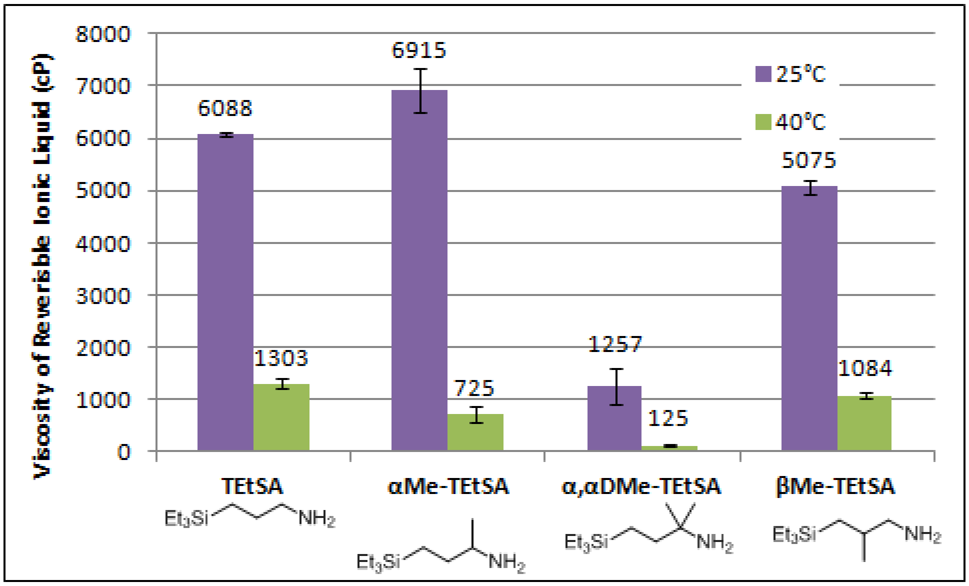

Figure 2.46 - Reversible ionic liquid viscosity of TEtSA, αMe-TEtSA, α,αDMe-TEtSA, and βMe-TEtSA at 25 and 40°C

2.4.3.5 Viscosity versus CO_2 uptake of a branched trialkyl silylpropylamine

The effect of CO_2 uptake on viscosity was also investigated for the branched silylamine α,αDMe-TEtSA (Figure 2.47). While α,αDMe-TEtSA does not reach the same equilibrium uptake as TPSA, the shape of the curve in Figure 2.47 is very similar to that of the same curve presented for TPSA previously in Figure 2.37. The methyl branching of the α,αDMe-TEtSA silylamine affects only the end point of the curve; although the equilibrium CO_2 uptake is lower, the viscosity exhibits similar behavior to that of TPSA prior to the end point. At high CO_2 uptake values, α,αDMe-TEtSA deviates slightly with a sharper rise in viscosity. For example, at 0.45 moles of CO_2 per mole of amine, the viscosity of α,αDMe-TEtSA is nearly 1,500 cP while TPSA does not reach a similar viscosity until 0.50 moles of CO_2 per mole of amine.

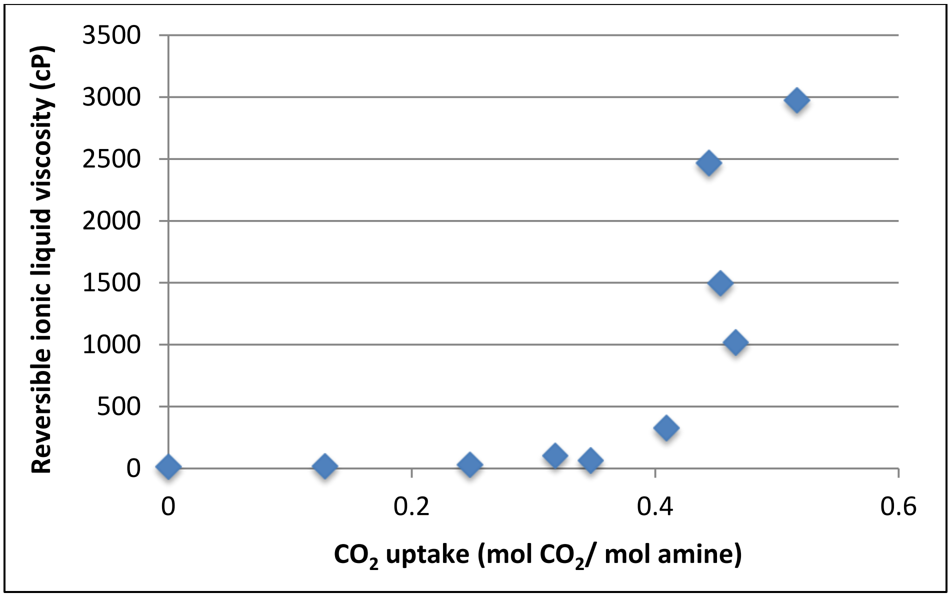

Figure 2.47 – Reversible ionic liquid viscosity as a function of CO_2 uptake for α,αDMe-TEtSA at 25°C under 1 bar of CO_2

2.4.3.6 Thermodynamics

Table 2.10 lists the thermodynamic properties for αMe-TEtSA, α,αDMe-TEtSA, and βMe-TEtSA. Branching of the propyl chain backbone on average reduces the reversal temperature by 20°C. The silylamine evaporation temperature is nearly the same between TEtSA, αMe-TEtSA, and α,αDMe-TEtSA but decreases by nearly 30°C in the case of βMe-TEtSA.

The branched amines have comparable enthalpies of regeneration to that of TEtSA with the exception of α,αDMe-TEtSA. At first glance, this enthalpy is higher than expected. The increased steric hindrance at the reactive amine site should destabilize the carbamate formed, thus lowering the enthalpy. This is indeed the case. The enthalpy presented is calculated with respect to the CO_2 uptake observed. Because a lower CO_2 uptake is observed (0.46 moles of CO_2 per mole of amine) than the other reversible ionic liquids, the calculated enthalpy of regeneration appears higher.

Table 2.10 – Thermodynamic properties of TEtSA, αMe-TEtSA, α,αDMe-TEtSA, and βMe-TEtSA

Reversible ionic liquid	Reversal temperature (°C)	Silylamine evaporation temperature (°C)	Enthalpy of regeneration (kJ/mol CO_2)
TEtSA	71±3	168±12	83±6
αMe-TEtSA	56±5	164±20	90±5
α,αDMe-TEtSA	41±6	171±7	114±16
βMe-TEtSA	57±7	130±3	89±8

2.4.3.7 Structure-property notes

Adding a methyl branch to the α or β carbon relative to the amine has a minor effect on the CO_2 uptake observed at 25°C. In the case of the β methyl branch (βMe-TEtSA), viscosity of the reversible ionic liquid is reduced by 1,000 cP at 25°C. While the enthalpy of regeneration is not affected for a single methyl branch, the reversal temperature is lowered by approximately 20°C (71°C for TEtSA, 56 and 57°C for αMe-TEtSA and βMe-TEtSA respectively).

Addition of two methyl groups to the α carbon relative to the amine negatively affects CO_2 uptake at 25°C. CO_2 uptake is reduced by approximately 25%. The reversible ionic liquid viscosity drops significantly, though it is likely a result of the incomplete conversion of the silylamine to the reversible ionic liquid. Further the reversal temperature drops by 30°C compared to only 20°C in the case of the branched amines with only a single methyl branch (αMe-TEtSA and βMe-TEtSA).

2.4.4 Unsaturation in the backbone of trialkyl silylpropylamines

The effect of unsaturation in the silylamine propyl backbone was investigated for *trans*-TEtSA, *trans*-α,αDMe-TEtSA, and *trans*-α,αDMe-TPSA. It was hypothesized that a locked *trans* conformation could help lower the reversible ionic liquid by increasing the room for movement in reversible ionic liquid network.

2.4.4.1 CO_2 uptake

The CO_2 uptake for *trans*-TEtSA, *trans*-α,αDMe-TEtSA, and *trans*-α,αDMe-TPSA is shown in Figure 2.48. *Trans*-TEtSA exhibits a similar CO_2 uptake as its saturated analogue (TEtSA, 0.63). The same is true for the CO_2 uptake of *trans*-α,αDMe-TEtSA (0.47) vs. α,αDMe-TEtSA (0.46). When branching, propyl chains around the silicon atom, and unsaturation are combined as shown for *trans*-α,αDMe-TPSA, the CO_2 capacity drops to 0.40 moles of CO_2 per mole of amine. The decreased equilibrium CO_2 uptake of the branched silylamines is a result of the steric hindrance around the reactive amine site, as explained for α,αDMe-TEtSA.

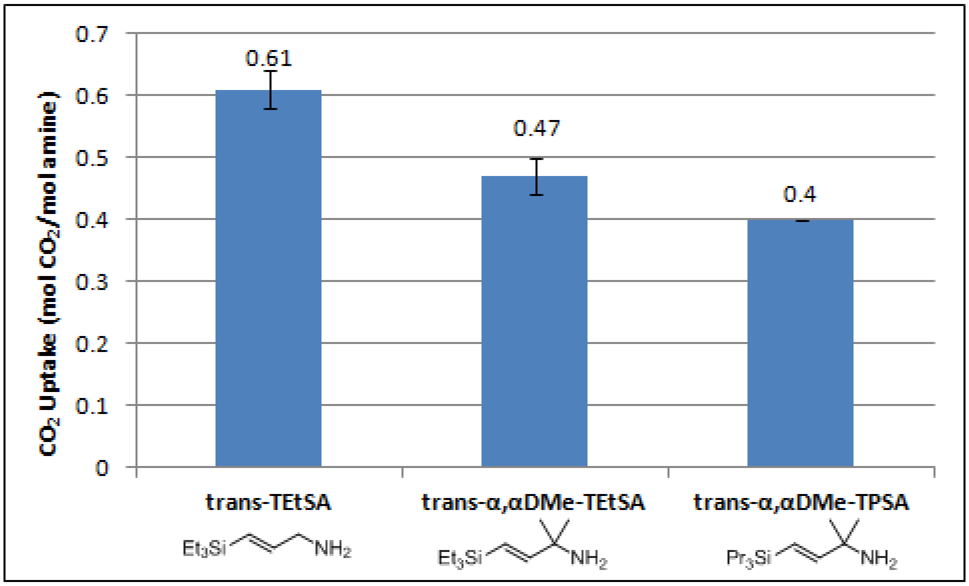

Figure 2.48 - Equilibrium CO_2 uptake for *trans*-TEtSA, *trans*- α,αDMe-TEtSA, and *trans*- α,αDMe-TPSA at 25°C under 1 bar of CO_2

2.4.4.2 Reversible ionic liquid viscosity

The reversible ionic liquid viscosity of the three unsaturated silylamines is shown in Figure 2.49. Unsaturation in the alkyl chain backbone has a profound effect on the reversible ionic liquid viscosity. *Trans*-TEtSA has a reversible ionic liquid viscosity nearly 50% less than its saturated TEtSA analogue. This drastic viscosity decrease is attributed to the locked conformation the *trans* species. The locked conformation should decrease the "packing" ability of the ionic species relative to each other and thereby reduce the overall viscosity of the reversible ionic liquid system.

Both the branched unsaturated amines exhibit viscosities too low to measure on our viscometer (limited to samples above 100 cP). As will be discussed, both *trans*-α,αDMe-TEtSA, and *trans*-α,αDMe-TPSA have low reversal temperatures, so the viscosity reported cannot be taken without qualification that significant reversal and release of the CO_2 absorbed likely occurred during testing.

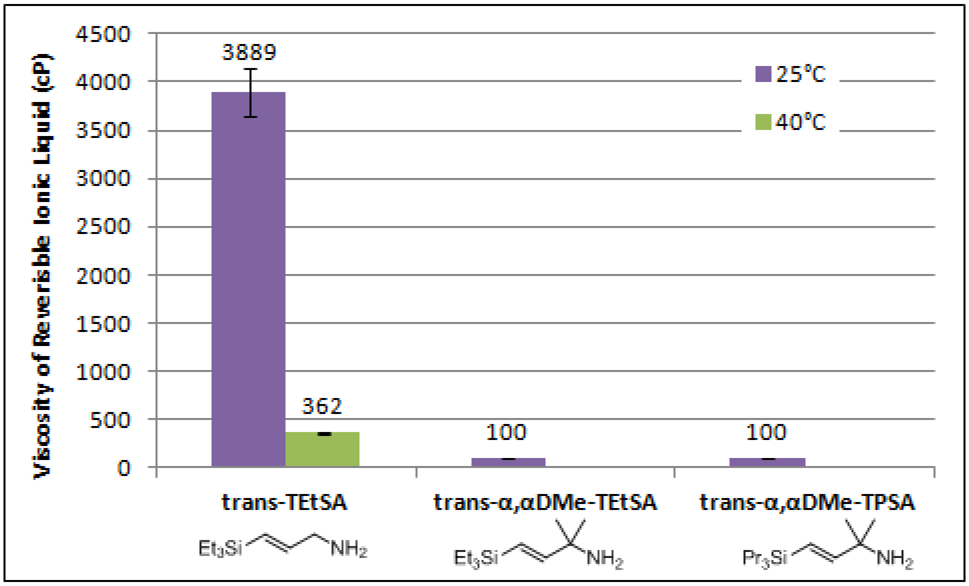

Figure 2.49 - Reversible ionic liquid viscosity of *trans*-TEtSA, *trans*- α,αDMe-TEtSA, and *trans*- α,αDMe-TPSA at 25 and 40°C

2.4.4.3 Thermodynamics

The thermodynamic properties of the unsaturated silylamines compared to the saturated silylamine TEtSA are shown in Table 2.11. Compared to TEtSA, *trans*-TEtSA has a reversal temperature that is 20°C less; the same is true for the silylamine evaporation temperature, while the enthalpy of regeneration remains the same.

Both *trans*-α,αDMe-TEtSA and *trans*-α,αDMe-TPSA have reversal temperatures less than room temperature. However, the bottom of the reversal curve event in the DSC thermogram is closer to 30-40°C for both. This explains the decreased CO_2 capacity observed. Further, the low reversal temperatures suggest that the low viscosities observed for *trans*-α,αDMe-TEtSA and *trans*-α,αDMe-TPSA are likely the result of incomplete conversion to the reversible ionic liquid. The enthalpy of regeneration for both is also much less than that observed for the other silylamines studied (10-20 kilojoules per mole of CO_2 compared to 80-90 kilojoules per mole of CO_2 respectively).

Table 2.11 – Thermodynamic properties of *trans*-TEtSA, *trans*- α,αDMe-TEtSA, and *trans*- α,αDMe-TPSA

Reversible ionic liquid	Reversal temperature (°C)	Silylamine evaporation temperature (°C)	Enthalpy of regeneration (kJ/mol CO_2)
TEtSA	71±3	168±12	83±6
trans-TEtSA	48±1	144±4	85±7
trans-α,αDMe-TEtSA	11±0[a]	140±0	8±0
trans-α,αDMe-TPSA	15±2[b]	206±11	21±6
[a]Bottom of reversal curve at 30°C [b]Bottom of reversal curve at 40°C			

2.4.4.4 Structure-property notes

Unsaturation by itself does not negatively affect CO_2 capacity. Both TEtSA and *trans*-α,αDMe-TEtSA achieve similar CO_2 uptake values (0.61, 0.47) compared to their saturated analogues (TEtSA, 0.63; α,αDMe-TEtSA, 0.46). Unsaturation does however affect significantly both the reversible ionic liquid viscosity as well as the thermodynamic properties. The viscosity of *trans*-TEtSA is reduced by nearly 40% compared to TEtSA. Further the reversal temperature of *trans*-TEtSA is lowered by 20°C. The di-methyl branched silylamines show the lowest reversal temperatures and enthalpies of regeneration observed out of all of the silylamines studied. Though not viable, they show the drastic effect of combining silylamine structural modifications on the reversible ionic liquid properties.

2.4.5 Varying the amine order from primary to secondary

N-methylated secondary amines were investigated for TEtSA and DMESA (to give STEtSA and SDMESA). Several authors have investigated secondary amines similar in structure to monoethanolamine.[40,41] They showed that if only a short alkyl substituent is used on the secondary amine, CO_2 uptake does not decrease drastically. Further, they evidenced only mildly reduced rates of reaction.[40] We hypothesized that while basicity is expected to increase in the case of secondary amines likely leaving CO_2 uptake unaffected, reversal temperature and enthalpy of regeneration could be lowered as a result of the steric hindrance at the amine.

2.4.5.1 CO_2 uptake

The equilibrium CO_2 uptake at 25°C under 1 bar of CO_2 of the two secondary silylamines investigated is reported in Figure 2.50. Both of the secondary amines exhibit CO_2 capacities similar to that of TEtSA. Though the reactive amine is secondary, the position of the equilibrium in the reaction with CO_2 is apparently not affected. As reported by Sartori and Savage, secondary amines still maintain exceptional reactivity towards CO_2; only the kinetics of the reaction are slightly affected.[40]

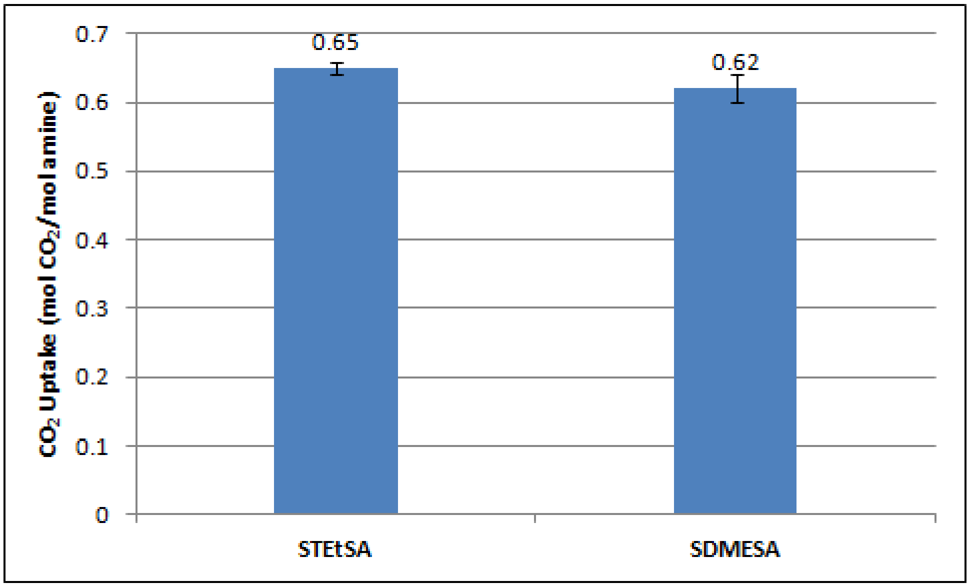

Figure 2.50 - Equilibrium CO_2 uptake of STEtSA and SDMESA at 25°C under 1 bar of CO_2

2.4.5.2 Reversible ionic liquid viscosity

The viscosity of the secondary silylamines is significantly less than the primary silylamines (Figure 2.51). Whereas TEtSA has a viscosity of 6,088 cP at 25°C, STEtSA has a viscosity of 135 cP – an industrially viable level. Further, while DMESA forms a solid at 25°C after reaction with CO_2, the reversible ionic liquid of SDMESA has a viscosity of only 117 cP. We hypothesize that these low viscosities are due to the decrease in ionic strength of the reversible ionic liquid. Because the nucleophilicity of the nitrogen is slightly reduced, it can be expected that the ionic salts in the reversible ionic liquid may not be held as tightly together. As such, more freedom of movement and lower viscosities could be expected.

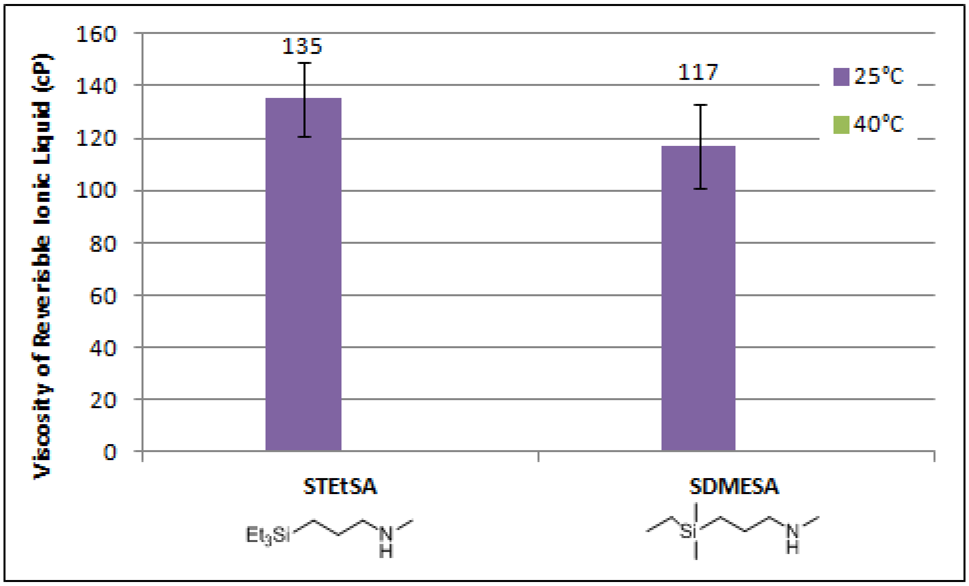

Figure 2.51 - Reversible ionic liquid viscosity of STEtSA and SDMESA at 25°C; 40

2.4.5.3 Thermodynamics

Both STEtSA and SDMESA have significantly reduced reversal temperatures (40°C decrease) compared to TEtSA as shown in Table 2.12. The low reversal temperatures are a concern when examining CO_2 capture properties at the standard operating temperature of 40°C. STEtSA was prepared initially; its low reversal temperature led to the synthesis of SDMESA. An increase in the reversal temperature is observed, as was similarly seen when examining TEtSA vs. DMESA. A decline of 10 kilojoules per mole of CO_2 is seen in the enthalpy of regeneration for both of the secondary silylamines when compared to TEtSA. This reduction would translate into a significant reduction in the amount of energy required during the regeneration stage.

Table 2.12 - Thermodynamic properties of TEtSA, STEtSA, and DMESA

Reversible ionic liquid	Reversal temperature (°C)	Silylamine evaporation temperature (°C)	Enthalpy of regeneration (kJ/mol CO_2)
TEtSA	71±3	168±12	83±6
STEtSA	30±3	155±6	77±6
DMESA	37±2	139±16	76±2

2.4.5.4 Structure-property notes

Adding a methyl group to the reactive amine functionality to form a secondary silylamine does not adversely affect the equilibrium CO_2 capacity at 25°C. The reversible ionic liquid viscosities exhibit an enormous drop compared to their primary silylamine analogues. At 25°C the secondary silylamines have industrially viable viscosities. While the low reversal temperatures would prevent use at 40°C, our work suggests further structural modification could aid in raising the reversal temperature to a desired value. Secondary silylamines also have a depressed enthalpy of regeneration relative to their primary analogues, lowering the energy required for regeneration.

2.5 Conclusions

A systematic process for designing CO_2 capture solvents that achieve a high CO_2 uptake – while minimizing viscosity and the energy required for reversal – has been presented. The influence of the silicon-amine proximity as well as adding or changing the position of one or more methyl groups in the silylamine structure has a significant effect on the pertinent CO_2 capture properties of the reversible ionic liquids. 3-(aminopropyl)triethylsilane (TEtSA) was used as a baseline silylamine to which structural modifications were made in order to establish structure-property relationships.

2.5.1 Key structure-property relationships

Changing the alkyl chain length of trialkyl silylpropylamines	
Property	*Effect of Structure*
CO_2 uptake	Caution must be exercised in lengthening the alkyl chain around the silicon atom, as the increased molecular weight of THSA negatively affects its CO_2 uptake capacity on a mole of CO_2 captured per kilogram of amine basis under 1 bar of CO_2.
Reversible ionic liquid viscosity	Major effect on the viscosity of the reversible ionic liquid formed. By lengthening the alkyl chain, reversible ionic liquid viscosity was decreased by 60% from TEtSA to THSA at 25°C.
Thermodynamics	The reversal temperature dropped by nearly 30°C over the range of alkyl chains investigated while the evaporation temperature rose by almost 100°C.
Varying the silicon-atom amine proximity	
Property	*Effect of Structure*
CO_2 uptake	With the exclusion of the silylamines that formed solids upon reaction with CO_2, CO_2 uptake at 25°C was not significantly affected.
Reversible ionic liquid viscosity	As the silicon atom is placed closer to the reactive amine, viscosity decreases. When a butyl linker is used in the case of TEtSBA, a solid is formed upon reaction with CO_2. However, when only a methylene linker is used the reversible ionic liquid viscosity is on the order of 2,000 cP at 25°C under 1 bar of CO_2.
Thermodynamics	With the exclusion of the silylamines that formed solids upon reaction with CO_2, the reversible ionic

	liquid thermodynamic properties were not significantly affected.
Effect of branching in trialkyl silylpropylamines	
CO_2 uptake	Adding a methyl branch to the α or β carbon relative to the amine has a minor effect on the CO_2 uptake observed at 25°C. Addition of two methyl groups to the α carbon relative to the amine negatively affects CO_2 uptake at 25°C. CO_2 uptake is reduced by approximately 25%.
Reversible ionic liquid viscosity	A single methyl branch does not have a significant effect on the reversible ionic liquid viscosity. The lowered viscosity of α,αDMe-TEtSA is likely the result of incomplete conversion to the reversible ionic liquid.
Thermodynamics	It is apparent the branching lowers the reversal temperature of the ionic liquid (20-30°C).
Unsaturation in the backbone of trialkyl silylpropylamines	
CO_2 uptake	Unsaturation by itself does not negatively affect CO_2 capacity.
Reversible ionic liquid viscosity	Unsaturation causes a significant decrease in the reversible ionic liquid viscosity. The viscosity of *trans*-TEtSA is reduced by nearly 40% compared to TEtSA.
Thermodynamics	It is apparent that unsaturation causes a decrease in the reversal temperature of the ionic liquid. The reversal temperature of *trans*-TEtSA is lowered by 20°C compared to TEtSA.
Varying the amine order from primary to secondary	
CO_2 uptake	Adding a methyl group to the reactive amine functionality to form a secondary silylamine does not adversely affect the equilibrium CO_2 capacity at 25°C.
Reversible ionic liquid viscosity	The reversible ionic liquid viscosities exhibit an enormous drop compared to their primary silylamine analogues. At 25°C the secondary silylamines have industrially viable viscosities.
Thermodynamics	While the low reversal temperatures would prevent use at 40°C, our work suggests further structural modification could aid in raising the reversal temperature to a desired value. Secondary silylamines also have a depressed enthalpy of regeneration relative to their primary analogues, lowering the energy required for regeneration.

2.5.2 Recommended silylamines for CO_2 capture

While selection of a particular CO_2 capture solvent is dependent on the specifications of its end use application, we have identified two silylamine solvents to recommend for further investigation – TEtSMA and *trans*-TEtSA. Their properties are summarized in Table 2.13. They both exhibit high CO_2 uptake capacities relative to the other silylamines studied, viable reversible temperatures, and reasonable enthalpies of regeneration. Their reversible ionic liquids have lower viscosities than most other silylamine reversible ionic liquids, and further, by controlling the CO_2 uptake, viscosity could be reduced to meet industry-operating specifications.

Table 2.13 - Summary of the properties of TEtSMA and *trans*-TEtSA

Summary of the properties of TEtSMA and *trans*-TEtSA		
Property	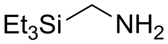 TEtSMA	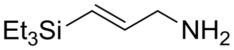 *trans*-TEtSA
CO_2 uptake (mol CO_2/mol amine, 25°C)	0.59±0.01	0.61±0.03
CO_2 uptake (mol CO_2/kg amine, 25°C)	4.09±0.08	3.56±0.20
Reversal temperature (°C)	78±5	48±2
Enthalpy of regeneration (°C)	76±7	85±7
Reversible ionic liquid viscosity at 25°C (cP)	2373±206	3889±252
Reversible ionic liquid viscosity at 40°C (cP)	625±58	362±19

2.5.3 Initial process scale-up simulation

As an initial step towards considering the CO_2 capture process as a whole, we used Aspen HYSYS to model 3-(aminopropyl)tripropylsilane (TPSA) as an example silylamine. TPSA and its reversible ionic liquid were modeled as hypotheticals and the E-NRTL package was used. A flow diagram of the process is shown in Figure 2.52. For the initial simulation, water was removed from the flue gas before entering the absorber. Further studies would need to include water to obtain a more realistic simulation.

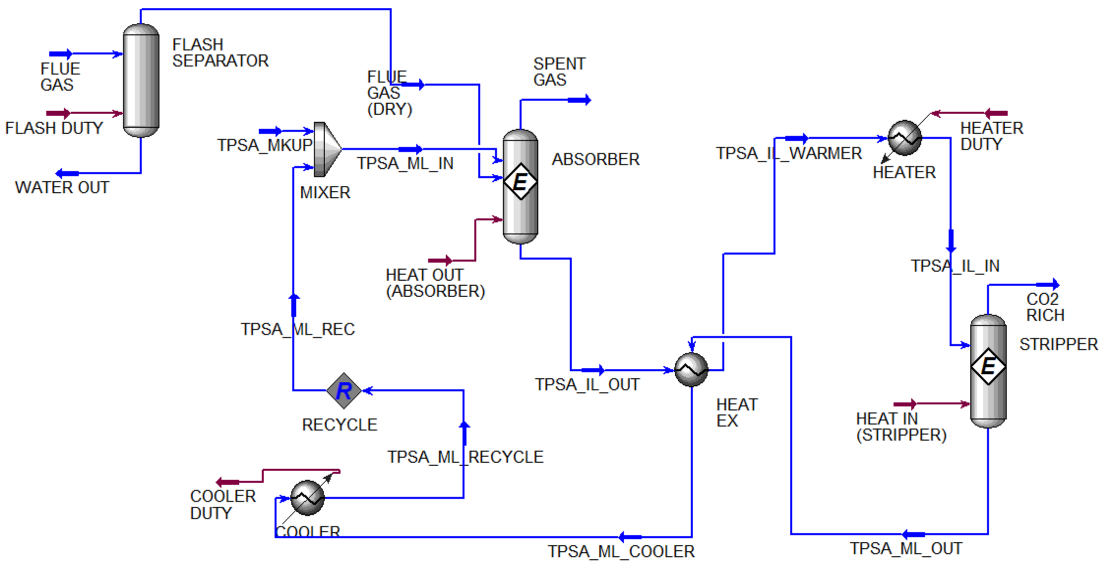

Figure 2.52 – Aspen HYSYS flow diagram of CO_2 capture process modeled

The composition of the flue gas is given below in Table 2.14. The flue gas leaving the flue gas desulfurization unit and entering the CO_2 capture process was modeled at a flow rate of 5,118,399 pounds per hour (based on a 550 MW net pulverized coal power plant). The flue gas was modeled at a pressure of 14.7 psia and a temperature of 135°F.

Table 2.14 - Modeled flue gas composition (wet basis)

Component	Volume %
CO_2	13.17
H_2O	17.25
N_2	66.44
O_2	2.34
Ar	0.80
SO_x	43 ppm
NO_x	74 ppm

The process starts with the dry flue gas entering the bottom of the absorber. An equilibrium reactor is used for modeling the absorber. This allows us to use the equilibrium constant data found using FTIR measurements and COSMO-RS calculations.[42] The unit is operated at 40°C. The CO_2 lean solvent (TPSA) enters the top of the absorber and reacts with the CO_2 available in the dry flue gas. In the absence of water there is no formation of bicarbonates. Enthalpies of formation of the TPSA silylamine and its reversible ionic liquid are automatically adjusted to match the reaction enthalpy of the silylamine-CO_2 reaction. The scrubbed gas primarily containing nitrogen leaves from the top of the absorber while the CO_2-rich reversible ionic liquid exits from the bottom. The composition and the physical conditions of these streams are given in Appendix A.

The CO_2-rich solvent is fed to the stripper via a heat exchanger. As with the absorber, an equilibrium reactor is used for modeling the stripper. Stoichiometry and equilibrium constants of the reverse reaction are entered in the design specifications of the stripper. The stripper is operated at 85°C, which is a temperature above the onset reversal temperature (64°C) found from DSC. A CO_2 stream exits from the top of the stripper while the CO_2-lean silylamine exits from the bottom. The CO_2-lean silylamine is passed through the heat exchanger that simultaneously cools the stream and heats the returning CO_2-rich stream. After cooling, a make-up steam of TPSA molecular liquid is added to the CO_2-lean stream, and re-fed to the absorber to complete the loop.

Details of the operating conditions and the calculation for the amount of energy required for the DOE target of 90% CO_2 captured are given in Appendix A. Our non-aqueous TPSA solvent required 1.39 MJ/kg of CO_2 captured in the simulation. This nearly a third of the 4MJ/kg of CO_2 reported using an aqueous monoethanolamine process.

While the assumptions made limit the utility of the simulation, it does provide a useful starting point for further optimization and development. Future studies would need to incorporate the water present in the flue gas stream and the associated additional unit operations that would be necessary to handle its presence (i.e. possible decantation and separation if water is accumulated in excess).[43] Additionally, the viscosity of the reversible ionic liquid would need to be considered as it would greatly influence the energy required to transfer the CO_2-rich solvent from the absorber to the stripper for regeneration.

2.6 References

(1) Kohl, A. L.; Nielsen, R. *Gas purification*; 5th edition ed.; Gulf Publishing Company: Houston, 1997.

(2) Kim, I.; Svendsen, H. F. *Industrial & Engineering Chemistry Research* **2007**, *46*, 5803.

(3) Anderson, S.; Newell, R. *Annual Review of Environment and Resources* **2004**, *29*, 109Rao, A. B.; Rubin, E. S. *Environmental Science & Technology* **2002**, *36*, 4467Rubin, E. S.; Chen, C.; Rao, A. B. *Energy Policy* **2007**, *35*, 4444.

(4) Davis, J.; Rochelle, G. *Energy Procedia* **2009**, *1*, 327.

(5) Bedell, S. A. *International Journal of Greenhouse Gas Control* **2011**, *5*, 1Bollini, P.; Choi, S.; Drese, J. H.; Jones, C. W. *ENERGY & FUELS* **2011**, *25*, 2416.

(6) Bello, A.; Idem, R. *Industrial & Engineering Chemistry Research* **2005**, *44*, 945.

(7) Sathe, A. A.; Hartline, D., R.; Radosevich, A. T. *ChemComm* **2013**Liu, A.-H.; He, L.-N.; Hua, F.; Yang, Z.-Z.; Huang, C.-B.; Yu, B.; Li, B. *Advanced Synthesis & Catalysis* **2011**, *353*, 3187Godec, M. L.; Kuuskraa, V. A.; Dipietro, P. *Energy & Fuels* **2013**Yang, Z.-Z.; Zhao, Y.-N.; He, L.-N.; Gao, J.; Yin, Z.-S. *Green Chemistry* **2012**, *14*, 519Mikkelsen, M.; Jørgensen, M.; Krebs, F. C. *Energy & Environmental Science*, *3*, 43Liu, A. H.; Li, Y. N.; He, L. N.; Liu, A.-H.; Li, Y.-

N.; He, L.-N. *Pure and Applied Chemistry*, *84*, 581D'Alessandro, D. M.; Smit, B.; Long, J. R. *Angewandte Chemie International Edition* **2010**, *49*, 6058.

(8) McGhee, W.; Riley, D.; Christ, K.; Pan, Y.; Parnas, B. *Journal of Organic Chemistry* **1995**, *60*, 2820.

(9) Freemantle, M. *Chemical and Engineering News London* **2000**, *78*, 37.

(10) Goodrich, B. F.; de la Fuente, J. C.; Gurkan, B. E.; Zadigian, D. J.; Price, E. A.; Huang, Y.; Brennecke, J. F. *Industrial & Engineering Chemistry Research* **2011**, *50*, 111.

(11) Wang, C.; Luo, X.; Luo, H.; Jiang, D.-e.; Li, H.; Dai, S. *Angewandte Chemie International Edition* **2011**, *50*, 4918.

(12) Gurkan, B. E.; de la Fuente, J. C.; Mindrup, E. M.; Ficke, L. E.; Goodrich, B. F.; Price, E. A.; Schneider, W. F.; Brennecke, J. F. *Journal of the American Chemical Society* **2010**, *132*, 2116.

(13) Almantariotis, D.; Gefflaut, T.; Pádua, A. A. H.; Coxam, J. Y.; Costa Gomes, M. F. *The Journal of Physical Chemistry B* **2010**, *114*, 3608.

(14) Shannon, M. S.; Bara, J. E. *Separation Science and Technology* **2012**, *47*, 178.

(15) Jessop, P. G.; Heldebrant, D. J.; Li, X.; Eckert, C. A.; Liotta, C. L. *Nature* **2005**, *436*, 1102Liu, Y. X.; Jessop, P. G.; Cunningham, M.; Eckert, C. A.; Liotta, C. L. *Science* **2006**, *313*, 958Mercer, S. M.; Jessop, P. G. *ChemSusChem* **2010**, *3*, 467Jessop, P. G.; Phan, L.; Carrier, A.; Robinson, S.; Durr, C. J.; Harjani, J. *Green Chemistry* **2010**, *12*, 809Chen, C.-S.; Lau, Y. Y.; Mercer, S. M.; Tobias, R.; Horton, J. H.; Jessop, P. G. *ChemSusChem* **2012**, *6*, 132Robert, T.; Mercer, S. M.; Clark, T. J.; Mariampillai, B. E.; Champagne, P.; Cunningham, M. F.; Jessop, P. G. *Green Chemistry* **2012**, *14*, 3053Xin, B.; Hao, J. *Chemical Society Reviews* **2010**, *39*, 769Su, X.; Cunningham, M. F.; Jessop, P. G. *ChemComm* **2013**, *49*, 2655.

(16) Blasucci, V. M.; Hart, R.; Pollet, P.; Liotta, C. L.; Eckert, C. A. *Fluid Phase Equilibria* **2010**, *294*, 1.

(17) Blasucci, V.; Dilek, C.; Huttenhower, H.; John, E.; Llopis-Mestre, V.; Pollet, P.; Eckert, C. A.; Liotta, C. L. *Chemical Communications* **2009**, 116.

(18) Hart, R.; Pollet, P.; Hahne, D. J.; John, E.; Llopis-Mestre, V.; Blasucci, V.; Huttenhower, H.; Leitner, W.; Eckert, C. A.; Liotta, C. L. *Tetrahedron* **2010**, *66*, 1082.

(19) Blasucci, V.; Hart, R.; Mestre, V. L.; Hahne, D. J.; Burlager, M.; Huttenhower, H.; Thio, B. J. R.; Pollet, P.; Liotta, C. L.; Eckert, C. A. *Fuel* **2010**, *89*, 1315.

(20) Jessop, P. G.; Heldebrant, D. J.; Li, X. W.; Eckert, C. A.; Liotta, C. L. *Nature* **2005**, *436*, 1102.

(21) Rohan, A. L.; Switzer, J. R.; Flack, K. M.; Hart, R. J.; Sivaswamy, S.; Biddinger, E. J.; Talreja, M.; Verma, M.; Faltermeier, S.; Nielsen, P. T.; Pollet, P.; Schuette, G. F.; Eckert, C. A.; Liotta, C. L.

(22) Switzer, J. R.; Ethier, A. L.; Hart, E. C.; Flack, K. M.; Rumple, A. C.; Donaldson, J. C.; Bembry, A. T.; Scott, O. M.; Biddinger, E. J.; Talreja, M.; Song, M.-G.; Pollet, P.; Eckert, C. A.; Liotta, C. L. *ChemSusChem* **2013**.

(23) Kost, D.; Gostevskii, B.; Kalikhman, I. *Pure and Applied Chemistry* **2007**, *79*, 1125.

(24) Shirota, H.; Castner, E. W. *Journal of Physical Chemistry B* **2005**, *109*, 21576.

(25) Voronkov, M. G.; Frolov, Y. L.; D'Yakov, V. M.; Chipanina, N. N.; Gubanova, L. I.; Gavrilova, G. A.; Klyba, L. V.; Aksamentova, T. N. *Journal of Organometallic Chemistry* **1980**, *201*, 165Chuit, C.; Corriu, R. J. P.; Reye, C.; Young, J. C. *Chemical Reviews* **1993**, *94*, 1371.

(26) Perry, R. J.; O'Brien, M. J. *Energy & Fuels* **2011**, *25*, 1906Perry, R. J.; Grocela-Rocha, T. A.; O'Brien, M. J.; Genovese, S.; Wood, B. R.; Lewis, L. N.; Lam, H.; Soloveichik, G.; Rubinsztajn, M.; Kniajanski, S.; Draper, S.; Enick, R. M.; Johnson, J. K.; Xie, H.-b.; Tapriyal, D. *ChemSusChem* **2010**, *3*, 919.

(27) Rohan, A. L.; Switzer, J. R.; Flack, K. M.; Hart, R. J.; Sivaswamy, S.; Biddinger, E. J.; Talreja, M.; Verma, M.; Faltermeier, S.; Nielsen, P. T.; Pollet, P.; Schuette, G. F.; Eckert, C. A.; Liotta, C. L. *ChemSusChem* **2012**, *5*, 2181.

(28) Airgas; Airgas: http://www.airgassgcatalog.com/catalog/; Vol. 2012.

(29) Anthony, J. L.; Maginn, E. J.; Brennecke, J. F. *The Journal of Physical Chemistry B* **2002**, *106*, 7315.

(30) Bondi, A. *Journal of Physical Chemistry* **1964**, *68*, 441.

(31) Poling, B. E. *The properties of gases and liquids*; 5th ed. ed.; McGraw-Hill: New York :, 2001.

(32) Kvamsdal, H. M.; Jakobsen, J. P.; Hoff, K. A. *Chemical Engineering and Processing: Process Intensification* **2009**, *48*, 135Mofarahi, M.; Khojasteh, Y.; Khaledi, H.; Farahnak, A. *Energy* **2008**, *33*, 1311.

(33) Scovazzo, P.; Camper, D.; Kieft, J.; Poshusta, J.; Koval, C.; Noble, R. *Industrial & Engineering Chemistry Research* **2004**, *43*, 6855.

(34) Wright, H. B.; Moore, M. B. *Journal of the American Chemical Society*, *70*, 3865Danckwerts, P. V. *Chemical Engineering Science* **1979**, *34*, 443Caplow, M. *Journal of the American Chemical Society*, *90*, 6795Crooks, J. E.; Donnellan, J. P. *Journal of the Chemical Society, Perkin Transactions 2*, 331Versteeg, G. F.; Van Dijck, L. A. J.; Van Swaaij, W. P. M. *Chemical Engineering Communications* **1996**, *144*, 113.

(35) Switzer, J. R.; Ethier, A. L.; Flack, K. M.; Biddinger, E. J.; Gelbaum, L.; Pollet, P.; Eckert, C., A; Liotta, C. L. *Energy & Environmental Science* **2013**, *submitted*.

(36) Danon, A.; Stair, P. C.; Weitz, E. *The Journal of Physical Chemistry C* **2011**, *115*, 11540Soutullo, M. D.; Odom, C. I.; Wicker, B. F.; Henderson, C. N.; Stenson, A. C.; Davis, J. H. *Chemistry of Materials* **2007**, *19*, 3581Knöfel, C. a. M. C. l. a. H. V. a. L. P. L. *The Journal of Physical Chemistry C* **2009**, *113*, 21726Pinchas, S.; Ishai, B. D. *Journal of the American Chemical Society* **1957**, *79*, 4099Bossa, J.-B.; Borget, F.; Duvernay, F.; Theule, P.; Chiavassa, T. *Journal of Physical Chemistry A* **2008**, *112*, 5113Dijkstra, Z. J.; Doornbos, A. R.; Weyten, H.; Ernsting, J. M.; Elsevier, C. J.; Keurentjes, J. T. F. *The Journal of Supercritical Fluids*, *41*, 109.

(37) Strazisar, B. R.; Anderson, R. R.; White, C. M. *Energy & Fuels* **2003**, *17*, 1034Goff, G. S.; Rochelle, G. T. *Industry and Chemistry Engineering Research* **2004**, *43*, 6400.

(38) Sartori, G.; Savage, D. W. *Industrial & Engineering Chemistry Fundamentals* **1983**, *22*, 239.

(39) Hook, R. J. *Industry & Engineering Chemistry Research* **1997**, *36*, 1779Pei, Z.; Yao, S.; Jianwen, W.; Wei, Z.; Qing, Y. *Journal of Environmental Sciences* **2008**, *20*, 39Park, J.-Y.; Sang, J. Y.; Huen, L. *Environmental Science Technology* **2003**, *37*, 1670.

(40) Sartori, G.; Savage, D. *Industry & Engineering Chemistry Fundamentals* **1983**, *22*, 239.

(41) Hartono, A.; Svendsen, H. *Energy Procedia* **2009**, *1*, 853.

(42) Palomar, J.; Gonzalez-Miquel, M.; Polo, A.; Rodriguez, F. *Industrial & Engineering Chemistry Research* **2011**, *50*, 3452.

(43) Deschamps, J.; Gomes, M. F. C.; Padua, A. A. H. *Chemphyschem* **2004**, *5*, 1049Ficke, L. E.; Brennecke, J. F. *Journal of Physical Chemistry B* **2010**, *114*, 10496Lawal, A.; Wang, M.; Stephenson, P.; Koumpouras, G.; Yeung, H. *Fuel* **2010**, *89*, 2791Matin, N. S.; Remias, J. E.; Neathery, J. K.; Lui, K. *Industrial & Engineering Chemistry Research* **2012**, *51*, 6613.

CHAPTER 3 - CARBON DIOXIDE AS A PROTECTING GROUP IN CHEMICAL SYNTHESES

3.1 Abstract

The goal of this project is to reversibly protect nitrogen functionalities *in-situ* using CO_2. Our studies have focused on exploring the effect of solvent, temperature and the addition of base on the stability of CO_2-protected amines. We have targeted utilization of the CO_2 protection technology in proof-of-concept reactions including a chemoselective reaction with 4-(aminomethyl) phenyl methanol. The CO_2 protection strategy will ultimately be transferred for use in protecting nitrogen-containing substrates in Suzuki coupling reactions; however the technology has wide applicability in greatly simplifying multi-step industrial syntheses.

3.2 Introduction

3.2.1 Chemical syntheses involving nitrogen functionalities

Chemical syntheses that involve nitrogen functionalities can be found throughout the literature. Examples of relevant nitrogen containing structures include alkyl amines, anilines, pyridines, and pyrroles (Figure 3.1).[1]

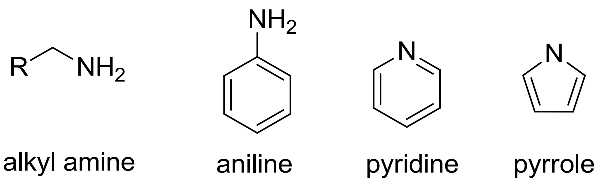

Figure 3.1 - Example structures of nitrogen containing compounds

Of the four examples shown, alkyl amines are the most reactive, often serving as a base in nucleophilic reactions, while aniline is much less reactive.[2] The nitrogen atoms of pyridine and pyrroles are comparatively much less reactive due to their decreased nucleophilicity/basicity; however their lone pair of electrons is still capable of coordinating with metal centers (i.e. catalysts). This project focuses on preventing the unwanted reaction or interaction of these nitrogen containing substrates. Traditionally this achieved through the use of a protecting group.[3]

3.2.2 Amine protection in syntheses

Protecting groups are widely used in synthetic chemistry to allow a chemical reaction to proceed at one reaction site while temporarily blocking another. Careful selection of protecting groups is necessary to achieve a reaction with high yields of the desired product. In Greene's Protective Groups in Organic Synthesis, it is proposed that a protecting group must:[3]

(1) react with the substrate in good yield to achieve sufficient protection,
(2) form a protected species that can be separated from side products, and
(3) avoid sites for further reaction.

Several examples of protecting groups used for protection of nitrogen functionalities are shown in Figure 3.2.[3,4] An important point is that all of these protecting groups require at least two additional steps be added to the synthetic procedure. A step must be added to protect the nitrogen as well as one for the deprotection. Additional separation steps are also often needed to remove the cleaved protecting group as well as any side products.[5]

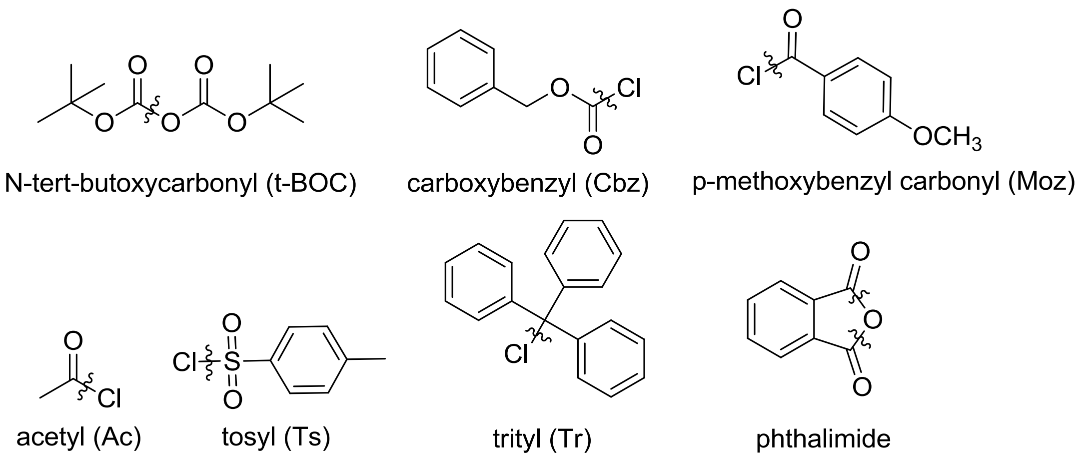

Figure 3.2 - Common protecting groups used for amines; name corresponds to the actual protecting group

The protection groups shown in Figure 3.2 are widely applied in organic synthesis. Di-tert-butyl dicarbonate reacts with amines to give the N-tert-butoxycarbonyl (t-BOC) protecting group. Removal requires the use of a strong acid such as trifluoroacetic acid or HCl. Carboxybenzyl chloride reacts with amines to give the carboxybenzyl (Cbz) protecting group.[6] It is removed by hydrogenation or treatment with HBr. P-methoxybenzyl chloride (Moz) reacts in the same manner but it is easier to remove than the Cbz protecting group. The acetyl group (Ac, accessible via reaction with acetyl chloride) is a common protecting group but can be difficult to remove due to the stable amide it forms. A strong base is required, with some syntheses using ammonia or methylamine. The compound 4-toluenesulfonyl chloride forms the amide of toluenesulfonic acid upon reaction with amines. It is removed by hydrolysis using a strong acid. The trityl (derived from triphenylchloride) and phthalimide groups (derived from potassium phthalimide) are additional protecting groups removed usually removed by weak acid and hydrazine respectively.[1,3,4]

All of the protecting groups exemplified add complication to both the front end of a desired reaction in terms of (1) choosing a protecting group and (2) introducing it to the reaction. Further, on the back end, the protecting group must then be (1) removed and then (2) separated. The majority of the examples shown require a strong acid or base to cleave the protecting group, causing potential interference with other products or reagents in the reaction mixture.

3.2.3 Example of a syntheses requiring nitrogen protection

Complex nitrogen containing compounds are especially prevalent in the pharmaceutical and specialty chemicals industry. One example is Penicillin V; its synthesis is shown in Figure 3.3.[7,8] The end pharmaceutical contains two nitrogen functionalities, several carboxyl groups, and a sulfur-containing functionality. Of note are the steps to prepare compounds **B** and **G**. In the synthesis of **B**, the nitrogen circled in red is not involved; it is protected by a phthalimide protecting group. It must be protected to prevent unwanted reaction and ensure that only the green-labeled nitrogen reacts. This chemistry requires a step to prepare the phthalimide protected compound as well as a step to deprotect the amine (**C**).[8,9]

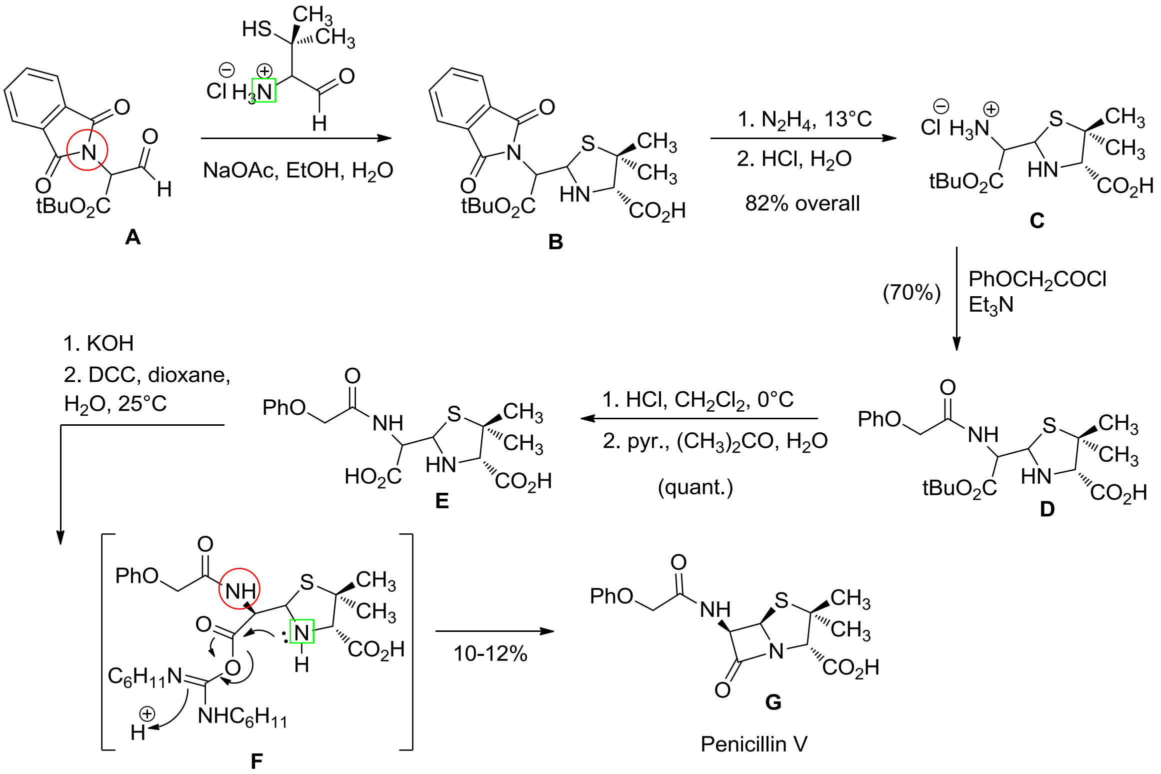

Figure 3.3 - Synthesis of Penicillin V

In the final step to prepare **G**, there are two reactive nitrogen functionalities, one in red and the other in green. Reaction is desired at only the green-labeled nitrogen. However, because the red-labeled nitrogen is unprotected, it can undergo an azlactonization to yield an unwanted product. This side reaction is the major cause of the low yield shown in Figure 3.3 (10-12%). The yield of **G** can be increased to 67% through the use of bulky protecting group such as a trityl group.[10] Note, protection with trityl, would also require a separate synthetic step to protect and deprotect the offending nitrogen.

An additional example of a complex-nitrogen containing molecule is Oseltamivir (Tamiflu, Figure 3.4). The synthesis involves over twelve steps, several of which involve selective reaction at an amine or hydroxyl group site. While the industrial synthesis is proprietary, there is little doubt that reactive protecting groups are used during the synthesis.[11]

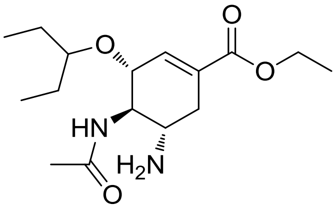

Figure 3.4 - Chemical structure of Oseltamivir (Tamiflu)

3.2.4 Suzuki couplings of nitrogen-containing substrates

In addition to avoiding reaction at unwanted sites, protecting groups are also used to prevent unwanted interaction of nitrogen functionalities with metal centers. The Suzuki reaction has become one of the most widely employed carbon-carbon bond forming processes.[12] The coupling of aryl halides with organoboronic acids is one of the most important palladium-catalyzed cross-coupling reactions of both academic and industrial interest. Suzuki couplings are often performed with amine containing compounds. It has been shown in the literature that the coupling reaction involving free amines suffers from low yields. The low catalyst activity in these reactions is attributed to the interaction of the free nitrogen to the metal center. This undesired interaction of nitrogen with palladium necessitates its protection. For substrates containing free amines, it is common practice to protect these functional groups prior to the coupling step[13] or use highly active catalyst systems.[14]

Recently, a number of publications have discussed conducting Suzuki coupling reactions in supercritical carbon dioxide (CO_2).[15] Supercritical CO_2 – while not the best solvent in terms of its solvent parameters – is considered green, as it is naturally abundant, non-toxic, and recyclable. Recently, mention has also been made of the interaction of supercritical CO_2 with amine-containing substrates. In one example, Wittmann et al. state, "Supercritical carbon dioxide ($scCO_2$) acts simultaneously as solvent and temporary protecting group during homogenously rhodium-catalyzed hydroaminomethylation of ethyl methallylic amine."[16] Though the reaction investigated is not a Suzuki coupling, a similar procedure may be transferable. Christopher Rayner conducted Heck reactions (similar to Suzuki couplings) with amine substrates in supercritical CO_2 and saw dramatic increases in yields over comparative couplings in traditional solvents. Rayner attributes this to interaction of the CO_2 with the amine as a temporary protecting or modifying group to prevent the amine's interaction with the palladium catalyst.[17] We have sought to expand these initial postulates. In this Chapter, work focuses on exploring the interaction of CO_2 with amines at atmospheric pressures of CO_2, however, later work is planned that will be conducted at higher pressures of CO_2.

3.2.5 Using CO_2 to protect nitrogen functionalities in-situ

While protection of nitrogen functionalities is often necessary in syntheses, it requires a minimum of two extra unit operations to any industrial process, adding to both the cost and waste generated in the synthesis. We propose CO_2 as an alternative protecting group for nitrogen functionalities. CO_2 is reactive towards amine functionalities and can be reversed with only moderate heating. We hypothesize that CO_2 can not only at be used at high pressures, but also could be useful at low, more industrially-friendly pressures of CO_2.

The idea of using low-pressure CO_2 as a protecting group originated from our group's work on CO_2 capture (Chapter 2), wherein we developed a class of silylamines for use as reversible ionic liquids. Silylamines react with 1 bar of CO_2 to form ionic liquids consisting primarily of ammonium carbamate ion pairs (non-aqueous conditions, Figure 3.5). The ionic liquid is easily reversed back to its starting amine under moderate heating. The general reaction chemistry is shown below in Figure 1.

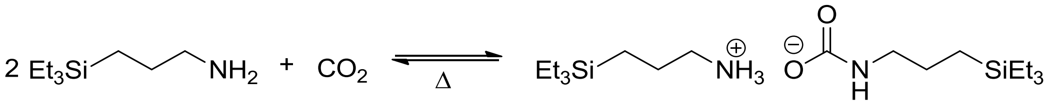

Figure 3.5 - Reaction of 3-(aminopropyl)tripropylsilane with CO_2 to form a reversible ionic liquid

Based on this reactivity, we asserted that the nitrogen atoms in the reversible ionic liquid were essentially protected species (as ammonium and carbamate ions, respectively). We have sought to capitalize on this reactivity with benzylamine substrates. What follows is discussion of three protection strategies developed employing CO_2 as well as several proof of concept reactions conducted to evidence the utility of CO_2 protection of benzylamines.

Aside from the postulates of supercritical CO_2 interacting with amines to serve as a temporary protecting group as presented earlier, the idea of using CO_2 as a protecting group is fairly novel. Only a handful of examples exist where a similar strategy has been investigated. Katritzky et al. have published a number of articles on using CO_2 for the protection of nucleophilic centers.[18] However, their method of protection requires harsh chemicals (n-Butyllithium) as they relied on formation of the lithium salt of the carbamate species. Our research group investigated CO_2-protected amine formation from nitrile and imine hydrogenation in gas-expanded liquids in 2004, however, only elevated pressures were used (30 bar).[19] A CO_2-protection strategy was recently published (April 2013) similar to our proposal, however we evidence differences in our investigation of the strategy.[20] Further discussion is included in the conclusions section.

3.3 Experimental methods

3.3.1 Materials

3.3.1.1 General model amine compounds

Benzylamine, 4-chlorobenzylamine, 4-bromo-α-methylbenzylamine, 4-bromoaniline, and (4-aminomethyl)-phenyl methanol were used as model nitrogen containing compounds (Figure 3.6). The halogen containing compounds were chosen as they were of interest for use as substrates in Suzuki coupling reactions as well. All were used as received from Sigma-Aldrich except for (4-aminomethyl)-phenyl methanol. It was synthesized from 4-aminomethyl benzoic acid as described below.

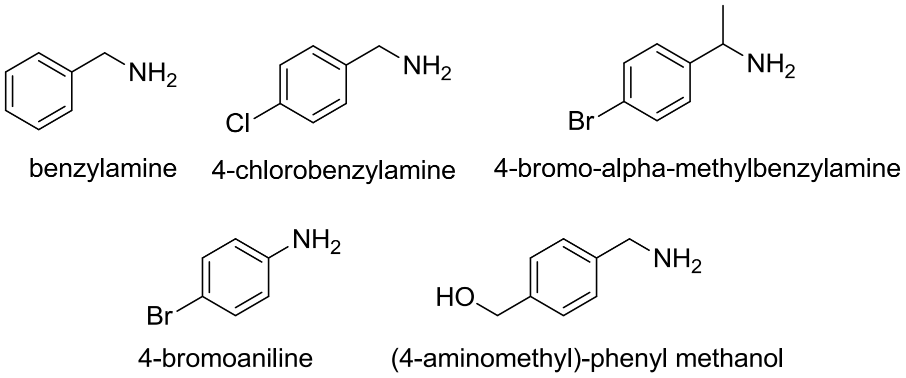

Figure 3.6 - Model amine compounds studied

3.3.1.2 Synthesis of 4-(aminomethyl)-phenyl methanol

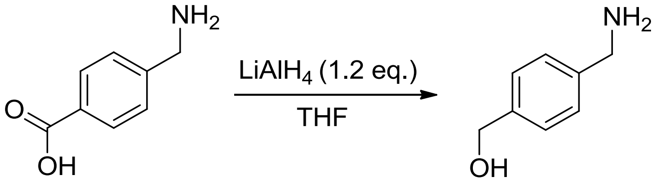

Figure 3.7 - Synthesis of 4-(aminomethyl)-phenyl methanol

The model benzylamine, 4-(aminomethyl)-phenyl methanol was prepared from 4-aminomethyl benzoic acid by reduction with $LiAlH_4$ (Figure 3.7) following literature precedent.[21] In general, one equivalent of 4-aminomethyl benzoic acid was added to a round bottom flask with a stir bar and condenser. The flask was sealed and purged with argon at which point anhydrous tetrahydrofuran (THF) was added. The solution was cooled to near 0°C using an ice bath. Approximately 1.2 equivalents of $LiAlH_4$ (powder) was added in portions slowly to limit the exotherm and byproduct H_2 gas produced. Once added, the solution was heated to reflux (66°C). After 12 hours, the reaction mixture was cooled again to 0°C. The remaining $LiAlH_4$ was quenched slowly with methanol followed by water/30% sodium hydroxide solution. The organic layer was extracted with dichloromethane and rotovapped to yield 4-(aminomethyl)-phenyl methanol as a pale yellow solid in 30% isolated yield.

3.3.1.3 Synthesis of pivaloyl benzatriazole

Pivaloyl benzatriazole was synthesized from benzatriazole and pivaloyl chloride (Figure 3.8). The procedure was adapted from literature precedent.[22] Anhydrous THF was added to an argon-purged round bottom flask with a stir bar. An equivalent of benzatriazole was added and the solution was cooled to 0°C using an ice bath. An equimolar equivalent of pivaloyl chloride and triethylamine (TEA) was added. The reaction was brought to room temperature and allowed to stir for 4 hours. The mixture was then quenched with methanol and water. The organic layer was extracted with dichloromethane and brine. The collected organic layer was then rotovapped to yield pivaloyl benzatriazole as a yellow oil (68% isolated yield).

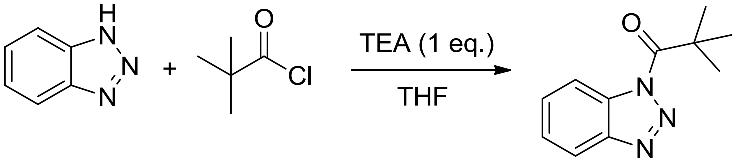

Figure 3.8 - Synthesis of pivaloyl benzatriazole

3.3.1.4 General model acyl substrates

Three acyl substrates were chosen for use in a model nucleophilic acyl substitution reaction – pivaloyl chloride, pivaloyl benzatriazole, and isopropenyl acetate (Figure 3.9). Pivaloyl chloride and isopropenyl acetate were used as received from Sigma-Aldrich. Pivaloyl benzatriazole was prepared from benzatriazole and pivaloyl chloride as detailed above.

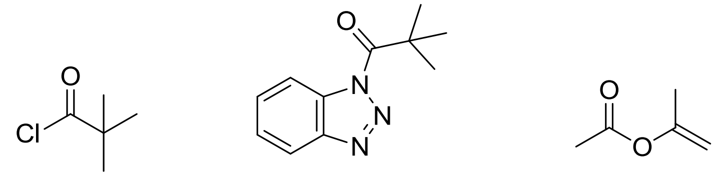

pivaloyl chloride pivaloyl benzatriazoyl isopropenyl acetate

Figure 3.9 - Acyl substrates investigated in a nucleophilic substitution reaction

3.3.2 Nucleophilic acyl substitution reactions

The model reaction focused on is a nucleophilic substitution reaction of an acyl substrate adding to a benzylamine to form the corresponding amide. The details of the individual reactions conducted are discussed in the Results and Discussion section based on the method of CO_2-protection used. The general form of the reaction is shown in Figure 3.10. The rate of the reaction with benzylamines is largely determined by the reactivity of the acyl species and the leaving ability of its corresponding leaving group (labeled LG). By protecting the amine with CO_2, the reaction should not proceed to give the amide product in Figure 3.10. Instead, the protected benzylamine should either 1) not react or 2) react to give an anhydride (see following sections). The anhydride can easily be cleaved by quenching with an alcohol.

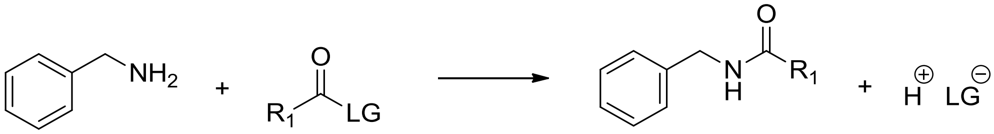

Figure 3.10 - General scheme of nucleophilic acylation of a benzylamine

3.3.3 ^{13}C NMR

^{13}C NMR spectroscopy was used to examine the protection and reversal of the amine substrates in solution as well as to monitor product formation in the reactions (400.13 Mhz Bruker instrument). For measurements above room temperature, following addition of a deuterated solvent, the NMR tube was flame-sealed. Several experiments involve the use of isotopically labeled $^{13}CO_2$ as indicated in the results sections.

3.3.4 ATR-FTIR

To better understand the *in situ* protection of the amine substrates in various solvents Attenuated Total Reflectance-Fourier Transform Infrared (ATR-FTIR) spectroscopy was used (Shimadzu IR-Prestige 21 with a Golden Gate ATR cell). Solid and liquid samples were analyzed for characteristic absorption peaks. In general, 32 scans were performed scanning from 4000 to 400 cm^{-1}.

3.3.5 Differential scanning calorimetry (DSC)

Differential scanning calorimetry was used to determine the reversal and/or melting temperature of any solid carbamate salts formed. DSC measurements are performed using a Q20 TA DSC Instrument. The DSC method included equilibrating the cell at -40°C and ramping the temperature 5°C per minute until 400°C was reached. The reversal temperature is defined from the DSC thermogram as the intersection of tangent lines drawn from the onset and bottom of the reversal events – as shown in the results section.

3.4 Results and discussion

3.4.1 Use of CO_2 to form the protected salt (solvent-free)

The first protection technique evaluated used the reaction of CO_2 with the amine substrate to form an ammonium-carbamate ionic salt (Figure 3.11).

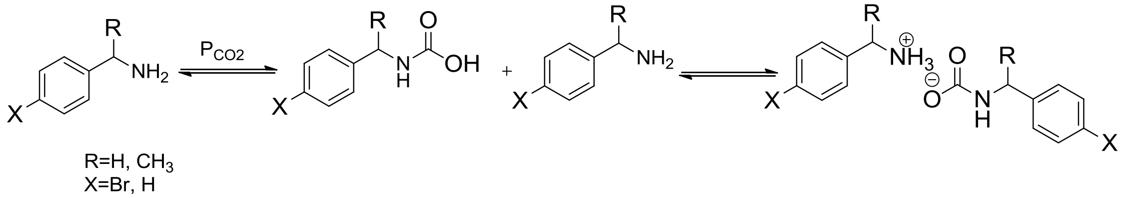

Figure 3.11 – Reaction of benzyl-type amines with CO_2 to form an ammonium-carbamate ionic salt

As shown in Figure 3.11, the benzylamine species first reacts with CO_2 to form a carbamic acid species. The carbamic acid is rapidly deprotonated in the presence of unreacted benzylamine in neat conditions to form an ammonium-carbamate ion pair – isolated as a white solid. Figure 3.12 shows an IR spectrum of the ammonium-carbamate salt of 4-bromo-α-methylbenzylamine formed after reaction with 1 bar of CO_2 at 25°C. There are two characteristic peaks in the IR spectrum. The first is the broad ammonium

(NH_3^+) vibration between 2800 and 3200 cm^{-1} and the second is the characteristic carbonyl stretch (C=O) at ~1630 cm^{-1}.

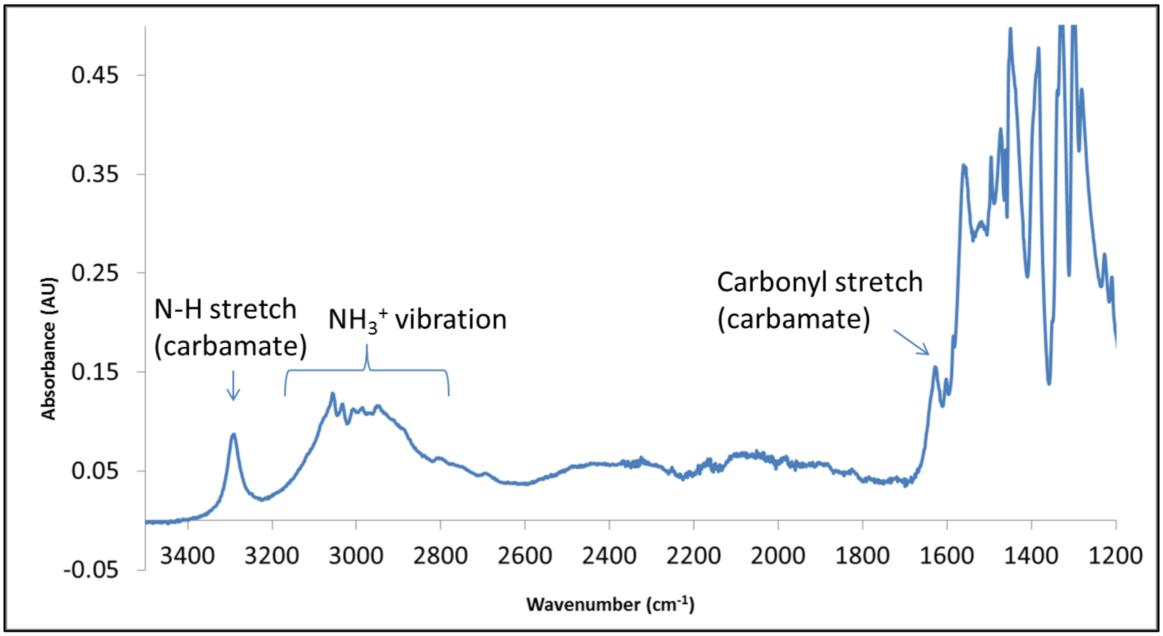

Figure 3.12 - FTIR spectrum of 4-bromo-α-methylbenzylamine salt after reaction with 1 bar of CO_2 at 25°C

The DSC thermogram of the CO_2-protected 4-bromo-α-methylbenzylamine salt (Figure 3.13) shows two events. The first is representative of the release of CO_2 and consequent melting of the salt. The second event corresponds to the evaporation of the amine substrate. Of note, the reversal of the neat salt is recorded at 101°C. The elevated reversal temperature suggests that synthesis could be carried out above room temperature without reversal of the CO_2 protecting group. However, the solid salt formed would imply a solid-liquid heterogeneous reaction. As such, the effect of solvent on the reversal temperature and the solubility of the protected salt were then investigated.

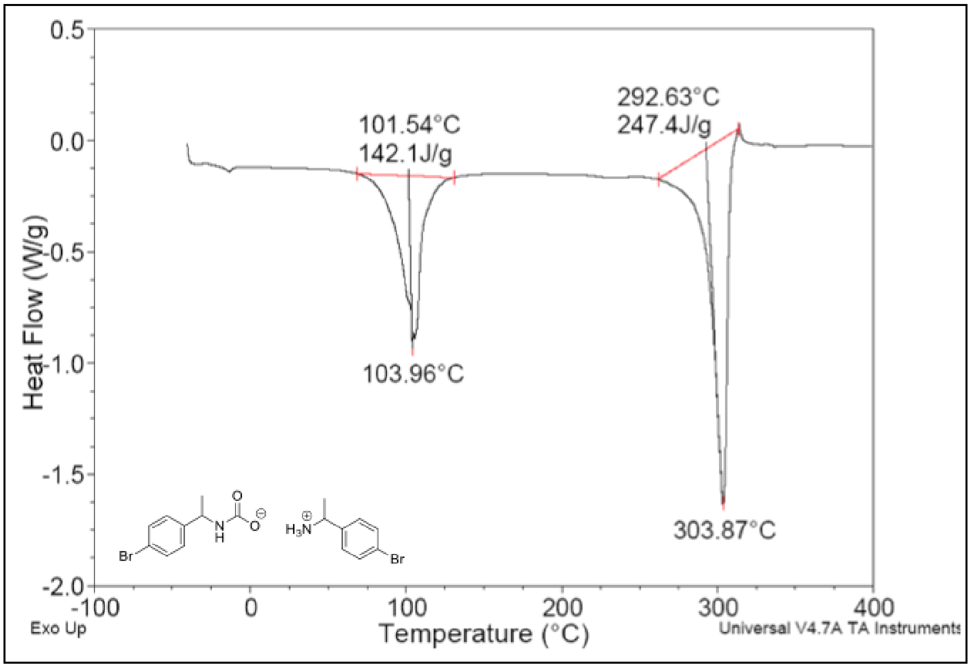

Figure 3.13 - DSC thermogram of 4-bromo-α-methylbenzylamine salt after reaction with 1 bar of CO_2 at 25°C

3.4.2 The effect of solvent on the ammonium-carbamate salt

To investigate the effect of solvent on reversal temperature, the CO_2-protected salt was added to a volume of solvent. Methanol was first used as the solvent to promote the formation of the ammonium carbamate and ammonium methyl carbonate ion pairs. Experimentally, 4-bromo-α-methylbenzylamine was reacted with isotopically labeled $^{13}CO_2$ at 25°C and then added to an NMR tube containing deuterated methanol (0.4 M). An NMR spectrum was recorded at 25 and 50°C. To record a spectrum at 50°C, the NMR spectrometer was heated to temperature and the sample was allowed to equilibrate for 15 minutes.

At 25°C the protected 4-bromo-α-methylbenzylcarbamate salts are soluble in methanol, and the equilibrium concentration of the ammonium carbamate and ammonium methyl carbonate ion pairs are nearly equivalent as evidenced by the carbonyl peaks labeled **x** and **y** in Figure 3.14. Note: standard NMR spectra are presented in the Appendix.

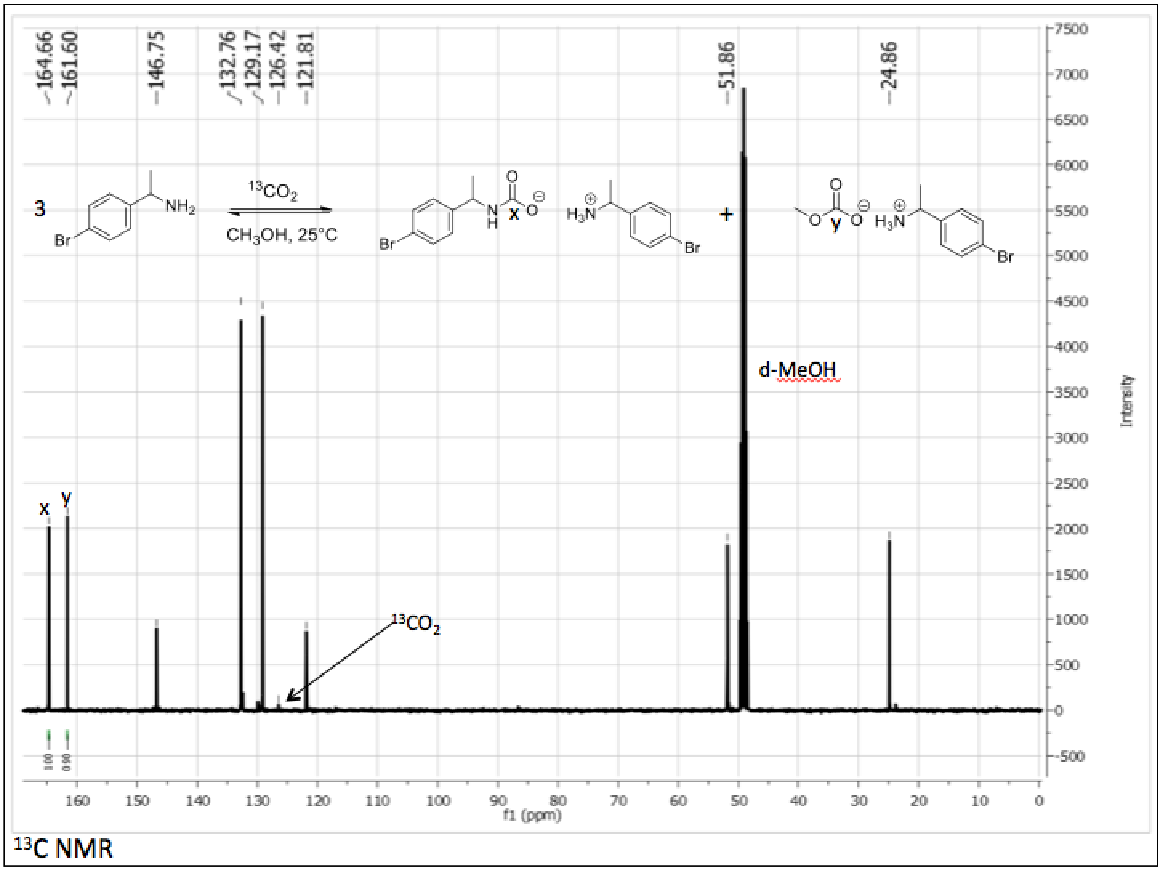

Figure 3.14 - ^{13}C NMR spectrum of 4-bromo-α-methylbenzylamine in methanol at 25 °C under 1 atm CO_2

A NMR spectrum was also recorded at 50°C. As shown in Figure 3.15, a significant decrease in the carbamate carbonyl carbon is observed (labeled **x**) while the $^{13}CO_2$ peak (~126 ppm) increases. Additionally, an equilibrium exists between the ammonium carbamate and ammonium methyl carbonate ion pairs. The increase in temperature shifts the equilibrium towards the ammonium methyl carbonate species. The spectra show that 4-bromo-α-methylbenzylamine does remain protected and is soluble in methanol. However, it was decided that it would be more desirable to use a polar aprotic solvent in which only one type of protected species could form, as opposed to the two types of ion pairs as evidenced in methanol.

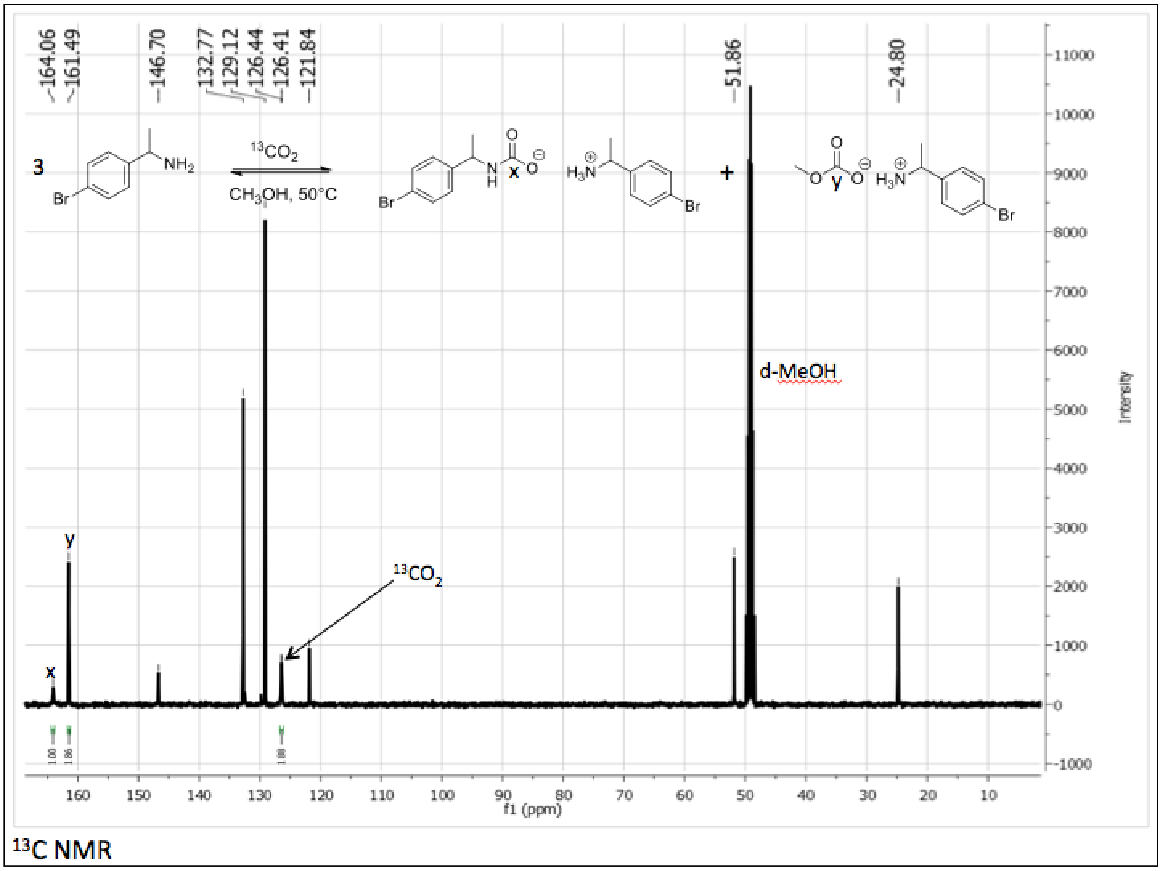

Figure 3.15 - NMR spectrum of 4-bromo-α-methylbenzylamine in methanol at 50 °C under 1 atm CO_2

As an alternative to methanol, THF was used as the solvent for the protected salt. At 25°C and a concentration of 0.4M, the 4-bromo-α-methylbenzylamine CO_2-protected salt is largely insoluble in the THF. At 50°C, the solid dissolves into the solvent; however, NMR suggests significant reversal of the salt back to the starting amine substrate (Figure 3.16). The relatively small size of the carbamate peak suggests that the protected carbamate-containing species is present in solution only in small concentrations. Since isotopically labeled $^{13}CO_2$ was used to form the protected salt, it should appear much larger than the rest of the non-isotopically labeled peaks. Of note, the peak shown near 126 ppm is representative of free isotopically labeled $^{13}CO_2$ in solution. Its peak height suggests it is present in much higher concentration than the carbamate species. It is realized that this ^{13}C NMR experiment is only semi-quantitative; however, peak heights are often at least qualitatively indicative of concentration.

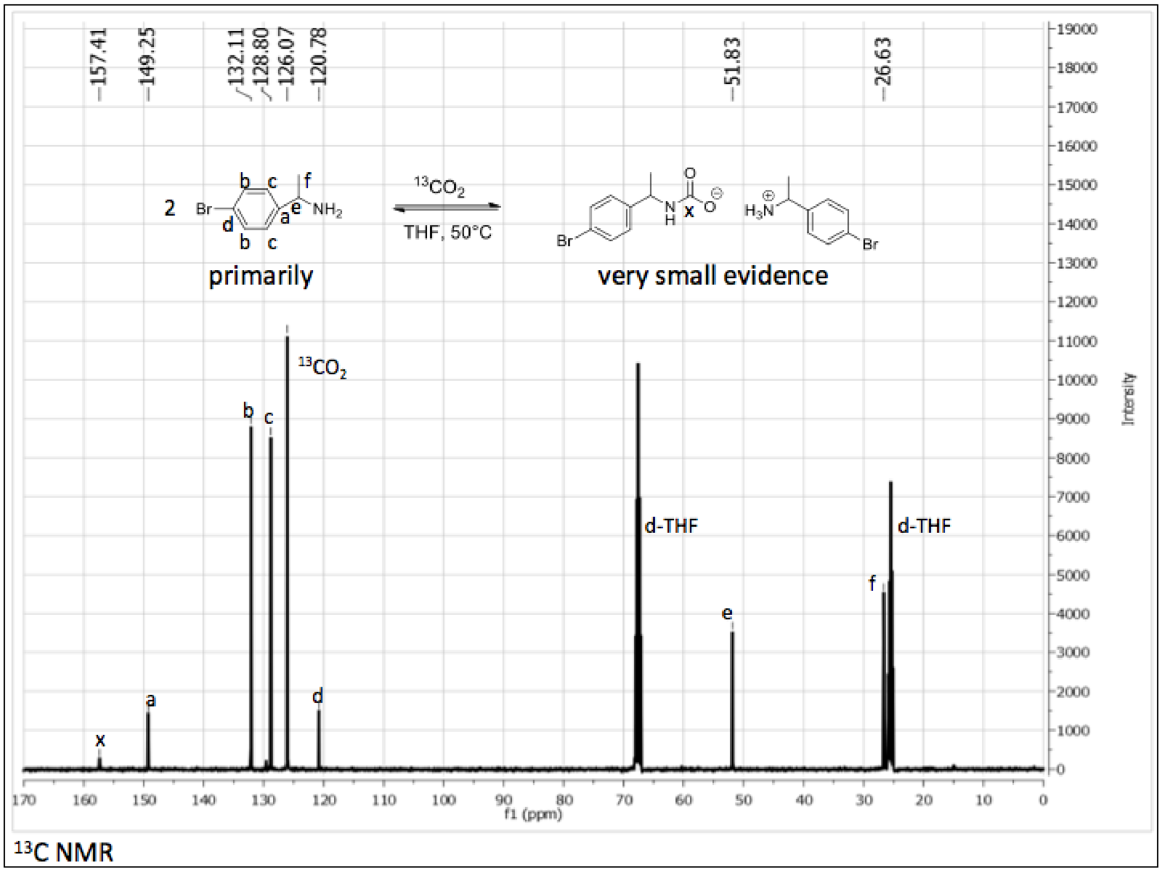

Figure 3.16 - ^{13}C NMR spectrum of the 4-bromo-α-methylbenzylamine in THF at 50°C under 1 atm CO_2

In addition to THF, several additional aprotic solvents were investigated. The additional solvents investigated include ethyl acetate, acetone, 1,4 dioxane, chloroform, and acetonitrile (Figure 3.17). In all cases, it was found that the CO_2-protected salt was insoluble at 25°C and underwent significant reversal when heated to 50°C. Due to the negligible solubility of the CO_2-protected benzyl-type amines in these aprotic solvents, two highly dipolar, protophilic, aprotic solvents were investigated – dimethyl sulfoxide (DMSO) and dimethylformamide (DMF).

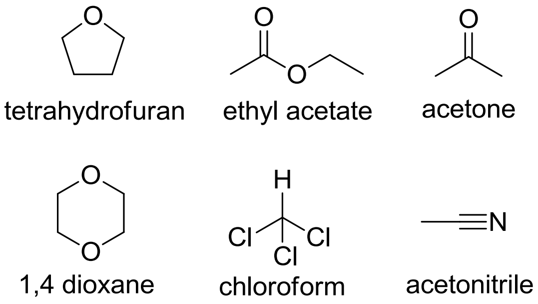

Figure 3.17 – Solvents investigated for solubility of the CO_2-protected ammonium-carbamate benzyl-type amine salt

3.4.3 Formation of carbamic acid in DMSO and DMF

In protophilic, highly dipolar, aprotic solvents such as dimethyl sulfoxide (DMSO) and dimethyl formamide (DMF), it was discovered that benzylamine reacts with an atmosphere of CO_2 at room temperature to form its corresponding carbamic acid (benzyl-carbamic acid).[23] In literature, carbamic acid formation has been used as a replacement for phosgene to synthesize ureas and carbamates.[24]

In most organic solvents as shown in section 3.4.1, the reaction proceeds further – a molecule of unreacted amine deprotonates the carbamic acid to form an ammonium-carbamate ion pair. However, because of the hydrogen bonding accepting ability of both DMSO and DMF, the carbamic acid species is solvent-stabilized (Figure 3.18). The ^{13}C NMR spectra of the carbamic acid formed in DMSO and DMF respectively are shown in Figure 3.19 and Figure 3.20. Forming carbamic acid as opposed to the ion pair is advantageous for two reasons: 1) all of the amine moieties are protected by a single functionality, and 2) no ionic species are formed which precipitate out of solution, eliminating the issue of solubility of the protected species.

Figure 3.18 - Equilibrium reaction of benzylamine to form benzyl-carbamic acid

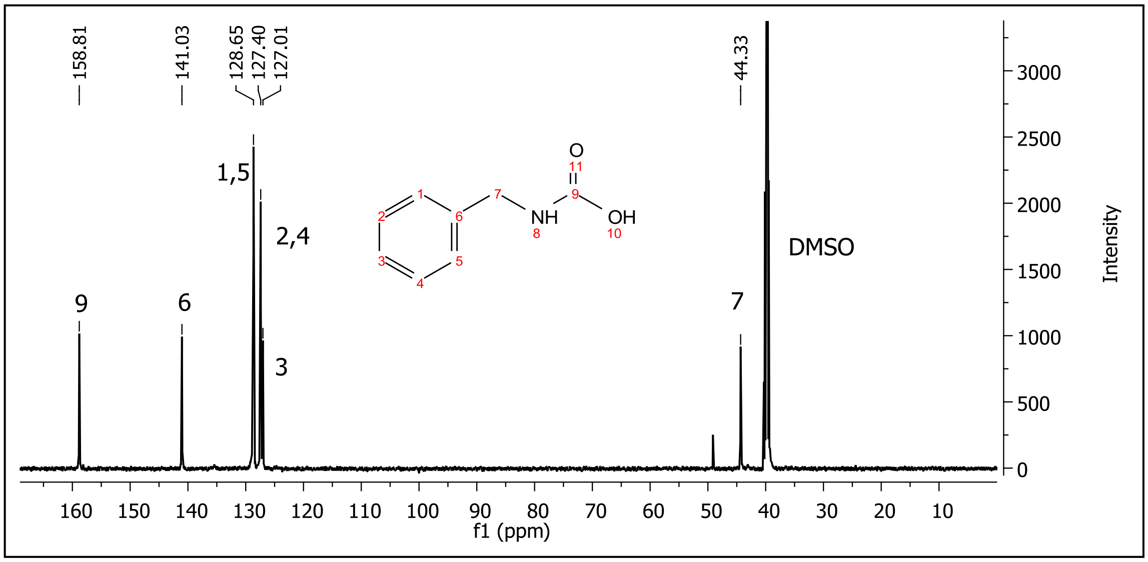

Figure 3.19 - ^{13}C NMR of benzyl-carbamic acid formed in DMSO

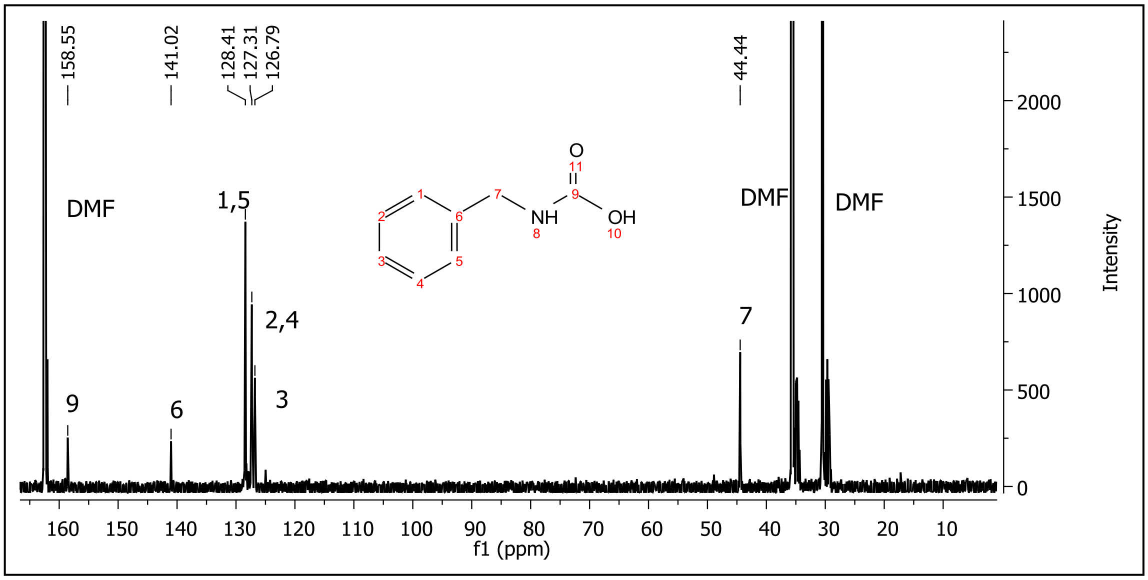

Figure 3.20 - ^{13}C NMR of benzyl-carbamic acid formed in DMF

3.4.4 Model reaction: nucleophilic acyl substitution

With the success of forming carbamic acid in DMSO and DMF, the utility of carbamic acid as a protecting group for benzylamine using a nucleophilic acyl substitution reaction. Several acyl substrates were investigated as detailed in the following sections.

3.4.4.1 Pivaloyl chloride

The first acyl substrate investigated was pivaloyl chloride. It was expected that in the presence of the carbamic acid of benzyl amine no reaction would take place other than possible formation of the anhydride shown in Figure 3.21.

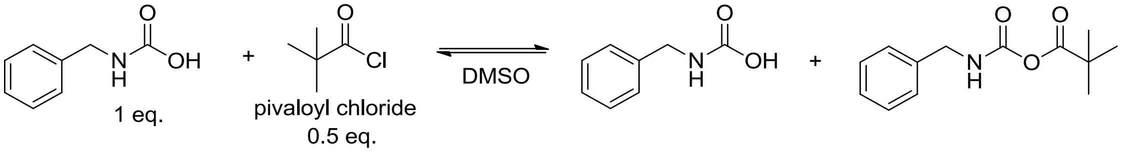

Figure 3.21 - Expected reaction of benzyl-carbamic acid with a model acyl substrate (pivaloyl chloride)

A control reaction was first run with unprotected benzylamine and pivaloyl chloride to determine the extent of reaction and products formed. The reaction was analyzed by ^{13}C NMR, which showed the formation of two products. One product resulted from the expected reaction of pivaloyl chloride with benzylamine to give the corresponding benzylpivalamide. The second product resulted from the unexpected reaction of the pivaloyl chloride with the solvent – DMSO. The reaction is depicted in Figure 3.22. Surprisingly, the HCl salt of benzylamine was not observed. It was expected that the HCl byproduct would react with the free benzylamine to form the ionic salt.

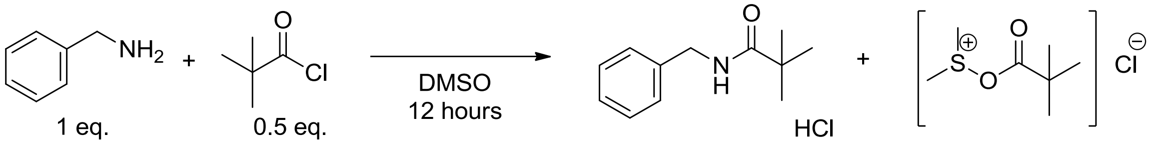

Figure 3.22 - Observed reaction of benzylamine with pivaloyl chloride in DMSO

Though pivaloyl chloride reacted with the DMSO solvent, a reaction was run with the protected carbamic acid form of benzylamine. Benzylamine (0.4 M) was sparged with CO_2 in DMSO for approximately 30 minutes. Complete formation of the corresponding carbamic acid was verified by ^{13}C NMR. The solution was then cooled to 0°C using an ice bath. A half-molar equivalent of pivaloyl chloride was added dropwise. The reaction was stirred for three hours. After three hours an aliquot was taken for NMR analysis.

Two products were identified via ^{13}C NMR. The first product was the DMSO-pivaloyl chloride reacted species. The second product was unreacted carbamic acid (only 0.5 eq. of pivaloyl chloride was used). The results were encouraging in terms of maintaining the carbamic acid protection as none of the benzylpivalamide product was observed (Figure 3.23).

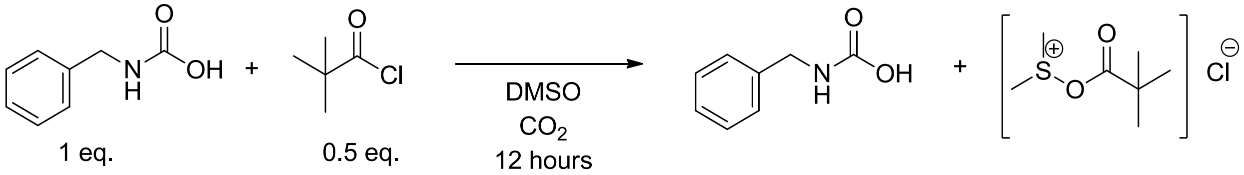

Figure 3.23. Observed reaction of benzyl-carbamic acid with pivaloyl chloride in DMSO

However, the formation of the DMSO-pivaloyl chloride reacted species was undesirable. Introducing the potential for two competitive reactions added the complexity of needing to determine the relative rates of each reaction. As such, DMF was investigated as an alternate solvent, since it was also found to stabilize the carbamic acid species. However, DMF also readily reacts with pivaloyl. The reaction observed between pivaloyl chloride with DMSO and DMF was confirmed in literature.[25]

3.4.4.2 Benzatriazole

As an alternative to pivaloyl chloride, pivaloyl benzatriazole was investigated as an acyl substrate. We hypothesized that its decreased reactivity would prevent it from reacting with the DMSO solvent. It is further useful because it prevents generation of HCl as a byproduct, which could in turn react with the CO_2-protected benzylamine.

A control reaction was run with benzylamine (1 equivalent, 0.4 M) and 1-(2,2,2-trimethylacetyl)-1H-benzotriazole (0.5 equivalents). The reaction was conducted at room temperature and allowed to proceed for 24 hours. The resulting ^{13}C NMR analysis evidenced formation the benzylpivalamide product as well as the presence of remaining starting material. The scheme is shown in Figure 3.24.

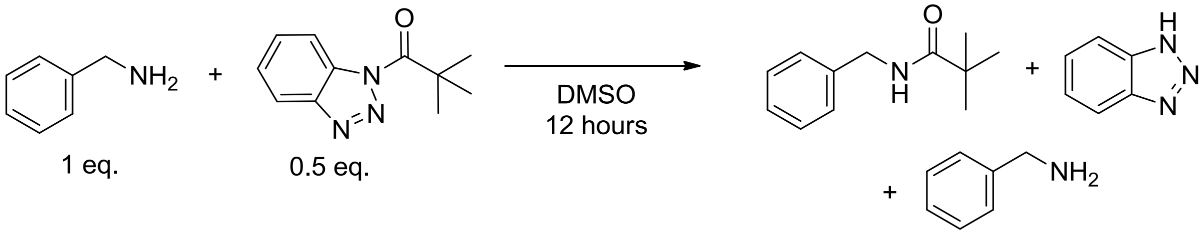

Figure 3.24 - Observed reaction of benzylamine with 1-(2,2,2-trimethylacetyl)-1H-benzotriazole in DMSO

Reactions were then conducted with the CO_2-protected carbamic acid form of benzylamine. The reaction was repeated twice; reactions were run at room temperature for 4 hours with 1 equivalent of the CO_2-protected carbamic acid of benzylamine and 0.5 equivalents of 1-(2,2,2-trimethylacetyl)-1H-benotriazole. The carbamic acid of benzylamine was first formed by sparging a 0.4 M solution of benzylamine in DMSO with CO_2. The acyl benzotriazole was then added dropwise. In both reactions, the products were benzylpivalamide and remaining benzyl-carbamic acid (

Figure 3.25). The formation of benzylpivalamide was undesired as it indicated that the amine did not maintain protection as carbamic acid. Upon investigation of the literature it was found that the pKa of benzotriazole is 8.2.[26] We hypothesize that if any of the benzyl-carbamic acid was reversed to benzylamine upon addition of the pivaloyl benzatriazole, then any small concentration of benzatriazole formed would have led to deprotonation and reversal of additional benzyl-carbamic acid.

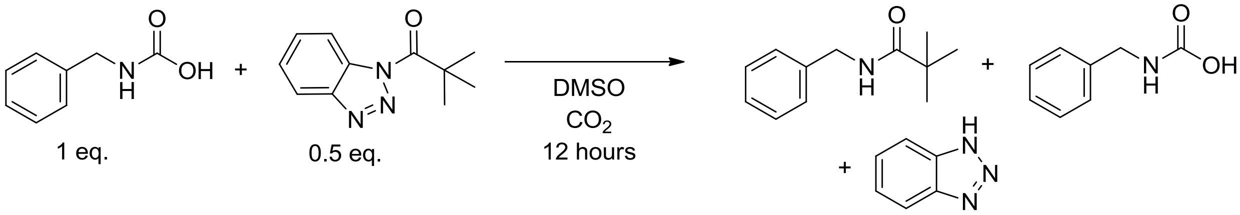

Figure 3.25. Observed reaction of benzyl-carbamic acid with 1-(2,2,2-Trimethylacetyl)-1H-benzotriazole in DMSO

3.4.4.3 Isopropenyl acetate

Isopropenyl acetate was also investigated as a substrate for the nucleophilic acyl substitution. Isopropenyl acetate is a mild acylating agent.[27] A reaction using 4-(aminomethyl)-phenyl methanol protected as its carbamic acid was carried out with 1 equivalent of isopropenyl acetate. It was postulated that the bifunctionality of 4-(aminomethyl)-phenyl methanol would consume the isopropenyl acetate, aiding in maintaining protection of the amine over time.[28] The carbamic acid was first formed by sparging a 0.4 M solution of 4-(aminomethyl)-phenyl methanol with CO_2 for 30 minutes. A 0.5 molar equivalent of isopropenyl acetate was then added at room temperature. After

4 hours an aliquot was extracted for NMR analysis. The resulting ^{13}C NMR spectrum showed formation of the undesired acetamide product as well as remaining carbamic acid (

Figure 3.26). Continued monitoring of the reaction by ^{13}C NMR showed increased formation of the acetamide product over time.

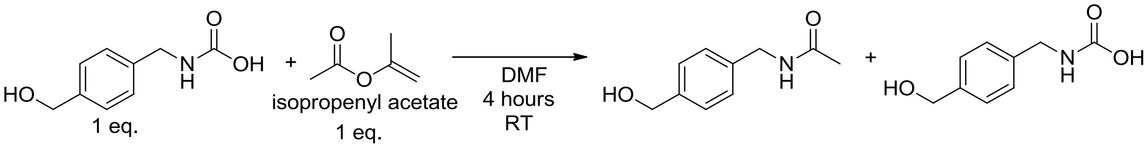

Figure 3.26 - Reaction of CO_2-protected 4-(aminomethyl)-phenyl methanol with isopropenyl acetate

3.4.5 Use of an added base to shift equilibrium with CO_2

As the CO_2-protected ammonium carbamate salts of benzyl-type amines showed low solubility in organic solvents, and the CO_2-protected carbamic acid form of benzylamine showed limited stability in the presence of reactive acyl substrates, an additional method of CO_2-protection was sought.

To promote the forward reaction while using a non-interacting polar aprotic solvent, we proposed the addition of a strong base to the solvent and benzylamine prior to reaction with CO_2. The reaction scheme is shown in Figure 3.27. The base shifts the equilibrium to the right by accepting the proton of the carbamic acid to form an ion pair with the carbamate species.[29] This has been utilized in the synthesis of urethanes and carbonated from amine/alcohols, CO_2, and allylic chlorides.[30]

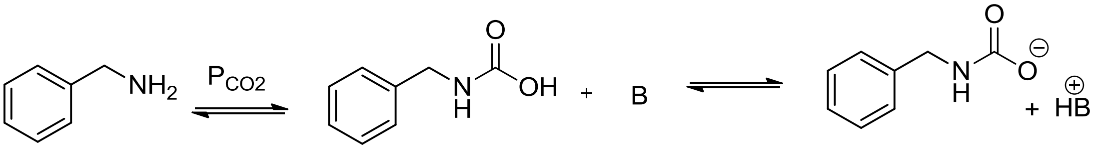

Figure 3.27. Reaction of benzylamine with CO_2 in acetonitrile or THF with added base.

The added base must be carefully selected as we found it has a strong influence on the degree of amine protection and solubility of the protected species in the polar aprotic solvent. Four bases were tested – triethylamine (TEA), 1,1,3,3-tetramethylguanidine (TMG), diisopropylethylamine (DIPEA), and 1,8-diazabicyclo[5.4.0]undec-7-ene (DBU) (Figure 3.28). For each, the protected species was formed and its solubility in tetrahydrofuran (THF) and acetonitrile (ACN) was tested. When TEA, TMG, or DIPEA was used, a white solid was formed that was not soluble in THF or ACN. However, when DBU was used a viscous light yellow liquid formed that is soluble in both THF and ACN. With these results, characterization of the protected species when using DBU was carried out.

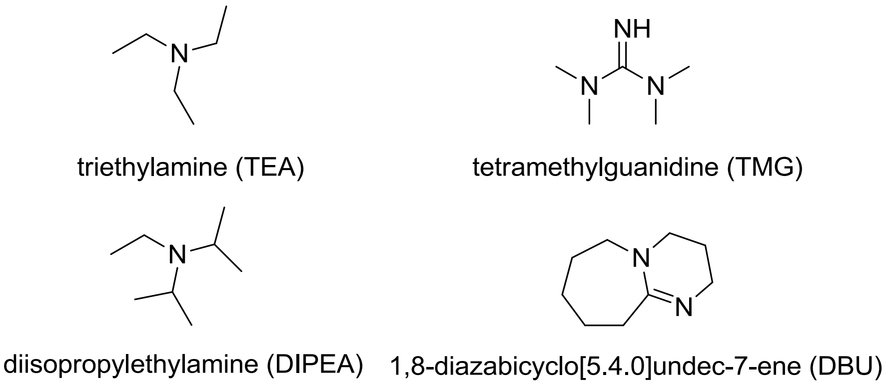

triethylamine (TEA)

tetramethylguanidine (TMG)

diisopropylethylamine (DIPEA)

1,8-diazabicyclo[5.4.0]undec-7-ene (DBU)

Figure 3.28 - Bases investigated: TEA, TMG, DIPEA, and DBU

3.4.5.1 Characterization of the CO_2-protected benzylamine using DBU

Figure 3.29 depicts the equilibrium reaction of benzylamine with CO_2 in the presence of DBU. Two ion pairs (A and B) are shown as potential products in the reaction. Ion Pair A is formed when the DBU deprotonates the carbamic acid, stabilizing the carbamate species. Ion Pair B is formed when an additional mole of benzylamine accepts the carbamic acid proton instead of DBU. It was hypothesized that the higher pKa of DBU (pKa~12) compared to benzylamine (pKa~9.5) would result in the dominance of Ion Pair A, which is soluble in acetonitrile.

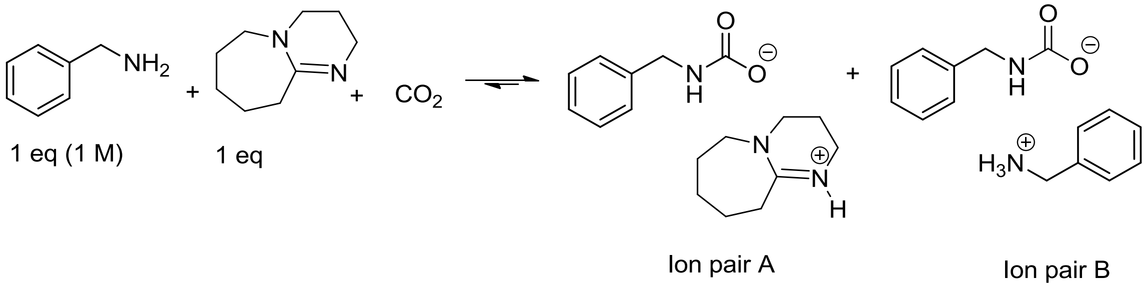

Figure 3.29. Equilibrium reaction of benzylamine with added base (DBU) and CO_2.

A ^{13}C NMR is shown in Figure 3.30 of the CO_2-protected benzylamine in the presence of DBU. Using NMR standards (see Appendix), peak assignments were made and are shown in Figure 3.31. The self-associated ammonium carbamate ion pair (Ion pair B in Figure 3.29) was not observed. Two species were identified as being associated with a molecule of protonated DBU. The first is the carbamate of benzylamine as depicted Figure 3.29 (Ion pair A). The second species is a carbamate-carbamic acid benzylamine moiety resulting from the addition of two molecules of CO_2 to the benzylamine nitrogen. The species was confirmed using ^{13}C, ^{1}H, and ^{15}N NMR. 2-D NMR coupling experiments showed that of the two nitrogen benzylamine species observed, one did not have any attached protons, supporting the proposed bis-anion (see Appendix). While the observance of the bis-anion was surprising, it exists as a protected amine species as does the carbamate. As such, nucleophilic acyl substitution reactions were again investigated to test the utility of the protection using CO_2 with added DBU.

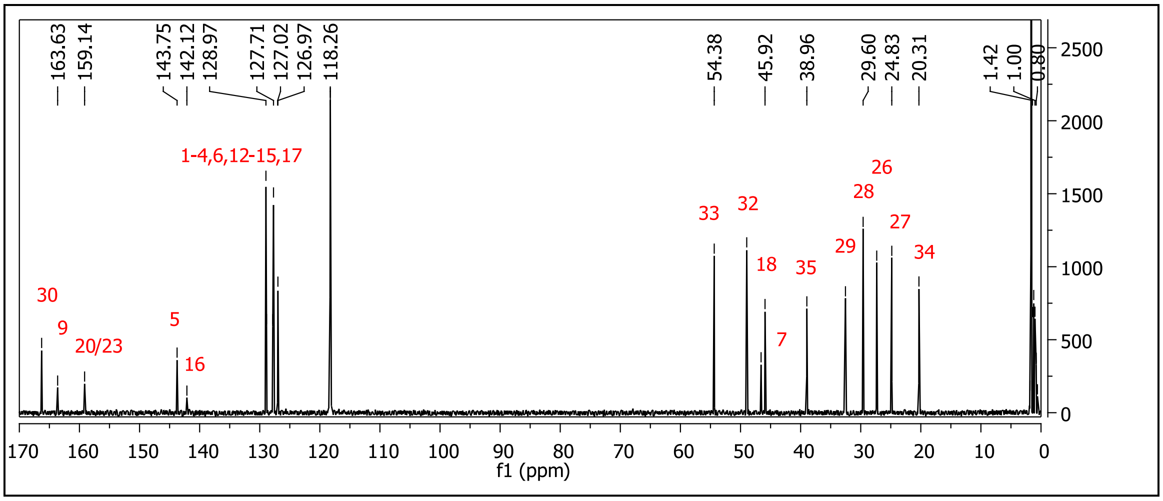

Figure 3.30 – ^{13}C NMR of CO_2-protected benzylamine using DBU

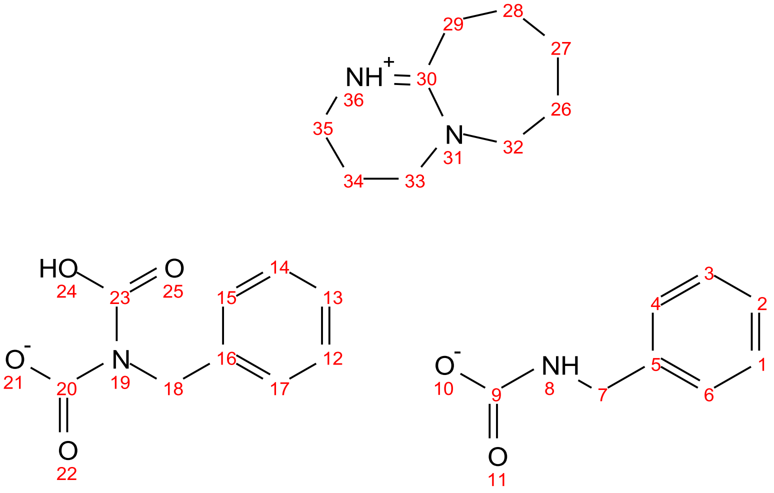

Figure 3.31 – Carbon peak assignments for the 13C NMR of CO_2-protected benzylamine using DBU

3.4.6 Model reaction: nucleophilic acyl substitution

3.4.6.1 Pivaloyl chloride

To demonstrate the utility of the *in-situ* protection of benzylamine using CO_2 and and DBU as an added base, a nucleophilic acyl substitution reaction was attempted using pivaloyl chloride as the acyl substrate. Shown in Figure 3.32 and Figure 3.33 are the proposed reaction pathways with and without CO_2 protection. With CO_2 protection, in the presence of DBU, the benzylamine forms the stabilized carbamate species. Upon addition of pivaloyl chloride, in red, the carbamate may (1) remain unreacted or (2) react with the pivaloyl chloride to form an anhydride species. Without CO_2 protection, the benzylamine and pivaloyl chloride should react to immediately form the benzylpivalamide (as shown earlier).

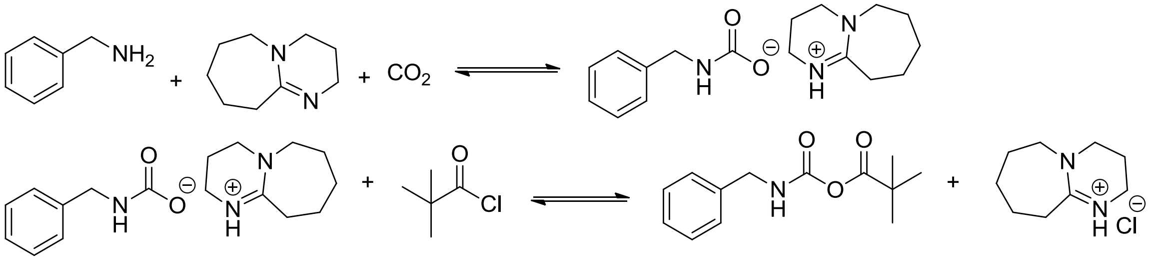

Figure 3.32 - Proposed reaction pathway with CO_2 protection

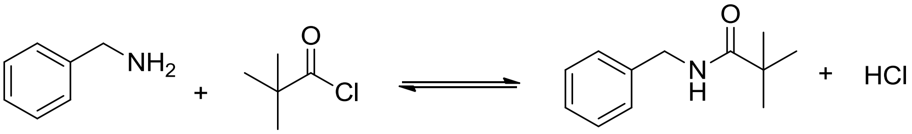

Figure 3.33. Proposed reaction pathway without CO_2 protection.

The results of the protection study completed using ^{13}C NMR indicate that the acetylation reaction with CO_2-protected benzylamine did not proceed, however the pivaloyl chloride species reacted with the DBU, forming Species A, shown in Figure 3.34. A ^{13}C NMR is shown in Figure 3.35 of the reaction. Experimentally, the CO_2-protected benzylamine species with DBU (1 M) was first formed in acetonitrile. A slight excess (1.2 equivalents) of DBU was used to account for any water present in the DBU (Completely drying the DBU proved difficult.). The solution was then cooled to 0ºC using an ice bath. Approximately 0.5 equivalents of pivaloyl chloride were then added dropwise and the reaction mixture was allowed to return to room temperature. After one hour, an aliquot was taken for NMR analysis.

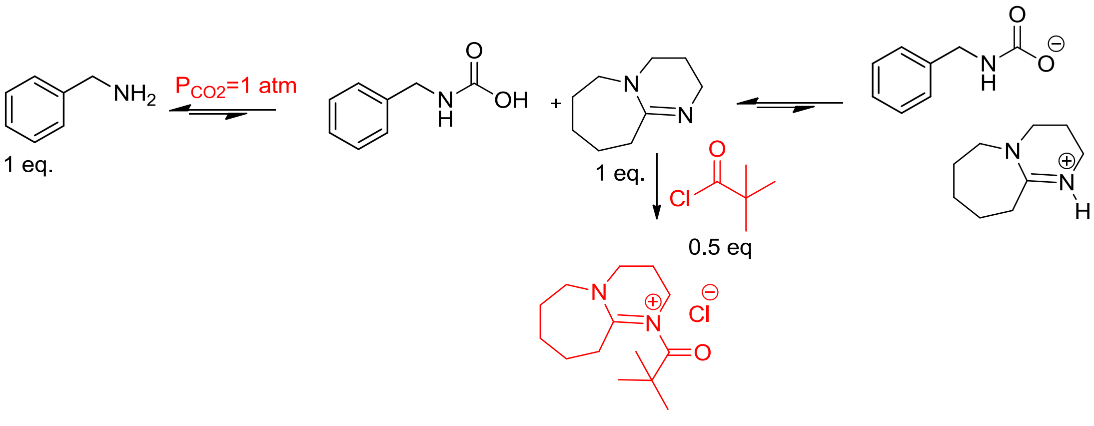

Species A

Figure 3.34 - Scheme showing the reaction of pivaloyl chloride with DBU

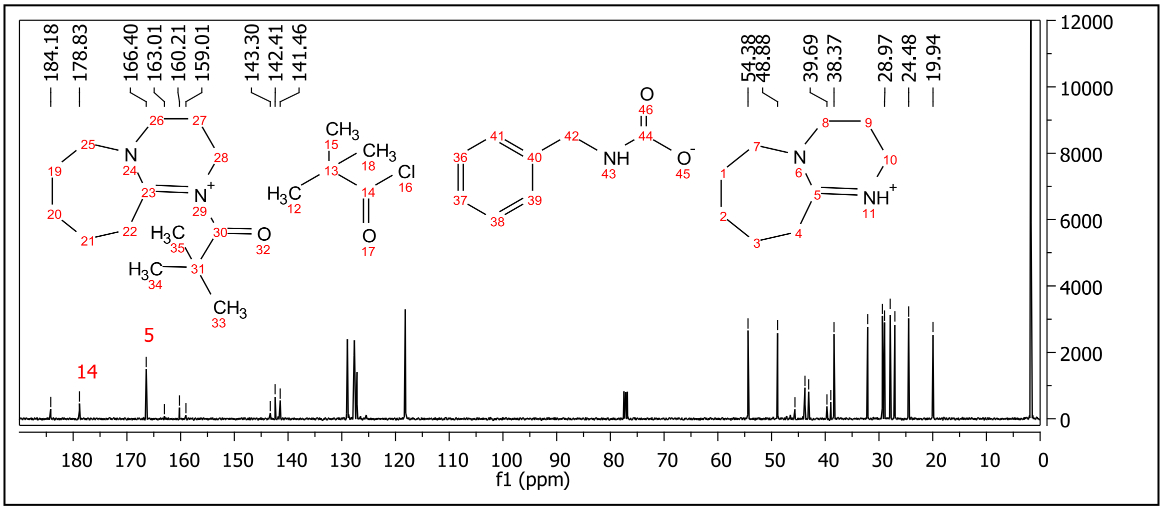

Figure 3.35 – ^{13}C NMR of the reaction of CO_2-protected benzylamine using DBU and pivaloyl chloride

A control reaction was also run using unprotected benzylamine with pivaloyl chloride. Benzylamine in acetonitrile (1 M) was cooled to 0ºC with an ice bath. Pivaloyl chloride (0.5 equivalents) was added dropwise and then the reaction mixture was returned to room temperature. After 1 hour, an aliquot was taken for NMR analysis. The ^{13}C NMR showed complete consumption of the pivaloyl chloride to form N-benzylpivalamide.

It is important to emphasize that the reaction using the CO_2-protected benzylamine using DBU was completed with 1 atm of CO_2 pressure, and although the pivaloyl chloride reacted with the DBU, we demonstrated the ability to manipulate reaction chemistry through CO_2 protection. In the control, no reaction of the pivaloyl chloride with DBU was observed, evidencing that reaction with the amine was preferential. However, in the reaction utilizing CO_2 protection, the pivaloyl chloride reacted with the DBU as the amine was not available for reaction with the acyl substrate.

The results from these initial reactions were promising in terms of developing the CO_2 protection using added base (DBU) strategy. However, the reaction of the acyl substrate with DBU was undesired. To attempt to mitigate the reaction of the acyl substrate with the DBU an alternate acyl substrate was explored.

3.4.6.2 Pivaloyl benzatriazole

Pivaloyl benzatriazole was investigated as an alternate to the pivaloyl chloride acyl substrate. We hypothesized that pivaloyl benzatriazole would be less reactive than pivaloyl chloride, hoping to mitigate potential reaction of the acyl substrate with the added base in the CO_2-protection strategy. Further, the only byproduct from the reaction of pivaloyl benzatriazole is benzatriazole. In the reactions with pivaloyl chloride a chloride salt was formed as a byproduct.

To test our hypothesis, CO_2-protection and control reactions were conducted in a similar fashion to those investigated with pivaloyl chloride. The CO_2-protected benzylamine using DBU species in acetonitrile was formed as previously described. A slight excess of DBU was used. The reaction mixture was cooled to 0ºC using an ice bath and then 1 equivalent of pivaloyl benzatriazole was added drop wise. The reaction mixture was returned to room temperature after addition and allowed to stir for 1 hour.

After 1 hour, an aliquot was removed for NMR analysis. The ^{13}C NMR spectrum showed that the protected species was unstable in the presence of the pivaloyl benzatriazole, reaction between the pivaloyl benzatriazole and the excess DBU was observed (Figure 3.36). As in the case of the investigation with the carbamic acid, the basicity of benzatriazole likely played a role in causing reversal of the CO_2-protected benzylamine. At this point, another acyl substrate was found that would not react with the added base (DBU).

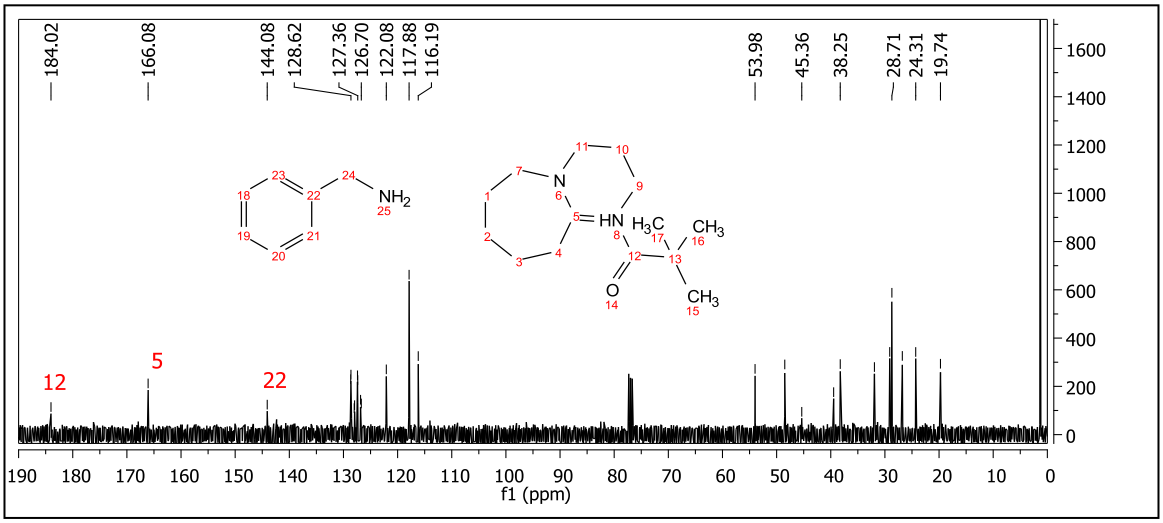

Figure 3.36 – ^{13}C NMR of the reaction of CO2-protected benzylamine using DBU and pivaloyl benzatriazole

3.4.6.3 Isopropenyl acetate

After investigation of the literature, we decided isopropenyl acetate would be an ideal candidate for the proof-of-concept nucleophilic acyl substitution we wanted to investigate.[27] The first reaction ran was between the CO_2-protected benzylamine using DBU and isopropenyl acetate. The CO_2-protected benzylamine was prepared as previously described in acetonitrile (1.1 equivalents DBU to benzylamine). Isopropenyl acetate (1 equivalent) was then added at room temperature. The reaction was allowed to proceed for 6 hours. After 6 hours, no reaction was observed by ^{13}C NMR (Figure 3.37). The benzylamine remained protected by CO_2 as the carbamate associated with the protonated DBU. Further, the isopropenyl acetate did not react with the DBU base.

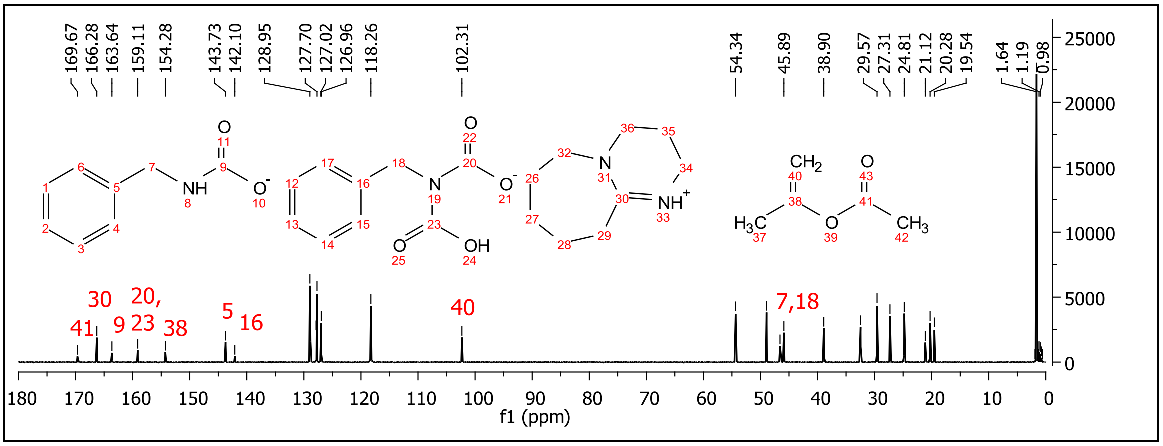

Figure 3.37 -^{13}C NMR of reaction investigated between CO_2-protected benzylamine using DBU and isopropenyl acetate

A control reaction was conducted with unprotected benzylamine and isopropenyl acetate. The same conditions were used as in the reaction with CO_2 protection using DBU as an added base. After 6 hours significant evidence of the N-benzylacetimide product was observed (Figure 3.39). The reaction is shown in Figure 3.38. Comparing this result with the CO_2-protected benzylamine shows the success of the CO_2-protection strategy using an added base. When protected, no reaction of the amine was observed; however, when unprotected reaction of the amine does occur.

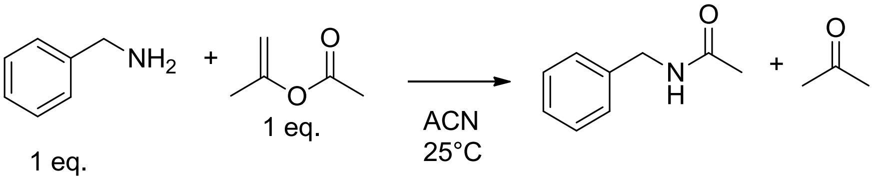

Figure 3.38 - Control reaction of isopropenyl acetate with benzylamine

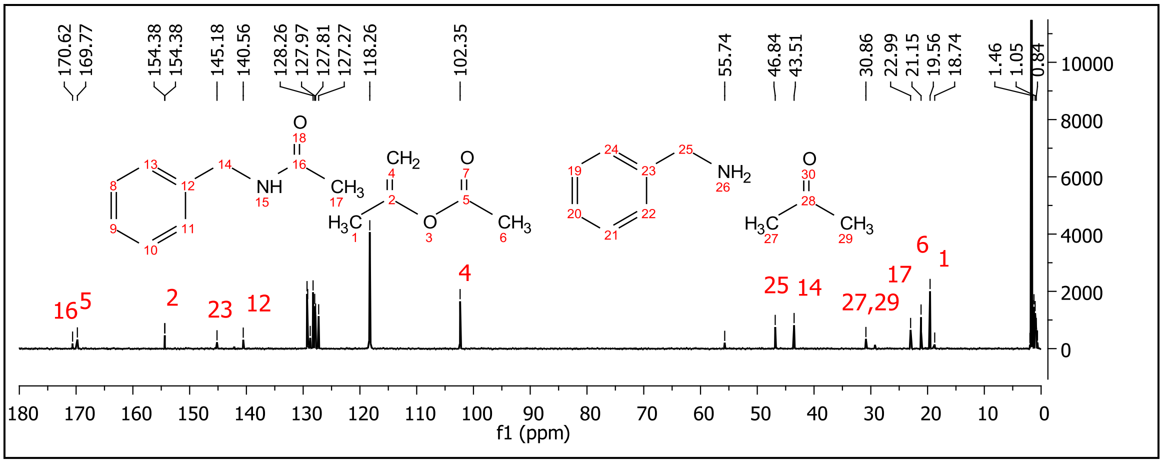

Figure 3.39 – ^{13}C NMR control reaction of unprotected benzylamine with isopropenyl acetate

3.4.6.4 Chemoselective reaction with 4-(aminomethyl)-phenyl methanol

To further investigate whether or not the CO_2-protection technology could be used to further alter the reaction chemistry, benzylalcohol was added in an equimolar quantity in addition to CO_2-protected benzylamine (using DBU). After 6 hours, at room temperature, a ^{13}C NMR sample was taken. The resulting NMR is shown in Figure 3.40. No reaction of the CO_2-protected benzylamine is observed; however, reaction of the benzylalcohol was observed to yield the phenyl acetate. This was the first evidence we found that by protecting the benzylamine using CO_2, we could direct reactivity toward a less reactive molecule (benzylalcohol). A control reaction is presented in the Appendix.

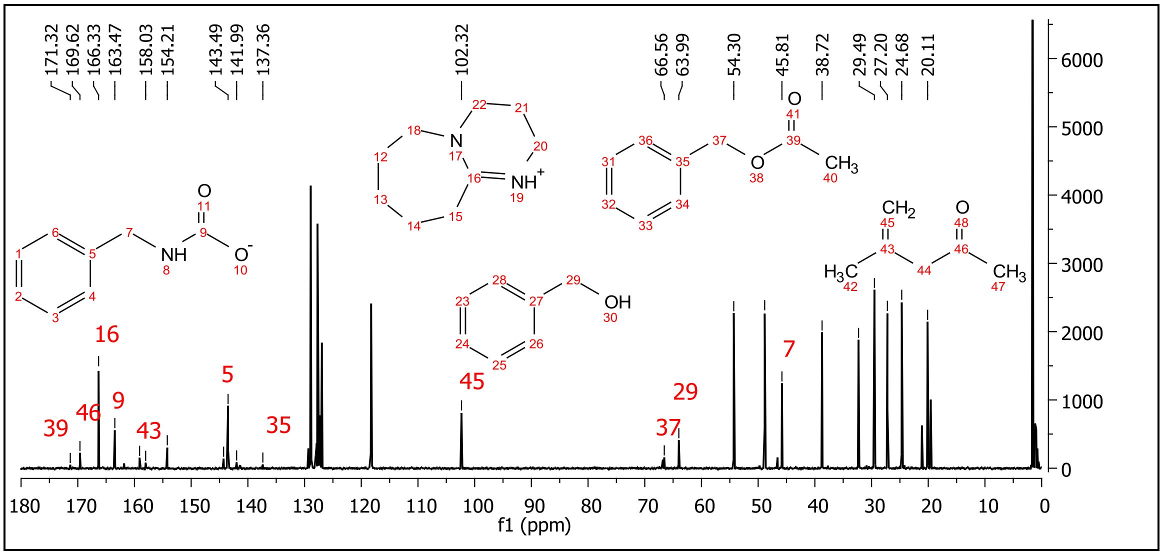

Figure 3.40 - ^{13}C NMR of reaction between CO_2-protected benzylamine using DBU and benzylalochol with isopropenyl acetate

To further investigate the reaction of benzylalcohol in the presence of a CO_2-protected benzylamine using DBU, the bifunctional molecule 4-(aminomethyl)-phenyl methanol was used. A control reaction was first run with the bifunctional molecule and isopropenyl acetate (1.7 equivalents). The expected reaction is shown in Figure 3.41. The reaction was carried out for 6 hours; a small amount of catalyst (0.5 mol%, 1,2,4-triazole) was used to speed the reaction. A ^{13}C NMR was taken after 6 hours. By NMR analysis (Figure 3.42), 100% of the available amine reacted and 70% of the hydroxyl group reacted.

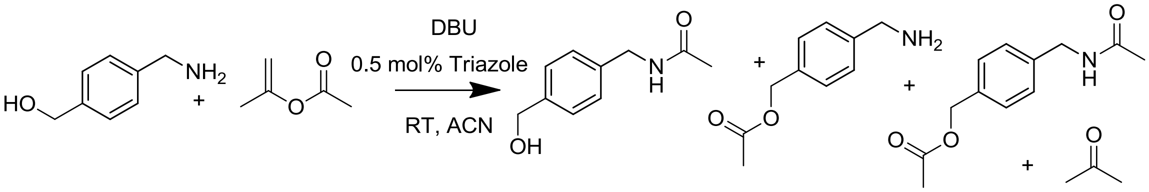

Figure 3.41 – Control reaction scheme of 4-(aminomethyl)-phenyl methanol with isopropenyl acetate

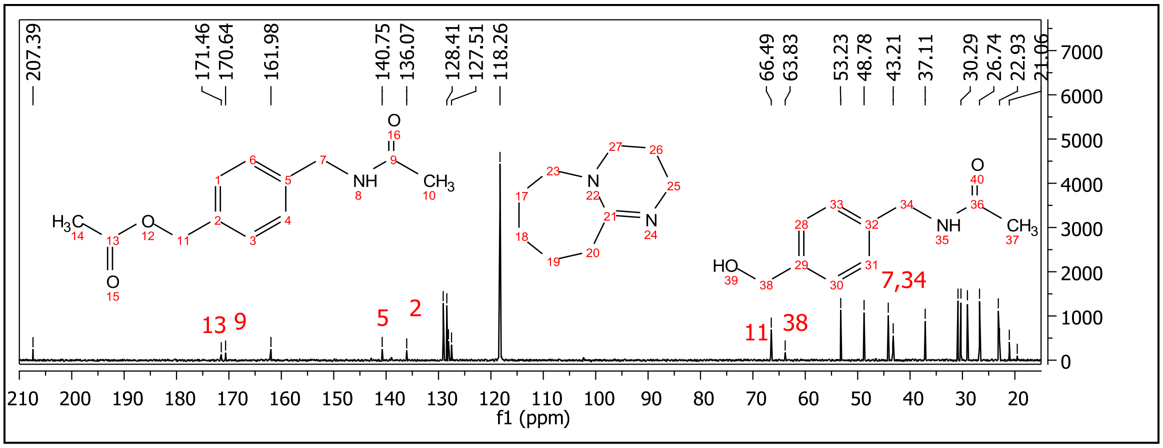

Figure 3.42 - ^{13}C NMR control reaction of unprotected 4-(aminomethyl)phenyl methanol in the presence of isopropenyl acetate and DBU (no CO_2)

A reaction was then carried out using 4-(aminomethyl)-phenyl methanol with the amine protected by CO_2 using DBU. Using 1.7 equivalents of isopropenyl acetate and 0.5 mol% catalyst, after 6 hours NMR analysis showed 30% of the hydroxyl group had reacted while none of the amine reacted; it remained CO_2-protected. The reaction was also carried out at a longer time period (24 hours) using 1 mol% catalyst. By NMR 80% of the hydroxyl group reacted while none of the amine reacted. The amine remained CO_2-protected (Figure 3.43). The reaction scheme is shown in Figure 3.44.

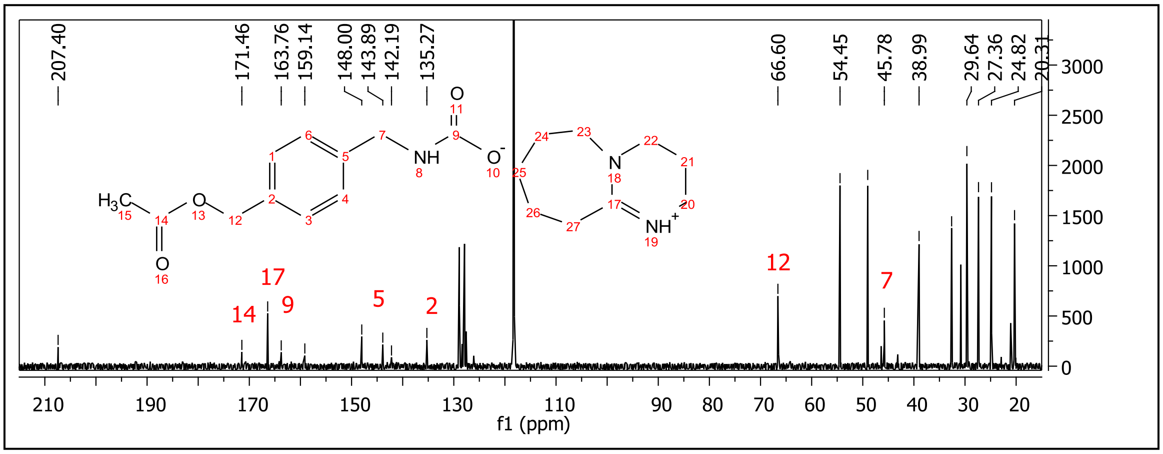

Figure 3.43 - ^{13}C NMR of reaction CO_2-protected 4-(aminomethyl)phenyl methanol using DBU in the presence of isopropenyl acetate

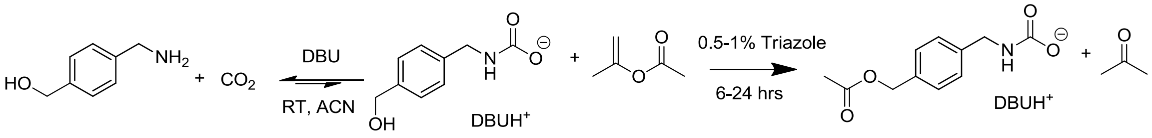

Figure 3.44 – Reaction shceme of CO_2-protected 4-(aminomethyl)-phenyl methanol using DBU with isopropenyl acetate

3.5 Conclusions

3.5.1 Key findings and accomplishments

Three strategies for the protection of benzyl amines using CO_2 were developed. They are as follows: (1) reaction of CO_2 with benzylamine to form the self-associated ammonium carbamate salt, (2) reaction of benzylamine in DMSO or DMF with CO_2 to form the corresponding carbamic acid, and (3) reaction of benzylamine with CO_2 in the presence of an added strong base to form a benzylamine carbamate – protonated base species. Of the three strategies, the most success was seen when a strong base was added.

Several nucleophilic acyl substitution reactions were carried out using CO_2-protected benzylamine and DBU as the added strong base. When protected by CO_2 using DBU, no reaction of the amine was observed in the presence of a nucleophilic acyl substituent (isopropenyl acetate). Further, when a bifunctional molecule was used – 4-(aminomethyl)-phenyl methanol – with the CO_2-protected benzylamine using DBU – reactivity was directed away from the amine to the hydroxyl group. Whereas in a control reaction 100% of the amine was consumed by reaction with the nucleophilic acyl substituent, in the CO_2-protected reaction no reaction at the amine was observed. We thereby successfully used CO_2 to protect a reactive amine functionality and direct reactivity elsewhere within the same molecule in a chemoselective manner.

Recent literature supports our initial results.[20] In the latest issue of *Green Chemistry*, de Vos et al. report similar acylation reactions using CO_2 to protect benzylamine with DBU as an added strong base. Their results further show that our idea does indeed have potential and warrants further investigation. The chemoselectivity reaction we demonstrated using 4-(aminomethyl)-phenyl methanol is certainly novel.

3.6 References

(1) March, J. *Advanced Organic Chemistry: Reactions, Mechanisms, and Structure*; Fourth Edition ed.; Wiley-Interscience: New York, 1992.

(2) Anslyn, E. V.; Dougherty, D. A. *Modern Physical Organic Chemistry*; University Science Books, 2006.

(3) Wuts, P. G. M. *Greene's protective groups in organic synthesis*; 4th ed. / ed.; Wiley-Interscience: Hoboken, N.J. :, 2007.

(4) Kocienski, P. J. *Protecting Groups*; 3rd edition ed.; Thieme: New York, 2005.

(5) Agami, C.; Couty, F. *Tetrahedron* **2002**, *58*, 2701.

(6) Bora, P. B.; Vanlaldinpuia, K.; Rokhum, L.; Bez, G. *Synthetic Communications* **2011**, *41*, 2674.

(7) Bentley, P. H.; USPTO, Ed.; Beechem Group Limited: US, 1981; Vol. 4416883.

(8) Sheehan, J. C.; Henery-Logan, K. R. *Journal of the American Chemical Society* **1957**, *79*, 1262Sheehan, J. C.; Henery-Logan, K. R. *Journal of the American Chemical Society* **1959**, *81*, 3089.

(9) Sheehan, J. C.; USPTO, Ed. US, 1966; Vol. 3487074.

(10) Poore, T. In *Classics in Heterocyclic Chemistry*; Chemistry, C. U., Ed.; Columbia University, 2011.

(11) Karpf, M.; Trussardi, R. *Journal of Organic Chemistry* **2001**, *66*, 2044.

(12) Miyaura, N.; Suzuki, A. *Chemical Reviews* **1995**, *95*, 2457Hassan, J.; Sevignon, M.; Gozzi, C.; Schulz, E.; Lemaire, M. *Chemical Reviews* **2002**, *102*, 1359Littke, A. F.; Fu, G. C. *Angewandte Chemie-International Edition* **2002**, *41*, 4176.

(13) Caron, S.; Massett, S. S.; Bogle, D. E.; Castaldi, M. J.; Braish, T. F. *Organic Process Research & Development* **2001**, *5*, 254.

(14) Wolfe, J. P.; Singer, R. A.; Yang, B. H.; Buchwald, S. L. *Journal of the American Chemical Society* **1999**, *121*, 9550Billingsley, K. L.; Anderson, K. W.; Buchwald, S. L. *Angewandte Chemie-International Edition* **2006**, *45*, 3484Fu, G. C.; Littke, A. F.; Dal, C. Y.; Schwarz, L. *Abstracts of Papers of the American Chemical Society* **2000**, *219*, U195Itoh, T.; Mase, T. *Tetrahedron Letters* **2005**, *46*, 3573.

(15) Shezad, N.; Oakes, R. S.; Clifford, A. A.; Rayner, C. M. *Tetrahedron Letters* **1999**, *40*, 2221Leitner, W. *Accounts of Chemical Research* **2002**, *35*, 746Leeke, G. A.; Santo, R. C. D.; Bushra, A.-D.; Seville, J. P. K.; Smith, C. J.; Lee, C. K. Y.; Holmes, A. B.; McConvey, I. F. *Organic Process Research & Development* **2007**, *11*, 144Gordon, R. S.; Holmes, A. B. *ChemComm* **2002**, 640Fernandes, R. R.; Lasri, J.; da Silva, M. F. C. G.; Palavra, A. M. F.; da Silva, J. A. L.; da Silva, J. J. R. F.; Pombeiro, A. J. L. *Advanced Synthesis and Catalysis* **2011**, *353*, 1153Feng, X.; Yan, M.; Zhang, T.; Lui, Y.; Bao, M. *Green Chemistry* **2010**, *12*, 1758Early, T. R.; Gordon, R. S.; Carroll, M. A.; Holmes, A. B.; Shute, R. E.; McConvey, I. F. *Chemical Communications* **2001**, 1966Kuchurov, I.; A., V. e. A.; Zlotin, S. G. *Mendeleev Communications* **2010**, *20*, 140.

(16) Wittmann, K., WisniewskiMynott, RichardLeitner, Wlater *Chemistry - A European Journal* **2001**, *7*, 4854.

(17) Rayner, C. M. *Organic Process Research & Development* **2007**, *11*, 121.

(18) Katritzky, A. R. *Organic Synthesis: Modern Trends* **1987**, 203Katritzky, A. R.; Akutagawa, K. *Tetrahedron Letters* **1985**, *26*, 5935.

(19) Xie, X. F.; Liotta, C. L.; Eckert, C. A. *Industrial & Engineering Chemistry Research* **2004**, *43*, 7907.

(20) Peeters, A.; Ameloot, R.; De Vos, D. E. *Green Chemistry* **2013**, *15*, 1550.

(21) Pignataro, L.; Boghi, M.; Civera, M.; Carboni, S.; Piarulli, U.; Gennari, C. *Chemistry European Journal* **2012**, *18*, 1383Colombo, R.; Mingozzi, M.; Belvisi, L.; Arosio, D.; Umberto, P.; Carenini, N.; Perego, P.; Zaffaroni, N.; De Cesare, M.; Castiglioni, V.; Scanziani, E.; Gennari, C. *Journal of Medicinal Chemistry* **2012**, *55*, 10460.

(22) Wilkerson, C., University of Florida, 2003Katritzky, A. R.; He, H.-Y.; Suzuki, K. *Journal of Organic Chemistry* **2000**, *65*, 8210.

(23) Masuda, K.; Ito, Y.; Horiguchi, M.; Fujita, H. *Tetrahedron* **2005**, *61*, 213Dijkstra, Z. J.; Doornbos, A. R.; Weyten, H.; Ernsting, J. M.; Elsevier, C. J.; Keurentjes, J. T. F. *The Journal of Supercritical Fluids*, *41*, 109.

(24) Peterson, S. L.; Stucka, S. M.; Dinsmore, C. J. *Organic Letters*, *12*, 1340.

(25) Dubey, A.; Kandula, S. R. V.; Kumar, P. *Synthetic Communications* **2008**, *38*, 746.

(26) Katritzky, A. R., Rachwal, Stanislaw, Hitchings, Gregory J. *Tetrahedron* **1991**, *47*, 2683.

(27) Hagemeyer Jr., H. J.; Hull, D. C. *Industrial and Engineering Chemistry* **1949**, *41*, 2920.

(28) Sinning, C.; Watzer, B.; Coste, O.; Nusing, R. M.; Ott, I.; Ligresti, A.; Marzo, V. D.; Imming, P. *Journal of Medicinal Chemistry* **2008**, *51*, 7800.

(29) Carrera, G. V. S. M.; da Ponte, M. N.; Branco, L. C. *Tetrahedron* **2012**, *68*, 7408.

(30) McGhee, W. D.; Riley, D. P.; Christ, M. E.; Christ, K. M. *Organometallics* **1993**, *12*, 1429.

CHAPTER 4 - MITIGATING THE THERMAL DEGRADATION OF POLYVINYL CHLORIDE (PVC)

4.1 Abstract

The thermal degradation of polyvinyl chloride (PVC) is a significant processing challenge which can lead to deleterious mechanical and optical properties in a wide range of products. Synergetic studies on PVC model compounds and blends of bulk PVC were performed; together they provide unique insights into the thermal degradation and stabilization pathways of PVC in the presence of common additives. Model PVC compounds were selected to replicate specific defects (e.g., allylic, vicinal and tertiary) and tacticity (i.e., utilizing stereochemistry to investigate tacticity) commonly found in PVC. Model studies were conducted neat (solvent-free) with metal carboxylates. Thermal weight loss studies using blends of bulk PVC proved critical in transferring mechanistic insights into the context of a polymeric matrix. Blends of PVC with both phthalate- and bio-based plasticizers were studied in addition to blends incorporating metal stearate thermal stabilizers. In addition, two novel stabilizers for incorporation into PVC blends were developed based on the mechanistic understanding of the pathways of PVC degradation, combining both the model and bulk PVC studies.

4.2 Introduction

4.2.1 Polyvinyl chloride (PVC)

Polyvinyl chloride (PVC) is one of the most used plastics globally, with an annual use of over 26 million metric tons. It is second only to polypropylene in plastics use.[1] Its chemistry and polymeric properties give it wide application to a number of industries including piping, construction, signage, clothing and furniture, healthcare, and electrical cabling. For the purposes of this Chapter, PVC will be studied as relevant to the electrical cabling industry.

PVC was first introduced in the electrical cabling industry in World War II. During the War, the US Navy was involved in an enormous ship building campaign, using thousands of miles of rubber-coated wiring. However, the rubber used was in limited supply and furthermore was ignitable; when ignited, it caused fires that could spread throughout a ship. In response, the Navy turned to plasticized PVC to use as fire-resistant insulation for wiring on the ships. PVC provides excellent fire resistance as more than half of the PVC monomer by weight is chlorine. Chlorine inhibits burning by scavenging free radicals to form HCl. Since World War II, PVC has made its way into home wiring applications as well. PVC now holds 58% of the wire and cable plastics market.[1]

4.2.2 PVC polymerization

PVC is made commercially by the free-radical polymerization of vinyl chloride (Figure 4.1). Vinyl chloride is produced industrially from the pyrolysis of ethylene dichloride (1,2 dichloroethane) in a cracking operation. Ethylene dichloride is produced on large scale from reaction of ethylene with chlorine. Though sometimes regarded as environmentally unfriendly, production of PVC uses less than 0.3% of the world's annual oil and gas production; further, as its chlorine content is nearly 57%, it is much less dependent on oil and gas than other polymers. Chlorine is considered readily available as it can be produced from sodium chloride (naturally abundant).[1]

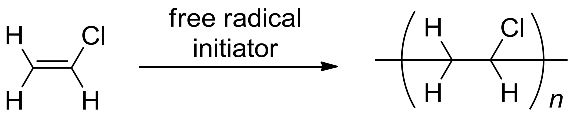

Figure 4.1 - Radical polymerization of vinyl chloride to yield polyvinyl chloride; n ranges from 625 to 2700 commercially

The vast majority of PVC produced today is polymerized using a suspension polymerization (80%). Approximately 12% is made using emulsion polymerization techniques and 8% is made by bulk polymerization. In the suspension polymerization process, dispersant chemicals are used to suspend drops of vinyl chloride monomer (boiling point, -13°C) in water. A free radical initiator is used to commence the polymerization. This process produces a slurry of PVC grains in water. Due to health concerns surrounding the vinyl chloride monomer – It is a known carcinogen – the polymerization is a closed process. Unique to PVC, the vinyl chloride monomer is largely insoluble in the PVC polymer, facilitating its removal. The molecular weight of the polymer after polymerization, removal of excess monomer, and drying can range from M_w = 39,000 to 168,000 depending on the intended application.[1,2]

4.2.3 PVC plasticizers

PVC – by itself – is a hard, brittle, white solid. For use in electrical cabling as insulation, a number of additives are incorporated into the polymer to improve its properties. Chief among them is the use of a plasticizer. Plasticizers serve to increase the flexibility, workability, and distensibility of the polymer; they can be used at levels as high as 30-45 weight percent or parts per hundred resin (phr). The most common plasticizers used are derived from phthalates. An example plasticizer used throughout this Chapter is diisodecyl phthalate as shown in Figure 4.2.[1]

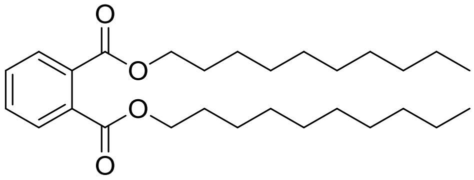

Figure 4.2 - Diisodecyl phthalate (DIDP) – a common PVC plasticizer

There is growing interest in investigating alternate plasticizers to phthalates as they are undergoing increasing scrutiny from a health standpoint.[3] Further, they are directly derived from petroleum, so there is an inherent desire to switch to a material source with a non-volatile price-point. One such alternative plasticizer is epoxidized soybean oil (ESO) as shown in Figure 4.3.

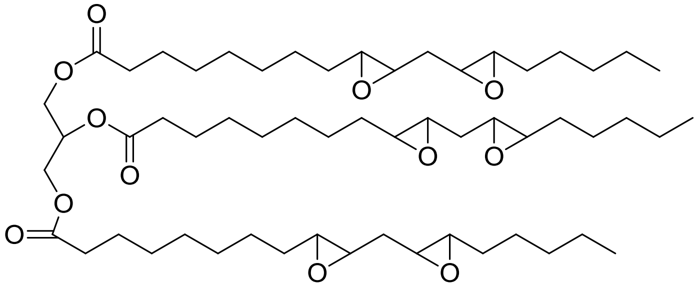

Figure 4.3 - Epoxidized soybean oil (ESO) - a bio-based PVC plasticizer

As its name implies, it is derived from soybeans, a renewable resource. It is often referred to as a bio-based plasticizer. Soybean oil has a high content of double bonds, which are epoxidized using a peroxide or peracid. The epoxide groups serve to increase the plasticizers compatibility with the PVC, aiding to prevent migration of the plasticizer from the polymer.[4] Additionally, described further in this Chapter and in its accompanying Appendix, the epoxide groups are effective HCl scavengers. HCl results from the thermal degradation of the polymer.

4.2.4 Thermal degradation of PVC

Thermal degradation of PVC presents a significant problem for maintaining polymer performance after processing.[5] Thermal degradation can occur when the polymer is exposed to high temperatures (during or post-processing) and continues even after the temperature is lowered – though at a slower rate. PVC processing occurs at temperatures between 17-220°C.[1] The thermal degradation of PVC occurs through release of HCl from the PVC backbone forming the corresponding alkene, shown in Figure 4.4. HCl is a known catalyst for the thermal degradation process; thus as the thermal degradation process proceeds, the rate of degradation increases in an autocatalytic manner.[6]

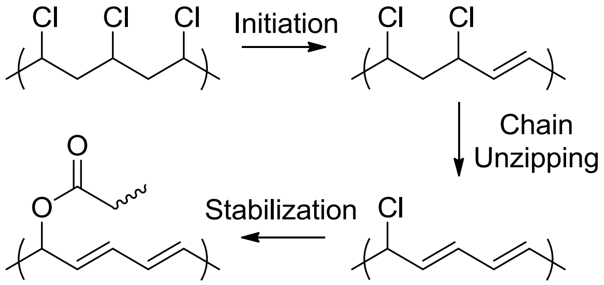

Figure 4.4 - Degradation, chain unzipping, and stabilization of PVC

Figure 4.5 shows several structural arrangements of PVC believed to affect the dehydrochlorination. Defects occur during polymerization and are weak points which can initially trigger thermal degradation.[7,8] After the initial dehydrochlorination, the newly formed allylic chloride is highly reactive and likely to trigger "chain-unzipping." This dehydrochlorination becomes even more favored as the conjugation increases, practically resulting in a chain-dehydrochlorination phenomenon. Practically, this will yield to conjugated double bond domains within the polymer that reduce the optical properties of the PVC (i.e. causing discoloration).[5]

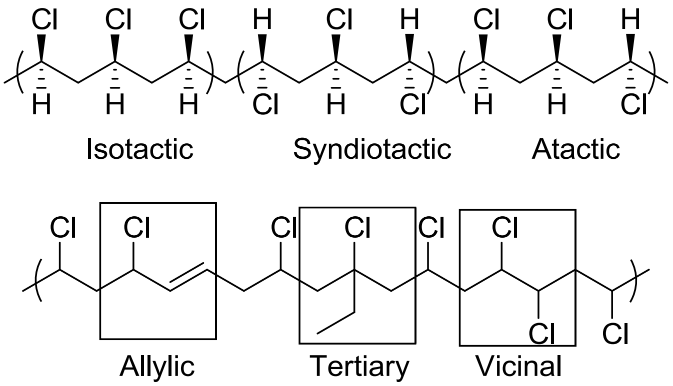

Figure 4.5 - Structural arrangements of PVC that affect the degradation and stabilization of PVC

4.2.5 Thermal stabilizers used in PVC formulations

Thermal degradation is typically mitigated through the addition of thermal stabilizers such as metal carboxylates (e.g., combinations of zinc and calcium stearate, Figure 4.6).

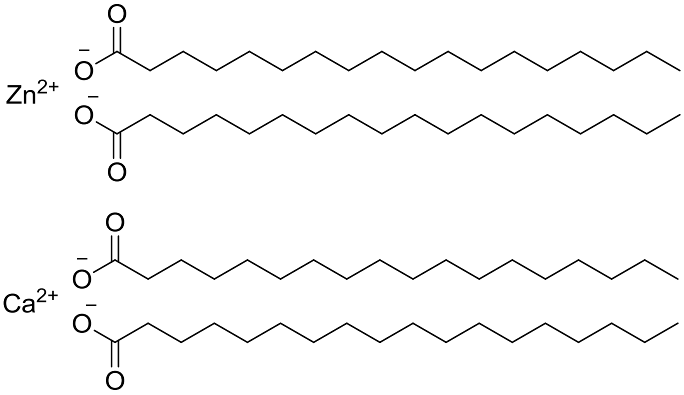

Figure 4.6 - Zinc stearate ($ZnSt_2$) and calcium stearate ($CaSt_2$) – two of the most common thermal stabilizers used in PVC

These metal carboxylates, specifically zinc stearate ($ZnSt_2$), are believed to stabilize PVC via two actions: (1) sequestration of HCl to prevent autocatalysis and (2) substitution of stearate at an allylic chloride to prevent chain-unzipping.[7,9] The sequestration of HCl and the stearate substitution lead to the formation of zinc chloride ($ZnCl_2$), which has been shown to enhance the rate of degradation further.[10] A proposed role of the additional metal stearates, specifically calcium stearate ($CaSt_2$), is to ion exchange with $ZnCl_2$ to regenerate $ZnSt_2$ and form calcium chloride ($CaCl_2$).[11] We hypothesize that these various processes (sequestration of HCl, preventing chain-unzipping, and avoiding formation of species that enhance degradation rates) encompass the overall picture of metal carboxylate stabilization.

4.2.6 Studying the thermal degradation of PVC

Investigating the thermal degradation of PVC itself using standard analytical techniques is intricate due to the inherent complexity of polymer systems. Small structural changes in a PVC blend can be difficult to observe, analyze, quantify and interpret. Labile chlorides account for less than 0.5% of all chlorides in PVC, but their effect on heat stability is critical.[1] Polymer systems are often studied using model compounds or small molecules that replicate the important structural features of the system. For example, the thermal degradation of PVC has been studied extensively via model compounds.[12,13] These studies provide a great deal of understanding of the degradation and stabilization process; however, many of these studies utilize dilute solutions of model compounds that may not directly replicate a bulk polymer system, while others have not investigated the commercial Zn/Ca stabilizer systems.

Herein, parallel studies using PVC model compounds and blends of bulk PVC are presented to study the mechanisms and pathways of degradation and stabilization. Further, based on the understanding developed, novel stabilizers are presented and evaluated against traditional metal carboxylate stabilizers.

4.2.7 Model compounds for PVC

A library of the PVC model compounds which were chosen to simulate defects of PVC is shown in Table 4.1. 1,3-Dichlorobutane **1** models primary and secondary chlorides and is a commercially available candidate. 2,4-Dichloropentane **2** models tacticity (*meso* stereoisomer models isotactic and enantiomeric pair models syndiotactic). Tertiary chloride and vicinal defect were mimicked by 3-ethyl-3-chloropentane **3** and 3,4-dichlorohexane **4**, respectively. 3-Chloro-1-butene **5** and (*E*)-6-chloronon-4-ene **6** specifically model allylic defects. Reactivity studies were performed which compared each of the model compounds with a reactive metal acetate system (model of a metal stearate) in order to compare directly the relative reactivity of each defect and tacticity. Mechanistic studies were conducted in which a single, defect-free, model compound was reacted with various metal stearates to determine rates of reaction and color formation.

Table 4.1 – Library of model compounds

#	Structure/name	Model	Source
1	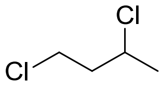 1-,3-dichlorobutane	1° Cl 2° Cl	Commercial
2	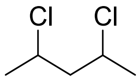 2,4-dichloropentane	2° Cl Tacticity	Synthesized
3	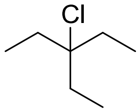 3-ethyl-3-chloropentane	3° Cl	Synthesized
4	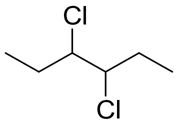 3,4-dichlorohexane	Vicinal	Synthesized
5	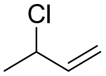 3-chloro-1-butene	Allylic	Commercial
6	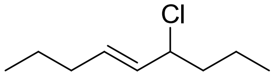 (*E*)-6-chloronon-4-ene	Allylic	Synthesized

4.2.8 Comparison with PVC blends

Model compound studies are only as valid as the degree of similarity to the real system. To provide a direct comparison between the neat model compounds with additives and the plasticized PVC with additives, PVC blends were also studied as a function of additives (i.e. plasticizer and/or stearates), temperature and time. Typical industrial blends of PVC, DIDP or ESO, and metal stearates were prepared (3 g PVC, 30 phr DIDP/ESO, and 5 phr total metal stearates equally divided) and thermally treated. The concentrations used are slightly exaggerated, but on the same relative scale as those used industrially. The overall weight loss of the blend and discoloration were monitored during thermal treatment.

4.2.9 Development of novel stabilizers for PVC

Our research on the performance of traditional stearates in both the PVC model compounds as well as plasticized PVC blends containing DIDP or ESO suggests that there is room for improving their performance. Based on our understanding of the role of metal stearates in mitigating the thermal degradation of PVC we were able to propose, formulate, and evaluate two novel stabilizers for the thermal stabilization of PVC. Both of the developed thermal stabilizers are discussed in detail in the Results and Discussion section.

4.3 Experimental

4.3.1 PVC model compound studies

4.3.1.1 Synthesis of PVC model compounds

Detailed syntheses and characterization of the non-commercial model compounds are available in Appendix C.

4.3.1.2 Reactivity studies using PVC model compounds

Reactivity studies were performed on all of the model compounds with various metal acetates (NaOAc, $Ca(OAc)_2$, or $Zn(OAc)_2$). A solution of the phase transfer catalyst (PTC) tetra-*n*-butylammonium chloride in tetrahydrofuran (THF, 3.0 mL of a 0.33 M solution, 0.001 mol, 0.10 eq) was added to the acetate salt (0.020 mol $^{-}$OAc, 1 eq) under an argon atmosphere with a condenser, heated to 60°C, and stirred overnight to allow the PTC to condition the acetate salt. The THF was then evaporated and tetradecane (0.001 mol) was added as an internal standard and heated to 100°C. The model compound (0.0400 mol, 2 eq) was added and the resulting slurry was stirred throughout the reaction. Aliquots were taken periodically, filtered to remove any solids, and quantitatively diluted in THF for analysis.

Mechanistic studies using 2,4-dichloropentane with various stearates (e.g., $ZnSt_2$ and $CaSt_2$) at the parts per hundred resin scale (phr, grams of additive per 100 grams of polymer or model) were performed in sealed glass reaction vessels. For example, 2,4-dichloropentane (5.655 mmol) was added to zinc stearate (0.0315 mol, 2.5 phr) and calcium stearate (0.0328 mol, 2.5 phr). The resulting slurry was transferred to the reaction vessel (thick walled NMR tube or Ace Glass pressure tube #8648-03) which was subsequently purged with argon and sealed (i.e., the NMR tube was flame sealed or the glass pressure tube capped). The reaction vessel was then heated *via* an oil bath for the desired reaction time then cooled. Higher concentration studies were also performed with 0.10 equivalents of additive (to 1 eq of 2,4-dichloropentane).

4.3.1.3 Model reaction analysis

Model compounds reactions were monitored via gas chromatography-mass spectroscopy (GC-MS) using a Shimadzu GCMS-QP2010P fitted with a Supelco PTA-5 (30m x 0.32 mm x 1.00 µm, length x inside diameter x film thickness) capillary column and/or nuclear magnetic resonance (NMR). Reaction samples were diluted quantitatively in THF and injected into the GC at 250°C with a mobile phase of helium (70.1 kPa, 40 cm/sec). The oven temperature was ramped from 50°C to 250°C at a rate of 15°C/min.

The MS was operated in electron impact mode with an ion source and interface temperature of 225°C. For NMR, a 1 mm d_6-DMSO capillary was used as the lock solvent. An elevated temperature (e.g., 100°C) was necessary to ensure homogeneity of the reaction mixture.

4.3.2 PVC blend studies

4.3.2.1 PVC blend preparation

Initially, attempts were made to cast PVC samples as films using tetrahydrofuran (THF) as the solvent. A solution of PVC powder (6 wt. %) in THF was cast on a glass plate at room temperature. The film was exposed to air for three hours and then dried in a vacuum oven at 6 mm Hg and 35℃ for 12 hours. After vacuum, the film was exposed to CO_2 at 50℃ and 850 psi for two hours in a stainless steel high pressure vessel. After two hours, the pressure vessel was rapidly depressurized to remove any residual THF. However, thermogravimetric analysis (TGA) and ATR-FTIR demonstrated that approximately 1 wt% THF remained in the cast film (Figure 4.7).

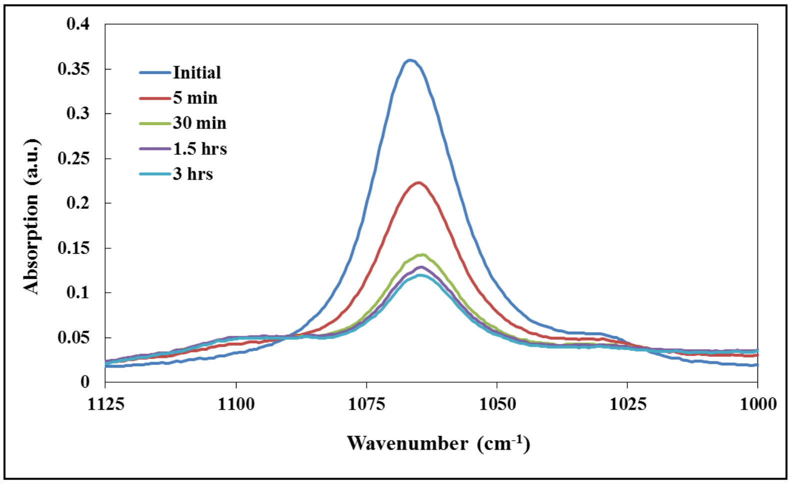

Figure 4.7 - FTIR of PVC films cast with THF and oven dried for various amounts of time; the peak at 1070 cm^{-1}, is indicative of THF

Dry-blended samples were prepared to remove the possibility of residual solvent (e.g., THF) effects. Dry-blended samples consisted of 3 g of PVC powder, 30 phr (0.9 g) plasticizer (DIDP or ESO), and 5 phr (0.15 g) additional additives ($ZnSt_2$ and/or $CaSt_2$ and/or novel additives prepared). The PVC powder and one-half of the plasticizer (0.45 g) were physically combined, heated to 95°C in an oil bath, and thoroughly mixed. Separately, the remaining plasticizer and all other additives were combined and heated to 95°C. The two mixtures were then combined and heated to 95°C and thoroughly mixed. This temperature was chosen as it is above the glass transition temperature of PVC (approximately 80°C) and should facilitate absorption of the additive by the PVC. Blending the plasticizer with the PVC in two separate steps allowed the complete uptake and uniform distribution of the additives which do not blend well with PVC on their own.

4.3.2.2 Thermal analysis of PVC blends

Thermogravimetric analysis (TGA) was performed using a TA Instruments TGA Q50-0500 to investigate thermal degradation of the various blends. Several isothermal weight loss studies were conducted at 150, 160, 170, and 180°C for three hours under a flow of nitrogen (100 mL/min). Most isothermal weight loss studies were conducted at 170°C for two hours under a flow of nitrogen (100 mL/min). Constant temperature ramp rate studies were conducted at 1, 5, and 10℃ per minute from 20℃ to 500℃. In all cases, approximately 20 mg of a dry blended sample was used. Each blend was prepared at least twice for repeatability and the data and images shown are representative examples.

4.3.2.3 UV-visible spectroscopy study of PVC

UV-visible studies of PVC were performed using an Agilent Cary Series UV-visible spectrophotometer. Scans were recorded over a range of 200-600 nanometers.

PVC samples (~50 mg) were first loaded into the TGA and an accurate mass was recorded. The TGA was used to precisely heat the sample to 180°C for a specific duration. The heated samples were immediately removed from the TGA upon completion of the run and dissolved in THF to obtain equal concentrations. UV-visible spectra were obtained in triplicate to ensure repeatability between samples.

4.3.2.4 Color studies of model compounds and PVC blends

Photographs were taken after thermal treatment of several in several of the PVC model compound studies as well as of the heat PVC blends studied. The photographs were used to compare discoloration of the model compound or PVC polymer. Discoloration was not quantified but was rather only used in a qualitative sense.

4.3.3 Synthesis of novel sacrificial epoxide stabilizers

The synthesis of the two novel sacrificial epoxide stabilizers is shown in Figure 4.8. The detailed experimental procedure is provided in the associated Appendix. In general, linolenic acid, a natural occurring compound, was reacted with peracetic acid at 0°C over two hours. Sodium hydroxide in a methanol solution was added to form the corresponding sodium salt. Following addition, zinc or calcium acetate (depending on the metal salt desired) in water was added and the solution was cooled to 0°C. A white precipitate evident of the product was formed. The solid was then filtered and characterized for use.

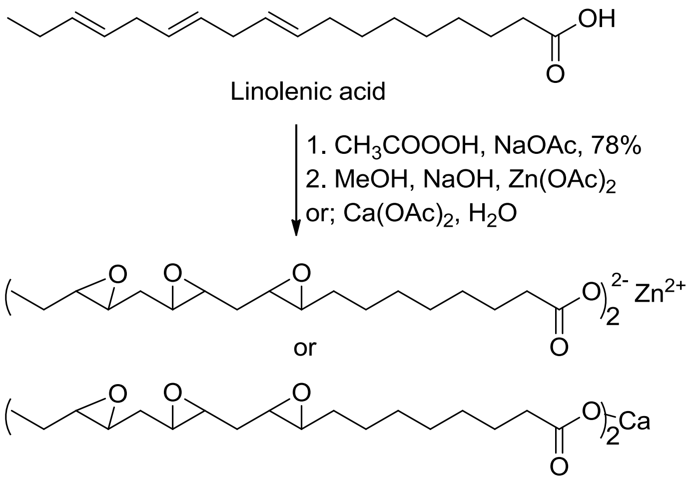

Figure 4.8 - Synthesis of novel sacrificial epoxide stabilizers

4.3.4 Synthesis of novel maleimide stabilizers

The two novel maleimide stabilizers were prepared from the commercially available 11-maleimido-decanoic acid. A sodium hydroxide solution was added to the 10-maleimide-decanoic acid in water to form the sodium salt. Zinc or calcium acetate was then added to form the corresponding zinc or calcium salt. The solution was cooled to 0°C and a white precipitate was collected to yield the desired product.

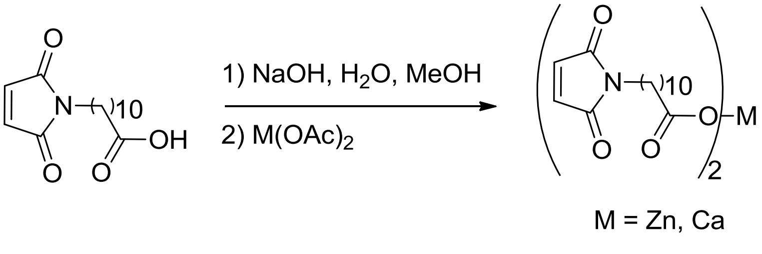

Figure 4.9 - Synthesis of novel maleimide stabilizers

The detailed experimental procedure is included in the associated Appendix.

4.4 Results and Discussion

The Results and Discussion section is divided between the model compound studies and the studies of the bulk PVC blends. Where relevant, comparisons between the two are made. Near the end of the section, the performance of the two novel stabilizers proposed is evaluated.

4.4.1 PVC model compound studies

4.4.1.1 Kinetic studies using model PVC compounds with acetates

Neat reactions of the model compounds (i.e. no additional solvents) were used to replicate the polymer matrix by preventing any solvent effects from influencing the reactions.[12] As such, relatively large amounts of each model compound were synthesized to be able to perform each reaction under neat conditions. Calcium, zinc, and sodium acetates were chosen as models for common metal stearates that are often added to PVC. Our goal was to determine the relative reactivities of the various model compounds and provide a measure of how susceptible defects and tacticities are to various degradation/stabilization pathways, as shown in Figure 4.10. While the reaction rates would not be identical to those in PVC, the relative rates of reaction are not expected to vary significantly.

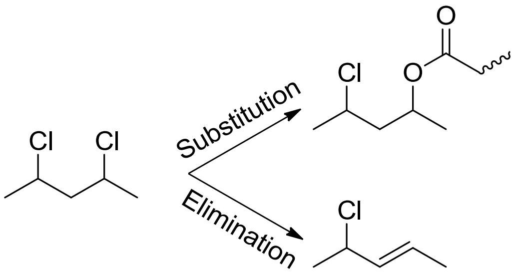

Figure 4.10 - Expected reaction pathways for the model compounds through substitution (stabilization) or elimination (degradation) when reacted with metal carboxylates

Initially, 1,3-dichlorobutane **1** was reacted with NaOAc, $Ca(OAc)_2$ or $Zn(OAc)_2$ at 100°C, but no reaction was detected after two days. The lack of reaction was attributed to the poor solubility of the metal acetates in the model compound. Tetra-*n*-butylammonium chloride, a phase transfer catalyst (PTC), was employed to improve the solubility of the metal acetate and resulted in a successful reaction. The apparent, pseudo-first order reaction rates (k_{app}) of **1** with the various metal acetates and a PTC are summarized in Table 4.2 given

$$-\frac{dC_1}{dt} = kC_1C_{MOAc} = k_{app}C_1$$

where k is the reaction rate, C_1 is the concentration of the model compound, and C_{MOAc} is the concentration of the metal acetate (assumed constant due to the presence of a PTC [14]).

Table 4.2 - Summary of Apparent Reaction Rates - 1,3-Dichlorobutane with various metal acetates (0.1 eq $^{-}$OAc) at 100°C

Metal Acetate	$\boldsymbol{k_{app}}$ ($\cdot 10^{-4}$ min^{-1})
NaOAc	4.61 ± 0.44
$Ca(OAc)_2$	1.13 ± TBD
$Zn(OAc)_2$	0.612 ± TBD

The overall rate of disappearance of **1** decreases as the metal acetate is changed from NaOAc to $Ca(OAc)_2$ to $Zn(OAc)_2$. The reaction resulted in various substitution products (chloride substituted by acetate) and the product selectivities were found to be independent of the metal cation. While the difference in apparent reaction rates can be attributed to the solubility effects of the PTC on the metal acetates, for the purpose of determining the relative reactivities of the various model compounds, as shown in Table 4.3, (and hence, the defects/tacticities they model) NaOAc was chosen for further model compound screening as it was the fastest to react.

Table 4.3 - Summary of apparent reaction rates - Model compounds with sodium acetate (0.1 eq NaOAc) at 100°C

#	Structure	k_{app} ($\cdot 10^{-4}$ min^{-1})
1	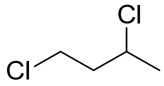	4.61 ± 0.44
2a	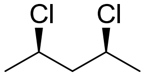	6.51 ± 0.53
2b	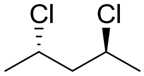	2.86 ± 0.03
3	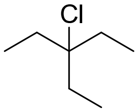	3.91 ± 1.28[1]
4a	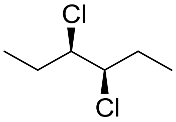	2.25 ± 0.13
4b	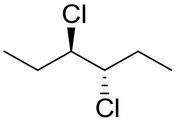	0.40 ± 0.25
5	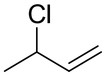	27.8 ± 2.1
6	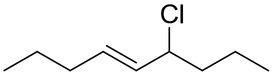	17.9 ± 1.3

[1] Proceeds via a zero-order reaction (k_{app} units of 10^{-4} mol min^{-1}L^{-1})

2,4-Dichloropentane provides the opportunity to explore tacticity as the *meso* stereoisomer **2a** is a model for isotactic PVC whereas the enantiomeric pair **2b** is model for syndiotactic PVC. The diastereomeric ratio is approximately 1.6 (*meso*:enantiomeric pair) and the two stereoisomers are easily discernible by GC-MS and NMR. **2a** reacts faster than **2b** (due to the steric hindrance of **2b** slowing substitution) with 0.1 eq of NaOAc at 100°C forming the corresponding 4-chloropentan-2-yl acetate and, eventually, the pentan-2,4-diyl diacetate. This agrees with reported findings that isotactic PVC is more readily stabilized than syndiotactic PVC .[15]

The tertiary chloride model **3** showed small amounts of the substitution product (pentan-3-yl acetate) at short reaction times (1 hour); however, the only product when the reaction was completed (1 day) was the elimination product (3-ethylpent-2-ene). The vicinal defect models **4a** and **4b** (representing the *meso* and enantiomeric pair stereoisomer, respectively) are less reactive than **2a** and **2b** and are therefore not believed to play a significant role in the degradation or stabilization processes. The allylic models **5** and **6** react very quickly to form their elimination products (1,3-butadiene, and (3*E*,5*E*)-nona-3,5-diene, respectively) while no detectable amounts of the substitution products were detected. As the reaction conditions are favorable for acetate substitution, by analogy chloride substitution by a stearate would be expected to be slower and not a major stabilization pathway.

These elimination and substitution pathways are analogous to degradation and stabilization processes, respectively. The allylic model compounds (**5** and **6**) and the tertiary model compound (**3**) form the corresponding eliminated (or degraded) alkenes. It is likely, as proposed in the literature, that these defects would be the weak links in the

PVC backbone by which the degradation process initiates.[7,8] After initiation at one of these sites, an α-chloroalkene is formed which is likely to eliminate further, propagating the degradation process. However, contrary to previous reports, we found no evidence of substitution of allylic chlorides by carboxylates. In terms of substitution (i.e. stabilization), the isotactic PVC models undergo substitution faster than the syndiotactic PVC models.

4.4.1.2 Mechanistic studies using model PVC compounds with stearates

The metal acetates and the phase transfer catalysts were replaced with metal stearates, which are more soluble at elevated temperatures, do not require a PTC, and provide a more realistic model system. 2,4-Dichloropentane, as a mixture of stereoisomers **2a** and **2b** of Table 4.3, was used for these studies as it is the most representative of defect-free PVC. The reactions were carried out in sealed vessels. The evolution of color as a function of heat and time was monitored to gain further insights as color changes are one of several indicators of degradation.[16] Upon heating, the initial colorless reaction mixture would typically turn yellow, deep brown and finally black as seen in Figure 4.11.

Figure 4.11 - Typical color change of 2,4-dichloropentane with $ZnSt_2$ and $CaSt_2$ during the degradation process

The rate of color change varied greatly depending on the additives as summarized in Table 4.4. 2,4-Dichloropentane without any additives exhibited no color change after 3 days. However, when 5 phr of $ZnSt_2$ was added, the color of the reaction mixture changed rapidly (~8 min) to brown suggesting a fast degradation (and implies that the $ZnSt_2$ may contribute to the thermal degradation of PVC). This was anticipated since $ZnSt_2$ can act as a Lewis acid, facilitating dehydrochlorination to yield stearic acid and $ZnCl_2$, an even stronger Lewis acid. In fact, when $ZnSt_2$ was replaced with $ZnCl_2$ (equimolar in Zn), the color change was accelerated (~5 min) despite its much lower solubility.

Table 4.4 - Qualitative color change study for the reaction of 2,4-dichloropentane with various additives. NR - No reaction in 180 minutes; NA - Color change not seen

Additive 1	Additive 2	Time to Color Change (minutes)		
		Yellow	**Brown**	**Black**
None	None	NR	NR	NR
$ZnSt_2$ (5 phr)	None	NA	8±2	11±1
$ZnSt_2$ (2.5 phr)	$CaSt_2$ (2.5 phr)	102±10	131±6	159±20
$ZnSt_2$ (5 phr)	$CaSt_2$ (2.5 phr)	85±5	100±0	119±12
$ZnCl_2$[1]	None	NA	5±2	8±2
$ZnCl_2$[1]	$CaSt_2$ (2.5 phr)	21±0	27±2	43±2

[1] Equimolar in Zn to 5 phr of $ZnSt_2$.

Zinc stearate is rarely used as the sole stabilizer; it is often used in combination with other stearates, namely calcium stearate.[17] In all cases, the addition of $CaSt_2$ delayed the formation of color compared to identical mixtures without the $CaSt_{2.}$ This reaction is enthalpically favored and would delay the formation of the potent $ZnCl_2$. Color change is one measure of stability and degradation but it does not indicate the structural changes that occur.

Reactions of 2,4-dichloropentane with higher concentrations of additives were used to monitor structural changes of the 2,4-dichloropentane by NMR after 3 hours at 140°C. Typical ^1H NMR spectra of 2,4-dichloropentane and zinc stearate are shown in Figure 4.12. All NMR spectra were acquired at 100°C to ensure all solids were solubilized and the sample homogeneous. It is easy to discern the *meso* stereoisomer **2a** (denoted by primes " ′ " in Figure 4.12) from the enantiomeric pair **2b** using the signal from the ipso proton to the chloride (b and b′ in Figure 4.12). The aliphatic protons of the stearate (CH_2's labeled f in Figure 4.12) can be used as an internal standard to evaluate the disappearance (i.e., degradation) of 2,4-dichloropentane.

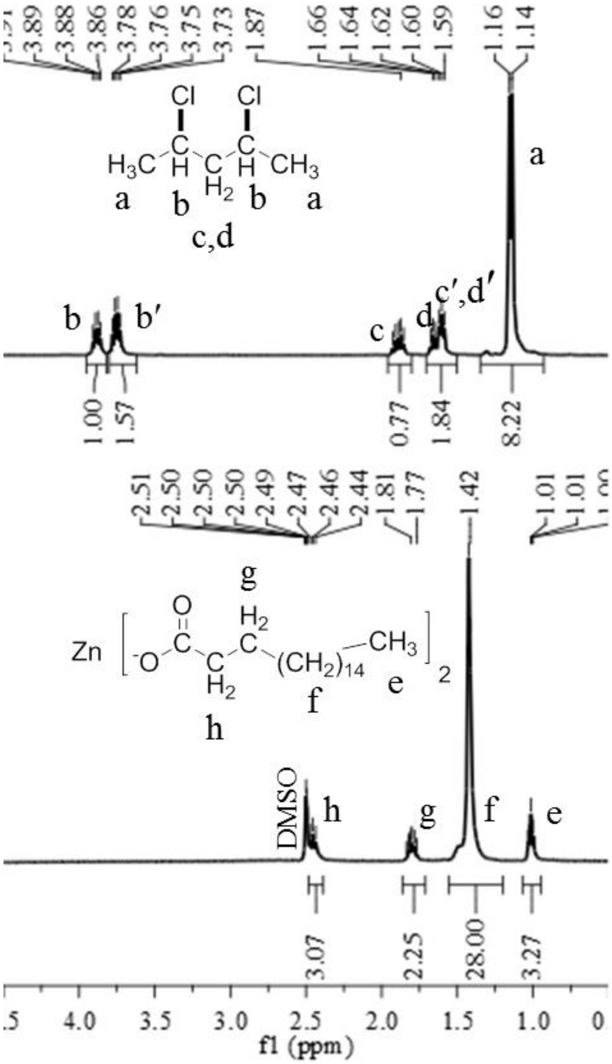

Figure 4.12 - Selected NMR spectra at 100°C - TOP - ^{1}H NMR of neat meso-2,4-dichloropentane (denoted with ′) and (2*S,4*S**)-dichloropentane with DMSO capillary - BOTTOM – ^{1}H NMR of zinc stearate in o-dichlorobenzene (a nonreactive solvent) with a DMSO capillary**

Stereoisomer ratios and conversions for reactions of 2,4-dichloropentane with various additives are shown in Table 4.5. Typical NMR spectra of the reaction between 2,4-dichloropentane and $ZnSt_2$ are shown in Figure 4.13.

Table 4.5 – Summary of reactions of 2,4-dichloropentane with various additives at 140°C for 3 hours

Additive 1	Additive 2	*Meso*:Enantiomeric Pair	2,4-Dichloropentane Conversion (%)
PRIOR TO REACTION		1.57	--
NONE	NONE	1.57	0
$ZnSt_2$ (0.1 eq)	NONE	0.71	75
$ZnSt_2$ (0.05 eq)	$CaSt_2$ (0.05 eq)	0.99	42
$ZnSt_2$ (0.1 eq)	$CaSt_2$ (0.05 eq)	0.74	56

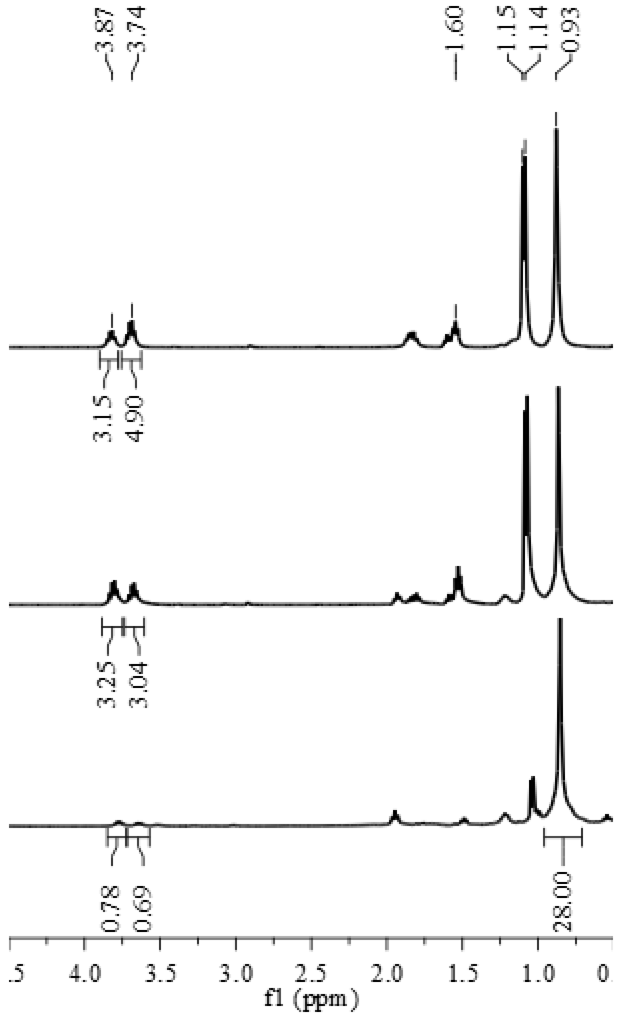

Figure 4.13 – ^{1}H NMR spectra from the reaction of 2,4-dichloropentane with $ZnSt_2$ at 140°C. TOP – Prior to reaction. MIDDLE – 1.5 hours of reaction time. BOTTOM – 3 hours of reaction time. Each spectra is normalized to the aliphatic protons of the stearate (CH_2's labeled f in Figure 4.12)

The two main observations are (1) **2a** (*meso*) reacts much faster than **2b** (enantiomeric pair) and (2) no new significant product peaks appear in the reactions with $ZnSt_2$; we see only disappearance of the model compound. These results mirrors the ones obtained in the NaOAc + PTC studies (Table 4.3) and are consistent with literature reports.[7,9] This also indicated that while the isotactic model is stabilized faster than the syndiotactic model, the isotactic model also degrades faster. This reaction demonstrates that $ZnSt_2$ can cause the degradation of defect-free systems.

Once the reaction is complete (i.e., when the 2,4-dichloropentane was no longer detectable), the only species that is present is stearic acid, confirmed by ^{13}C NMR. As each NMR spectrum is recorded at an elevated temperature, we should caution that any volatile compounds (i.e., the alkene elimination products) in the vapor phase would not be seen through the NMR analysis. We therefore complemented our NMR study with GC-MS head-space analyses. And in fact, the vapor phase analysis indicates the presence of products supporting the formation of carbocation intermediates (e.g., chloride abstraction by $ZnSt_2$ resulting in a carbocation).

As the qualitative color studies indicated that the presence of $CaSt_2$ mitigated the deleterious effects of $ZnSt_2$, it was necessary to investigate similar mixtures containing $CaSt_2$ with ^{1}H NMR. The presence of $CaSt_2$ in a mixture containing either $ZnSt_2$ or $ZnCl_2$ slowed the consumption of 2,4-dichloropentane as compared to mixtures without $CaSt_2$. This corroborates and validates the conclusions from the color studies (i.e., that the color is indicative of degradation of the 2,4-dichloropentane and that $CaSt_2$ mitigates the negative impact caused by zinc compounds).

The proposed overall mechanism for the reactions between PVC and metal carboxylates as determined by reactions involving model PVC compounds is shown in Figure 4.14. Zinc stearate could complex with a chloride on the backbone to promote its abstraction, forming a carbocation (as supported by the analysis of the reactions' vapor phase). The carbocation could then undergo elimination as no substitution products were seen. The stearate in the zinc complex could abstract a proton (Step 2, Figure 4.14) to form stearic acid, ZnClSt, and the corresponding alkene. This process could repeat until $ZnCl_2$ is formed.[18] $ZnCl_2$ and $CaSt_2$ could then ion exchange (Step 3, Figure 4.14) to prevent accumulation of $ZnCl_2$, regenerate $ZnSt_2$, and form the enthalpically favored $CaCl_2$. The regenerated $ZnSt_2$ could then continue to react with the PVC backbone (Step 4, Figure 4.14). As there was no substitution of stearate detected with the model compounds and reactions with NaOAc + PTC have shown that allylic chlorides are much more likely to eliminate rather than substitute, the primary stabilization mechanism seems to be the prevention of the very strong Lewis acid $ZnCl_2$. We have also demonstrated evidence of $ZnSt_2$ causing degradation of a defect-free system.

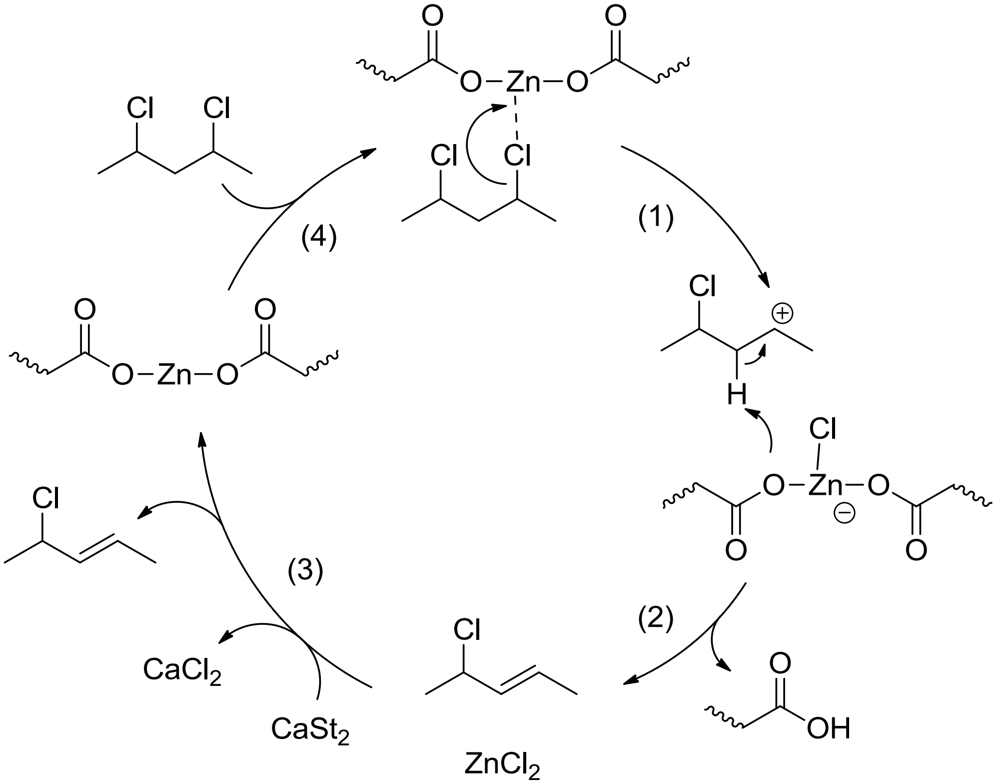

Figure 4.14 - Proposed mechanism of the degradation and stabilization of PVC as indicated by reactions of model compounds

4.4.2 Studies of bulk PVC blends

4.4.2.1 PVC and plasticizer blends at an elevated temperature

Figure 4.15 shows the weight loss of virgin PVC along with blends of PVC with two plasticizers – DIDP and ESO (in 30 phr concentrations) during thermal treatment at 170°C for 2 hours. The temperature 170°C was chosen as an ideal temperature to study because it is within the typical industrial processing window of temperatures used, and it allowed adequate differentiation of weight loss between blends. Initially temperature ranges of 150, 160, 170, and 180°C were studied, but for comparison studies, 170°C was found to be sufficient. Weight loss is reported with respect to PVC, excluding the additives.

From Figure 4.15, it is immediately clear that PVC + DIDP lost significantly more weight than virgin PVC or PVC + ESO. In a control experiment, the plasticizer DIDP was treated at 170°C for 2 hours; using the data obtained (available in the Appendix), the loss of DIDP only accounts for 0.027% of the weight loss. This is plausible as it is the minor component in the blend. We hypothesize the increased weight loss of PVC + DIDP compared to PVC is due to a plasticization effect. The DIDP plasticizer facilitates movement of the polymer chains, facilitating the escape of HCl.

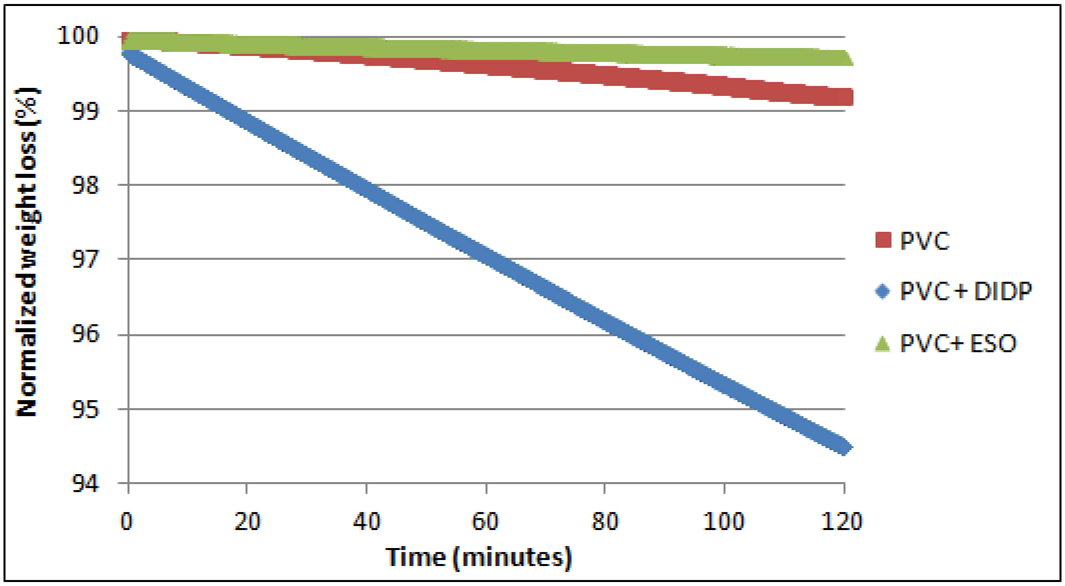

Figure 4.15 - Weight loss at 170°C over 2 hours for PVC of PVC and plasticizer blends; weight normalized against the mass of PVC in each blend

The blend of PVC + ESO actually loses less weight after 2 hours than virgin PVC; it exhibits a stabilization effect. The stabilization effect is a result of the epoxide rings on the backbone of the epoxidized soybean oil. As HCl is released from the degrading PVC polymer, it is scavenged by the epoxide rings of ESO as shown in Figure 4.16. The point at which release of HCl loss dominates as a result of the opening of all available epoxide rings is not evident in the 2 hour period studied. While scavenging of HCl was initially considered a desirable feature of epoxidized soybean oil, it is important to note that as the HCl is scavenged, the plasticizer properties of ESO change, leading to deleterious polymer blend performance. Maintaining the integrity of the ESO plasticizer is a desired. The opening of epoxide rings by HCl was studied and the results are included in the Appendix.

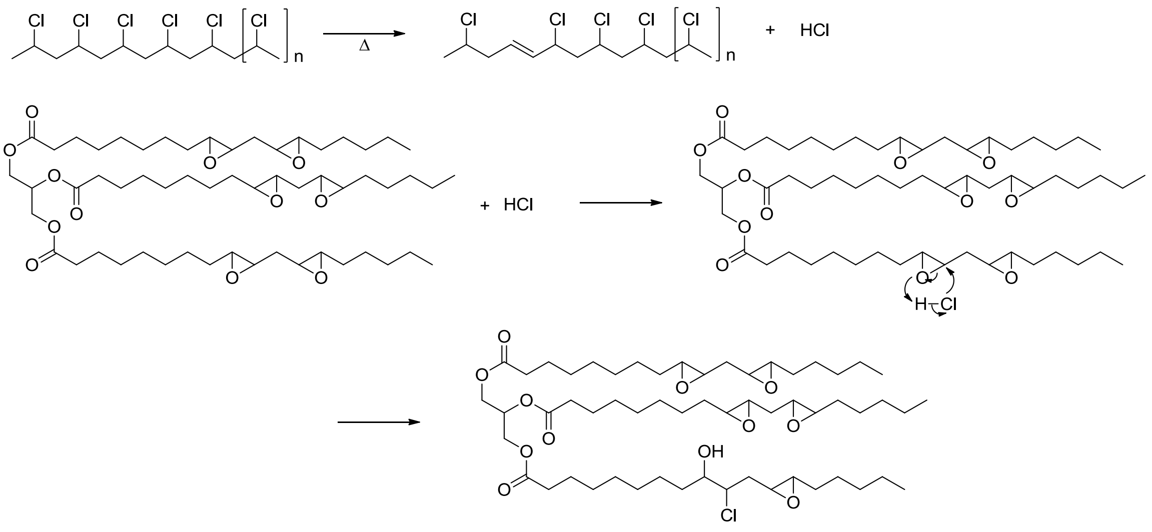

Figure 4.16 - Method of HCl scavenging by epoxidized soybean oil

Virgin PVC loses less than 1 percent of its weight after thermal treatment at 170°C for 2 hours. While the weight loss profile is certainly desirable, it is important to remember that virgin PVC is too rigid and brittle for most applications, and plasticizers are required to increase processibility. However, virgin PVC provided a good starting point to begin the thermal studies. To further confirm that the weight loss observed was a result of the previously explained ‘chain unzipping’ (section 4.2.4) and HCl release, UV-visible measurements were taken for samples heated at 180°C over a period of 45 minutes (180°C was chosen to accelerate degradation). The resulting spectra are shown in Figure 4.17. A clear increase in the overall absorption area as a function of time heated can be seen, corresponding to an overall increase in conjugation in the polymer system. Overlaid on top of the spectra are markers corresponding to the absorption of various lengths of conjugated alkenes. As the spectra shows, degraded PVC contains olefins in conjugation from 3 to over 11 double bonds in length. It was initially expected that the area of the high wavelengths – representing extended conjugation – would increase over time. However, it was found from prior studies that as conjugation increases, rearrangements and other chemistries can take place leading to the loss of volatile compounds, effectively limiting the maximum amount of conjugation observed.

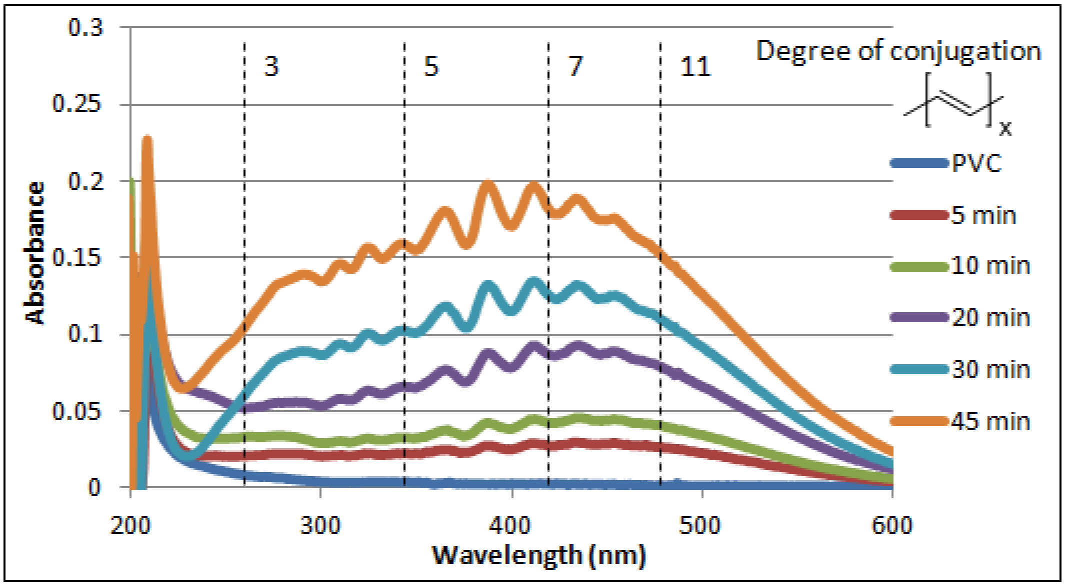

Figure 4.17 - UV-visible spectra of virgin PVC heated at 180°C for varying time increments

Shown in Table 4.6 is the discoloration of virgin PVC and the plasticized PVC blends after thermal treatment at 170°C for 2 hours as reported initially in Figure 4.15. Though the differences are hard to observe from the photographs shown, the ESO-plasticized PVC blend evidences the least discoloration; however all of the blends are relatively similar. These photographs will be used as a reference for the remainder of the Chapter. Not only is thermal weight loss an important indicator of degradation, discoloration of the polymer is as well. Combined with the quantitative thermal studies, the qualitative photographs provide a more holistic picture of the degradation occurring.

Table 4.6 - Color comparison of PVC and plasticizer blends after thermal treatment

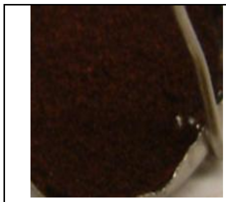 PVC	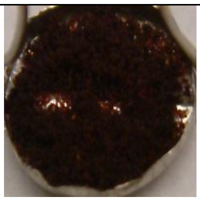 PVC + DIDP	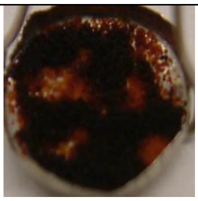 PVC + ESO

4.4.2.2 Determination of activation energy of dehydrochlorination

Activation energies for the initial steps of the PVC degradation process were determined by thermogravimetric analysis (TGA) for PVC and PVC + ESO. PVC weight percent was calculated with respect to the amount of PVC in the blend excluding the additives. The weight of any ESO in the blend was assumed constant. The Arrhenius equation was used to calculate the activation energy $k = Ae^{-\frac{E_a}{RT}}$ where k is the rate of degradation, A is the frequency factor, E_a is the activation energy of degradation, R is the gas constant, and T is the temperature. The isothermal weight loss data of virgin PVC at various temperatures is shown in Figure 4.18 as an example. The first 30 minutes of the isothermal weight loss data were used to determine the initial rate of degradation assuming first order kinetics at each temperature. The activation energy for the initial degradation for PVC is 117 ± 4 $\mathrm{kJ \cdot mol^{-1}}$ while that for PVC with 30 phr of ESO is 61.7 ± 0.4 $\mathrm{kJ \cdot mol^{-1}}$. The weight loss of ESO alone using the same procedure showed minimal weight loss (see Appendix).

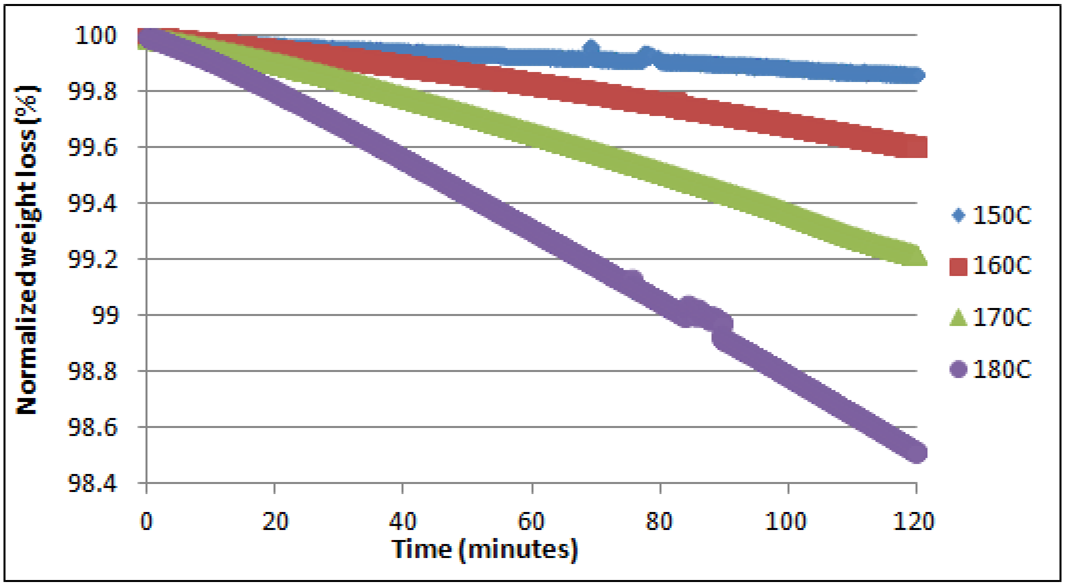

Figure 4.18 - Isothermal weight loss of virgin PVC over 2 hours at 150, 160, 170, and 180°C

The ASTM E698 method[19] for determining activation energies through the use of constant heating rate weight loss studies determined that the activation energies of the bulk thermal degradation of PVC and PVC with 30 phr ESO are 147 kJ·mol^{-1} and 102 kJ·mol^{-1}, respectively. In both cases (i.e., initial degradation and bulk degradation), the activation of the PVC alone was higher than that of the PVC with 30 phr ESO. However, the overall weight loss is less when PVC is mixed with 30 phr ESO than the weight loss of PVC alone. This could indicate that when a plasticizer (e.g., ESO) is used along with PVC, the release of HCl occurs more readily but the ability of ESO to scavenge the HCl prevents autocatalytic degradation, thus reducing the overall amount of thermal degradation. In practice this is undesirable, as ring-opened epoxides increase the hydrophilicity of the blend leading to migration of the plasticizer from the polymer.

4.4.2.3 PVC, DIDP, and stearate blends at elevated temperature

Figure 4.19 shows weight loss of DIDP-plasticized PVC with metal stearate stabilizers at 170°C for 2 hours. DIDP-plasticized PVC blended with $ZnSt_2$ showed very little weight loss for the first 10 minutes of the thermal treatment; however, a catastrophic weight loss occurred thereafter losing a total of 30% of its original mass. Plasticized PVC with $CaSt_2$ lost 7.5% of its original PVC. Plasticized PVC with a mixture of $ZnSt_2$ and $CaSt_2$ lost 9.9%; it is buried in the graph between the PVC+ DIDP and PVC + DIDP + $CaSt_2$ blends. Plasticized PVC with $ZnCl_2$ (equimolar in zinc compared to the plasticized PVC with $ZnSt_2$) showed a rapid weight loss, losing 51.5% of the original PVC mass.

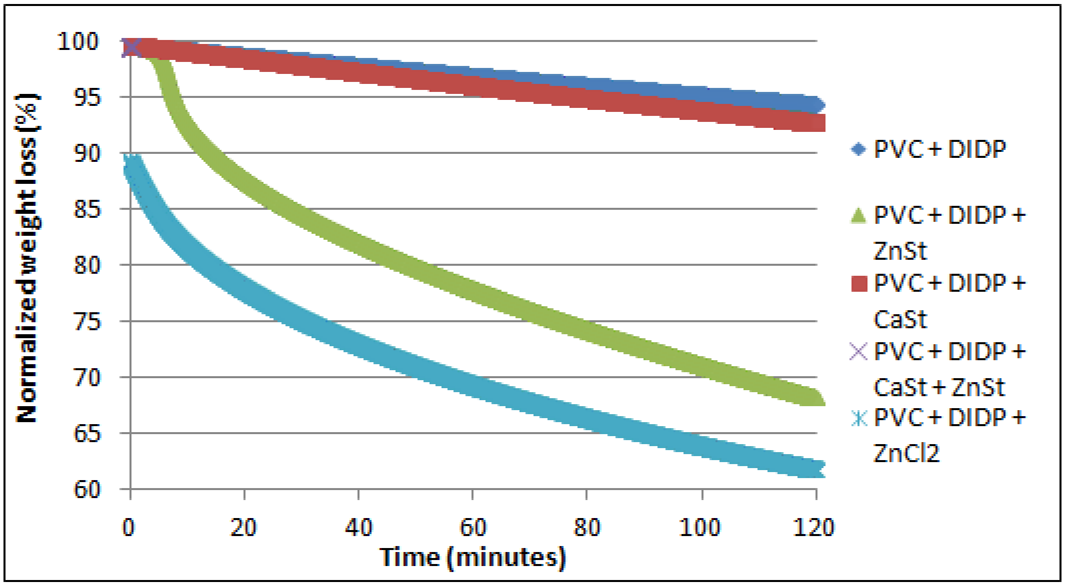

Figure 4.19 - Weight loss of DIDP-plasticized PVC blends during the heat treatment and degradation process at 170°C; weight normalized against the mass of PVC in each blend

DIDP-plasticized PVC displays poor color stability (Table 4.7); the discoloration is similar to that of virgin PVC. The blend of DIDP-plasticized PVC and $ZnSt_2$ showed very poor color stability as it changed from a white powder to a black powder. Plasticized PVC with $CaSt_2$ showed similar color stability to that of the DIDP-plasticized PVC without additives and the virgin PVC. Plasticized PVC with a mixture of $ZnSt_2$ and $CaSt_2$ lost 9.9% of its original PVC mass but showed the best color stability of the blends prepared. Whereas all other blends changed from a white powder to a dark brown or black powder, the plasticized PVC with a mixture of $ZnSt_2$ and $CaSt_2$ changed from a white powder to a heterogeneous mix of yellow and black powder.

Table 4.7 - Color comparison of DIDP-plasticized PVC blends after thermal treatment

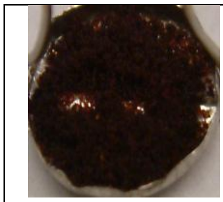	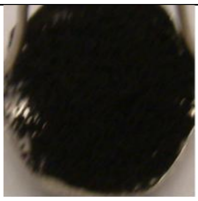	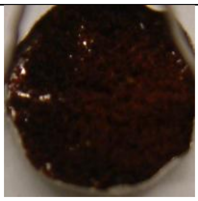	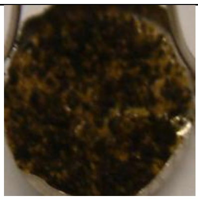
PVC + DIDP	+ $ZnSt_2$	+ $CaSt_2$	+ $ZnSt_2$ + $CaSt_2$

The thermal weight loss and discoloration results correlate well with the results from the model compound studies. $ZnSt_2$ contributes detrimentally to the degradation of PVC in terms of weight loss and color stability just as $ZnSt_2$ contributes detrimentally the degradation of 2,4-dichloropentane. Similarly $ZnCl_2$ has a catastrophic effect on the stability of both PVC and 2,4-dichloropentane. The plasticized PVC with $ZnSt_2$ is thermally stable (in terms of weight loss) for an appreciable time, during which $ZnCl_2$ is likely formed and then causes the catastrophic weight loss and color degradation. This is evidenced by the similarity in the weight loss trends. These experiments also demonstrate the validity of using neat model compound studies to investigate the degradation of PVC. The mechanistic cycle presented in Figure 4.14 holds true.

4.4.2.4 PVC, ESO, and stearate blends at an elevated temperature

The thermal weight loss profiles of ESO-plasticized PVC blends with metal stearates at 170°C over 2 hours are shown in Figure 4.20. What should immediately stand out is that compared to the DIDP-plasticized blends shown in Figure 4.19, the overall weight loss is much less (less than 2% for all blends presented here). However, upon comparison, it is apparent that the shapes of the individual weight loss curves are the same. As presented earlier, ESO exhibits a stabilization effect; in these results this stabilization effect delays the onset of degradation. A drastic drop in weight is still seen for the ESO-plasticized blend with $ZnSt_2$, however it occurs much later – near the 2 hour mark.

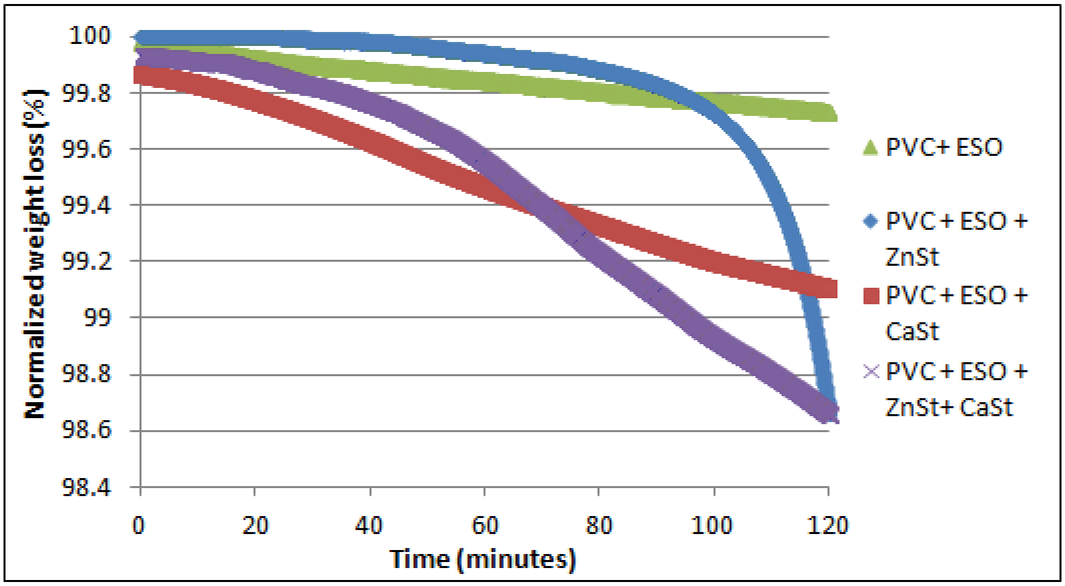

Figure 4.20 - Weight loss of ESO-plasticized PVC blends during the heat treatment and degradation process at 170°C; weight normalized against the mass of PVC in each blend

A comparison of the discoloration of the ESO-plasticized blends is shown in Table 4.8. The ESO-plasticized blend with no additive closely resembles that of PVC, as does the blend with $CaSt_2$. The ESO-plasticized blends with $ZnSt_2$ and a combination of the stearates ($ZnSt_2$ + $CaSt_2$) exhibit excellent color stability however. The blend of ESO-plasticized PVC with $ZnSt_2$ and $CaSt_2$ exhibited the most admirable qualities, with a slow rate of degradation in the weight loss study (Figure 4.20) and minimal discoloration (Table 4.8). The results further confirm the synergistic effect of using both calcium and zinc stearate. As shown in the model studies, we believe the calcium stearate serves to ion exchange with any zinc chloride formed as a result of the reaction of the zinc stearate with the degrading polymer.

Table 4.8 - Color comparison of ESO-plasticized PVC blends after thermal treatment

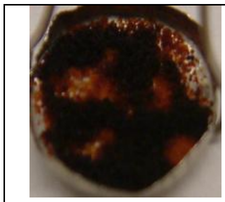 PVC + ESO	 + $ZnSt_2$	 + $CaSt_2$	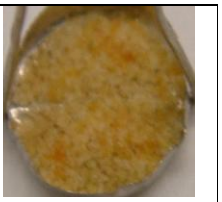 + $ZnSt_2$ + $CaSt_2$

4.4.3 Development of novel stabilizers

Based on the results presented, two novel stabilizers were invented. The first incorporates sacrificial epoxides into the traditional stearate structure. The second utilizes Diels-Alder chemistry in attempt to mitigate the discoloration that occurs during the degradation of PVC. The two inventions are described below along with performance evaluations as compared to the metal stearate results presented in prior sections.

4.4.3.1 Novel epoxide stabilizer

Epoxidized soybean oil (ESO) was investigated as a bio-based plasticizer to substitute for traditional petroleum-based phthalate plasticizers (DIDP) in PVC. ESO is readily compatible with PVC and is suitable as a plasticizer. However, as shown, the thermal degradation of PVC releases HCl. The epoxide rings present in ESO are vulnerable to attack and opening by HCl molecules (study presented in Appendix). The stabilization effect exhibited by the opening of the epoxide rings on ESO to scavenge

HCl alters the compatibility of ESO with PVC, changing the plasticizer's properties. We hypothesize that by incorporating sacrificial epoxides into a thermal stabilizer we can aid in maintaining the integrity of the ESO plasticizer while mitigating the thermal degradation of the PVC polymer.

The novel epoxide stabilizer invented is a metal (zinc and calcium) cation salt of epoxidized linolenic acid (Figure 4.21). The structure is analogous to the traditional zinc and calcium stearates used for the stabilization of PVC; however it has the added functionality of sacrificial epoxides. The epoxide stabilizer therefore acts as both a traditional stearate as well as an HCl scavenger through the opening of its sacrificial epoxides, ideally to protect the plasticizer properties (epoxides rings) of ESO.

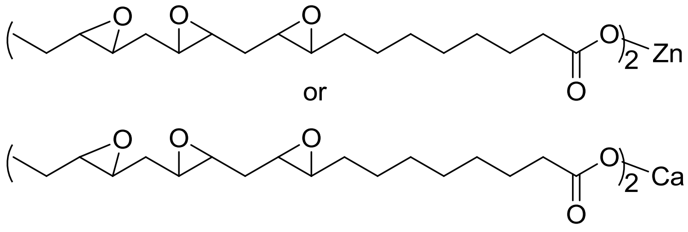

Figure 4.21 - Zinc and calcium novel epoxide stabilizers for PVC

4.4.3.2 Investigation of literature precedence

As invention disclosures were filed with Dow on the novel epoxide stabilizers created, a significant effort was made to search for similar ideas in the literature. A reference to the structure created was found in patent literature, although the claim for its use was vague and largely unsubstantiated.[20]

Benanbiba et al. found similar results to ours in that plasticizers containing epoxide rings exhibit a stabilization effect. In their case, epoxidized sunflower oil was investigated.[21] They cited two important stabilizing influences: 1) epoxides increase the induction time to raped dehydrochlorination and 2) epoxides decrease the overall rate of dehydrochlorination after the induction time.

Taking it a step further, Odilora et al. showed that there is advantage when metal carboxylates were used with epoxidized oils.[22] The study demonstrates that the time to reach 1 percent dehydrochlorination and the rate of dehydrochlorination at that time are both improved when metal carboxylates are used in addition to epoxidized oils. Similarly, Iida et al. studied epoxidized polybutadiene as a thermal stabilizer alongside calcium and zinc stearate.[23]

Similar to the stabilizer we invented, Okieiman et al. examined the stabilizing effects of epoxidized oils of which they created metal soaps.[24] Oils included jatropha seed oil, khaya seed oil, and rubber seed oil. These oils are comprised of mixtures of various fatty acids. Metal soaps were prepared directly from the oils. Of note, rubber seed oil contains 22.5 weight percent linolenic acid (the precursor to the epoxidized metal salts we created). Worschech et al. conducted a similar study, creating calcium and zinc salts of epoxidized metal glycerides.[25]

4.4.3.3 Performance of novel epoxide stabilizer blends

The performance of the zinc and calcium epoxide stabilizers (abbreviated ZnEp and CaEp, respectively) is shown in Figure 4.22. Weight loss with respect to PVC is plotted for DIDP-plasticized blends heated isothermally at 170ºC for 2 hours. All blends exhibit similar or improved performance when compared to their non-epoxidized stearate analogs. In Figure 4.19, PVC + DIDP + $ZnSt_2$ exhibit a greater than 30% weight loss, however, when ZnEp is substituted for $ZnSt_2$, a weight loss of less than 15% is observed.

PVC + DIDP + CaEp and PVC + DIDP + ZnEp + CaEp exhibit similar weight loss when compared to their stearate blend analogs (PVC + DIDP + $CaSt_2$ and PVC + DIDP + $ZnSt_2$ + $CaSt_2$, respectively).

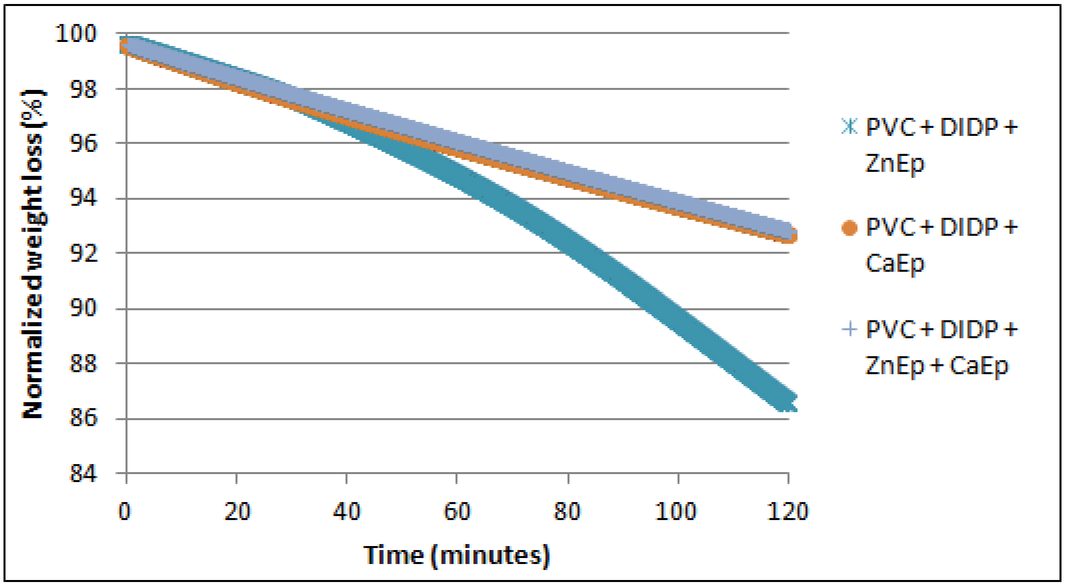

Figure 4.22 - Weight loss of DIDP-plasticized PVC blends incorporating novel epoxide stabilizers during the heat treatment and degradation process at 170°C; weight normalized against the mass of PVC in each blend

In terms of discoloration, the DIDP-plasticized novel epoxide blend that shows the most enhanced performance is the DIDP-plasticized PVC with ZnEp and CaEp (Table 4.9). When compared with DIDP-plasticized PVC with $ZnSt_2$ and $CaSt_2$, a significant improvement in color sability is observed. Whereas, the ZnEp + CaEp blend still appears mildly heterogeneous in color, it is a much lighter shade than the $ZnSt_2$ + $CaSt_2$ blend.

Table 4.9 - Color comparison of DIDP-plasticized PVC blends incorporating novel epoxide stabilizers after thermal treatment

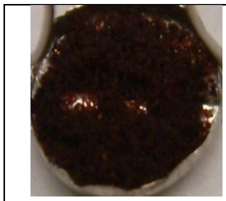 PVC + DIDP	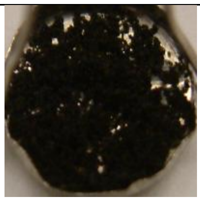 + ZnEp	 + CaEp	 + ZnEp + CaEp

Blends of ESO-plasticized PVC with the ZnEp and CaEp stabilizers are shown in Figure 4.23. Again, weight loss is plotted with respect to PVC over a period of 2 hours under isothermal heating at 170ºC. The drastic increase in the rate of weight loss seen with the ESO-plasticized PVC with $ZnSt_2$ blend is not evidence in the ESO-plasticized PVC blend with ZnEp. Further, a performance improvement is also observed in the ESO-plasticized PVC blend with both ZnEp and CaEp.

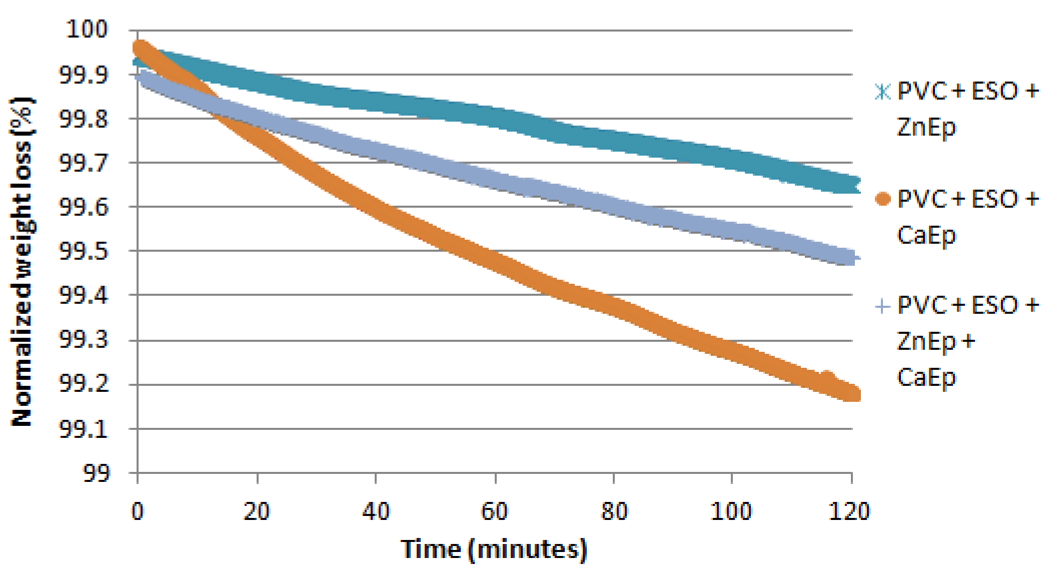

Figure 4.23 - Weight loss of ESO-plasticized PVC blends incorporating novel epoxide stabilizers during the heat treatment and degradation process at 170°C; weight normalized against the mass of PVC in each blend

The discoloration of the ESO-plasticized PVC blends with the novel epoxide stabilizers after thermal treatment is shown in Table 4.10. Each of the blends closely resembles its ESO-plasticized PVC with stearate analog (Table 4.8). The blends with the novel epoxide stabilizer appear to have a slightly increased red tint, although it is not quantifiable. The similarity in color is expected, both the stearate and novel epoxide stabilizer blends contain ESO, which has a large number of epoxide rings susceptible to opening by HCl , effectively mitigating further autocatalytic degradation.

Table 4.10 - Color comparison of ESO-plasticized PVC blends incorporating novel epoxide stabilizers after thermal treatment

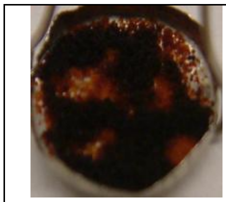		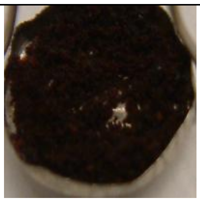	
PVC + ESO	+ ZnEp	+ CaEp	+ ZnEp + CaEp

4.4.3.4 Novel maleimide stabilizer

Conjugated polyene sequences caused by liberation of HCl from the PVC backbone are active in the visible color spectrum when the sequences reach five or more conjugated double bonds. This is a primary origin of color formation in PVC. Color change of the PVC polymer is undesirable both in terms of polymer integrity and industrial application / consumer preferences.

We have invented a stabilizer that 1) decreases weight loss (HCl release) at elevated temperatures and 2) decreases color formation (extended conjugated olefin chain formation) at elevated temperatures. We incorporate a highly reactive dienophile combined with a non-volatile metal salt that is compatible with PVC formulations (Figure 4.24).

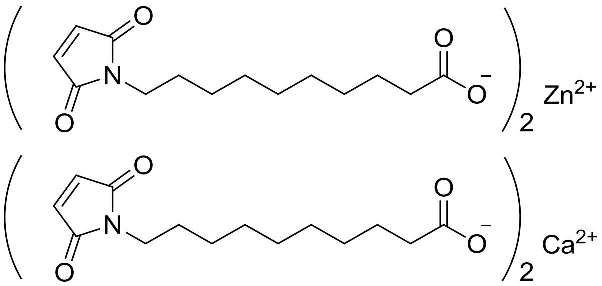

Figure 4.24 - Examples of the novel maleimide stabilizers invented (Zn11M and Ca11M, respectively)

The dienophile portion of the added stabilizer reacts with conjugated segments formed on the PVC backbone to give the Diels-Alder reaction product, thereby reducing the degree of conjugation and reducing color formation (Figure 4.25). The metal stearate-like portion of the stabilizer package scavenges HCl to aid in preventing extended conjugated double bond sequence formation.

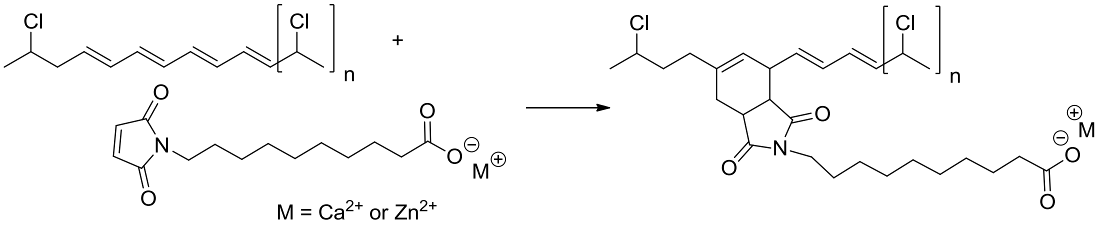

Figure 4.25 - Mode of maleimide stabilization via Diels-Alder chemistry

4.4.3.5 Investigation of literature precedence

No direct literature reference was found to the maleimide stabilizers we created. However, Diels-Alder chemistry has been utilized in enhancing the thermal stability of PVC blends. Pourahmady et al. used similar Diels-Alder chemistry be incorporating N-alkyl maleimides into PVC blends. They suggest a synergistic and positive enhancement of thermal stability when used with traditional stabilizers to include calcium and zinc stearates.[26] Yassin et al. conducted a similar study, using UV experiments to show increased color stability; their focus was on designing N-substituted maleimides as replacements for traditional thermal stabilizers.[27] Several authors have also investigated N-aryl and N-phenyl maleimides for use as thermal stabilizers.[28]

Wang et al. synthesized a tin maleimide for use a thermal stabilizer in PVC blends. They cite an increase in color stability after thermal treatment at 180°C. They do not investigate calcium or zinc salts of N-alkyl maleimides.[29]

In an interesting article, Mohamed et al. use a biologically active maleimide to impart Diels-Alder type stabilization on the degrading PVC polymer.[30] However, because their stabilizer is also biologically active, they demonstrate good microbial activity towards two types of bacteria and fungi. This is pertinent to plasticized-PVC formulations for use in the food industry. While not directly evident, it does similarly show the use of a multi-purpose/dual-role thermal stabilizer.

4.4.3.6 Performance of novel maleimide stabilizer blends

The novel maleimide stabilizers were first substituted for $ZnSt_2$ and $CaSt_2$ in DIDP-plasticized PVC blends. Figure 4.26 shows weight loss of the new blends at 170°C over a period of 2 hours. In comparison with the corresponding stearate blends (Figure 4.19), the most glaring difference is that Zn11M does not exhibit the drastic decline in weight as evidenced by $ZnSt_2$. The DIDP-plasticized PVC blend with Ca11M exhibits approximately the same degree of weight loss as the DIDP-plasticized PVC with $CaSt_2$

blend. Interestingly the synergistic blend with both Zn11M and Ca11M loses more weight than the corresponding $ZnSt_2$ + $CaSt_2$ blend. This is an unexpected result, as each of the individual blends (Zn11M and Ca11M, respectively) performs better than or as well as the corresponding stearate blends.

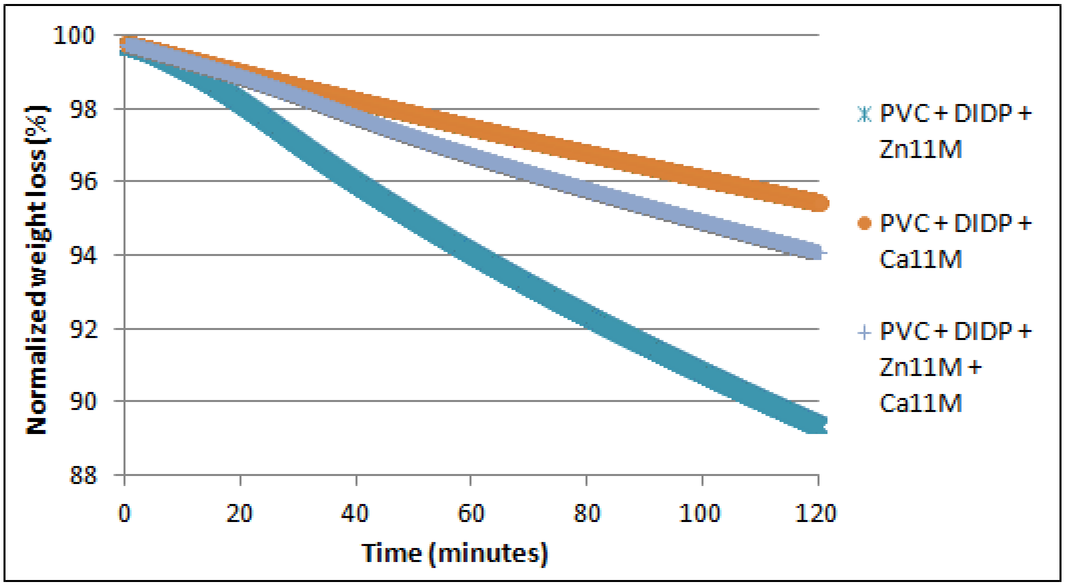

Figure 4.26 - Weight loss of DIDP-plasticized PVC blends incorporating novel maleimide stabilizers during the heat treatment and degradation process at 170°C; weight normalized against the mass of PVC in each blend

The color stability of the DIDP-plasticized blends with Zn11M and Ca11M stabilizers are shown in Table 4.11. Compared to the corresponding stearate blends after thermal treatment, the blend incorporating Zn11M and the synergistic blend incorporating Zn11M and Ca11M both show decreased discoloration. The results suggest that indeed Diels-Alder chemistry is likely taking place, mitigating the color change of the degrading polymer.

Table 4.11 - Color comparison of DIDP-plasticized PVC blends incorporating novel maleimide stabilizers after thermal treatment

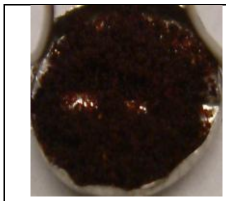 PVC + DIDP	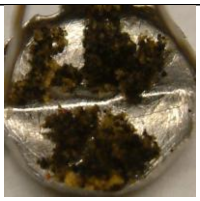 + Zn11M	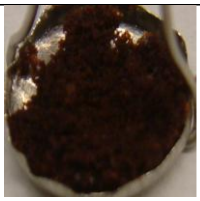 + Ca11M	 + Zn11M + Ca11M

Blends incorporating the Zn11M and Ca11M in ESO-plasticized PVC exhibit the best performance out of all blends studied. As shown in Figure 4.27, over a period of 2 hours at 170°C, none of the blends lose more than 0.4 weight percent PVC. All of the blends show decreased weight loss relative to the analogous stearate blend (compare to Figure 4.20).

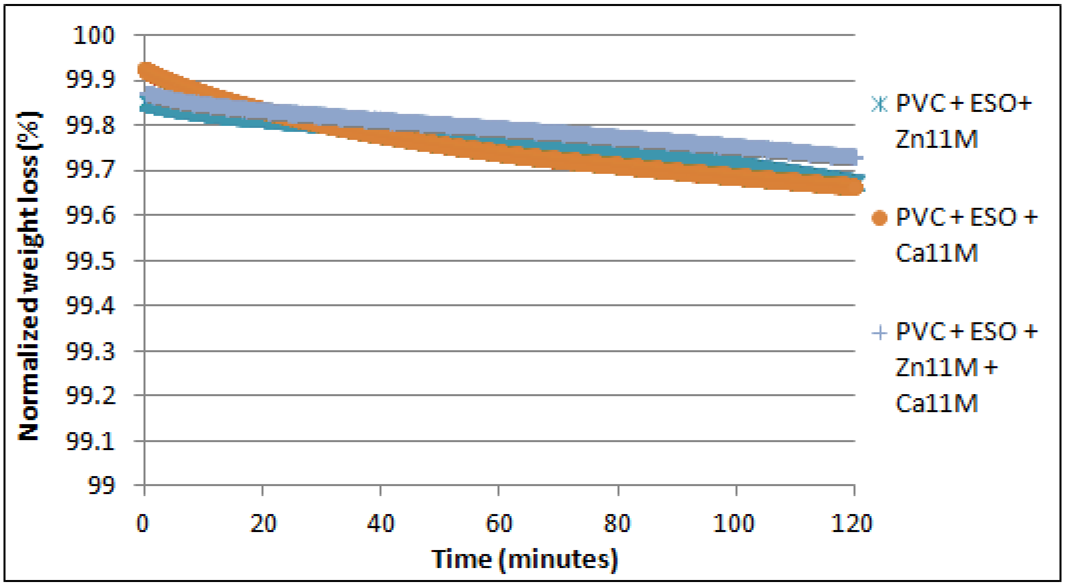

Figure 4.27 - Weight loss of ESO-plasticized PVC blends incorporating novel maleimide stabilizers during the heat treatment and degradation process at 170°C; weight normalized against the mass of PVC in each blend

In addition to the most admirable weight loss profiles, the maleimide stabilizers also exhibit the least amount of discoloration at 170°C over 2 hours. The ESO-plasticized blend containing Zn11M exhibits excellent color stability while the ESO-plasticized PVC blend incorporating Ca11M discolors to nearly the same extent as the blend containing $CaSt_2$ (Table 4.12).

All of the results regarding calcium substituted carboxylates presented suggest that calcium stabilizers have very limited solubility in the polymer and do not engage in a significant level of reactivity with the polymer itself. However, when combined with Zn11M, a significant improvement in color stability is observed. The ESO-plasticized PVC blend with Zn11M and Ca11M shows best color stability of any blend studied. This further confirms that zinc and calcium carboxylates engage in a synergistic mechanism as initially presented with the model studies in Figure 4.14.

Table 4.12 - Color comparison of ESO-plasticized PVC blends incorporating novel maleimide stabilizers after thermal treatment

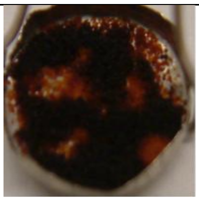 PVC + ESO	 + Zn11M	 + Ca11M	 + Zn11M + Ca11M

4.5 Conclusions

4.5.1 Key findings and accomplishments

Synergistic studies using model PVC compounds and blends of powder PVC were used to study the mechanism of degradation and stabilization of PVC. A library of PVC compounds was selected to characterize various tacticities and defects. Neat reactions of the model compounds with metal acetates (models for metal stearates) with a phase transfer catalyst indicated that tertiary chlorides and allylic chlorides degrade rapidly to form the corresponding alkene, confirming that these defects lead to the initial degradation. Isotactic models showed better stabilization (reacts 127% faster) than syndiotactic models.

In all cases, when the model compounds or the PVC were blended with $ZnSt_2$ alone an undesirable degradation occurred rapidly: the model compound was consumed rapidly and showed color formation in 8 minutes while the PVC blend showed a catastrophic weight loss after 10 minutes. When the $ZnSt_2$ was replaced with $ZnCl_2$, all degradation metrics were accelerated indicating that formation of $ZnCl_2$ causes catastrophic degradation. However, when $ZnSt_2$ were blended in combination with $CaSt_2$ the rate at which the model compound was consumed was reduced by 40%, color formation was delayed by 90 minutes and the bulk PVC never showed a catastrophic weight loss. The results support that: (1) the Lewis acidity of the $ZnSt_2$ facilitates the degradation process to form the stronger Lewis acid $ZnCl_2$, (2) $CaSt_2$ is an ion exchange support to prevent the formation of $ZnCl_2$ by regenerating $ZnSt_2$ and forming $CaCl_2$.

Thermogravimetric analysis studies using blends of PVC and ESO-plasticized PVC have provided the activation energy of the initial thermal degradation reaction and for the bulk degradation reactions. We have determined the activation energy for the initial degradation (117 ± 4 $kJ \cdot mol^{-1}$) and bulk degradation (147 $kJ \cdot mol^{-1}$) of PVC. These may correspond to different pathways of degradation. The activation energy for the initial thermal degradation for PVC with ESO is less (by 48%) than that for PVC alone however the overall rate of degradation is less for PVC with ESO. Studies with model epoxides and HCl (that simulate the undesirable and fast uptake of HCl by ESO), have indicated that cyclic epoxides are able to scavenge HCl more rapidly than linear epoxides (see Appendix). This seems to imply that it may be possible to develop better HCl scavengers as "sacrificial" epoxides (ensuring the structural integrity of ESO).

Thermogravimetric analysis studies on DIDP- and ESO-plasticized PVC blends with metal stearates further support and reinforce the conclusions from the model studies. Color formation after thermal treatment closely mirrors the model studies as well. These metrics for determining degradation and stabilization are critical for industrial applications as they consider all important material properties (structural changes and color performance).

The synergism between $ZnSt_2$ and $CaSt_2$ is the major driving force in thermal stability. $CaSt_2$ alone does not add benefit or detriment to the plasticized PVC while $ZnSt_2$ only shows a detriment; therefore it must be the added benefit of both the $ZnSt_2$ and $CaSt_2$. This is evidence by the preservation of structure (as determined by ^1H NMR) and color of the 2,4-dichloropentane in the model compound studies and the similar results (in terms of weight loss and color) of the PVC blend studies. As hypothesized above the $CaSt_2$ can act as an ion exchange support preventing the formation of $ZnCl_2$.

Two novel stabilizers were invented based on the mechanistic understanding of DIDP and ESO plasticized PVC degradation with metal stearates. A novel epoxide stabilizer was created and tested in both DIDP- and ESO-plasticized PVC blends. The stabilizer showed superior weight loss performance and color stability in DIDP-plasticized blends. A second thermal stabilizer, utilizing Diels-Alder chemistry through incorporation of a highly reactive dienophile (maleimide) was also presented. The ESO-plasticized PVC with maleimide stabilizer exhibited the best color stability of any PVC blend studied.

4.6 References

(1) Wilkes, C. E.; Summers, J. W.; Daniels, C. A. *PVC Handbook*; Carl Hanser Verlag, 2005.

(2) Titow, V. W. *PVC Plastics: Properties, Processing and Applications*; Elsevier Applied Science: New York, 1990Sarvetnick, H. A. *Polyvinyl Chloride*; Van Nostrand Reinhold Company, 1969.

(3) Europa Europa.eu, 2005; Vol. 2013.

(4) Matthysen, L.; Martinz, D. O.; Solvay, 2011; Vol. 2013Sun, B.; Chaudhary, B. I.; Shen, C.-Y.; Mao, D.; Yuan, D.-M.; Dai, G.-C.; Li, B.; Cogen, J. M. *Polymer Engineering and Science* **2012**.

(5) Wypych, G.; ChemTec Publishing.

(6) Patel, K.; Velazquez, A.; Calderon, H. S.; Brown, G. R. *Journal of Applied Polymer Science* **1992**, *46*, 179.

(7) Frye, A. H.; Horst, R. W. *J Polym Sci* **1959**, *40*, 419.

(8) Bengough, W. I.; Onozuka, M. *Polymer* **1965**, *6*, 625Iván, B.; Kennedy, J. P.; Kelen, T.; Tüdös, F. *Journal of Macromolecular Science: Part A - Chemistry* **1982**, *17*, 1033.

(9) Frye, A. H.; Horst, R. W. *J Polym Sci* **1960**, *45*, 1Frye, A. H.; Horst, R. W.; Paliobagis, M. A. *Journal of Polymer Science Part A: General Papers* **1964**, *2*, 1765.

(10) Owen, E. D.; Msayib, K. J. *Journal of Polymer Science Part A: Polymer Chemistry* **1989**, *27*, 399.

(11) Atakul, S.; Balköse, D.; Ülkü, S. *Journal of Vinyl and Additive Technology* **2005**, *11*, 47Bensemra, N.; Tran Van, H.; Guyot, A.; Gay, M.; Carette, L. *Polym Degrad Stabil* **1989**, *24*, 89Ureta, E.; Cantú, M. E. *Journal of Applied Polymer Science* **2000**, *77*, 2603.

(12) Varma, I. K.; Grover, S. S. *Die Makromolekulare Chemie* **1974**, *175*, 2515.

(13) Asahina, M.; Onozuka, M. *Journal of Polymer Science Part A: General Papers* **1964**, *2*, 3505Asahina, M.; Onozuka, M. *Journal of Polymer Science Part A: General Papers* **1964**, *2*, 3515Ayrey, G.; Siddiqui, I. H.; Poller, R. C. *J Polym Sci A1* **1972**, *10*, 725Ayrey, G.; Poller, R. C.; Siddiqui, I. H. *Journal of Polymer Science Part B: Polymer Letters* **1970**, *8*, 1Klemchuk Peter, P. In *Stabilization of Polymers and Stabilizer Processes*; AMERICAN CHEMICAL SOCIETY, 1968; Vol. 85Bacaloglu, R.; Fisch, M. *Polym Degrad Stabil* **1994**, *45*, 325Bacaloglu, R.; Fisch, M. *Polym Degrad Stabil* **1995**, *47*, 33Bacaloglu, R.; Fisch, M. *Polym Degrad Stabil* **1995**, *47*, 9.

(14) Starks, C. M.; Liotta, C. L.; Halpern, M. *Phase-transfer catalysis : fundamentals, applications, and industrial perspectives*; Chapman & Hall: New York, 1994.

(15) Martínez, G.; Mijangos, C.; Millán, J. *Journal of Macromolecular Science: Part A - Chemistry* **1982**, *17*, 1129Mijangos, C.; Martínez, G.; Millán, J. L. *European Polymer Journal* **1982**, *18*, 731.

(16) Bacaloglu, R.; Fisch, M. *Polym Degrad Stabil* **1994**, *45*, 301Fisch, M. H.; Bacaloglu, R. *Journal of Vinyl Technology* **1995**, *1*, 233Fisch, M. H.; Bacaloglu, R. *Plast Rubber Compos* **1999**, *28*, 119.

(17) Kaseler, T. G. *Soc Plast E* **1993**, *39*, 717.

(18) Wypych, J. *Journal of Polymer Science: Polymer Letters Edition* **1984**, *22*, 425.

(19) "ASTM E698 - Standard Test Method for Arrhenius Kinetic Constants for Thermally Unstable Materials Using Differential Scanning Calorimetry and the Flynn/Wall/Ozawa Method," 2011.

(20) Geigy, J. R.; Belgique, R. d., Ed. Belgium, 1963; Vol. 625282Herbst, H.; Hoffman, K.; Pfaedner, R.; Drewes, R.; Organization, W. I. P., Ed. Denmark, 1995Klemchuk, P.; Dexter, M.; USPTO, Ed. US, 1961; Vol. 3271338.

(21) Benaniba, M. T.; N., B.-B.; Gelbard, G. *Polymer Degradation and Stability* **2003**, *82*, 245.

(22) Odilora, C. A. *Acta Polymerica* **19889**, *40*, 541.

(23) Iida, T.; Kawato, J.; Tanie, S.; Goto, K. *Journal of Applied Polymer Science* **1989**, *37*, 1685Margaritis, A. G.; Kalfoglou, N. K. *European Polymer Journal* **1988**, *24*, 1043.

(24) Okieimen, F. E. *Industrial Crops and Products* **2002**, *15*, 71.

(25) Brand, E.-U.; Stoll, G.; Wedl, P.; Worschech, K.; USPTO, Ed. United States, 1990; Vol. US5302644 A.

(26) Pourahmady, N.; USPTO, Ed.; The B.F. Goodrich Company: United States, 1992.

(27) Yassin, A.; Mohamed, N.; Mikhael, M.; Sabaa, M. *Polymer Degradation and Stability* **1990**, *29*, 291.

(28) Al-Dossary, A.; Abdel-Naby, A. *Journal of Vinyl & Additive Technology* **2008**, *14*, 175Zhang, J.; Howell, B. *Journal of Vinyl & Additive Technology* **2006**, *12*, 88Al-Dossary; A. Abdel-Naby, A. *Journal of Vinyl & Additive Technology* **2008**, *14*, 167.

(29) Wang, X.; Yuan, W.; Liu, J. *Advanced Materials Research* **2012**, *535*, 1167.

(30) Mohamed, N.; Mohamed, R.; M., F. *Molecules* **2012**, *17*, 7927.

CHAPTER 5 - CONCLUSIONS AND RECOMMENDATIONS

5.1 Overall conclusions

5.1.1 Conclusions

The twelve green chemistry principles presented in Chapter 1 have served as a guide for three industrially-relevant projects. In the first project, silylamines were presented for use as reversible ionic liquids in application to CO_2 capture from post-combustion flue gas streams. The effect of silylamine structure was thoroughly researched to develop a comprehensive library of silylamines and an accompanying set of structure-property relationships. The proposed solvent systems have the potential to present significant energy savings, as design has focused on their use in a non-aqueous, solvent-free process.

The second project also dealt extensively with CO_2, but instead as a reversible, *in-situ* protecting group for amines. Three strategies for the reversible protection of amines using CO_2 were developed and evaluated. Further, a chemoselective reaction was performed using CO_2 to protect a reactive amine and consequentially direct reactivity elsewhere within the same molecule. The CO_2-protection technology developed has significant impact in multi-step industrial syntheses, as reversible, *in-situ* protection with CO_2 eliminates the need for separate protection and deprotection unit operations.

Lastly, a study was performed on the thermal degradation and stabilization of PVC in the presence of both plasticizers and thermal stabilizers. The study combined both model compound experiments as well as work with bulk PVC blends to gain a holistic understanding of the processes that take place during the degradation and stabilization of PVC. The bio-based plasticizer epoxidized soybean oil was investigated as a replacement for petroleum-based phthalate plasticizers. Additionally, two novel stabilizers were presented in attempt to further improve the performance of PVC thermal stabilizers.

5.1.2 Recommendations

For each of the projects presented below, individual and specific recommendations are given. However, in general, further study of the economics involved with each project is recommended. While the focus of this thesis is on the development of green chemistry methods and processes for application to industry, investigating each project's sustainability in terms of its actual economic viability would ensure its utility in an industrial setting. While this is often complicated when examined from a laboratory scale, with process simulation programs such as Aspen's HYSYS and the aid of our industrial sponsors (ConocoPhillips and Dow), intelligent approximations can be made concerning energy requirements and consequent costs.

5.2 Silylamines as Reversible Ionic Liquids for CO_2 Capture

5.2.1 Conclusions

A large library (15+) of silylamines was developed for use as reversible ionic liquids. Application of reversible ionic liquids to CO_2 capture from post-combustion flue gas streams was investigated and presented in Chapter 2. A strong structure-property relationship exists between the silylamines and the resulting reversible ionic liquid CO_2 capture properties. Several important conclusions were made; they are highlighted below.

- In a non-aqueous environment, silylamines exhibit enhanced CO_2 capacity resulting from the formation of carbamic acid in the ammonium carbamate ionic network of the reversible ionic liquid.
- Silylamine structure has an unambiguous impact on reversible ionic liquid viscosity and temperature of reversal.
- Hindering the reactive amine site through sterics or by varying the order of the amine affects both the reversal temperature and enthalpy of regeneration of the reversible ionic liquid.
- We can control the reversible ionic liquid viscosity by limiting conversion (CO_2 uptake) of the silylamine; industrially this translates to optimizing the residence time of the silylamine in the absorption tower.
- The use of silylamines in a non-aqueous environment could present significant energy savings over traditional aqueous alkanolamine processes.

Two silylamines were presented as excellent candidates for further investigation by our industrial partner, ConocoPhillips. They are 1-(aminomethyl)triethylsilane (TEtSMA) and (*trans*)-3-(triethylsilyl)prop-2-en-1-amine (*trans*-TEtSA). Both exhibit high CO_2 uptake capacities relative to the other silylamines studied, viable reversible temperatures, and reasonable enthalpies of regeneration (Table 5.1). Their reversible ionic liquids have lower viscosities than most other silylamine reversible ionic liquids, and further, by controlling the CO_2 uptake, viscosity could be reduced to meet industry-operating specifications.

Table 5.1- Summary of the properties of TEtSMA and *trans*-TEtSA

Summary of the properties of TEtSMA and *trans*-TEtSA		
Property	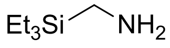 TEtSMA	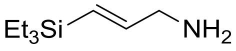 *trans*-TEtSA
CO_2 uptake (mol CO_2/mol amine, 25°C)	0.59±0.01	0.61±0.03
CO_2 uptake (mol CO_2/kg amine, 25°C)	4.09±0.08	3.56±0.20
Reversal temperature (°C)	78±5	48±2
Enthalpy of regeneration (°C)	76±7	85±7
Reversible ionic liquid viscosity at 25°C (cP)	2373±206	3889±252
Reversible ionic liquid viscosity at 40°C (cP)	625±58	362±19

5.2.2 Recommendations

While the project is now complete, there are several areas of research that would benefit from further study. First, further optimization of the two proposed silylamine candidates is necessary before they see industrial application. The reversal temperature of *trans*-TEtSA could be raised by substituting the triethyl substituents surrounding the silicon atom with dimethyl-ethyl substituents as used in 3-(aminopropyl)dimethylethylsilane (DMESA). Synthesis could be achieved using the same hydrosilylation reaction used to make many of the other silylamines (Figure 5.1).

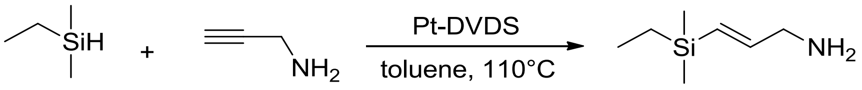

Figure 5.1 – Proposed synthesis of (*trans*)-3-(dimethylethylsilyl)prop-2-en-1-amine

Second, further structural investigation of secondary silylamines should be conducted to increased reversal temperature to an industrially-viable value. To increase the reversal temperature of the secondary silylamine, N-methyl-3-(aminopropyl)dimethylethylsilane (SDMESA), the length of the tether between the silicon atom and amine could be lengthened to a butylene linker. It was shown that as the tether length increases, reversal temperature also increases (Chapter 2). Synthesis of N-methyl-3-(aminobutyl)dimethylethylsilane could be achieved as shown in Figure 5.2.

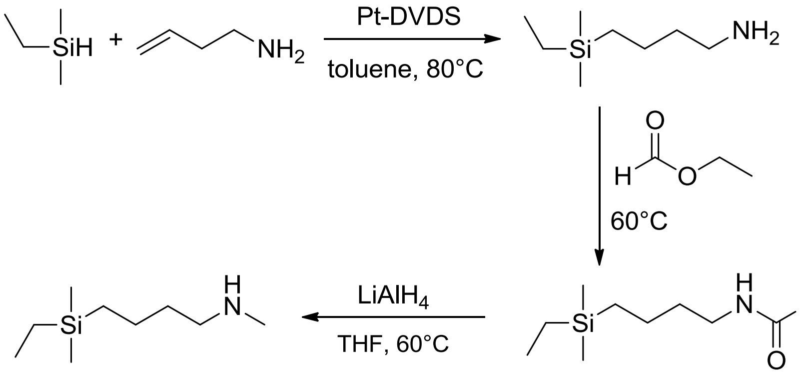

Figure 5.2 – Proposed synthesis of N-methyl-3-(aminobutyl)dimethylethylsilane

The effect of the residual water in the flue gas on the non-aqueous design of the reversible ionic liquid system should be investigated as well. Brennecke et al. recently published an article on the interaction of ionic liquids and water that would serve as a good starting point.[1] While traditional texts would suggest ionic liquids would have great solubility in water, as most salts are water-soluble, in practice that is not true. Due to the self-aggregation of the ionic species, dissolution of the ionic liquid in water is not facile. Thus, determining accurate water solubility is not straightforward.

Additionally, further investigation of the initial process simulation model should be conducted. Ideally, additional properties such as the reversible ionic liquid viscosity would be accounted for in the simulation. Further, running the process without removing the residual water in the flue gas stream should be investigated. This will likely require introduction of a decantation unit operation if excess water is found to accumulate over time.

Furthermore, alternate applications of reversible ionic liquids should be investigated. As the availability and access to natural gas increases, interest in post-combustion CO_2 capture has begin to decrease. However, the reversible ionic liquid system developed and has potential in many alternate applications[2], as evidenced by the similar use of CO_2 in Chapter 3.

Included in the appendix are two proposals that were submitted surrounding the use of reversible ionic liquids. The first is a proposal submitted to the Department of Energy (DOE) on developing a novel process for using reversible ionic liquids in a CO_2 capture process with a spray atomizer. The second proposal was submitted to the National Science Foundation (NSF) and discusses an idea of using reversible ionic liquids in the separation of bitumen from oil sands in Canada. As a significant amount of time was invested in preparing each of the proposals, they are included for reference and creative thinking.

5.3 CO_2 as a Protecting Group in Chemical Syntheses

5.3.1 Conclusions

Chapter 3 presented the use of CO_2 as a protecting group for use in chemical syntheses. Whereas traditional protecting groups require separate unit operations for the protection, deprotection, and subsequent separation of the protecting group used – all for the protection of a single amine – we demonstrated the reversible, *in-situ* protection of amines using CO_2. We found that by adding a strong base, a CO_2 protected species can be formed which is stable in the presence of reactive electrophilic acyl compounds. In addition, we demonstrated the use of the CO_2 protection technology in a chemoselective reaction; we showed that by protecting an amine with CO_2 we could direct reactivity towards a less reactive substituent, effectively preventing the reaction of the amine – all in the same molecule. This technology is directly applicable to our industrial partner, Dow, and could serve a wide application base, from multi-step synthesis to complex pharmaceutical synthesis as mentioned in Chapter 3.

5.3.2 Recommendations

The work presented in Chapter 3 is part of a multi-year project in collaboration with Dow; the project just completed its 2nd quarter of research. Moving forward, much of the work will focus on utilizing the CO_2 protection technology for amines in Suzuki coupling reactions as introduced in Chapter 3. However, in addition to the work with Suzuki coupling reactions, several other topics should also be investigated; they are suggested as follows:

- Strong bases other than DBU should be investigated to form the CO_2-protected species. As DBU is not favored in industry, other more industry-friendly and less costly bases should be investigated.
- Reversal of the CO_2-protected species, as a function of added base should be studied. Gaining control over the temperature at which the protected species releases the CO_2 protecting group will allow reactions to be conducted at elevated temperatures.
- A total synthesis should be conducted, to evidence in-situ protection, reaction at an alternate reaction site, in-situ deprotection, separation of the added base, and isolation of the product formed.

- In addition to the nucleophilic acyl substitutions investigated and the Suzuki coupling reactions discussed, alternate amine-containing reactions for application of the CO_2 protection technology could also be investigated. Relevant examples include Michael addition reactions and the selective formation of imines.
- Lastly, the work presented in Chapter 3 focused on the protection of primary amines. Primary amines are more nucleophilic and reactive than anilines and pyridines. However, protection of anilines and pyridines is often desired as well in chemical syntheses. Elevated pressures of CO_2 would likely be necessary. The protection of anilines and pyridines with CO_2 is a large area of research that is currently wide-open for exploration. While we have begun work in this area for application to Suzuki coupling reactions, developing an understanding of how the protection takes place under working CO_2 pressures would be of added value.

5.4 Mitigating the Thermal Degradation of Polyvinyl Chloride (PVC)

5.4.1 Conclusions

This research varied in topic significantly from the prior two chapters, but maintained a tie to green chemistry through the use of bio-based plasticizers and the development of a novel naturally-sourced thermal stabilizer through studying the degradation and stabilization of PVC. In Chapter 4, a comprehensive study using model compounds (neat) and bulk PVC blends was presented. Together the studies provided for the determination of a complete mechanistic pathway of not only the degradation of PVC but also the stabilization mechanisms provided by traditional metal stearates.

It was found that as PVC degrades, it undergoes chain unzipping to release HCl. Chain unzipping starts at the weak links in PVC and is autocatalytic; coordination by HCl aids in the release of further chloride ions. The thermal stabilizer zinc stearate is an excellent HCl scavenger, however it results in the formation of zinc chloride. Zinc chloride is a strong Lewis acid that was shown to drastically increase the rate of PVC degradation when present. For that reason, most industrial blends use a blend of both zinc stearate and calcium stearate. Calcium stearate is capable of ion exchanging with the zinc chloride formed from reaction of zinc stearate with HCl. The ion exchange results in the formation of calcium chloride, a non-acidic essentially-inert salt. Together zinc and calcium stearate impart important color and thermal stability to the polymer. The mechanistic pathway of degradation and stabilization was confirmed by both model studies and studies of bulk PVC blends.

PVC was studied in its neat form as well as in the presence of two plasticizers. The first, diisodecyl phthalate (DIDP), is a petroleum-based plasticizer that is commonly used in industry. The second, epoxidized soybean oil (ESO), is a bio-based plasticizer that was investigated as a replacement for DIDP. The presence of plasticizer increases the flexibility of the polymer chains, allowing for movement between chains. This increased movement provides for the easier escape of HCl at elevated temperatures and results in the increased weight loss in thermal studies when compared to PVC alone. ESO, however, acts not only as a plasticizer but also as a stabilizer. The epoxide groups on its backbone (added to increase its compatibility with PVC) act as HCl scavengers, preventing HCl release form the polymer blend. While this was initially thought to be desirable, maintaining the integrity of the plasticizer is a priority.

With these studies, two novel thermal stabilizers were developed. The first capitalized on the knowledge gained from the stabilization effect exhibited by ESO. Sacrificial epoxides were incorporated into a metal stearate-like structure that was derived from naturally occurring linolenic acid. The blends with the epoxidized stabilizer were exhibited similar weight loss and color performance to those with ESO present. The second stabilizer was designed to improve the color performance of PVC at elevated temperatures. A highly reactive dienophile (maleimide) was tethered to a stearate tail. The dienophile portion of the novel stabilizer is capable of reacting with conjugated sequences formed in the degrading PVC polymer to reduce color change by disrupting the level of conjugation. Both of the stabilizers are especially useful in that, not only do they have a specific added stabilization functionality, they also maintain a stearate backbone which is capable of scavenging HCl as reported with the traditional zinc and calcium stearate PVC blends.

5.4.2 Recommendations

The work on PVC resulted in two invention disclosures on the novel thermal stabilizers presented. While the work was initially focused around evaluating the performance of these novel stabilizers alone, future work should focus on optimization of the use of these stabilizers. Perhaps mixtures of these stabilizers with a traditional calcium or zinc stearate would prove beneficial. In addition, other metal cations, to include sodium and tin might also be advantageous.

Fundamental studies into the mechanism of stabilization of the maleimide stabilizer invented would be useful. While initial studies certainly suggest Diels-Alder chemistry is taking place, UV-visible spectroscopy studies would likely add further confirmation. In addition, an NMR study at an elevated temperature using a model compound along with the invented stabilizer would add further credence to its hypothesized mode of stabilization.

While PVC has been researched for several decades now, its use with bio-based plasticizers instead of those derived from petroleum is still a fairly novel topic. Additional studies investigating the change in properties of the plasticizer in ESO-plasticized PVC at elevated temperatures would be a great contribution to the field in terms of furthering green chemistry in the polymer industry. Additional studies on model epoxides were performed but not shown in Chapter 4. They are detailed in the Appendix. They show that tertiary epoxides scavenge HCl faster than secondary epoxides, which scavenge HCl faster than primary epoxides. Given this, in theory a tertiary epoxide stabilizer could be invented which would scavenge HCl faster than the ESO plasticizer to preserve its integrity. The invented epoxide stabilizer presented in Chapter 4 is a secondary epoxide, similar to the epoxides on ESO, and as such both epoxide forms scavenge HCl competitively.

Lastly, in cooperation with the same industrial sponsors at Dow, presented in the Appendix is a proposal on the stabilization of polyethylene during processing. While a different polymer structure, many of the same analytical techniques used to study PVC would be useful in investigating polyethylene. The proposal is included for reference.

5.5 References

(1) Ficke, L. E.; Brennecke, J. F. *Journal of Physical Chemistry B* **2010**, *114*, 10496.

(2) Xiong, D.; Li, Z.; Wang, H.; Wang, J. *Green Chemistry* **2013**, Advance Article.

APPENDIX A - ADDITIONAL INFORMATION ON SILYLAMINES AS REVERISBLE IONIC LIQUIDS FOR CARBON DIOXIDE CAPTURE

A.1 Introduction

This Appendix provides additional information referenced in Chapter 2. It includes the synthesis of the silylamines presented as well as details on the Aspen HYSYS simulation conducted. Syntheses were primarily performed by chemists in the Eckert-Liotta research group; however, several silylamines were synthesized with the assistance of chemical engineers.

A.2 Synthesis of Silylamines

A.2.1 Materials

All chemicals were purchased from Sigma-Aldrich and used as received unless otherwise noted. Chemicals used were: triethylsilane (99%); tripropylsilane (99%); trihexylsilane (99%); allylamine (99+%); platinum(0)-1,3-divinyl-1,1,3,3-tetramethyl disiloxane complex solution in xylene (Karstedt's catalyst; 2 wt% Pt) (Pt-DVDS); toluene (anhydrous, 99.8%); 0.5 *M* 2,8,9-triisobutyl-2,5,8,9-tetraaza-1-phospha bicyclo[3.3.3]undecane in diethyl ether; dimethylethylsilane (98%); 4-amino-1-butene (97%); tetrahydrofuran (THF; anhydrous, inhibitor-free, ≥99.9%); 3-chloro-1-butene (96%); potassium phthalimide (98%); hydrazine (anhydrous, 98%); 2-methyl-3-butyn-2-amine (95%); N-vinylphthalimide (99%); Pd on activated charcoal (5 wt% Pd basis); Celite 545; hexanes (anhydrous, mixture of isomers, ≥99%); and methanol (anhydrous, 99.8%). Propargylamine (95%) was acquired from TCI America, used as received, and stored in the dark under inert atmosphere at 5°C. 2-methylallylamine (97%) was purchased from Acros Organics and used as received. All chemicals were stored under inert dry atmosphere. The CO_2 employed was SFC grade from Airgas, certified to contain less than < 250 ppb H_2O with a purity of 99.9999%.

A.2.2 3-(aminopropyl)dimethylethylsilane (DMESA)

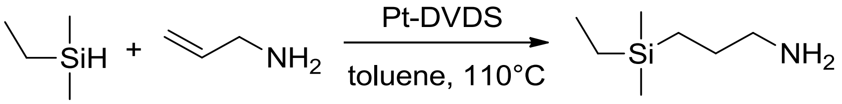

Figure A.1 – Synthesis of DMESA

To a 3-neck 250 mL round bottomed flask fitted with a condenser and magnetic stirbar under inert atmosphere was added anhydrous toluene (80 mL, 0.751 mol), dimethylethylsilane (10.56 mL, 80 mmol), and 2 wt% Pt-DVDS in xylenes (1.82 mL; 1.60×10^{-4} mol Pt; 0.20% catalyst loading wrt silane). This was allowed to stir at room temperature for approximately five minutes, at which point allylamine (12 mL, 0.160 mol) was added and the reaction was heated to 110°C overnight. Reaction progress was monitored via ^1H NMR for the disappearance of the silane proton (~3.7 ppm). When this peak was no longer present, the reaction mixture was allowed to cool to room temperature; the solvent and excess allylamine was then removed via rotary evaporator. The product 3-(aminopropyl)dimethylethylsilane (58% isolated yield) was distilled from the catalyst under reduced pressure (bp: 38°C at 2.5 mmHg).

^1H NMR (400.13 MHz, $CDCl_3$, 25°C) $\delta = 2.61$ (t, 2H), 1.37 (m, 2H), 1.15 (br, 2H), 0.44 (m, 4H), -0.09 (s, 6H)

^{13}C NMR (100.57 MHz, $CDCl_3$, 25°C) $\delta = 45.61, 28.22, 11.74, 7.24, 6.77, -4.04$

Calculated % for $C_7H_{19}NSi$ (MW: 145.32 g·mol^{-1}): C(57.86), H(13.18), N(9.64), Si(19.33); found: C (57.50), H(13.01), N(8.94)

A.2.3 3-(aminopropyl)triethylsilane (TEtSA), 3-(aminopropyl)tripropylsilane (TPSA), and 3-(aminopropyl)trihexylsilane (THSA)

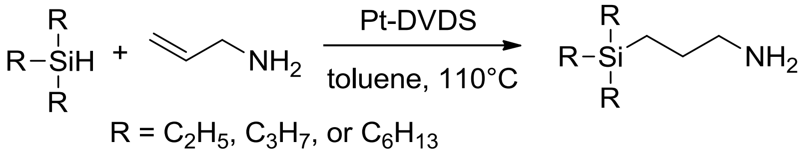

Figure A.2 – Synthesis of TEtSA, TPSA, and THSA

Trialkylsilane (80 mmol, 1 eq) and Pt-DVDS (0.8 mmol, 0.001 eq) were placed into a 3 neck round-bottom flask under nitrogen atmosphere at RT. The solution was dark yellow. Anhydrous toluene was then added (40 mL) under stirring. Allyl amine (160 mmol, 2 eq) was added in one portion (reddish color was first observed to then quickly turn dark brown). The reaction mixture was heated to reflux (110°C). ^{1}H NMR was used to monitor the disappearance of starting trialkylsilane. Upon complete reaction, the reaction solution was cooled to RT and the toluene and excess allyl amine were evaporated under vacuum. The crude material was then distilled under reduced pressure to afford the pure, desired silylamine.

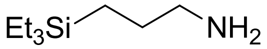

Figure A.3 - 3-(aminopropyl)triethylsilane (TEtSA)

Yield: 89%, Distillation temperature/pressure: 75°C at 4 mmHg.

^{1}H NMR (400.13 MHz, $CDCl_3$), δ: 2.63 (t, 2H), 1.39 (m, 2H), 1.08 (s), 0.90 (t, 9H), 0.49 (q, 6H),0.49 (t, 2H)

^{13}C NMR (400.13 MHz, $CDCl_3$), δ: 45.47, 27.88, 7.90, 6.95, 2.87

Calculated % for $C_9H_{23}NSi$ (MW: 173.37 g·mol^{-1}): C(62.35), H(13.37), N(8.08) Found: C(62.41), H(13.42), N(7.94)

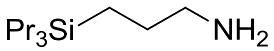

Figure A.4 - 3-(aminopropyl)tripropylsilane (TPSA)

Yield: 96%, Distillation temperature/pressure: 84°C at 0.3 mmHg.

^{1}H NMR (400.13 MHz, $CDCl_3$), δ: 2.63 (t, 2H), 1.39 (m, 2H), 1.30 (m, 6H), 1.05 (s, 2H), 0.93 (t, 9H), 0.48 (m, 8H)

^{13}C NMR (400.13 MHz, $CDCl_3$), δ: 45.85, 28.30, 18.63, 17.45, 15.27, 9.55

Calculated % for $C_{12}H_{29}NSi$ (MW: 215.45 g·mol^{-1}): C(66.90), H(13.57), N(6.50) Found: C(66.74), H(13.64), N(6.35)

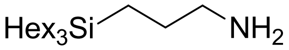

Figure A.5 - 3-(aminopropyl)trihexylsilane (THSA)

Yield: 92%, Distillation temperature/pressure: 155°C at 3 mmHg.

^{1}H NMR (400.13 MHz, $CDCl_3$), δ: 2.62 (t, 2H), 1.37 (m, 2H,), 1.25 (s(br)), 1.17 (s, 2H), 0.86 (t, 9H), 0.47 (m, 8H)

^{13}C NMR (400.13 MHz, $CDCl_3$), δ: 45.87, 33.58, 31.53, 28.34, 23.84, 22.61, 14.11, 12.40, 9.45

Calculated % for $C_{21}H_{47}NSi$ (MW: 341.69 g·mol^{-1}): C(73.82), H(13.86), N(4.10) Actual: C(72.87), H(13.59), N(4.07)

A.2.4 (aminomethyl)triethylsilane (TESMA)

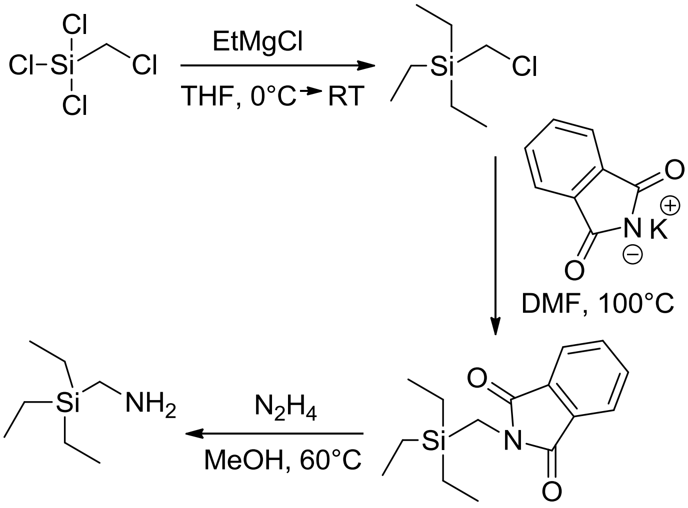

Figure A.6 – Synthesis of TESMA

2-((Triethylsilyl)methyl)isoindoline-1,3-dione (25.92 g, 0.0945 mol) was dissolved in anhydrous MeOH (315 mL) under an inert atmosphere and stirred with mechanical stirring. Anhydrous hydrazine (8.9 mL, 0.284 mol) was added in one portion to the MeOH solution and the temperature of the solution was brought to 60°C. During the course of the reaction, phthalylhydrazide formation was evidenced by a cloudy-gel like precipitate. After 5 hours of reaction, the solution was cooled and 2M HCl was added until a solid white precipitate was formed in the single aqueous phase. The solid was filtered under vacuum and washed with more 2M HCl. The collected liquid layer was then basified with 1M NaOH until a pH of 14 was reached. Diethyl ether was added to extract the amine product. The ether was then washed with brine, dried over $MgSO_4$ and removed at 45°C by distillation. The crude (aminomethyl)triethylsilane was attempted to be distilled under argon but it was noticed that as the temperature increased to 170°C a yellow sludge formed in the distillation flask. The heat was removed and the crude distilled at 25°C at 0.6 mmHg to give 3.63 g of pure (aminomethyl)triethylsilane in a 27% isolated yield.

^{1}H NMR (400 Hz, $CDCl_3$) 2.24 (s, 2H), 1.74 (s, 2H), 0.95 (t, 9H), 0.57 (q, 6H)

^{13}C NMR (400 Hz, $CDCl_3$) 26.68, 7.36, 2.10

Calculated % for $C_7H19NSi$ (MW: 145.32 g·mol^{-1}): Expected: C(57.86), H(13.18), N(9.64) found: C(56.56), H(13.28), N(9.13)

A.2.5 2-(aminoethyl)triethylsilane (TEtSEtA)

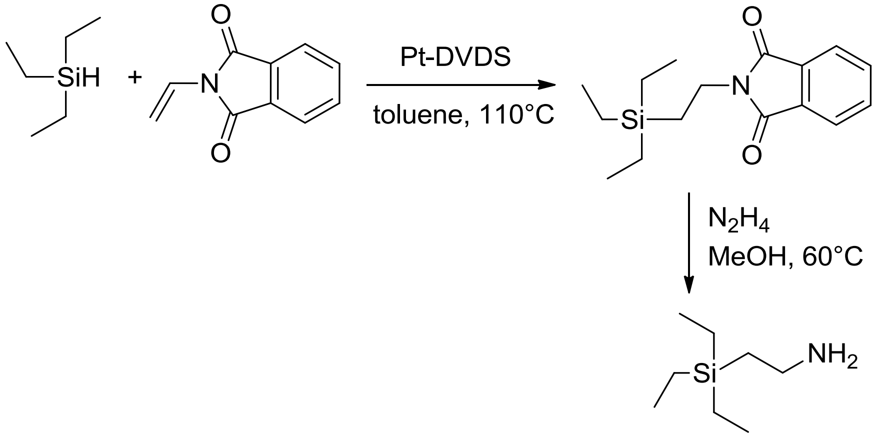

Figure A.7 – Synthesis of TEtSEtA

Triethylsilane (72.8 g, 0.626 mol) and Pt-DVDS (3.0 mL of 2 % Pt solution in xylene, 0.29 mmol) were added to a 3-neck round bottom flask fitted with a reflux condenser under inert atmosphere. To the mixture was transferred N-vinylphthalimide (25 g, 0.144 mol) dissolved in 250 mL anhydrous toluene using a double-tipped needle. The mixture was brought to 110 °C and stirred for 2 days. After cooling, the reaction mixture was filtered through celite and toluene was removed using a rotary evaporator. To the crude product was added hydrazine solution (35 wt. % in H_2O, 200mL, 2.16mol) and methanol 200 mL. The solution was heated to 60°C for 24 hours. After cooling, 150 mL of methanol was removed by distillation at atmospheric pressure, and the solution pH was adjusted to 1 using 6 N HCl aqueous solution at 0°C. The solution was filtered through celite, and the mother liquor pH was adjusted to 12 using 30 % NaOH aqueous solution at 0°C. It was extracted using Et_2O (300 mL, 6 times). The combined ether solution was dried over anhydrous $MgSO_4$, and ether was removed by evaporation. The residual crude was distilled under reduced pressure (bp: 30°C at 1mmHg) to give 2-(triethylsilyl)ethanamine (5.75g) in 25 % yield (2 steps).

^{1}H NMR (400 MHz, $CDCl_3$), δ (ppm): 2.73 (*t*,2H), 1.16 (broad, 2H), 0.92 (*t*,9H), 0.77 (*t*, 2H), 0.50 (*q*, 6H)

^{13}C NMR (100 MHz, $CDCl_3$), δ (ppm): 38.40, 17.83, 7.53, 3.56

Calculated % for $C_8H_{21}NSi$ (MW: 159.34 g·mol^{-1}): C(60.30), H(13.28), N(8.79), Si(17.63) found: C(59.89), H(13.24), N(8.65)

A.2.6 4-(aminobutyl)triethylsilane (TEtSBA)

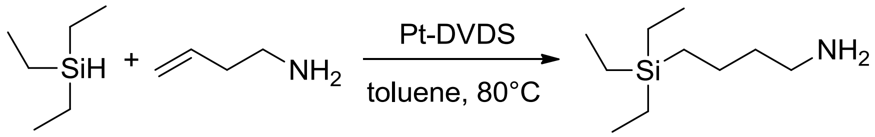

Figure A.8 – Synthesis of TEtSBA

To a 3-neck 250 mL round bottomed flask fitted with a condenser and magnetic stirbar under inert atmosphere was added 2 wt% Pt-DVDS in xylenes (0.6% catalyst loading wrt silane, 8.01 mL, 0.7 mmol) and triethylsilane (12.21 g, 105 mmol); the solution turned dark yellow. To this was added anhydrous toluene (40 mL) and 4-amino-1-butene (5.0 g, 70.3 mmol). The solution was heated to 80°C for 20 hours. Reaction progress was monitored via ^{1}H NMR for the disappearance of the silane proton (~3.7 ppm). When this peak was no longer present, the reaction mixture was allowed to cool to room temperature; the solvent and excess triethylsilane was then removed via rotary evaporator. The product 4-(aminobutyl)triethylsilane was distilled from the catalyst under reduced pressure (bp: 68°C at 1.95 mmHg) for an isolated yield of 66% (8.67 g; 46.3 mmol).

^{1}H NMR (400.13 MHz, $CDCl_3$, 25°C) δ = 2.62 (t, 2H), 1.40 (p, 2H), 1.27 (s, 2H), 1.17 (s, 2H), 0.86 (t, 9H), 0.44 (q, 8H)

^{13}C NMR (100.57 MHz, $CDCl_3$, 25°C) δ = 41.83, 37.95, 21.04, 11.09, 7.32, 3.16

Calculated % for $C_{10}H_{25}NSi$ (MW: 187.40 g·mol^{-1}): C(64.09), H(13.45), N(7.47), Si(14.99); found: C(62.34), H(13.33), N(7.47)

A.2.7 4-(triethylsilyl)-butyl-2-amine (αMe-TEtSA)

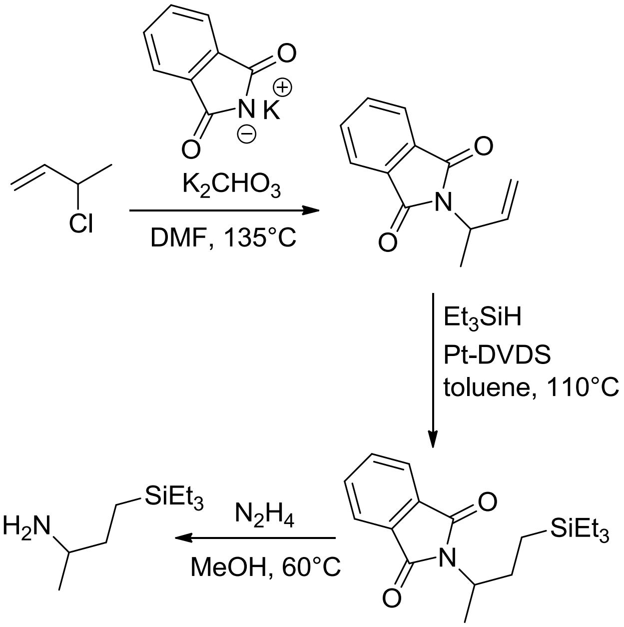

Figure A.9 – Synthesis of αMe-TEtSA

Gabriel Synthesis

A typical synthesis of αMe-TEtSA was achieved via the series of reactions detailed below. In a round-bottomed flask fitted with a condenser, 3-chloro-1-butene

(9.05 g, 100 mmol), potassium phthalimide (24.17 g, 130 mmol), and potassium carbonate (4.14 g, 30 mmol) were added to DMF (90 mL, 0.969 mol) and heated at reflux overnight. The reaction mixture was then poured over ice, forming a brown precipitate, which was isolated via vacuum filtration. The solid was washed with 1 M NaOH (200 mL, 0.2 mol), distilled water (100 mL, 5.6 mol), 1 N HCl (100 mL, 0.1 mol), and distilled water (100 mL, 5.6 mol); it was then vacuum dried, resulting in a 67% yield of the desired 3-phthalimido-1-butene (mp: 76-79°C).

^{1}H NMR (400.13 MHz, $CDCl_3$, 25°C) δ = 7.82 (m, 2H), 7.70 (m, 2H), 6.19 (m, 1H), 5.23 (d, 1H), 5.15 (d, 1H), 4.93 (p, 1H), 1.58 (d, 3H)

^{13}CNMR (100.57 MHz, $CDCl_3$, 25°C) δ = 167.92, 136.80, 133.84, 133.02, 123.11, 116.33, 48.93, 18.21

Hydrosilylation

In a 250 mL 3-neck round-bottomed flask fitted with a condenser, the isolated 3-phthalimido-1-butene (20.1 g, 100 mmol) and 2 wt% Pt-DVDS in xylenes (1.54 mL, 1.35×10^{-4} mol Pt, 0.104% loading wrt silane) was added to anhydrous toluene (60 mL, 0.563 mol) under inert atmosphere. The reaction mixture was then heated to 50°C, at which point the protected amine became soluble. Triethylsilane (20.7 mL, 130 mmol) was then added to the reaction mixture, which was then heated to 110°C and kept at that temperature overnight. The reaction was allowed to cool; the solvent was removed via rotary evaporator and the crude 3-(phthalimidobutyl)triethylsilane was distilled under reduced pressure with a 75% yield of the desired product 3-(phthalimidobutyl)triethylsilane (bp: 120°C at 0.7 mmHg).

^{1}H NMR (400.13 MHz, $CDCl_3$, 25°C) δ = 7.82 (m, 2H), 7.70 (m, 2H), 4.23 (s, 1H), 2.01 (m,1H), 1.72 (m,1H), 1.46 (d, 3H), 0.88 (trip, 9H), 0.48 (q,7H), 0.37 (t of d, 1H)

^{13}C NMR (100.57 MHz, $CDCl_3$, 25°C) δ = 168.61, 133.73, 132.01, 123.01, 50.58, 28.14, 18.30, 8.42, 7.37, 3.10

Ing-Manske Deprotection

3-(phthalimidobutyl)triethylsilane (16.9 g, 53 mmol) was dissolved in anhydrous methanol (250 mL, 6.172 mol). Anhydrous hydrazine (5 mL, 187 mmol) was slowly added and the reaction mixture was heated at 60°C for 4 hours. A cloudy white network formed, which was precipitated via addition of 2 M HCl. The resulting solid was removed from the desired liquid product mixture via vacuum filtration and washed with distilled water (100 mL, 5.6 mol). The solvent was removed via rotary evaporator and NaOH was added to the crude product until the pH was greater than 9. Extraction with ether, drying with $MgSO_4$, and distillation under reduced pressure yielded the pure product, 4-(triethylsilyl)-butan-2-amine in 62% yield (bp: 73°C at 2.7 mmHg).

^{1}H NMR (400.13 MHz, $CDCl_3$, 25°C) δ = 2.74 (s, 1H), 1.26 (m, 2H), 1.16 (s, 2H), 1.03 (d, 3H), 0.90 (t, 9H), 0.49 (q and m overlapping, 8H)

^{13}C NMR (100.57 MHz, $CDCl_3$, 25°C) δ = 49.71, 34.18, 23.25, 7.48, 7.37, 3.14

Calculated % for $C_{10}H_{25}NSi$ (MW: 187.40 g·mol^{-1}): C(64.09), H(13.45), N(7.47), Si(14.99); found: C(63.03), H(13.47), N(7.39)

A.2.8 2-methyl-4-(triethylsilyl)-butyl-2-amine (α,αDMe-TEtSA)

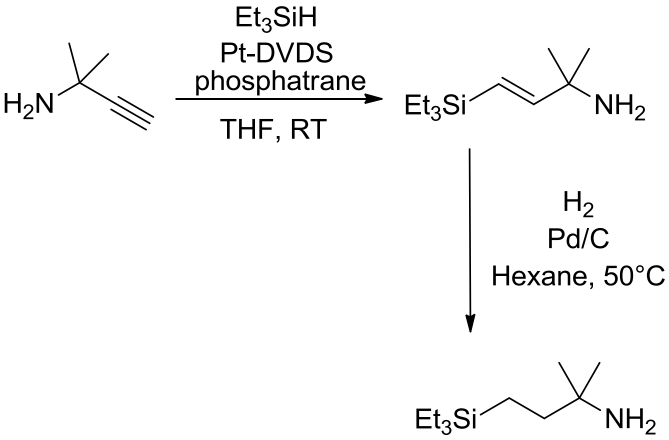

Figure A.10 – Synthesis of α,αDMe-TEtSA

Hydrosilylation

A 3-neck 250 mL round bottomed flask was fitted with a condenser and stirbar and placed under argon. To this was added 2 wt% Pt-DVDS in xylenes (13.75 mL, 1.205 x 10^{-3} mol Pt; 1.268% catalyst loading wrt silane) and 0.5 M 2,8,9-triisobutyl-2,5,8,9-tetraaza-1-phosphabicyclo[3.3.3]undecane solution in diethyl ether (2.4 mL, 1.200 x 10^{-3} mol). The reaction mixture was heated at 60°C for 10 minutes. After cooling to room temperature, anhydrous inhibitor-free THF (80 mL, 0.9865 mol) was added to the flask, which was then cooled to approximately -10°C in an ice-and-brine bath. Triethylsilane (21.25 mL, 0.133 mol) was then added dropwise to the flask and allowed to stir for approximately 5 minutes. 2-methyl-3-butyn-2-amine (10 mL, 9.503 x 10^{-2} mol) was then added dropwise to the reaction mixture, which was kept in the ice bath until the large exotherm had ceased. The reaction was then allowed to stir at room temperature overnight; reaction progress was monitored by the disappearance of the terminal alkyne carbon in the ^{13}C NMR (approximately δ91). The solvent and unreacted silane were removed via rotary evaporator. Distillation under reduced pressure yielded the alkene product 2-methyl-4-(triethylsilyl)but-3-en-2-amine as a clear oil (bp 60°C at 5 mmHg; 4.7772 g, 79.8% yield).

^{1}H NMR (400.13 MHz, $CDCl_3$, 25°C) δ = 6.10 (d, 1H), 5.55 (d, 1H), 1.17 (s, 2H), 1.14/1.13 (s overlapping, (6H)), 0.88 (t of d, 9H), 0.52 (q of d, 6H)

^{13}C NMR (100.57 MHz, $CDCl_3$, 25°C) δ = 157.50, 118.58, 52.24, 30.20, 7.28, 3.47

Hydrogenation

Hydrogenation of the alkene was carried out in a Parr reactor. The reactor was first loaded with 5 wt% Pd/C (0.1367 g, 6.42 x 10^{-5} mol Pd; 0.11% catalyst loading wrt alkene) and then purged several times with dry nitrogen. Anhydrous ethanol (30 mL, 0.513 mol) and 2-methyl-4-(triethylsilyl)but-3-en-2-amine (11.9032 mL, 59.69 mmol) were added to the reactor, which was then pressurized with hydrogen (80 psi) and heated at 50°C for 12 hours. Upon cooling, excess H_2 was vented, and the catalyst was removed from the reaction mixture via filtration with Celite. ^{1}H NMR of the product mixture revealed the total absence of any alkene peaks, indicating that the reaction had gone to completion. Removal of the solvent via rotary evaporator yielded the desired saturated crude product, which was then distilled at reduced pressure to yield 2-methyl-4-(triethylsilyl)-butyl-2-amine as a clear oil (9.1850 g, bp 65°C at 1.5 mmHg; 76.4% isolated yield).

^{1}H NMR (400.13 MHz, $CDCl_3$, 25°C) δ = 1.24 (m 2H), 1.09 (s, 2H), 0.99 (s, 6H), 0.86 (t, 9H), 0.42 (q, 8H)

^{13}C NMR (100.57 MHz, $CDCl_3$, 25°C) δ = 50.20, 39.02, 29.81, 7.59, 5.22, 3.30

Calculated % for $C_{11}H_{27}NSi$ (MW: 201.42 g·mol^{-1}): C(65.59), H(13.51), N(6.95), Si(13.94); found: C(64.03), H(13.51), N(6.67)

A.2.9 2-methyl-3-(triethylsilyl)propylamine (βMe-TEtSA)

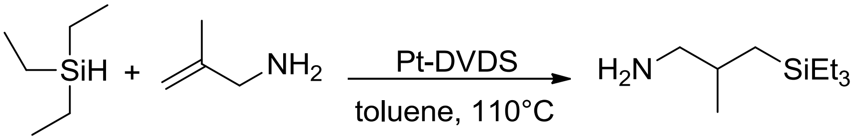

Figure A.11 - Synthesis of βMe-TEtSA

A 3-neck 250 mL round-bottomed flask was fitted with a condenser and stirbar and placed under argon. Anhydrous toluene (40 mL, 0.376 mol) was added to the flask, followed by triethylsilane (16.5 mL, 103 mmol; 2.58 M) and 2 wt% Pt-DVDS in xylenes (2.70 mL, 2.395 x 10^{-4} mol Pt; 0.23% loading wrt silane). The reaction mixture was allowed to stir at room temperature for several minutes; 2-methylallylamine (5 g, 70.3 mmol; 1.75 M) was then added and the reaction mixture was heated at 110°C for 24 hours. Reaction progress was checked via ^{1}H NMR for disappearance of the vinyl peaks of 2-methylallylamine. The solvent was removed via rotary evaporator and the product distilled under reduced pressure to yield 10.0744 g product (53.7 mmol; 76.4% isolated yield).

^{1}H NMR (400.13 MHz, $CDCl_3$, 25°C) $\delta = 2.51$ (m, 1H), 2.43 (m, 1H), 1.54 (m, 1H), 1.11 (s, 2H), 0.91 (t, 9H), 0.90 (d, 3H), 0.51 (q, 6H), 0.61 (d of d, 1H), 0.32 (d of d, 1H)

^{13}C NMR (100.57 MHz, $CDCl_3$) $\delta = 51.75, 32.79, 20.39, 16.69, 7.46, 4.01$

Calculated % for $C_{10}H_{25}NSi$ (MW: 187.40 g·mol^{-1}): C(64.09), H(13.45), N(7.47), Si(14.99); found: C(63.31), H(13.54), N(7.33)

A.2.10 (*trans*)-3-(Triethylsilyl)prop-2-en-1-amine (*trans*-TEtSA)

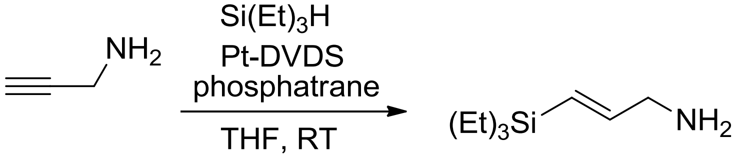

Figure A.12 - Synthesis of *trans*-TEtSA

A typical reaction was carried out as follows. In a 3-neck 250 mL round bottomed flask fitted with a condenser under inert atmosphere, 17.8 mL 2% Pt-DVDS in xylenes (1.560 x 10^{-3} mol Pt; 1.00% loading wrt silane) was combined with 3.1 mL 0.5 M 2,8,9-triisobutyl-2,5,8,9-tetraaza-1-phosphabicyclo[3.3.3]undecane solution (1.625 x 10^{-3} mol) in diethyl ether. The reaction mixture was heated at 60°C for 10 minutes and then allowed to cool to room temperature. 100 mL anhydrous inhibitor-free THF (1.233 mol) was added to the flask, which was then cooled to approximately -10°C in an ice-and-brine bath. 27.5 mL triethylsilane (0.172 mol) was then added dropwise to the flask and allowed to stir for approximately 5 minutes. 10 mL of propargylamine (0.156 mol) was then added dropwise to the reaction mixture, which was kept in the ice bath until the large exotherm had ceased. The reaction was then allowed to stir at room temperature overnight; reaction progress was monitored by the disappearance of the terminal alkyne carbon in the ^{13}C NMR (approximately δ91). The solvent and excess triethylsilane were then removed via rotary evaporator, and the product was distilled under reduced pressure (bp: 75°C at 6 mmHg) to yield 12.1926 g of the trans-isomer only (0.0711 mol; 45.57% yield).

^{1}H NMR (400.13 MHz, $CDCl_3$, 25°C) 6.13 (dt, J = 18.8, 4.8 Hz, 1H), 5.67 (dt, J = 18.9, 1.8 Hz, 1H), 3.33 (dd, J = 4.8, 1.8 Hz, 2H), 1.12 (s, 2H) 0.98 (t, J = 7.9 Hz, 9H) 0.57 (q, J = 7.9 Hz, 6H)

^{13}C NMR (100.57 MHz, $CDCl_3$, 25°C) 149.10, 124.22, 47.19, 7.55, 3.70

Calculated % for $C_9H_{21}NSi$ (MW: 171.36 g·mol^{-1}): C(63.08), H(12.35), N(8.17), Si(16.39); found: C(62.34), H(12.36), N(7.67)

A.2.11 (*trans*)-2-methyl-4-(triethylsilyl)but-3-en-2-amine (*trans*-α,αDMe-TEtSA)

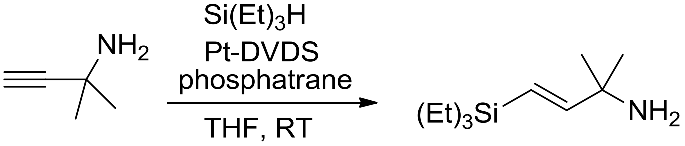

Figure A.13 – Synthesis of *trans*-α,αDMe-TEtSA

A 3-neck 250 mL round bottomed flask was fitted with a condenser and stirbar and placed under argon. To this was added 2 wt% Pt-DVDS in xylenes (13.75 mL, 1.205 x 10^{-3} mol Pt; 1.268% catalyst loading wrt silane) and 0.5 M 2,8,9-triisobutyl-2,5,8,9-tetraaza-1-phosphabicyclo[3.3.3]undecane solution in diethyl ether (2.4 mL, 1.200 x 10^{-3} mol). The reaction mixture was heated at 60°C for 10 minutes. After cooling to room temperature, anhydrous inhibitor-free THF (80 mL, 0.9865 mol) was added to the flask, which was then cooled to approximately -10°C in an ice-and-brine bath. Triethylsilane (21.25 mL, 0.133 mol) was then added dropwise to the flask and allowed to stir for approximately 5 minutes. 2-methyl-3-butyn-2-amine (10 mL, 9.503 x 10^{-2} mol) was then added dropwise to the reaction mixture, which was kept in the ice bath until the large exotherm had ceased. The reaction was then allowed to stir at room temperature overnight; reaction progress was monitored by the disappearance of the terminal alkyne carbon in the ^{13}C NMR (approximately δ91). The solvent and unreacted silane were removed via rotary evaporator. Distillation under reduced pressure yielded the alkene product 2-methyl-4-(triethylsilyl)but-3-en-2-amine as a clear oil (bp 60°C at 5 mmHg; 4.7772 g, 79.8% yield).

^{1}H NMR (400.13 MHz, $CDCl_3$, 25°C) $\delta = 6.10$ (d, 1H), 5.55 (d, 1H), 1.17 (s, 2H), 1.14/1.13 (s overlapping, (6H)), 0.88 (t of d, 9H), 0.52 (q of d, 6H)

^{13}C NMR (100.57 MHz, $CDCl_3$, 25°C) $\delta = 157.50$, 118.58, 52.24, 30.20, 7.28, 3.47

Calculated % for $C_{11}H_{25}NSi$ (MW: 199.41 $g\cdot mol^{-1}$): C(66.25), H(12.64), N(7.02), Si(14.08); found: C(64.81), H(12.41), N(6.55)

A.2.12 <u>(*trans*)-2-methyl-4-(tripropylsilyl)-butyl-2-amine (*trans*-α,αDMe-TPSA)</u>

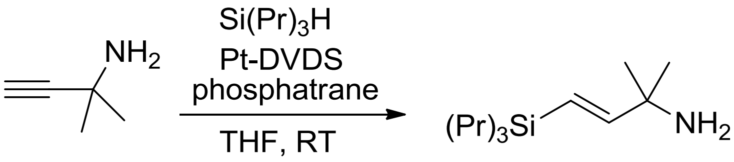

Figure A.14 – Synthesis of *trans*-α,αDMe-TPSA

Synthesized in the same manner as trans-α,αDMe-TEtSA. A 3-neck 250 mL round bottomed flask was fitted with a condenser and stirbar and placed under argon. To this was added 2 wt% Pt-DVDS in xylenes (13.75 mL, 1.205 x 10^{-3} mol Pt; 1.268% catalyst loading wrt silane) and 0.5 M 2,8,9-triisobutyl-2,5,8,9-tetraaza-1-phosphabicyclo[3.3.3]undecane solution in diethyl ether (2.4 mL, 1.200 x 10^{-3} mol). The reaction mixture was heated at 60°C for 10 minutes. After cooling to room temperature, anhydrous inhibitor-free THF (80 mL, 0.9865 mol) was added to the flask, which was then cooled to approximately -10°C in an ice-and-brine bath. Tripropylsilane (21.25 mL, 0.133 mol) was then added dropwise to the flask and allowed to stir for approximately 5 minutes. 2-methyl-3-butyn-2-amine (10 mL, 9.503 x 10^{-2} mol) was then added dropwise to the reaction mixture, which was kept in the ice bath until the large exotherm had ceased. The reaction was then allowed to stir at room temperature overnight; reaction progress was monitored by the disappearance of the terminal alkyne carbon in the ^{13}C NMR (approximately δ91). The solvent and unreacted silane were removed via rotary evaporator. Distillation under reduced pressure yielded the alkene product 2-methyl-4-(tripropylsilyl)-butyl-2-amine as a clear oil (68.1% yield).

^{1}H NMR (400.13 MHz, $CDCl_3$, 25°C) δ = 5.85 (d, 1H), 5.35 (d, 1H), 1.06 (s (br) overlapping sex, 8 H), 0.88 (s, 6H), 0.67 (t, 9H), 0.29 (d overlapping t, 6H)

^{13}C NMR (100.57 MHz, $CDCl_3$, 25°C) δ = 156.74, 119.31, 51.84, 29.79, 18.12, 17.01, 15.10

Calculated % for $C_{14}H_{31}NSi$ (MW: 241.49 g·mol^{-1}): C(69.63), H(12.94), N(5.80), Si(11.63); found: C(68.93), H(12.96), N(5.29)

A.2.13 N-methyl-3-(triethylsilyl)propan-1-amine (STEtSA)

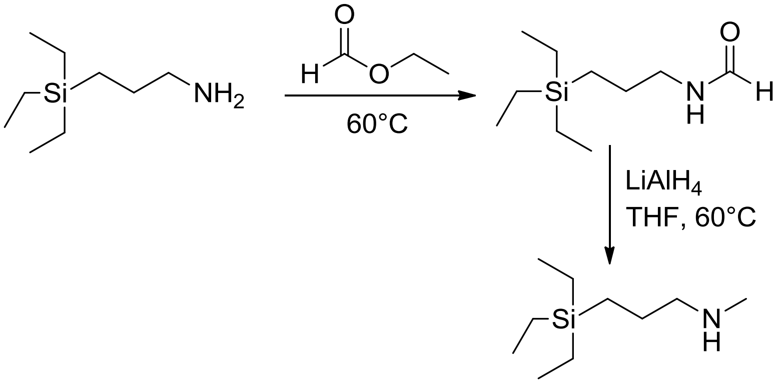

Figure A.15 – Synthesis of STEtSA

Formylation

To a round bottomed flask fitted with a condenser and magnetic stirbar under inert atmosphere was added 3-(aminopropyl)triethylsilane (8.69 g, 50 mmol). This was cooled to 10°C; ethylformate (5.25 mL, 65 mmol) was added then added dropwise over 15 minutes. The solution was then heated to 60°C and stirred for 3 hours. The byproduct EtOH and excess ethylformate were then removed under reduced pressure to yield 9.72 g (48.27 mmol) of the desired product N-(3-(triethylsilyl)propyl)formamide in 97% yield.

^{1}H NMR (400.13 MHz, $CDCl_3$, 25°C) δ = 8.13 (s)/8.01 (d)(1H), 5.96 (s, 1H), 3.23 (q)/3.15 (q) (2H), 1.47 (s, 2H), 0.89 (t, 9H), 0.48 (q, 8H)

^{13}C NMR (100.57 MHz, $CDCl_3$, 25°C) δ = 161.19, 41.43, 24.09, 8.51, 7.37, 3.13

Reduction

To a round bottomed flask fitted with a condenser and magnetic stirbar under inert atmosphere was added anhydrous THF (80 mL, 0.9865 mol) and N-(3-(triethylsilyl)propyl)formamide (8.49 g, 42 mmol). This solution was heated to 60°C, and $LiAlH_4$ in THF (50.7 mL, 50.7 mmol, 1 M) was added slowly over 45 minutes. An exotherm was observed. The reaction mixture was stirred for 18 hours at 60°C, at which point the resulting mixture was cooled to room temperature. DI H_2O (2.5 mL, 0.139 mol) and 10% NaOH (5 mL, 1.25 mmol) were added. An additional aliquot of H_2O (10.5 mL, 0.58 mol)) was then added; the mixture was filtered through Celite, then washed with hexane and MeOH. The organic layer was separated; the aqueous layer was washed with hexane, which was then combined with the previous organic layer. The solution was then washed with brine and dried with $MgSO_4$. The solvents were removed via rotary evaporator. The resulting liquid was distilled under reduced pressure at 1 mmHg and 48°C to provide N-methyl-3-(triethylsilyl)propan-1-amine (5.68 g, 30.3 mmol), corresponding to a 73% isolated yield.

^{1}H NMR (400.13 MHz, $CDCl_3$, 25°C) δ = 2.54 (t, 2H), 2.42 (s, 3H), 1.46 (s, 2H), 1.37 (s, 1H), 0.91 (t, 9H), 0.50 (q, 8H)

^{13}C NMR (100.57 MHz, $CDCl_3$, 25°C) δ = 55.70, 36.37, 24.09, 8.73, 7.42, 3.23

Calculated % for $C_{10}H_{25}NSi$ (MW: 187.40 g·mol^{-1}): C(64.09), H(13.45), N(7.47), Si(14.99); found: C(63.12), H(13.47), N(7.47)

A.2.14 N-methyl-3-(aminopropyl)dimethylethylsilane (SDMESA)

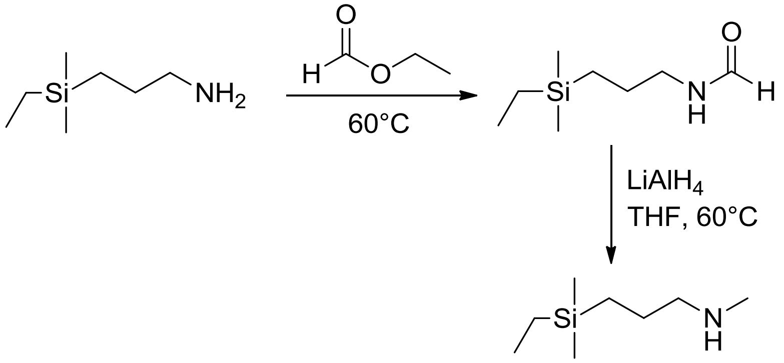

Figure A.16 – Synthesis of SDMESA

Formylation

3-(Aminopropyl)dimethylethylsilane (DMEtSA) (7.3 g, 0.05 mol) was added to a RB flask under argon. Ethylformate (5.25 mL, 0.065 mol) was added dropwise over 15 minutes at 10°C. The temperature of the solution was increased to 60°C and stirred for 4 hours. The solution was then cooled and rotovapped to remove the by-product, EtOH, and excess ethylformate to provide 8.47 g of N-(3-(dimethylethylsilyl)propyl)formamide in 98% yield.

^{1}H NMR (400 Hz, $CDCl_3$) 8.14 (s)/ 8.00 (d) (1H), 5.79 (s, 1H), 3.25 (q)/3.16(q) (2H), 1.48 (s, 2H), 0.89 (t, 3H), 0.47 (q, 4H), -0.06 (s, 6H)

^{13}C NMR (400 Hz, $CDCl_3$) 161.11, 41.28, 24.12, 11.92, 7.25, 6.68, 4.07

Reduction

N-(3-(dimethylethylsilyl)propyl)formamide (7.83 g, 0.0452 mol) was added to 120 mL of anhydrous THF under an inert atmosphere in a RB flask. The solution temperature was brought to 60°C and solid $LiAlH_4$ (3.091 g, 0.081 mol) was added slowly via solid addition arm over 30 minutes. After stirring for 18 hours at 60°C, the resulting mixture was cooled with a dry/ice acetone bath to keep the temperature at about 0°C. To it was added 3 mL H_2O followed by 6 mL of a 10% NaOH solution. 12 mL of H_2O were then added and the entire mixture was filtered through a pad of celite and washed with THF and H_2O. The collected solution was then introduced into a separatory funnel and heavily brined with NaCl. The organic layer was separated. The aqueous layer was washed with hexane and the organic layer was combined with the previous. They were both washed with brine and dried over $MgSO_4$. The solvents were removed via rotovap distillation. The resulting liquid was distilled under reduced pressure at 3.4 mmHg and 36°C to provide 3.54 g of the N-methyl-3-(dimethylethylsilyl)propan-1-amine corresponding to a 49% isolated yield.

^{1}H NMR (400 Hz, CDCl3) 2.47 (t, 2H), 2.35 (s, 3H), 1.40 (s, 2H), 1.00 (s, 1H), 0.84 (t, 3H), 0.40 (q, 2H), -0.12 (s, 6H)

^{13}C NMR (400 Hz, CDCl3) 55.47, 36.32, 24.10, 12.15, 7.21, 6.73, -4.10

Expected: C(60.30), H(13.28), N(8.79), Si(17.63) found: C(58.97), H(13.17), N(8.42)

A.3 Aspen HYSYS Simulation Details

The following tables provide details on the Aspen HYSYS simulation conducted to model a CO_2 capture process of 3-(aminopropyl)tripropylsilane.

Table A.1 – Capture conditions

CAPTURE CONDITIONS			
	Flowrate (kg/h)	Temperature C	Pressure (kPa)
TPSA Makeup	1.07E+04	40	101.3
Absorber	4.43E+06	40	101.3
Absorber / IL out (TPSA_IL_OUT)	4.73E+06	40	101.3
Heat exchanger (TPSA_IL_WARMER)	4.73E+04	50	120
Heater output (TPSA_IL_IN) = stripper op. T	4.73E+06	85	126
Stripper CO_2 rich gas	3.47E+05	85	126
Cooler	4.38E+06	74.42	120

Table A.2 – Inlet flue gas conditions

INLET FLUE GAS		
	Mass Flows (kg/h)	Mole Fraction
CO_2	305807.4	0.08
MEAmine	0	0
CO	0	0
H_2O	400545	0.26
Oxygen	54334.8	0.02
Nitrogen	154273.7	0.64
TPSA_ML	0	0
TPSA IL	0	0
Argon	18576	0.005

Table A.3 – CO_2-rich gas conditions

CO_2 RICH GAS		
	Mass Flows (kg/h)	Mole Fraction
CO_2	275200.02	0.72
H_2O	39921.98	0.26
Oxygen	21	0.0001
Nitrogen	845.64	0.004
TPSA_ML	31039.92	0.02
TPSA IL	0	0
Argon	7.94	0

Table A.4 – CO_2 spent gas conditions

CO_2 SPENT GAS		
	Mass Flows (kg/h)	Mole Fraction
CO_2	30621.3	0.01
H_2O	54312.6	0.05
Oxygen	54313.5	0.03
Nitrogen	1541889	0.9
TPSA_ML	11646	0.0009
TPSA IL	0.02	0
Argon	18567.95	0.008

Table A.5 - CO_2 recovery and energy required

CO_2 Removed	0.9
CO_2 Recovered	0.9
Total Energy Required = 3.83E+08 kJ/h	
Energy per kg of CO_2 captured = 1.39 MJ/kg	

$$CO2\ removed = \frac{C^{Flue}_{CO2} - C^{Spent}_{CO2}}{C^{Flue}_{CO2}} \qquad CO2\ recovered = \frac{C^{Rich}_{CO2}}{C^{Flue}_{CO2}}$$

Figure A.17 – Equations for CO_2 removed and CO_2 recovered

APPENDIX B - ADDITIONAL INFORMATION ON CARBON DIOXIDE AS A PROTECTING GROUP IN CHEMICAL SYNTHESES

B.1 Standard NMRs

The NMRs included below are for reference to those presented in Chapter 3.

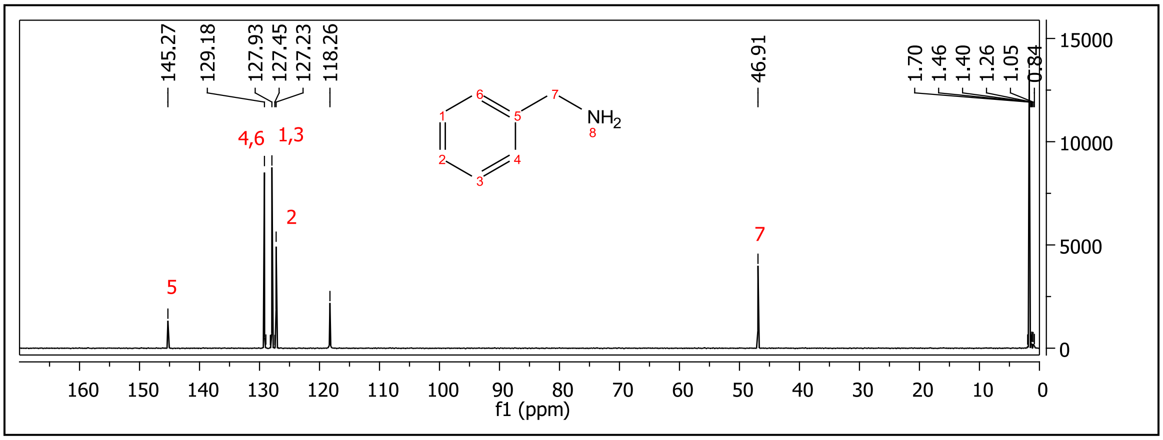

Figure B.1 – ^{13}C NMR spectrum of benzylamine in deuterated acetonitrile

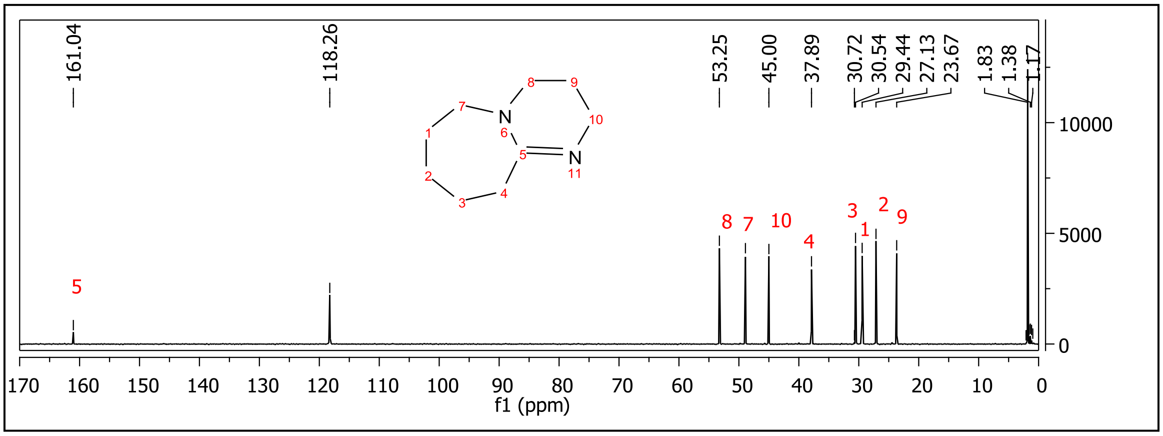

Figure B.2 – ^{13}C NMR spectrum of DBU in deuterated acetonitrile

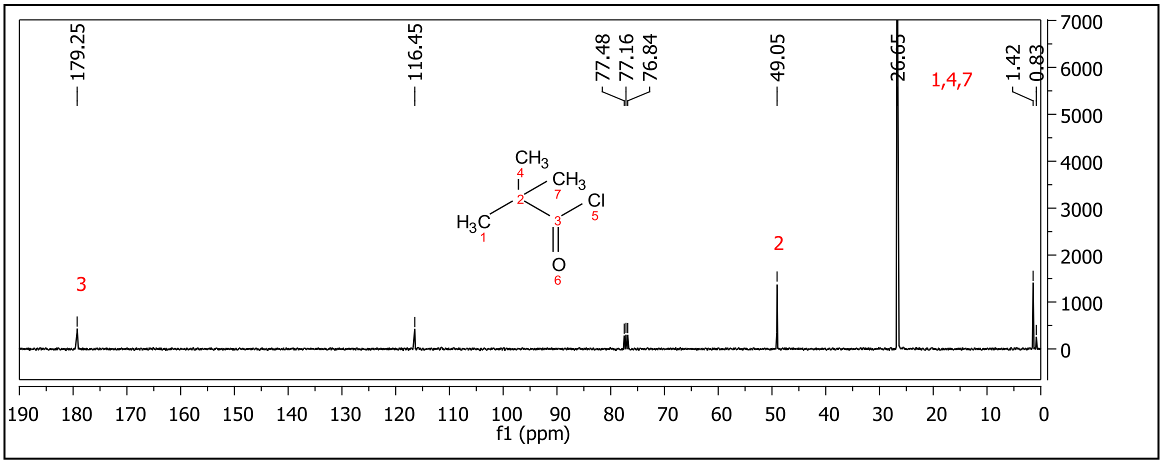

Figure B.3 - ^{13}**C NMR spectrum of pivaloyl chloride with a deuterated chloroform capillary**

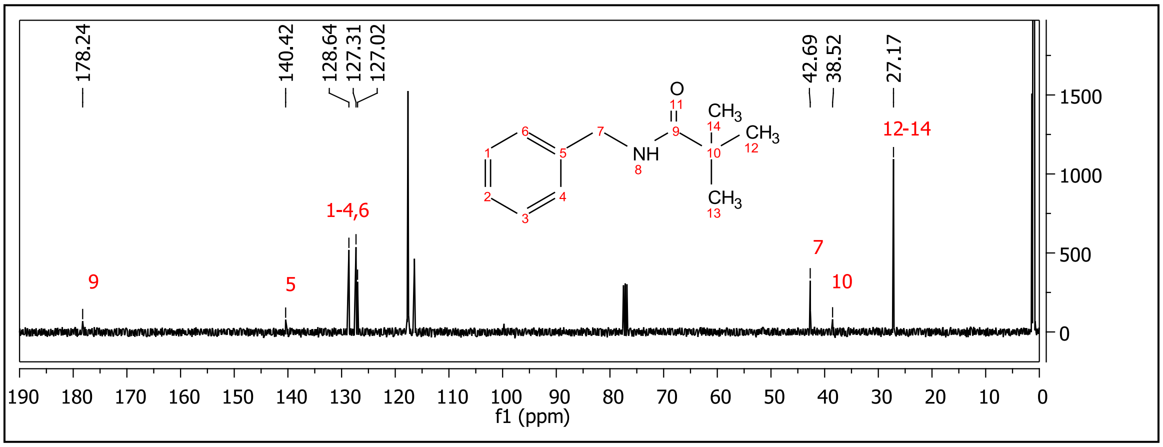

Figure B.4 – ^{13}**C NMR spectrum of benzylpivalamide with a deuterated chloroform capillary**

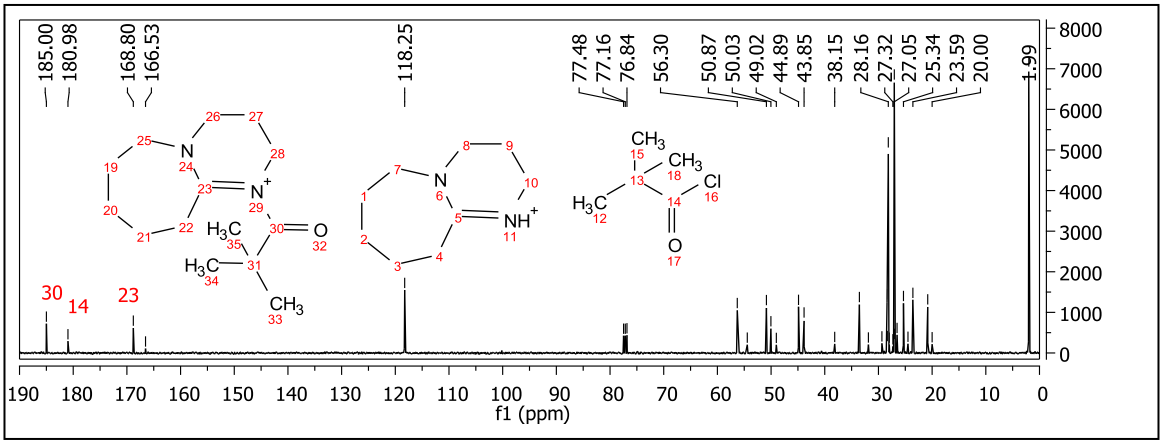

Figure B.5 – ^{13}**C NMR spectrum of pivaloyl chloride and DBU – reaction observed**

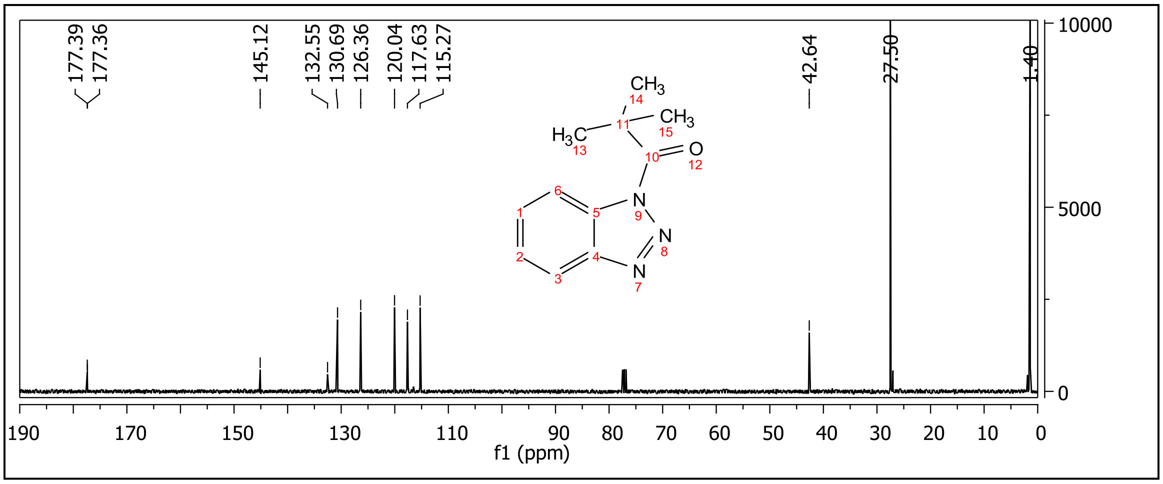

Figure B.6 – ^{13}C NMR spectrum of pivaloyl benzatriazole in deuterated chloroform

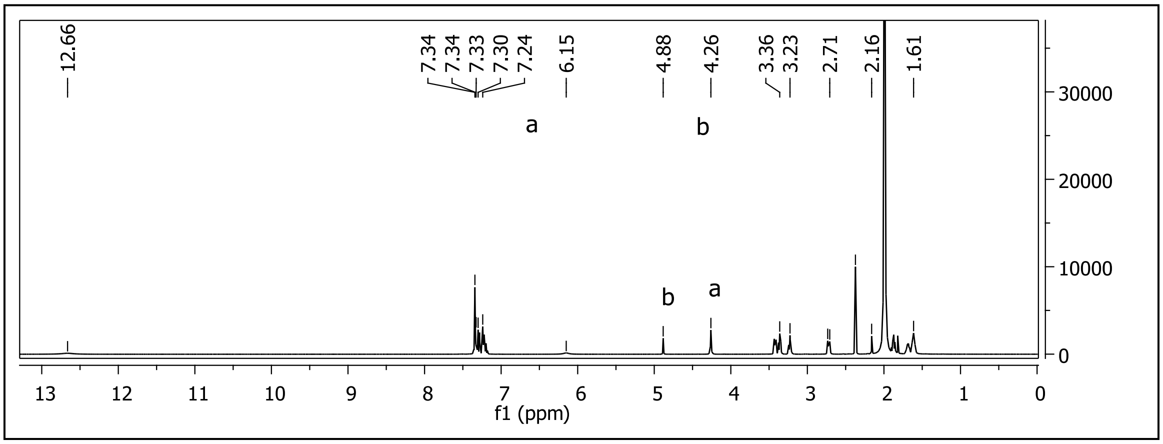

Figure B.7 - ^{1}H NMR of benzylamine + CO_2 + DBU, peaks assigned a and b are labeled below

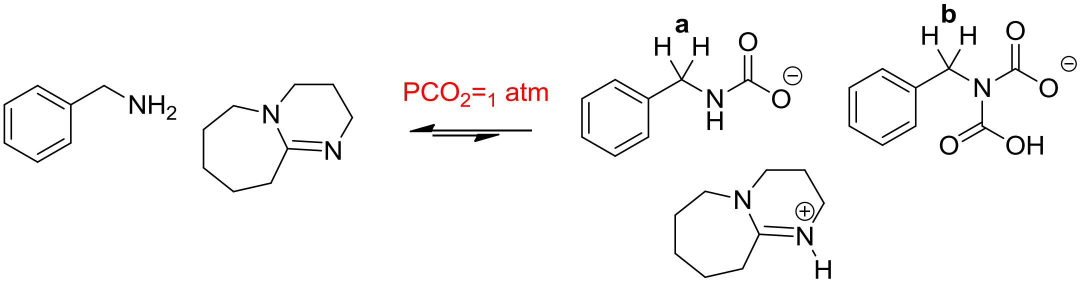

Figure B.8 – Reaction of benzylamine with CO_2 in the presence of DBU; peaks labeled are assigned in Figure B.7

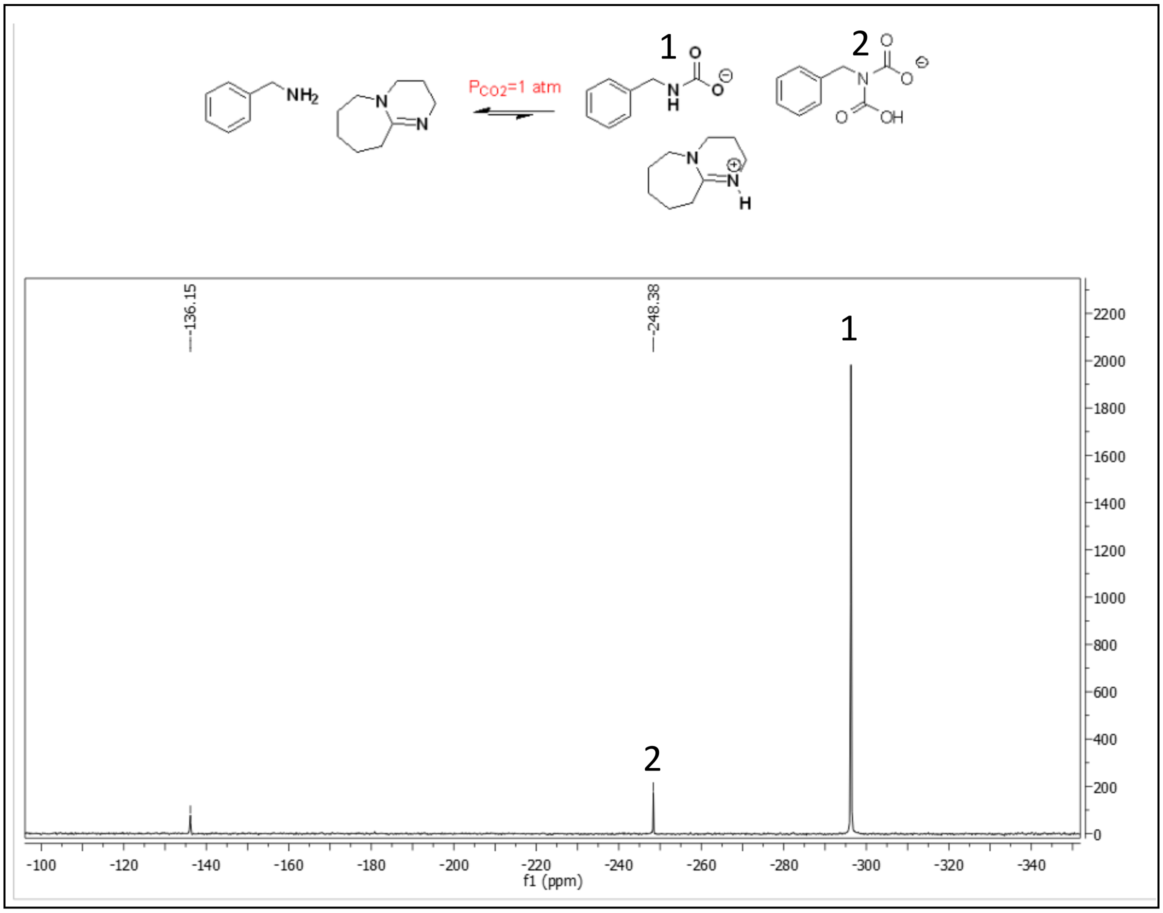

Figure B.9 – ^{15}N NMR of CO$_2$-protected benzylamine (^{15}N labeled) using DBU, nitrogen atoms are labeled above

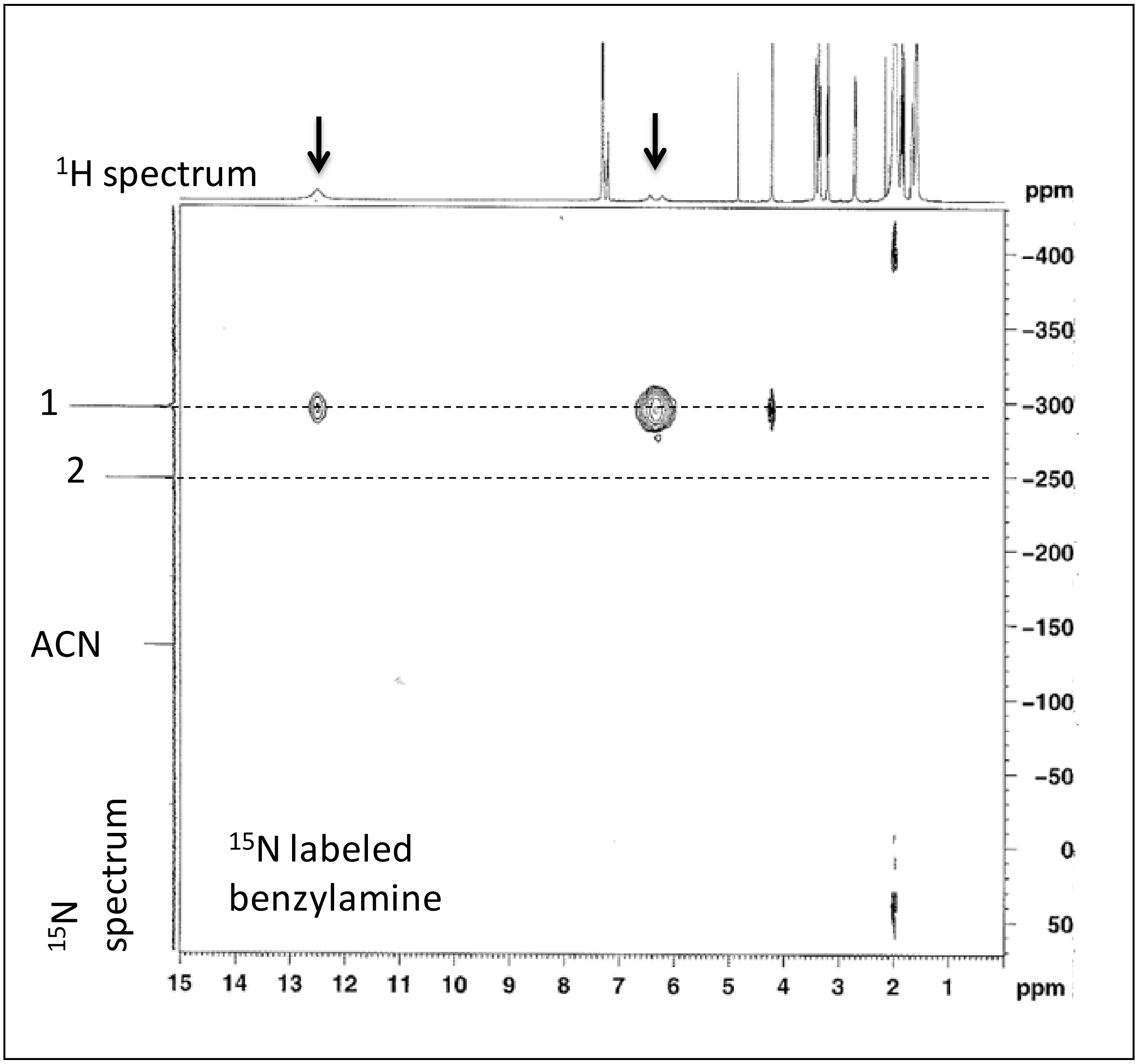

Figure B.10 – 2D NMR experiment coupling ^{15}N NMR and ^{1}H NMR. ^{15}N NMR peaks are labeled according to Figure B.9

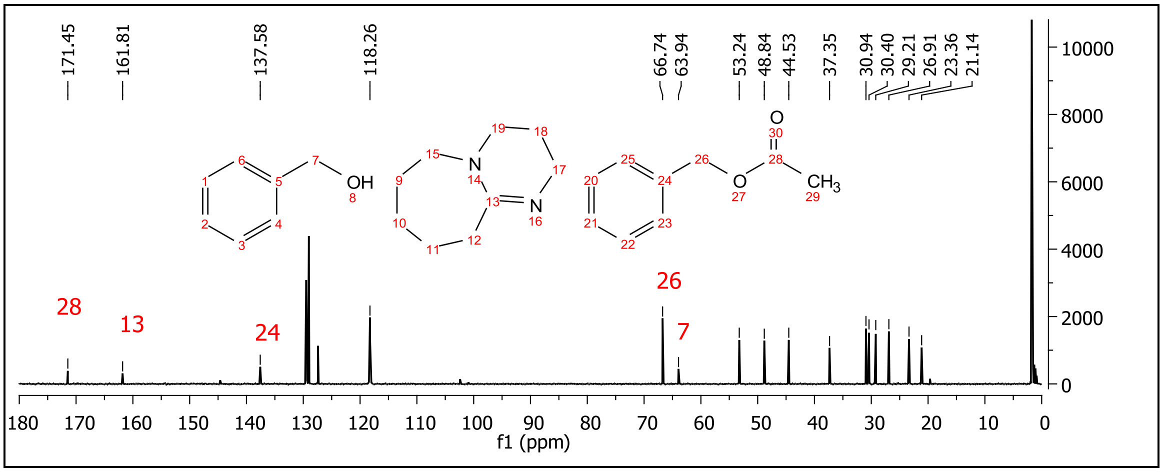

Figure B.11 - ^{13}**C NMR showing reaction products from benzylalcohol and isopropenyl acetate in the presence of DBU (no CO$_2$)**

APPENDIX C - ADDITIONAL INFORMATION ON MITIGATING THE THERMAL DEGRADTION OF POLYVINYL CHLORIDE

C.1 Introduction

This Appendix provides additional information referenced in Chapter 4. Syntheses of the model compounds and novel stabilizers were conducted by graduate chemists in the Eckert-Liotta research group.

C.2 Experimental

C.2.1 Materials for model studies

Calcium acetate ($Ca(OAc)_2$), *o*-dichlorobenzene (anhydrous), 1,3-dichlorobutane, diisodecyl phthalate (DIDP), deuterated dimethylsulfoxide (d_6-DMSO), sodium acetate (NaOAc, anhydrous), tetradecane, tetrahydrofuran (THF, anhydrous, inhibitor-free), tetra-*n*-butylammonium chloride (TBAC), zinc acetate ($Zn(OAc)_2$), and zinc stearate ($ZnSt_2$, purum, 10-12% zinc metal basis) were obtained from Sigma-Aldrich. Calcium stearate ($CaSt_2$) was obtained from Alfa Aesar. PVC powder (Oxyvinyls 240F) was provided by Dow Chemical Company. Helium and nitrogen were obtained from Airgas. All materials were >97% purity or ultra-high purity unless otherwise stated and used as received from the manufacturers.

C.2.2 Synthesis of 2,4-dichloropentane

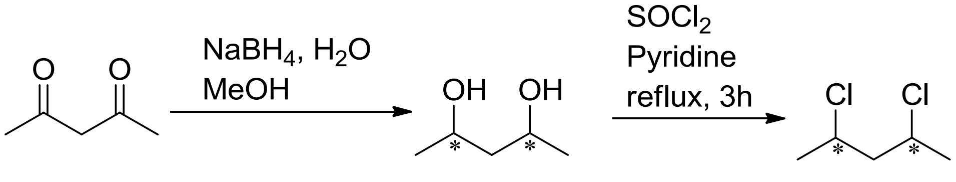

Figure C.1 - Synthesis of 2,4-dichloropentane

C.2.2.1 *Synthesis of 2,4-Pentanediol*

A solution of sodium borohydride ($NaBH_4$, 2.5 g, 0.066 mol) and sodium hydroxide (NaOH, 0.050 g, 0.0013 moles) in water (25 mL) was prepared and kept at approximately 20°C. A solution of acetylacetone (10 g, 0.099 moles) in methanol (MeOH, 30 mL) was added drop wise and stirred for 15 minutes. The solvent was removed *in vacuo*, yielding a white solid. The solid was then extracted into glycerol (50 mL). The extract was distilled at 60-70°C (0.45 mmHg) and, subsequently, fractionally distilled at 70-75°C (3.5 mmHg) in order to remove trace amounts of glycerol. 6.024 g (60% yield) of 2,4-pentanediol (colorless liquid) was obtained.

^{1}H NMR (400 MHz, acetone-d_6) δ 1.12 (t, J = 6.3 Hz, 6H), 1.47 (m, 2H), 3.97 (m, 2H), 4.06 (d, J = 4.68 Hz, 1H), 4.40 (d, J = 3.32 Hz, 1 H)

^{13}C NMR (400 MHz, acetone-d_6) δ 23.5 (2C), 47.1, 47.3, 64.1, 67.1.

C.2.2.2 Synthesis of 2,4-dichloropentane

Thionyl chloride ($SOCl_2$, 27.9 mL, 0.384 moles) was added drop wise to a solution of 2,4-pentanediol (10. g, 0.096 moles) in pyridine (1.17 mL, 0.0146 moles) at 0°C under argon atmosphere. The mixture was refluxed for 3 hours. After being cooled to room temperature, ice was added to quench any unreacted $SOCl_2$. The mixture was extracted twice with diethyl ether (50 mL). The combined organic layers were dried over magnesium sulfate ($MgSO_4$) and the solvent removed *in vacuo* (75 mmHg). Distillation (140-150°C, atm. pressure) yielded 5.558 g (41% yield) of 2,4-dichloropentane as a colorless liquid.

^{1}H NMR (400 MHz, $CDCl_3$) δ 1.52 (2d, J = 10.8, 7.5 Hz, 6H), 1.98 (m, 1.3H), 2.28 (dt, J = 14.2, 7.7 Hz, 0.6H), 4.13 (m, 1.2H), 4.30 (m, 0.7H)

^{13}C NMR (400 MHz, $CDCl_3$) δ 24.5, 25.5, 50.1, 50.4, 54.7, 55.8

C.2.3 Synthesis of 3-ethyl-3-chloropentane

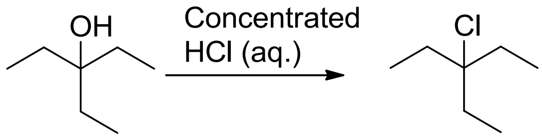

Figure C.2 - Synthesis of 3-ethyl-3-chloropentane

Hydrochloric acid (HCl, 10M, 40 mL) was added to 3-ethyl-3-pentanol (40 mL, 0.289 mol). The biphasic mixture was stirred at room temperature for 2 hours. The organic layer was then separated, dried over magnesium sulfate and purified over a silica plug with hexanes as the eluent. The solvent was removed under vacuum at 75 mmHg, 25°C to yield 40 mL (90% yield) of 3-ethyl-3-chloropentane as a clear liquid.

^{1}H NMR (400 MHz, $CDCl_3$) δ 0.95 (t, J = 7.4 Hz, 9H), 1.77 (q, J = 7.4 Hz, 6H)
^{13}C NMR (400 MHz, $CDCl_3$) δ 8.6, 22.6, 79.8

C.2.4 Synthesis of 3,4-dichlorohexane

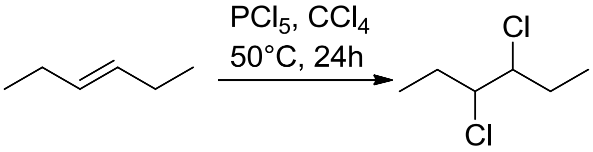

Figure C.3 - Synthesis of 3,4-dichlorohexane

Phosphorus pentachloride (PCl_5, 12.37 g, 60 mmol) was suspended in carbon tetrachloride (CCl_4, 23 mL) and heated to 50°C. 3-Hexene (5 g, 60 mmol) was slowly added to the suspension and stirred overnight at 50ºC. The PCl_5 and CCl_4 were removed by distillation. The 3,4-dichlorohexane was purified by distillation at 12-14 mmHg and 40°C to yield 1.72 g (20% yield) of 3,4-dichlorohexane as a clear liquid.

^{1}H NMR (400 MHz, $CDCl_3$) δ 1.05 (m, 6H), 1.58-1.81 (m, 2 H), 1.96-2.07 (m, 2H), 3.91-3.96 (m, 2H)

^{13}C NMR (400 MHz, $CDCl_3$) δ 10.4, 11.4, 27.9, 28.0, 66.9, 67.1

C.2.5 Synthesis of (E)-6-Chloronon-4-ene

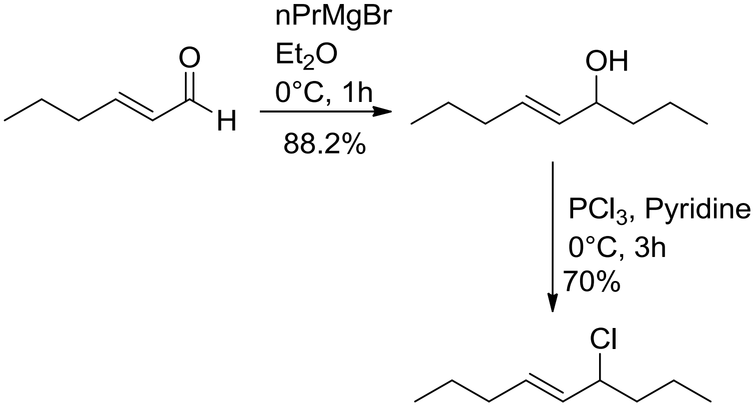

Figure C.4 - Synthesis of (E)-6-chloronon-4-ene

C.2.5.1 *Synthesis of (E)-Non-4-ene-6-ol*

2-Hexen-1-al (11.8 mL, 10.0 g, 0.102 mol) was mixed with anhydrous diethyl-ether (Et_2O, 148 mL). A solution of n-propylmagnesium bromide (nPrMgBr, 51 mL, 0.102 mol) dissolved in anhydrous diethyl ether (25 mL) was added drop wise over the course of 30 min at 0°C. The resulting pale yellow mixture was stirred for 1 hour at room temperature. After 1 hour, the reaction mixture was quenched with a saturated aqueous ammonia chloride solution (NH_4Cl, 100 mL). The organic layer was separated and the aqueous layer was extracted twice with diethyl ether (50 mL). The combined organic layer was dried over $MgSO_4$ and the solvent was removed to yield 12.8 g (88% yield) of (E)-non-4-ene-6-ol as a pale yellow oil.

^{1}H NMR (400 MHz, $CDCl_3$) δ 0.80 (m, 6H), 1.18-1.50 (m, 4H), 1.79 (q, 2H), 1.90 (q, 2H), 2.40 (s, 1H), 3.64 (m, 1H), 5.32 (m, 1H), 5.55 (m, 1H)

^{13}C NMR (400 MHz, $CDCl_3$) δ 13.48, 13.85, 18.58, 22.25, 34.18, 39.44, 67.73, 131.23, 133.36

C.2.5.2 *Synthesis of (E)-6-Chloronon-4-ene*

(E)-Non-4-ene-6-ol (12.8 g, 0.091 mol) and anhydrous pyridine (1.43 mL, 1.4 g, 0.018 mol) were combined and cooled to 0°C. Phosphorous trichloride (PCl_3, 2.9 mL, 7.2 g, 0.034 mol) was added drop wise over the course of 20 min at 0°C. The resulting pale yellow mixture was stirred for 3 hours at 0°C. After 3 hours, the upper layer was separated and distilled at reduced pressure (31°C, 0.3mmHg) to yield 10.1g (70% yield) of (E)-6-chloronon-4-ene as a pale yellow oil.

^{1}H NMR (400 MHz, $CDCl_3$) δ 0.9 (t, 6H), 1.4 (m, 4H), 1.79 (m, 2H), 2.0 (m, 2H), 4.37 (m, 1H), 5.5 (m, 1H), 5.59 (m, 1H)

^{13}C NMR (400 MHz, $CDCl_3$) δ 13.45, 13.57, 19.84, 22.18, 33.98, 40.93, 63.43, 131.22, 133.25

C.2.6 Synthesis of novel sacrificial epoxide stabilizers

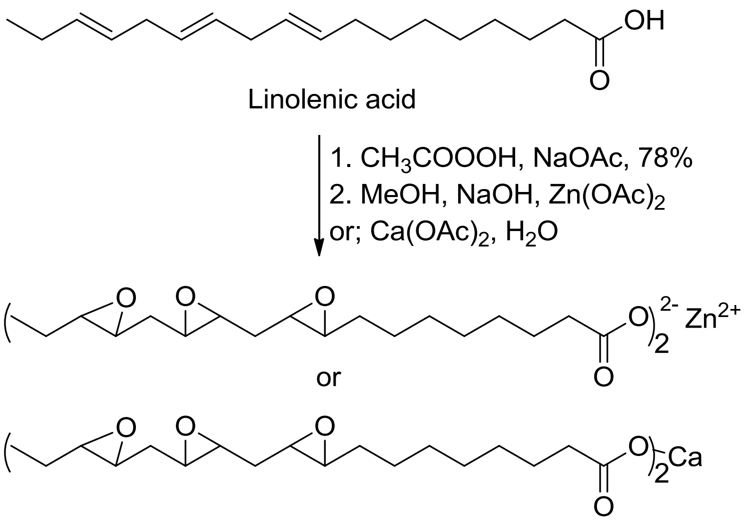

Figure C.5 – Synthesis of Zn or Ca salt of 9,12,15-triepoxylinolenic acid

C.2.6.1 *Synthesis of 9,12,15-triepoxylinolenic acid*

Peracetic acid (18mL, 0.069mol) and sodium acetate (1.1g, 0.069mol) was added to linolenic acid (5.4mL, 0.049mol) dropwise in 1h at 0^{o}C. The reaction was stirred for another period of 1h at the same temperature. The organics were then extracted with diethylether (2x10mL). The organic layer was washed with water (5x50mL), dried over $MgSO_4$ and rotovapped under vacuum to give 4.6g (yield 78%) of colorless semisolid product which was used as such for the next step.

C.2.6.2 *Synthesis of Zn or Ca salt of 9,12,15-triepoxylinolenic acid*

NaOH (0.5g, 0.132mol) in 15mL water was added to triepoxylinolenic acid (4.3g, 0.0132mol) dissolved in methanol (10mL). The reaction was stirred for another 15min at room temperature (homogeneous solution). $Zn(OAc)_2$ (1.2g, 0.007mol) (use $Ca(OAc)_2$ for preparation of Ca salt) in 15mL water was then added to the above homogeneous solution mixture. The appearance of a white precipitate was noted. The mixture was then cooled to 0°C. The solid was filtered and washed with water (3x20mL), acetone (2x10mL) and dried under vacuum to give 3.5g (yield 76%) of Zn-triepoxylinoleniate (yield 51% Ca-triepoxylinoleniate) as a white solid. Elemental analysis for Zn – Calc. 9.13; found 9.33; Ca – calc. 5.80; found 6.17.

C.2.7 Synthesis of novel maleimide stabilizers

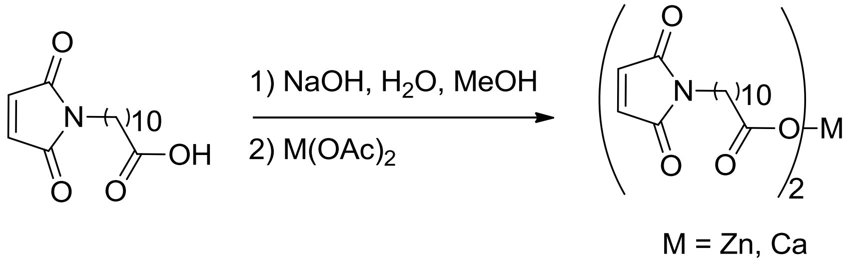

Figure C.6 - Synthesis of Zn or Ca salt of 11-maliemido-undecanoic acid

NaOH (0.95 g, 0.024 mol) in 15 mL water was added to 11-maleimido-undecanoic acid (5.0 g, 0.024 mol) dissolved in methanol (10 mL). The homogenous solution was stirred for 15 min at room temperature. $Zn(OAc)_2$ (2.2 g, 0.012 mol) (use $Ca(OAc)_2$ for preparation of Ca salt) in 15mL water was then added and a white precipitate formed. The reaction mixture was cooled to 0^oC, filtered and the solid washed with water (3 x 20 mL) and acetone (2 x 10 mL) then dried under vacuum resulting in 1.75 g (yield 32%) of Zn11M (yield 51% Ca11M) as white solid.

C.2.8 Epoxide ring opening studies

HCl (g) was bubbled (3 min) through o-dichlorobenzene (o-DCB, 35mL) at room temperature. The amount of HCl complexed with the o-DCB was determined by weighing the reaction vessel before and after HCl addition. The epoxide (cyclohexene oxide, 1,2-epoxyhexane or ESO) in a 1:1 or 20:1 (epoxide:HCl) molar ratio dissolved in o-DCB (2mL) was then added to the HCl solution. The reaction was stirred at room temperature and an aliquot of the mixture was taken and analyzed for the epoxide conversion and corresponding product formation by ^1H NMR spectroscopy.

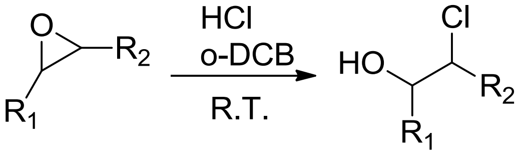

Figure C.7 - Example epoxide ring opening reaction

C.3 Results and Discussion

C.3.1 Weight loss of PVC additives

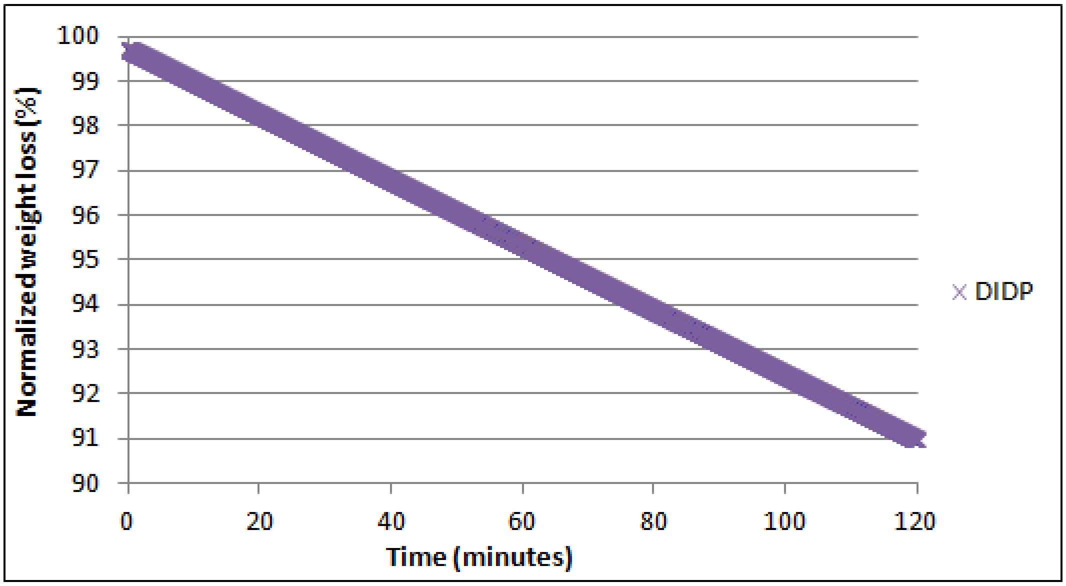

Figure C.8 - Weight loss of DIDP alone at 170°C

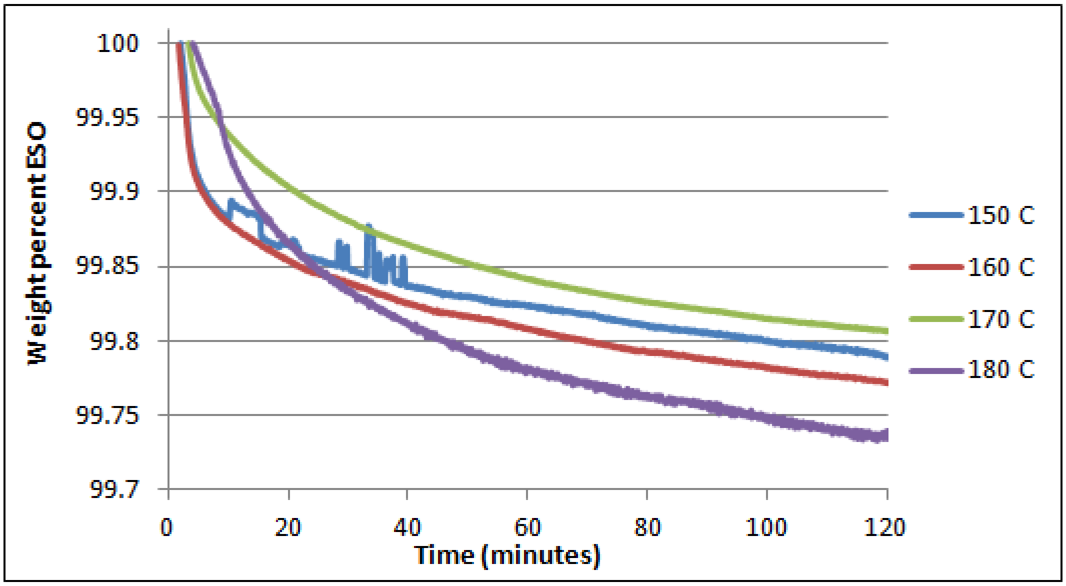

Figure C.9 – Weight loss of ESO alone at 150, 160, 170, and 180°C

C.3.2 Epoxide ring-opening studies

The thermal studies performed with PVC indicated that epoxidized soybean oil (ESO) scavenges the HCl released during the initial stages of thermal degradation. Epoxides are well known to react readily with HCl to generate chlorohydrins. In an effort to study and, later, develop a custom-designed HCl scavenger, reactions between a linear epoxide (1,2-epoxyhexane, EH) and a cyclic epoxide (1,2-cyclohexene oxide, CHO) with HCl were investigated.

The ^{1}H NMR spectrum of EH, shown in Figure C.10, shows peaks at 2.1, 2.4 and 2.6 ppm corresponding to the protons attached to the epoxide-adjacent carbons. The other aliphatic CH_3 and CH_2 protons appear up-field at 0.7 ppm and 1.00-1.31 ppm, respectively. The ^{13}C NMR of EH is shown in Figure C.11.

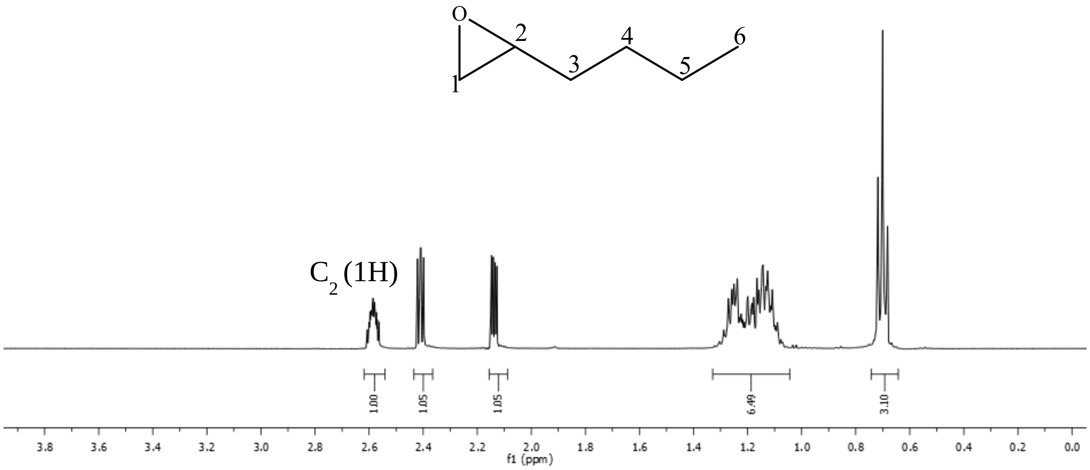

Figure C.10 – ^{1}H NMR of 1,2-epoxyhexane

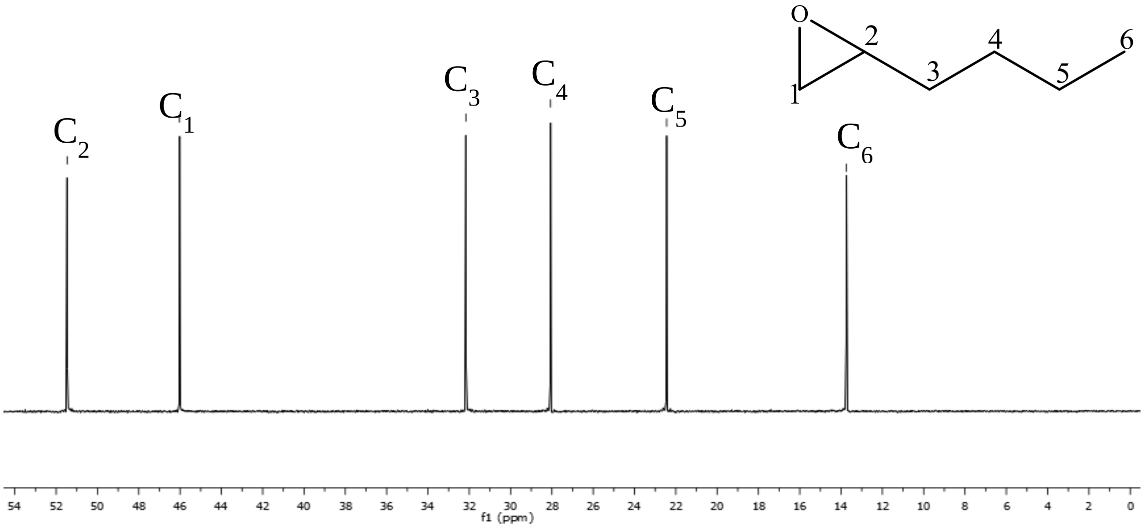

Figure C.11 - ^{13}C NMR of 1,2-epoxyhexane

The epoxide ring opening reaction of EH with HCl in o-dichlorobenzene (o-DCB), shown in Figure C.12, resulted in the two expected products. The major product, 2-hydroxy-1-chlorohexane, is formed by the epoxide ring opening and addition of chloride to the terminal carbon whereas the minor product, 1-hydroxy-2-chlorohexane, is formed by the epoxide ring opening and addition of the chloride to the internal, more sterically hindered, carbon. The ^{1}H NMR spectrum, shown in Figure C.13, of the products from the reaction of EH with HCl (1:1 molar ratio of EH:HCl) shows the ring-opened products and un-reacted starting material after 90 minutes. The ratio of the major and minor products to the starting material can be easily determined by the unique signatures of various protons of each species. The signals at 2.40, 3.10 and 3.70 ppm are attributed as shown in Figure C.13. The ratio of these peaks provides the ratio of each species in the mixture. The overall conversion of the EH was 27.3% with yields of 20.4% and 6.9% of 1-hydroxy-2-chlorohexane and 2-hydroxy-1-chlorohexane, respectively, after 90 minutes. The ^{13}C NMR spectrum of this reaction mixture is shown in Figure C.14.

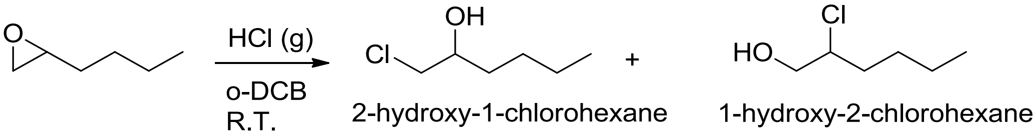

Figure C.12 - Epoxide ring opening reaction of 1,2-epoxyhexane with HCl (g)

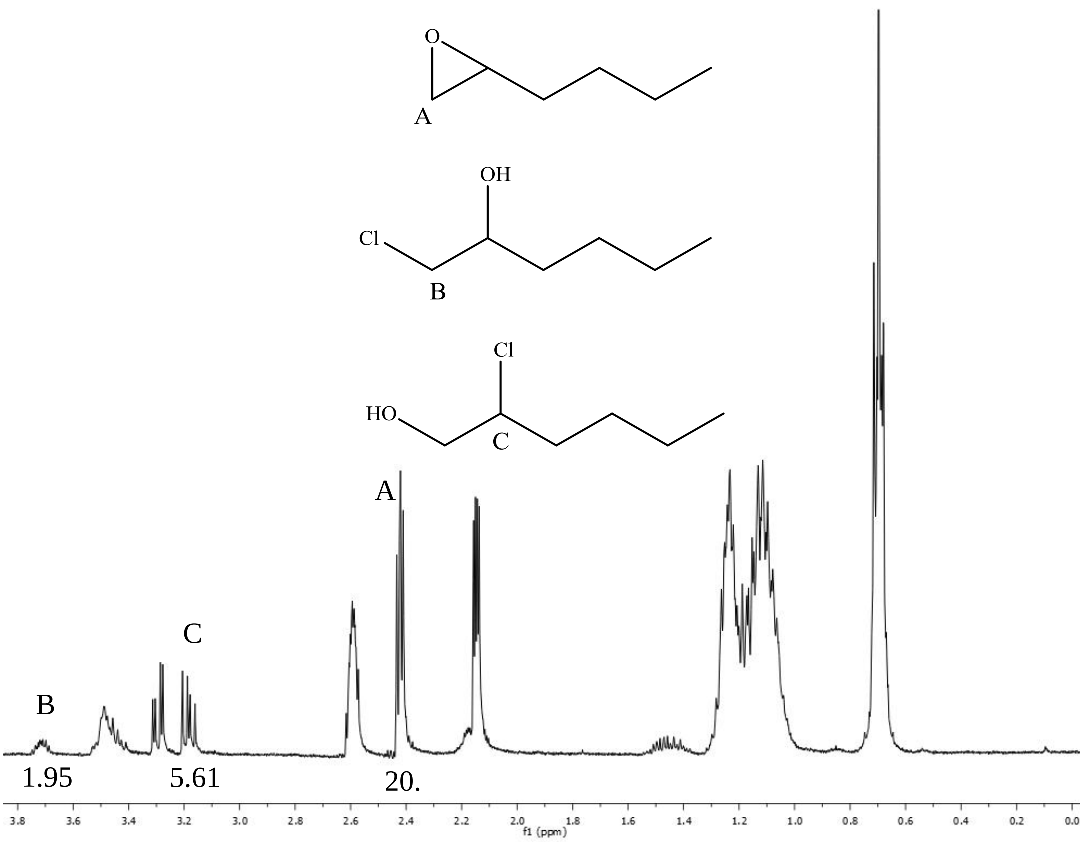

Figure C.13 - ^{1}H NMR spectrum of the reaction of 1,2-epoxyhexane with HCl

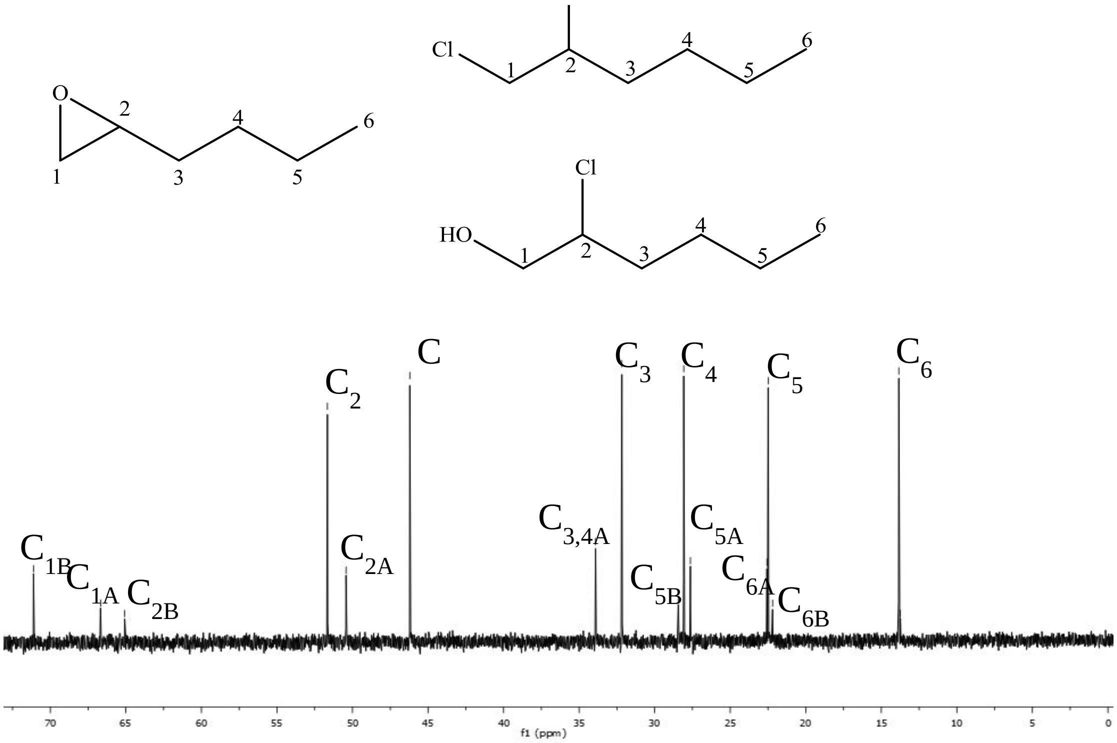

Figure C.14 - ^{13}C NMR spectrum of the reaction of 1,2-epoxyhexane with HCl

The epoxide ring opening reaction of the linear epoxide 1,2-epoxyhexane was compared with the cyclic epoxide cyclohexene oxide (CHO). The ^{1}H NMR spectrum of CHO is shown in Figure C.15 and the ^{13}C NMR spectrum is shown in Figure C.16. The signal corresponding to the CH adjacent to the epoxide appears most downfield at 2.74 ppm. The reaction of CHO with HCl (molar ratio of 1:1 CHO:HCl) gave the product 2-chlorocyclohexanol as seen in Figure C.17. The molar ratio of CHO to 2-chlorocyclohexanol was determined by the ratio of the distinct and representative peaks at 2.74 ppm (signal A, Figure C.18) and 2.58 ppm (signal B, Figure C.18) in the ^{1}H NMR spectrum. The ^{13}C NMR spectrum is shown in Figure C.15. The conversion of CHO was 55% after 90 minutes. This indicates that cyclic epoxides (55% conversion after 90 minutes) open significantly faster than linear epoxides (27% conversion after 90 minutes) when reacted with HCl.

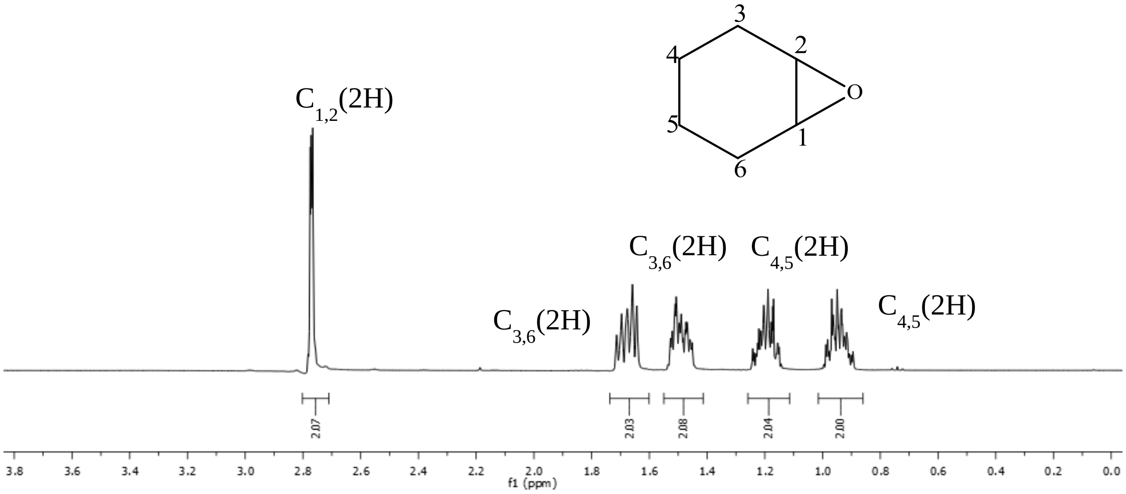

Figure C.15 – 1H NMR of cyclohexene oxide

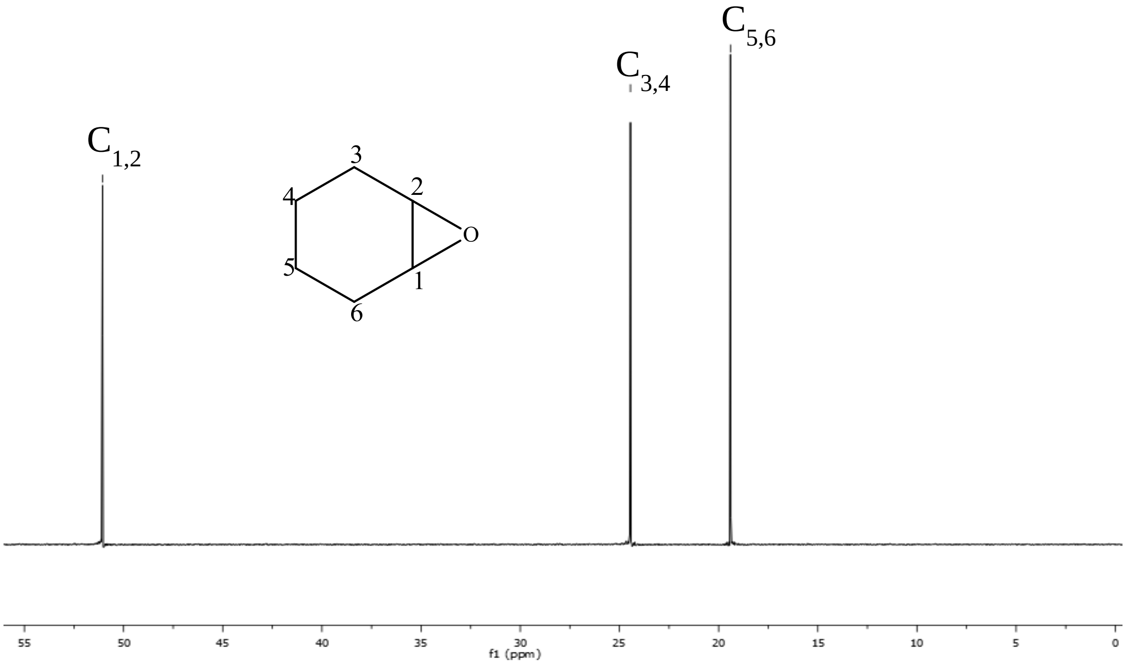

Figure C.16 – ^{13}C NMR spectrum of cyclohexene oxide

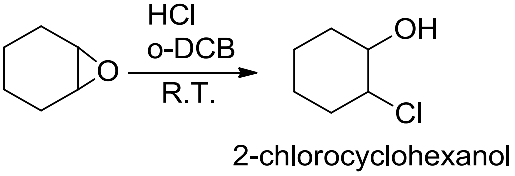

Figure C.17 - Epoxide ring opening reaction of cyclohexene oxide with HCl

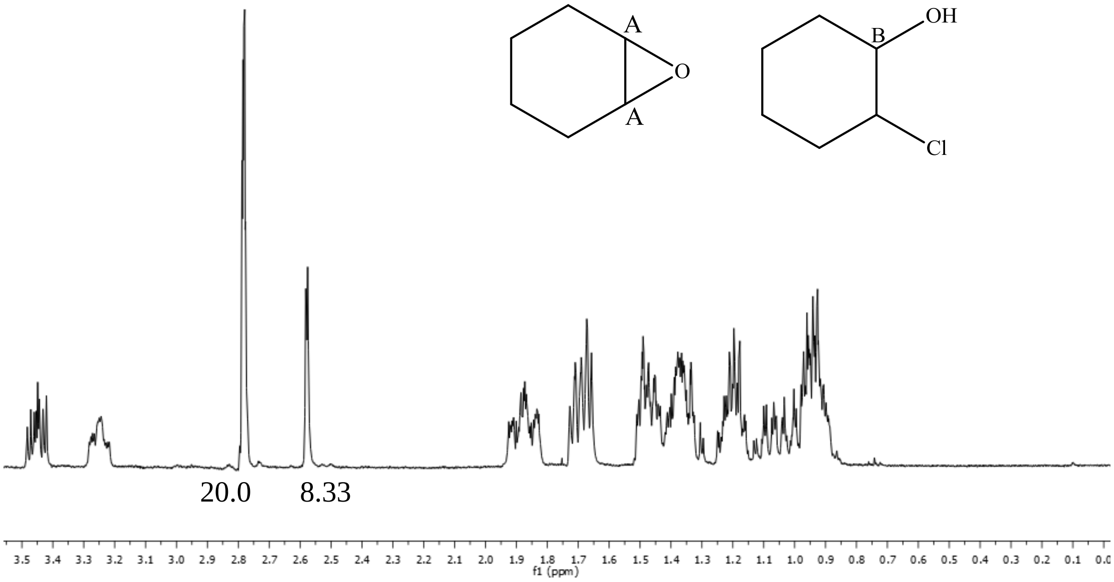

Figure C.18 - ^{1}H NMR spectrum of the reaction of cyclohexene oxide with HCl

In a competitive study performed with 0.5 equivalents each of EH and CHO with 1 equivalent of HCl, CHO was consumed faster than EH. The ^{1}H NMR spectrum of the reaction mixture after 90 minutes is shown in Figure C.19. The product distribution was determined based upon areas of the characteristic peaks of each product (peak deconvolution was used when necessary). The peak at 1.9 ppm (E in Figure C.19) for 2-chlorohexanol was used in this study. The signal at 3.2-3.3 ppm corresponds to both 1-chlorohexane and 2-chorohexanol, and was therefore deconvoluted to gain individual information. After 90 minutes, 26% of the 1,2-epoxyhexane was converted to 2-hydroxy-1-chlorohexane and 1-hydroxy-2-chlorohexane while 64% of cyclohexene oxide was converted to 2-chlorohexanol. This result provides additional evidence that cyclic epoxides open significantly faster (roughly 4 times faster, assuming first order kinetics) than linear epoxides.

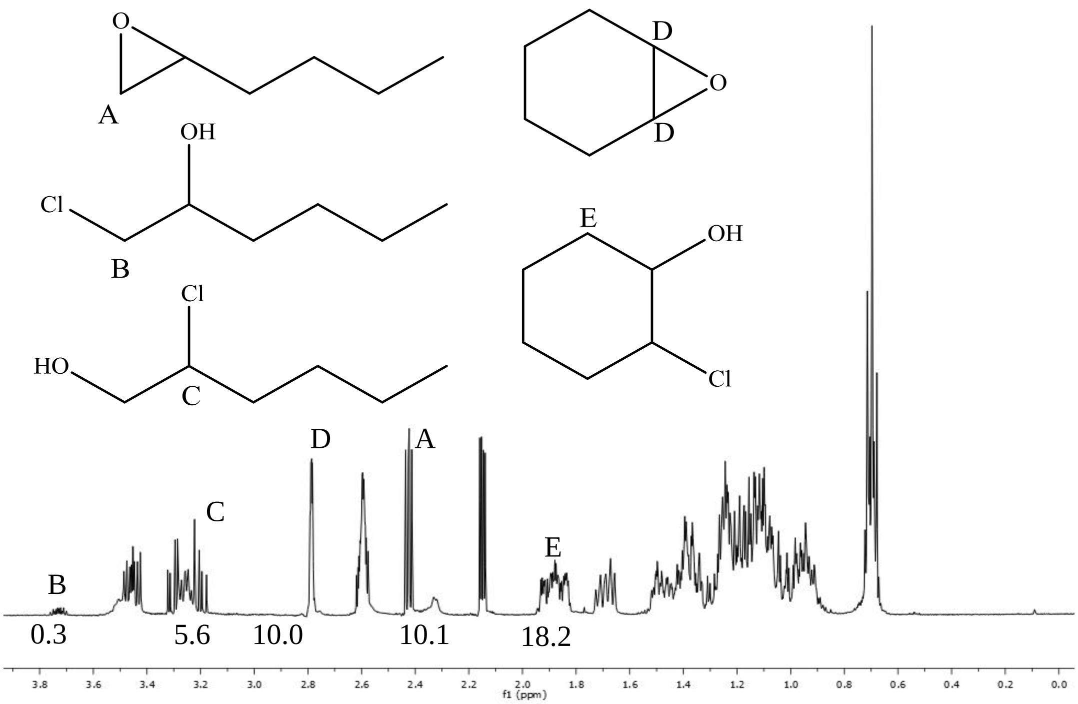

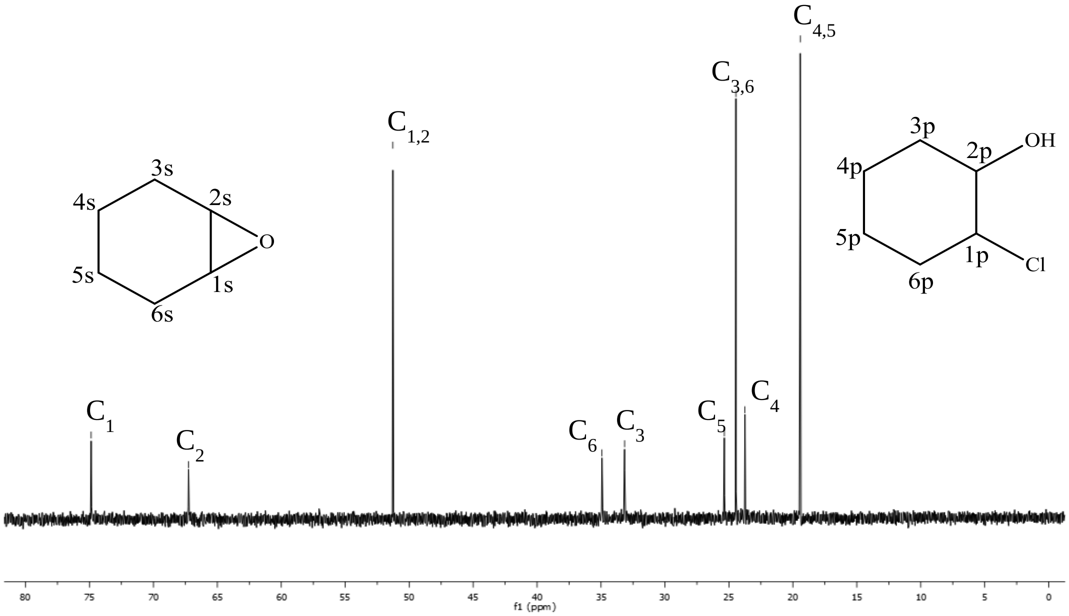

Figure C.20 - ^{13}C NMR spectrum of the reaction of cyclohexene oxide with HCl

Epoxidized soybean oil (ESO) was then reacted with HCl to determine the reactivity of the epoxide group present on ESO toward HCl, as shown in Figure C.21. A typical ^{1}H NMR spectrum of ESO is shown in Figure C.22. The signals corresponding to the C-H protons attached to the epoxide ring appear up-field around 2.70 and 2.89 ppm. The furthest downfield signal corresponds to the single tertiary C-H adjacent to the ester (labeled A in Figure C.22). If the ester signal is normalized to unity, the peak area of the C-H signal adjacent to the epoxides can be used to quantify of the number of unopened epoxides. In this case, the epoxide peak area is 11.31, within error to the theoretical 12 (i.e., two CH per epoxide with 6 epoxides per ESO molecule—it is recognized that 6 epoxides group per ESO is an approximation as shown in Figure C.21. As the epoxide rings open to form chlorohydrins, this number is expected to decrease.

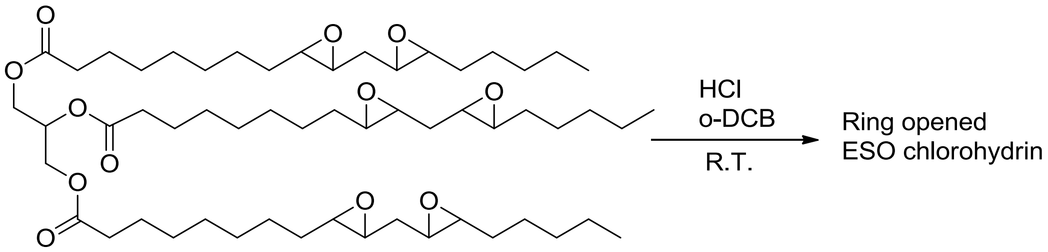

Figure C.21 - Structure of epoxidized soybean oil and reaction with HCl

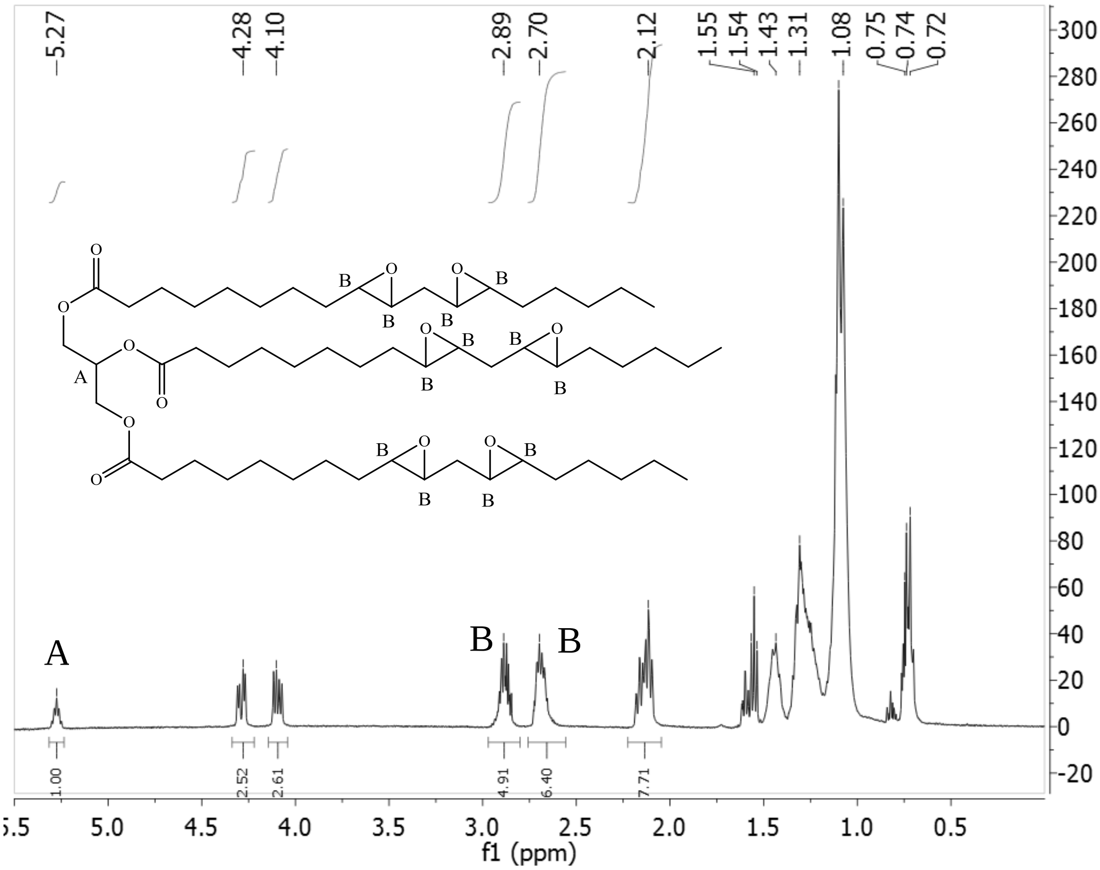

Figure C.22 – ^{1}H NMR spectrum of epoxidized soybean oil

When reacted with HCl, the epoxides of ESO open in a similar fashion to the linear epoxides shown above. Ring opened products appear in the ^{1}H NMR in the range of 3.4 – 4.0 ppm. The ^{1}H NMR spectrum of ESO reacted with HCl in a ratio of 20:1 is shown in Figure C.23. Again, normalizing the peak for the proton adjacent to the ester to unity, the integration corresponding to the epoxide signal is 5.54, indicating, semi-quantitatively, that some epoxides have opened. When reacted with 1:1 HCl, the epoxides completely open within five minutes, as evident by the ^{1}H NMR spectrum shown in Figure C.24.

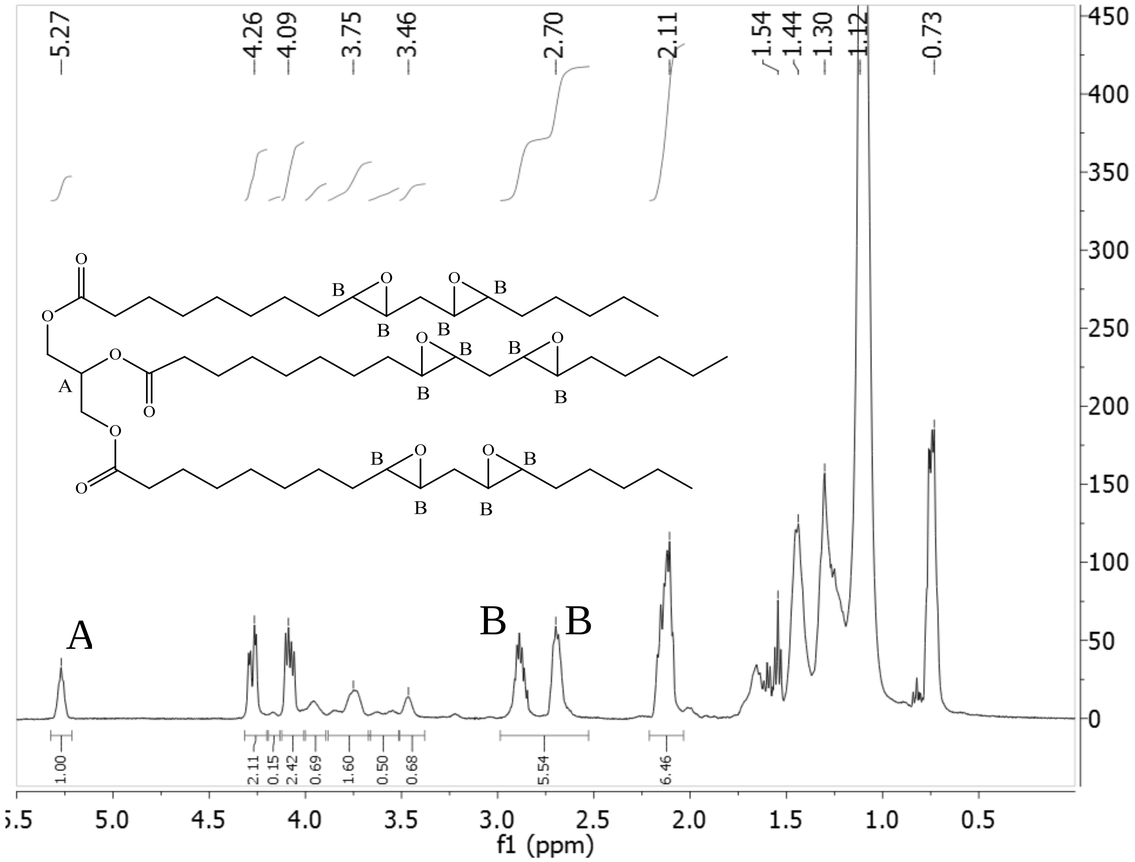

Figure C.23 - ^{1}H NMR spectrum of the products from the reaction of ESO with HCl (20:1 molar ratio, respectively)

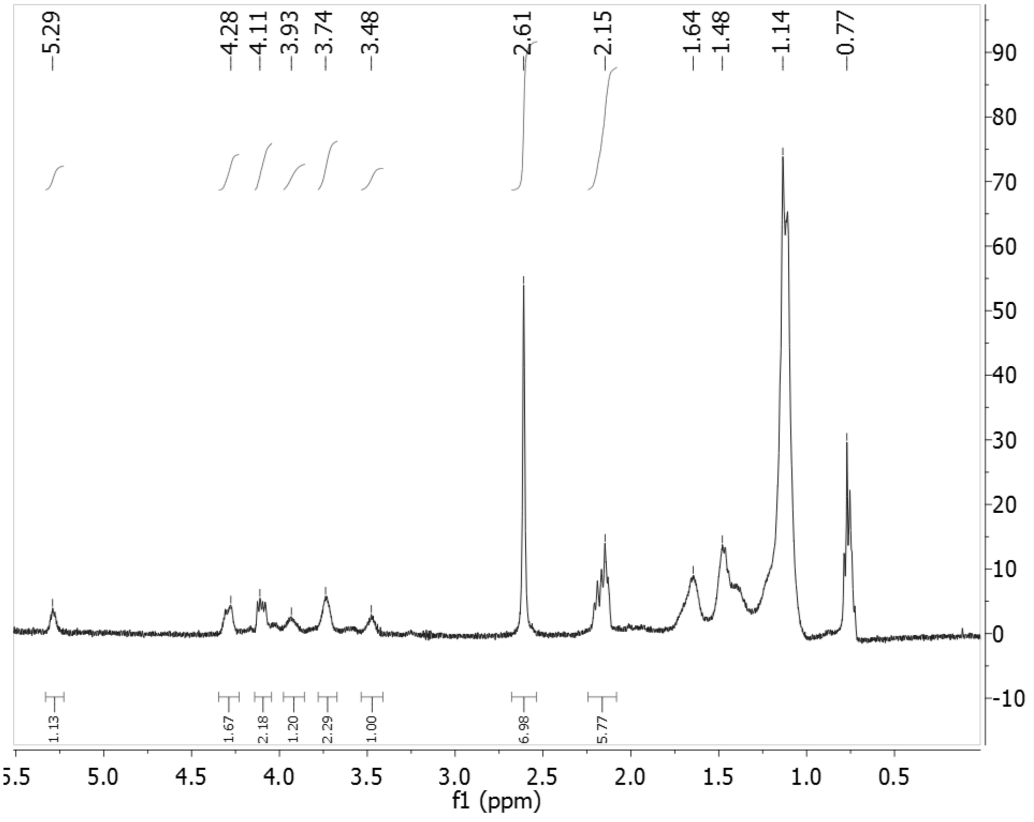

Figure C.24 – ^{1}H NMR spectrum of the products from the reaction of ESO with HCl (1:1 molar ratio)

APPENDIX D - REVERSIBLE IONIC LIQUIDS FOR SEPERATING BITUMEN FROM OIL SANDS: FUNDAMENTALS AND APPLICATION

D.1 Introduction

This Appendix details a proposal submitted to the National Science Foundation (NSF). The proposal deals with a potential process for separating bitumen from oil sands that uses silylamines as reversible ionic liquids. The proposal represents an additional application of reversible ionic liquids outside of CO_2 capture. Significant work was put into developing the idea of the process; it is included here for future reference and application.

D.2 Project summary

D.2.1 Intellectual merit

We propose to achieve an important separation using a class of novel solvent systems that we have developed – ***silylated reversible ionic liquid systems*** **–** to recover bitumen from oil sands. These solvent systems are such that they can achieve difficult separations by being reversibly switched from a non-ionic medium (molecular liquid) to an ionic medium (ionic liquid) with the simple addition of carbon dioxide. Heating the ionic liquid to eliminate carbon dioxide easily regenerates the molecular liquid. Preliminary experiments suggest that these solvent systems would provide excellent vehicles for efficient bitumen recovery by extracting bitumen from oil sands with the molecular liquid and subsequent phase separating the bitumen upon the formation of the ionic liquid. We propose to explore and establish structure-property relationships for selected silylated reversible ionic liquid systems to successfully design optimum solvent systems for recovery of this energy-rich hydrocarbon mixture from this abundant oil source. We propose to design novel chemistry, demonstrate its application in the laboratory, and substantiate its scale-up potential via process simulations.

The group proposing this work is a diverse team of chemical engineers and chemists. In addition, our research group is currently working with several industrial partners to develop sustainable chemical processes. Both the interdisciplinary nature of our research group and our extensive industrial collaborations contribute to the education and "real-world" experiences of our graduate students, our undergraduate students, our post-doctoral associates and our research scientist. Further this project will be an important demonstration of the newest paradigm in chemical engineering education—***product design***—where we are designing a solvent specifically to carry out an important separation.

D.3 Project description

D.3.1 Background

The depletion of conventional crude oil reserves and increase of crude oil prices has led to the use of oil sands as alternate fossil fuel resources in Canada and generated renewed interest in the oil sands of the western US. Currently, the isolation of hydrocarbons from oil sands is difficult mainly due to the physical properties of these materials, such as high viscosity and density.[1,2] Bitumen and the subsequent derived oil are recovered from oil sands mainly by two energy-intensive processes: hot water processing after oil sands mining or *in* situ steam injection.[2,3] Both of these methods rely heavily on water resources; although these water resources are abundant in the oil sands-rich regions in Canada, they are not in the oil sands-rich regions of the Western US. Additionally, many tailings ponds are produced of contaminated water preventing reclamation of the land and environmental concerns.

The silylated reversible ionic liquid solvent systems can solve water management problems and reduce energy requirements by including a built-in extraction and separation technology.[4-6] ***We propose to gain a fundamental understanding of the relationship between structure and properties of a wide variety of silylated-based reversible systems to allow us to custom-design solvent systems for the inexpensive, energy-efficient and environmentally conscious separation of bitumen from oil sands.*** The formation of the reversible ionic liquids is triggered by the addition of CO_2, resulting in dramatic changes in physical properties. Specifically, a molecular liquid (ML) is switched to an ionic liquid (RevIL) by the addition of CO_2 and subsequently reversed back to the "molecular liquid" by simply applying heat. Operationally, the bitumen is extracted from the oil sand by the molecular liquid and subsequently phase separated upon formation of the ionic liquid. Operationally the solids are contacted only with the relatively inviscid ML and not with the more-viscous RevIL.

Our solvent systems facilitate both recycle and reuse. Such separation capability affords us a selective extraction of hydrocarbons from sand, clay and other ionic species that will be both sustainable and economical. Importantly, this method will minimize the consumption of natural water resources and the need for downstream water purification—both having significant economic and environmental impact.

D.3.2 Preliminary research

A reversible ionic liquid is a solvent system which can switch back and forth between a medium which is ionic and a medium which is non-ionic; the latter is referred to as a molecular liquid (ML).[5-7] Reversible solvent systems were designed to address the separation limitations of conventional ionic liquids by including a "built-in" separations handle (Figure D.1).[5] There are two major classes of reversible ionic liquids (RevILs): two-component and one-component. Two-component RevILs are based on an equimolar mixture of a neutral alcohol and a neutral molecule containing at least one basic nitrogen functionality. Examples of the later are 1,8-diazabicyclo[5.4.0]undec-7-ene (DBU) and 2-butyl-1,1,3,3-tetramethylguanidine (TMBG).[5] In contrast, one-component systems eliminate the need for an alcohol as seen in the two-component RevILs; these systems employ solely a neutral molecule containing at least one basic nitrogen functionality.[5] Upon reaction with CO_2, the molecular liquids (silylated amines) form ionic liquids composed of the corresponding carbamate anion and ammonium cation pairs (Figure D.1).

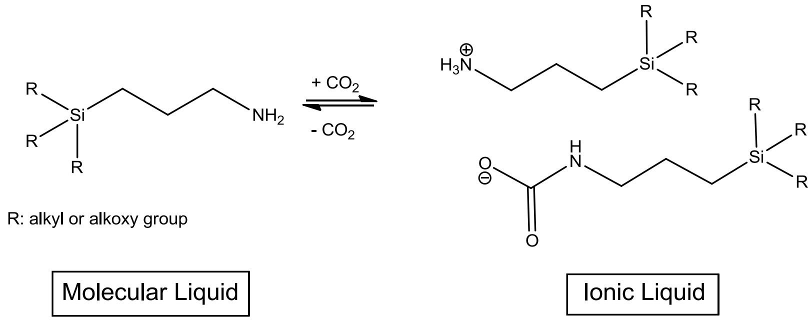

Figure D.1 - One-component system: reversible switch from a molecular liquid trialkoxy and trialkylsilylpropylamine to its corresponding ionic liquid upon addition of CO_2

We emphasize that the Lewis acid character of the silicon substituent will play an important role in controlling the temperatures at which formation and reversal of the ionic liquid takes place as well as influencing other important physical properties such as viscosity. In Figure D.2, a bar graph shows the reversal temperature as a function of the structure of the RevILs systems listed in Table D.1. In all cases, the RevIL was formed upon reaction of the ML with CO_2. The respective reversal temperature (RevIL to ML & CO_2) was measured by DSC (Differential Scanning Calorimetry). The silicon-containing reversible systems show lower reversal temperatures (from 20 to 80^{o}C lower) compared to amines with no silicon substituent present.

Table D.1 - Structure of RevIL systems involved in the reversal temperature study

TEtSA 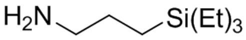	**TPSA** 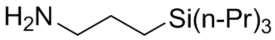	**THSA** 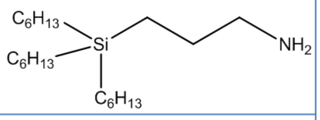
1 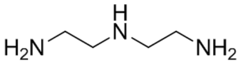	**2** 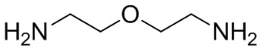	**3** 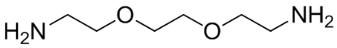

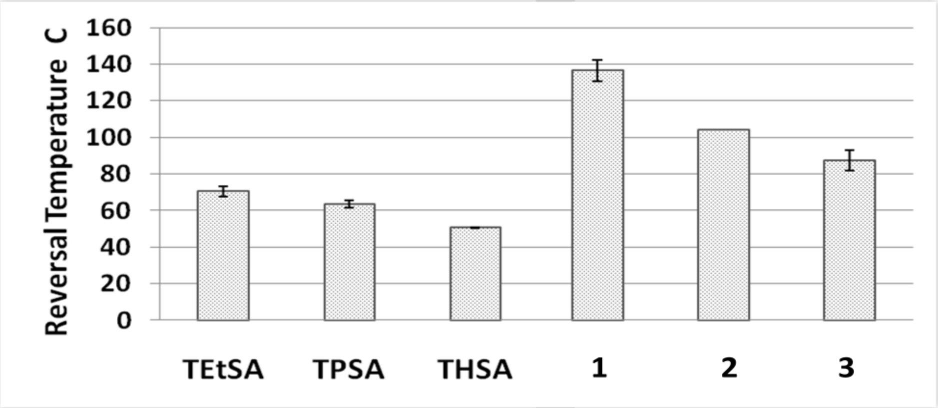

Figure D.2 - Temperature of reversal as a function of the structure of the RevILs system

The relative polarity of the ML/RevILs systems was determined via UV-Vis absorption measurement of the dye, Nile Red (a common solvatochromic probe). The experiments show that the conversion from the molecular solvent form to the ionic form results in a dramatic change in polarity.[6] The magnitude in change of polarity for all four RevILs in Figure D.3 is about 10 nm – the same as the spectral change of this probe going from chloroform to DMSO. Note that the polarity of both the molecular liquid and ionic liquid forms decrease as the alkyl chain length on the Si- group is increased. Also, alkoxy substituents on the silicon would not be employed for bitumen recovery since these substituents are unstable in the presence of water. They are included only as additional examples of the reversible ionic properties of this class of silicon-containing amines.

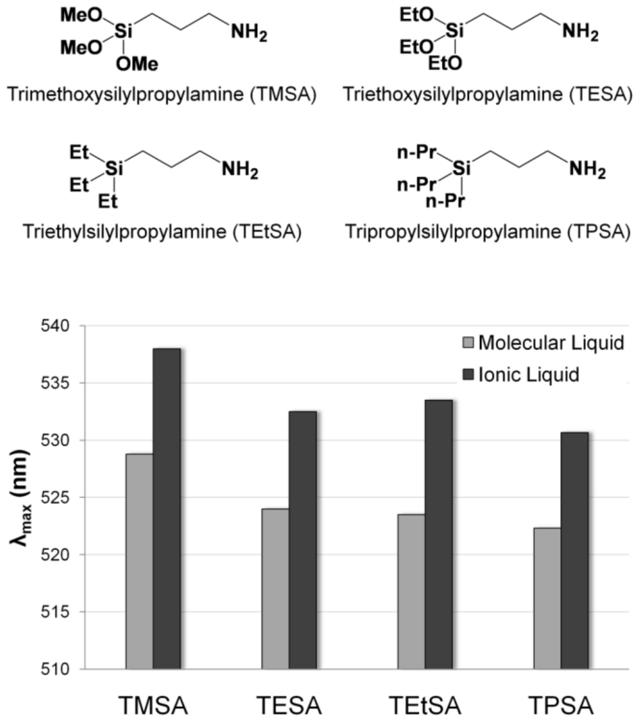

Figure D.3 - The polarity of the neutral and ionic forms of the one-component reversible ionic liquid solvents

In preliminary studies, we have demonstrated the principle of separation of hydrocarbons by taking advantage of the polarity switch between the neutral and ionic forms of our solvents. The switch from molecular liquid to ionic liquid is large enough to turn a homogenous mixture of hydrocarbon and molecular liquid into a heterogeneous liquid-liquid hydrocarbon and ionic liquid system. For example, a homogeneous mixture of octane and TMSA was reacted with CO_2 to form the corresponding ionic liquid

(TMSA-IL). We observed phase separation of the octane from the newly formed ionic liquid as shown in Figure D.4.

Figure D.4 - Phase split between octane and TMSA one-component ionic liquid

Equally important, these solvents can be recycled and reused. Figure D.5 displays the recyclable process employed for hydrocarbon extraction from oil. Crude oil was added at 50 wt% to TESA producing a single phase system. The crude oil sample that was used in this experiment was analyzed by Chevron for hydrocarbon cut and sulfur content.[1] Upon addition of CO_2 the extracted hydrocarbon phase separated from the ionic liquid phase. The hydrocarbon phase (top phase) was decanted and the ionic liquid phase (bottom phase) was heated at 120ºC to reverse the ionic liquid to the molecular liquid. The cycle was then repeated three times by reintroducing new samples of crude oil. After each cycle, the hydrocarbon phase had less than 0.4 mol% dissolved TESA-IL (Figure D.5). In addition, the separation efficiency did not significantly change over the course of three recycles, providing evidence that the integrity of our solvent system was maintained (0.4, 0.3, 0.3 mol% TESA in product phase, respectively).

---

[1] The hydrocarbon cut was determined by GC/MS and the corresponding spectra were analayzed by distillation simulated software. The major hydrocarbon cut was between 70ºC and 490ºC. ^{1}H NMR shown only aliphatic components. In addition, the oil was sour as it contained 1.17 wt% sulfur and medium grade as its density was 0.8835 g/mL (API density of 28.7).

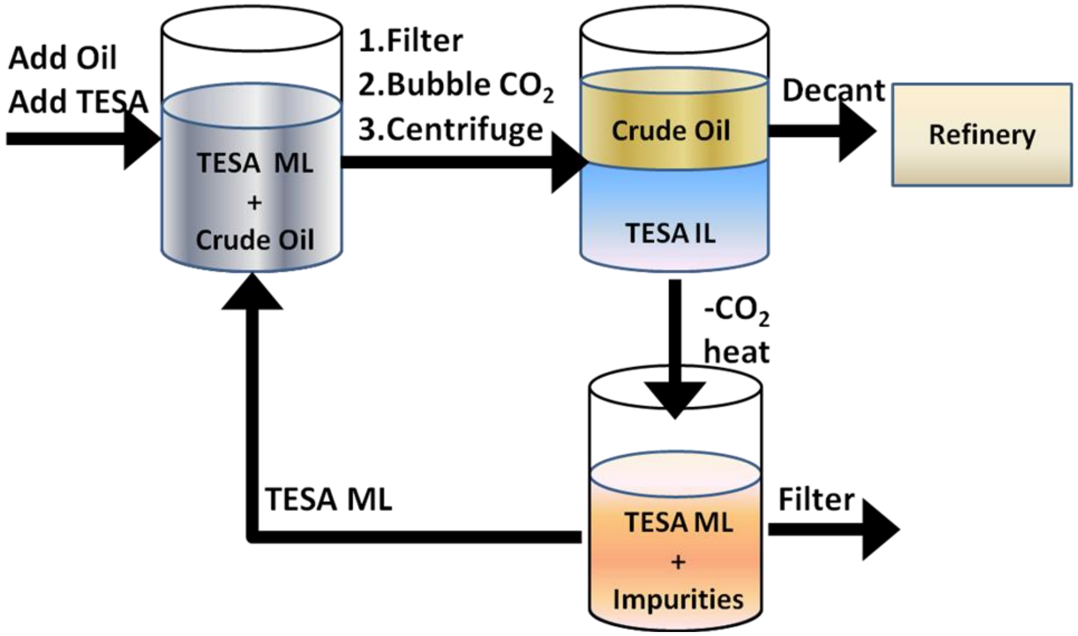

Figure D.5 - Recycling process diagram for hydrocarbon extraction from crude oil with one-component reversible ionic liquid

We have already demonstrated with both the two-component and one-component RevILs systems that properties like polarity changes can be easily manipulated by changing the molecular structure of the systems. This is true for viscosity as well which, along with polarity, is a crucial property for process design. For instance, we have shown that by going from a methoxy group (TMSA) to the ethoxy group (TESA) the viscosity of the ionic form goes from 2,160 cP to 930 cP, respectively. Therefore, making relatively minor changes in the skeletal backbone of the molecule results in dramatic changes in physical properties. The fundamental understanding of these changes is essential to developing the optimum solvent systems.

D.3.3 Solvent system design: structure-property relationships

Although a qualitative picture of how the reversible ionic liquid's properties are altered by tuning the structural features of the molecular liquid is beneficial, a more quantitative approach would enable a directed development of optimal solvent systems for actual commercial use. The relationship between molecular structure and molecular properties has been a cornerstone of physical-organic chemistry for more than half a century. These relationships establish a series of paradigms for predicting how various chemical structures reflect a plethora of physical and chemical properties. In particular, free energy, enthalpy, and entropy contributions to a given process step are essential to develop a viable overall process. Because our research group thrives on the synergy of chemistry with chemical engineering, we have successfully applied such approaches to a wide variety of chemical processes. For example we have used experimental and theoretical (molecular orbital theory) methods to characterize and modify many novel tunable solvents, such as supercritical fluids, near-critical water, and gas-expanded liquids.[8] Similarly we have exploited these relationships to correlate, predict, and modify a variety of thermodynamic properties, including heats of solution and phase equilibria.[9] This philosophy and approach will provide the basis for the proposed research dealing with the separation and recovery of bitumen from oil sands.

D.4 Proposed research

We determined experimentally that three critical elements are needed in designing RevIL systems: (1) the amine moiety for reaction with CO_2 to form the ionic liquid, (2) the alkyl chains for lipophilicity, and (3) the Si atom for tuning reactivity and viscosity. It is essential to understand the role of each of these elements to design the best possible system for extraction, and specifically hydrocarbon extraction from oil sands. As a consequence, the proposed research has two distinct components: (1) gaining a fundamental understanding of the structure-property relationship of silylated-based

RevILs, and (2) applying this knowledge towards the optimization of the extraction of oil sands with RevILs.

D.4.1 Structure-property relationships in silylated RevILs system

D.4.1.1 *Tuning physical and chemical properties: silicon's role in ML and IL forms*

We have discovered that amines containing silyl substituents proximate to the amine functionality have special properties related to both carbon dioxide capture and release. In order to determine the silyl amine structures which would optimize the thermodynamics and kinetics associated with the coordination of the amine with carbon dioxide and its subsequent release, it is critical to understand the intramolecular interactions between the silyl group (a Lewis acid) and the amine group (a Lewis base) and/or between the silyl group and the oxygen anion of carbamate. ***We propose to investigate the role of the silicon atom in the silylated amine molecular liquids and ionic liquids as a function of structural variations by two spectroscopic techniques NMR (^{29}Si, ^{1}H, and ^{13}C) and FTIR.***

In order to explore the relationship between structure and activity a series of silicon containing molecules will be synthesized. These are summarized in Figure D.6. To begin, we shall conduct control experiments using amine-free tetraalkylsilanes. These particular silanes will contain three identical alkyl groups with the remaining alkyl group varying in length. In these cases no intramolecular interactions with silicon can take place, thus establishing a baseline for comparison with other structures containing amine and carbamate functionalities. The literature has provided evidence that an increase in coordination number of the Si atom from 4 to 5 results in substantial upfield shifts of the

^{29}Si resonance.[10] We therefore propose to monitor the shift in ^{29}Si resonance (both in dilute and neat conditions) as function of structural changes for both the amine and the carbon dioxide adduct (the carbamate) by varying (1) the R groups on the Si and (2) the chain length between amine and Si from n = 1 to 4. The R group on the silicon atom will be varied from alkoxy (OCH_3, OC_2H_5), to alkyl (C_2H_5, C_3H_7, C_6H_7) to a variety of electron-donating and electron-withdrawing substituted benzenes. It is recognized that alkoxy-silanes and phenyl substituents will not be potential candidates for our applications, yet it can help us map the effect of the substituents on the bulk properties. The observation of the ^{1}H resonance of the CH_2 on alpha of the amine group and of the Si atom will be of interest as it could provide information as to the geometry of the five coordinate species formed. In the carbamate structure, the ^{13}C resonance of the carbonyl moiety (from the formed carbamate) and ^{13}C in alpha of the silicone will be monitored to further support such interaction with the Si atom. To maximize sensitivity, the reaction of the silylated amines will be conducted with ^{13}C labeled CO_2—yielding ^{13}C labeled carbamate. When working with neat samples, we shall also monitor changes in the ^{15}N NMR spectra as it can provide information as to the formation of coordination with the Si.

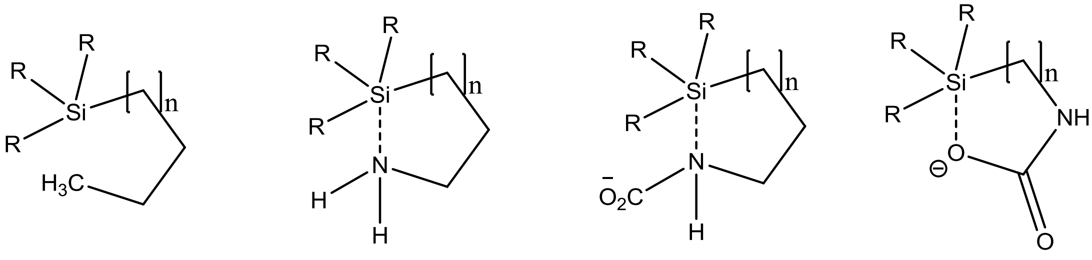

Control
No interaction

Molecular Liquid

Ionic Liquid

Ionic Liquid

R: OCH_3, OC_2H_5, C_2H_5, C_3H_7, C_6H_7, C_6H_5, $(R)C_6H_4$

Figure D.6 - Proposed compounds to study intramolecular coordination

With the exception of the alkoxy compounds that are commercially available, each model compound will be synthesized and characterized in our laboratories (^{1}H NMR, ^{13}C NMR, elemental analysis, MS (Mass spectroscopy), DSC (Differential Scanning Calorimetry), TGA (Thermogravimetry Analysis), viscosity, density). The synthesis will be conducted via the one-step hydrosilylation as shown in Figure D.7. The unsaturated amines and the silanes are commercially available and can be synthesized using literature procedure.[11]

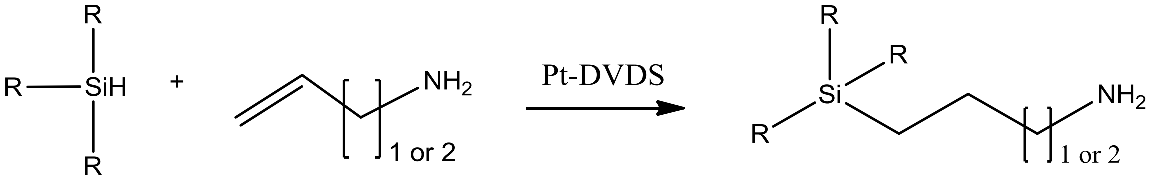

Figure D.7 - Hydrosilylation between trialkylsilane and allylamine

ATR-FTIR (Attenuated Total Reflectance–Fourier Transform Infrared Spectroscopy) will also be employed to investigate intramolecular interactions between the silicon substitute and the amine functionality. Voronkov *et al.* demonstrated that the sensitivity of the C–O bond vibration is such that a shift in wavenumber (frequency of vibration) of 80-100 cm^{-1} can be seen depending on the strength of the silicon-oxygen coordination.[12] By varying the separation distance between the silicon and oxygen atoms as well as varying the atoms' surrounding electronic environments (attached substituents), the effect of coordination between the two atoms can be studied. The ν(Si-C) and ν(C-N) will also be monitored but are expected to be less reliable as this region can become quite complex, leading to difficult assignments of the frequencies.

The results derived from NMR and FTIR investigations will subsequently be correlated with the measured chemical and physical properties (reversal temperature, viscosity, etc.) in order to determine trends and possible relationships between interaction at a molecular level and bulk properties. Such analyses and correlations will guide us in determining the optimum RevILs systems for extraction and separation of bitumen from oil sands.

D.4.1.2 *Polarity switch from molecular liquid to ionic liquid*

Preliminary work using octane (a simple model for hydrocarbons) demonstrated the separation of octane from the ML by switching to the RevIL. Although the TESA-IL phase separated from octane, analyses showed cross-contamination of the phases: 18 mol% of octane remained in the ionic liquid phase and 0.4 mol% of TESA-IL in the octane. This is a severe limitation both in terms of cost and efficiency. The premise behind our more quantitative approach is that increasing the "ionic character" of the ionic liquid can optimize the phase separation between the ionic liquid and hydrocarbons. We define "ionic character" as the ratio of the ion-pair volume (Vip) to the molecule's total volume (Vt). The ratio, Vip/Vt, can also be described qualitatively as *ion pair volume density*. The details of this approach are described in the subsequent paragraph. Vip/Vt can be used as a guide to design novel RevIL systems that will optimize bitumen separation.

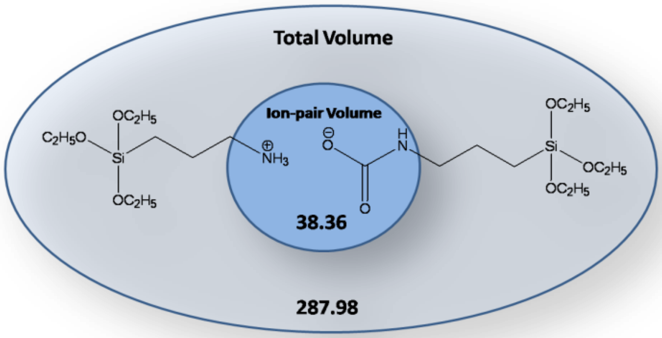

Figure D.8 - Ratio of the ion-pair volume (Vip) to the molecule total volume (Vt) for TESA

We propose to look at a selected group of silylated RevIL systems to minimize the loss of ionic liquid in the oil phase by defining and using a novel approach that considers the ratio of volume of ion pairs to total volume of the molecule (Vip/Vt). The closer the ratio to unity, the greater the salt-like character of the ionic liquid. The greater the salt-like character of the ionic liquid, the less it will dissolve in the oil phase. For example, Vip/Vt for TESA (Figure D.8) is calculated by adding the van der Waals volumes (V_w) for contributing groups comprising a molecular species as suggested by Bondi.[13] As a first approximation the ion-pair volume was calculated using the neutral intermediate: R-**NH_2···HO-C(=O)NH**-R (38.36 cm^3/mol). The total volume of the ionic liquid TESA was calculated to be 287.98cm^3/mol. Therefore the calculated Vip/Vt for TESA = 38.36/287.98 = 0.13. As a comparison an ionic salt like sodium chloride (Na^+Cl^-) has a Vip/Vt ratio of 1. Thus in the design of the optimum RevIL there are two competing factors that must be addressed: (1) maximizing the Vip/Vt ratio and (2) maintaining the room temperature liquid state of the molecular and ionic forms of the solvent system.

Operationally, each model compound will be synthesized via the hydrosilylation outlined in Figure D.7 (shown earlier). After formation of the RevILs, their respective solubility in octane, and the solubility of octane in the RevILs will be measured by NMR and GC analysis. We anticipate that octane's solubility in the ionic liquid phase will decrease as Vip/Vt increases. It should be recognized that the ML must exhibit complete miscibility with the hydrocarbon, while its ionic liquid counterpart must exhibit minimum solubility in the hydrocarbon. Hence, it is highly unlikely that the optimum Vip/Vt ratio will be very near unity. Model compounds like TEtSA and DHSA (as seen in Table D.2) were selected as they exhibit the same Vip/Vt ratio despite having different structures. This comparison will provide a reasonable indication of how the Vip/Vt ratio can realistically be correlated to the lipophobic character of the ionic liquids. If successful, these measurements would be a rapid test to provide additional guidance in the development of optimal RevIL solvent systems for the extraction and recovery of hydrocarbons from oil sand.

Table D.2 - Some proposed molecular liquids for bitumen extraction from oil sands along with their corresponding maximum potential Vip/Vt ratio

Molecular Liquid	Vip/Vt	Molecular Liquid	Vip/Vt
TESA 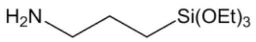	0.13	TMSA 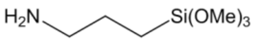	0.17
TPSA 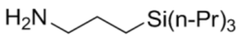	0.12	THSA 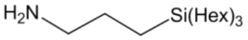	0.08
TEtSA 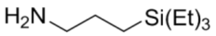	0.15	DTEtSA 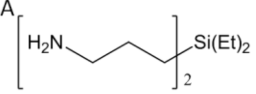	0.24
DHSA 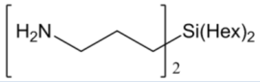	0.16	TRSA 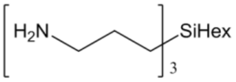	0.26

D.4.2 Oil Sand separation with RevIL systems

We propose to investigate the potential of two or three silylated RevIL systems selected from the structure-relationship studies for oil sand extraction. Each oil sand feedstock will be extracted using conventional organic solvent and characterized by GC/MS, elemental analysis and NMR and analyzed for sulfur content. Athabasca (Canadian) oil sands are readily available for purchase and will be used in the majority of our oil sands-based studies. Because of the contaminants and the complex nature of the oil sand feedstock, ***the efficiency of oil extraction and separation from crude materials will be investigated as a function of 1) loading of bitumen compared to RevIL system, 2) composition of the bitumen, 3) structure of the RevIL system, 4) temperature.*** The hydrocarbons phase and the ionic liquid phase will be analyzed by GC/MS, elemental analyses, and NMR.

While octane can be used as a preliminary model in the development of RevIL systems, oil sands are far more complex and will need to be analyzed directly to obtain realistic understanding of the recovery of bitumen from oil sands with RevILs. Figure D.9 described the bitumen recovery process that we propose:

A) Extraction of oil sands

B &C) Formation of the ionic liquid, resulting in the separation of the bitumen from the newly formed RevIL phase

D) Recovery of the bitumen

E) Recycle of the molecular liquid upon recovery and reversal of the ionic liquid phase,

F) Purification of the molecular liquid (This step is optional, its necessity will be determined during the experiments.)

G) Collection of insoluble materials from the molecular liquid (mostly sand)

We shall perform analyses (^{1}H, ^{13}C NMR, GCMS, LCMS) at each step to assess efficiency and performance. ***Finally from the experimental data we shall carry out HYSYS process simulations for one or more optimal solvents.*** Such simulations will demonstrate the design for scale-up and determine the cost and energy requirements for industrial recyclable solvent extraction of oil from oil sands. These simulations will be compared to Shell Canada's hot water processing of mined oil sands unit operating cost per barrel equivalent reported as US$38.15 in 2008.[14] ***Further, we shall also carry out a scale-up design for its bulk manufacture.***

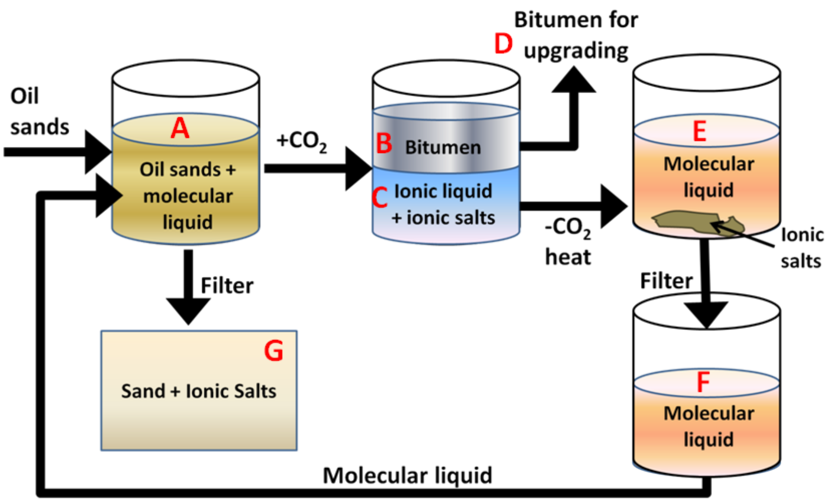

Figure D.9 - Process diagram used to study the extraction of bitumen from oil sands using RevILs

D.4.3 Technological Impact

The United States has large reserves of oil sands in Utah and surrounding areas, which are estimated be greater than 20 billion barrels of oil equivalent.[3] Additionally, even greater deposits lie in Canada with reserves greater than 1.17x10^{12} barrels of oil equivalent.[3] The barrier to using these North American resources lies in the problems surrounding the separation of useable feedstock from its contaminants. A single large-scale process using our method could produce more than half a million barrels a day, with the energy required furnished by a slipstream of the recovered oil. This project envisions extensive molecular design and process alternatives to optimize the operation of such a plant.

The success of this project could have an enormous impact, both economic and in terms of US security. We are already in contact with a number of oil companies about partnering with us. Each has its own agenda of course, but each seeks further data showing not only that the method works, which we basically already have shown, but that our tuning of the liquid structure can achieve some necessary economic goals. Examples of such goals would include (but are not limited to) more favorable phase equilibria and more manageable viscosities. Dr. Eckert and Dr. Liotta have extensive experience working with industrial partners, and it seems quite likely that we shall move forward into a partnership with one (or perhaps more) of the major oil companies. Such a partnership would bring some very practical scale-up know-how to the project to result in more realistic testing.

D.5 Conclusion

In this proposal we describe the development of a novel extraction technique for harvesting liquid fuel from oil sands. For this we shall employ the single-component reversible ionic liquids that have already solved a number of separation challenges. Using our strong background in structure-property relationships, we propose to develop our ability to tailor properties of the precursor silyl amines to form reversible ionic liquids in such a way to optimize the properties necessary for this extraction. These include:

- Low energy
- Lower losses
- Chemical stability
- Recyclability and reuse
- Water tolerance and usage
- Lower cost

With the compound(s) selected we shall carry out HYSYS designs and cost analyses of the proposed project in order to interact fruitfully with potential industrial users.

D.6 References

(1) Poska, F.; Company, P. P., Ed.; Phillips Petroleum Company: USA, 1980.

(2) Speight, J. G. In *Handbook of Alternative Fuel Technologies*; Lee, S., Speight, J. G., Loyalka, S., Eds.; Taylor & Francis Group, LLC: Boca Raton, 2007.

(3) Speight, J. G. In *Kirk-Othmer Enclyclopedia of Chemical Technology*; John Wiley & Sons, Inc., 2000.

(4) Jessop, P. G.; Heldebrant, D. J.; Li, X. W.; Eckert, C. A.; Liotta, C. L. *Nature* **2005**, *436*, 1102Vinci, D.; Donaldson, M.; Hallett, J. P.; John, E. A.; Pollet, P.; Thomas, C. A.; Grilly, J. D.; Jessop, P. G.; Liotta, C. L.; Eckert, C. A. *Chemical Communications* **2007**, 1427.

(5) Phan, L.; Chiu, D.; Heldebrant, D. J.; Huttenhower, H.; John, E.; Li, X. W.; Pollet, P.; Wang, R. Y.; Eckert, C. A.; Liotta, C. L.; Jessop, P. G. *Industrial & Engineering Chemistry Research* **2008**, *47*, 539.

(6) Blasucci, V.; Dilek, C.; Huttenhower, H.; John, E.; Llopis-Mestre, V.; Pollet, P.; Eckert, C. A.; Liotta, C. L. *Chemical Communications* **2009**, 116.

(7) Blasucci, V. M.; Husain, Z. A.; Fadhel, A. Z.; Donaldson, M. E.; Vyhmeister, E.; Pollet, P.; Liotta, C. L.; Eckert, C. A. *Journal of Physical Chemistry A* **2010**, *114*, 3932Blasucci, V. M.; Hart, R.; Pollet, P.; Liotta, C. L.; Eckert, C. A. *Fluid Phase Equilibria* **2010**, *294*, 1Blasucci, V.; Hart, R.; Mestre, V. L.; Hahne, D. J.; Burlager, M.; Huttenhower, H.; Thio, B. J. R.; Pollet, P.; Liotta, C. L.; Eckert, C. A. *Fuel* **2010**, *89*, 1315Jessop, P. G.; Heldebrant, D. J.; Li, X.; Eckert, C. A.; Liotta, C. L. *Nature* **2005**, *436*, 1102.

(8) Dillow, A. K.; Brown, J. S.; Liotta, C. L.; Eckert, C. A. *Journal of Physical Chemistry A* **1998**, *102*, 7609Brown, J. S.; Lesutis, H. P.; Lamb, D. R.; Bush, D.; Chandler, K.; West, B. L.; Liotta, C. L.; Eckert, C. A.; Schiraldi, D.; Hurley, J. S. *Industrial & Engineering Chemistry Research* **1999**, *38*, 3622Brown, R. A.; Pollet, P.; McKoon, E.; Eckert, C. A.; Liotta, C. L.; Jessop, P. G. *Journal of the American Chemical Society* **2001**, *123*, 1254Eckert, C. A.; Liotta, C. L.; Bush, D.; Brown, J. S.; Hallett, J. P. *Journal of Physical Chemistry B* **2004**, *108*, 18108Chandler, K.; Deng, F. H.; Dillow, A. K.; Liotta, C. L.; Eckert, C. A. *Industrial & Engineering Chemistry Research* **1997**, *36*, 5175Chandler, K.; Liotta, C. L.; Eckert, C. A.; Schiraldi, D. *Aiche Journal* **1998**, *44*, 2080Lesutis, H. P.; Glaser, R.; Liotta, C. L.; Eckert, C. A. *Chemical Communications* **1999**,

2063Patrick, H. R.; Griffith, K.; Liotta, C. L.; Eckert, C. A.; Glaser, R. *Industrial & Engineering Chemistry Research* **2001**, *40*, 6063Nolen, S.; Liotta, C. L.; Eckert, C. A.; Glaser, R. *Green Chemistry* **2003**, *5*, 663Thompson, R. L.; Glaser, R.; Bush, D.; Liotta, C. L.; Eckert, C. A. *Industrial & Engineering Chemistry Research* **1999**, *38*, 4220Nolen, S. A.; Lu, J.; Brown, J. S.; Pollet, P.; Eason, B. C.; Griffith, K. N.; Glaser, R.; Bush, D.; Lamb, D. R.; Liotta, C. L.; Eckert, C. A.; Thiele, G. F.; Bartels, K. A. *Industrial & Engineering Chemistry Research* **2002**, *41*, 316Ablan, C. D.; Hallett, J. P.; West, K. N.; Jones, R. S.; Eckert, C. A.; Liotta, C. L.; Jessop, P. G. *Chemical Communications* **2003**, 2972Jessop, P. G.; Stanley, R. R.; Brown, R. A.; Eckert, C. A.; Liotta, C. L.; Ngo, T. T.; Pollet, P. *Green Chemistry* **2003**, *5*, 123.

(9) Bush, D.; Eckert, C. A. *Fluid Phase Equilibria* **1998**, *150*, 479.

(10) Chuit, C.; Corriu, R. J. P.; Reye, C.; Young, J. C. *Chemical Reviews* **1993**, *94*, 1371Corriu, R. J. P.; Royo, G.; Desaxce, A. *Journal of the Chemical Society-Chemical Communications* **1980**, 892.

(11) Prince, P. D.; Bearpark, M. J.; McGrady, G. S.; Steed, J. W. *Dalton Transactions* **2008**, 271.

(12) Voronkov, M. G.; Frolov, Y. L.; Dyakov, V. M.; Chipanina, N. N.; Gubanova, L. I.; Gavrilova, G. A.; Klyba, L. V.; Aksamentova, T. N. *Journal of Organometallic Chemistry* **1980**, *201*, 165.

(13) Bondi, A. *Journal of Physical Chemistry* **1964**, *68*, 441.

(14) Shell Canada, 2010; Vol. 2010.

APPENDIX E - INTEGRATING REVERSIBLE IONIC LIQUIDS WITH ATOMIZER TECHNOLOGY FOR EFFICIENT CO_2 CAPTURE

E.1 Introduction

This appendix presents a proposal that was submitted to the Department of Energy (DOE) for continued funding on the project presented in Chapter 2 detailing the use of silylamines for CO_2 capture. The proposal presents novel atomizer technology for silylamine introduction into the absorption tower, outlining its potential advantages. The atomizer portion of the proposal was to be conducted with Dr. Andrei Federov of the School of Mechanical Engineering at Georgia Teach. The proposal was not acted on but is included for reference.

E.2 Abstract

The use of reversible ionic liquids for CO_2 capture from existing coal-fired power plants offers many advantages over conventional processes. We propose to bring our process nearer to commercialization by optimizing conditions and applying a powerful atomizer technology to eliminate limitations for heat and mass transfer. At the end of this project, (1) the method will be ready for pilot scale demonstration, (2) the process for large-scale manufacture of the solvent will have been defined, and (3) the economic and energy benefits will have been demonstrated.

Silylamine solvents are uncharged molecules which react with CO_2 to form reversible ionic liquids with moderate viscosity. Subsequently, modest heating reverses the reaction, yielding pure CO_2 for sequestration and pure solvent for reuse. The lower solvent viscosities reduce the water requirement and hence the parasitic energy penalty and the lower regeneration temperatures mitigate the energy requirements of the process.

Further, we propose bench-scale demonstration of these solvents using a state of the art atomizer unit, capable of producing uniform droplets only a few microns in diameter with minimum power input. Miniaturization of the droplets greatly increases the surface area to volume ratio to help overcome the heat and mass transfer limitations and reduce the residence times in the absorber. The droplets can be given a charge to prevent agglomeration. The net result is to render the CO_2 capture process highly efficient and cost-effective.

In parallel to our efforts towards improved capture technology through atomizer technology, we are also actively collaborating with our two industrial partners Evonik and ConocoPhillips. Through these collaborations, we propose (1) to determine the important design parameters and scale-up conditions for the industrial scale manufacture of our silylamines and (2) address corrosion, degradation, and toxicity issues related to our silylamines.

E.3 MRC 1: Scientific and technical merit

E.3.1 <u>Background</u>

We have developed a new class of solvent systems which we have termed reversible ionic liquids (RevIL). These switchable organic solvents can be taken reversibly from a relatively nonpolar state to an ionic liquid state by contact with ambient CO_2. Reversal back to the nonpolar state is accomplished by simply heating the ionic liquid to remove the CO_2. Such fluids have been applied to a host of reactions and separations.[1-4] In recent years, we have successfully demonstrated that these reversible ionic liquids also offer an alternative to the existing ethanolamine based CO_2 capture systems in coal-fired power plants.[1,3]

Figure E.1 illustrates the reversible reaction of our silylamines with CO_2. CO_2 is efficiently captured as an ammonium carbamate liquid salt. The subsequent release of the CO_2 is easily accomplished by modest heating. The unique feature of our amine solvent systems is the presence of the silyl group which (1) allows the tuning of the temperature range for the release of the captured CO_2 and (2) aids in the control of the viscosity of the system.[3-5]

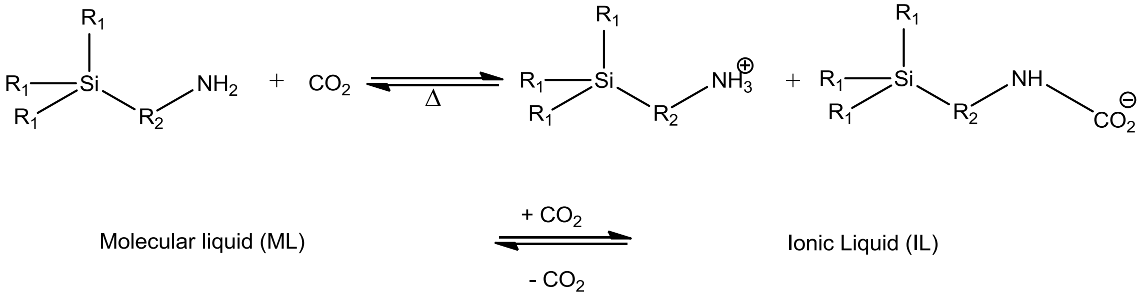

Figure E.1 –Reaction of silylamine with CO_2 to form a reversible ionic liquid

Through a systematic study of structure property relationships, we have determined that the three solvent systems listed in Table E.1 represent those systems with optimum properties with respect to CO_2 capture and release, viscosity, stability, and ease of synthesis. Table E.1 tabulates the critical properties of each of these solvent systems.

Table E.1 - Three silylamine solvents proposed in this project

Acronym	Compound	Structure
ML1	(3-aminopropyl) triethylsilane	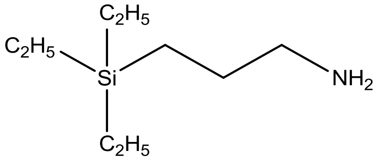
ML2	(3-aminopropyl) tripropylsilane	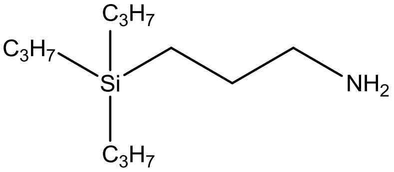
ML3	4-(triethylsilyl) butan-2-amine	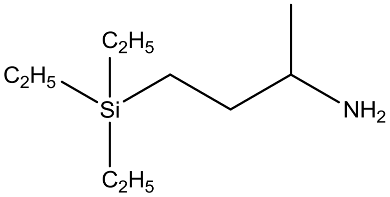

E.3.1.1 *Effect of water*

One of the major challenges in the ethanolamine based CO_2 capture solvent systems is the large quantities of water (70-80% by weight) used to bring down the viscosity and minimize amine degradation.[6] This results in large parasitic energy (165 KJ/mol of CO_2)[6] for heating water during regeneration as well as for separating CO_2 and steam in the exit stream of the stripper. However, some water will always be present because of water in the flue gas. In fact, in our method small quantities of water prove beneficial in improving the CO_2 capture capacity due to the formation of extra bicarbonate (HCO_3^-) and carbonate ions (CO_3^{2-}).

At STP, the solubility of water in our pure MLs prior to CO_2 capture is between 10-15 weight %, while less than 0.3 weight % of our MLs are soluble in the water phase. Thus our MLs have much lower water solubility than MEA, and they require far less water than MEA for corrosion prevention and for viscosity reduction. The viscosity of our neat ionic liquids (without water) varies between (400-2000cP at 40 ºC), significantly lower than that of MEA (8200cP). Therefore there are substantial processing advantages of our silylamines relative to MEA in minimizing the need for excess water, thus reducing the energy requirement for water separation in the cycle. For this proposal, as a standard working solution, we shall use 95% (by weight) ML/water solution.

Table E.2: State-point data table

		ML1		ML2		ML3	
	Units	**M/E P**	**PP**	**M/E P**	**PP**	**M/E P**	**PP**
Pure Solvent							
Molecular Weight	mol^{-1}	173		215		187	
Normal Boiling Point	^{o}C	168		180		160	
Normal Freezing Point	^{o}C	< -77		< -77		< -77	
Vapor Pressure @ 15^{o}C	bar	1x10^{-3}		0.5x10^{-3}		0.7x10^{-3}	
Working Solution							
Concentration	kg/kg	0.95		0.95		0.95	
Specific Gravity (15^{o}C/15^{o}C)	-	0.82		0.83		0.82	
Specific Heat Capacity @ STP	kJ/kg-K	2.20		2.21		2.20	
Viscosity @ STP	cP	2.2		2.19		1.97	
Surface Tension @ STP	dyn/cm	24.8		23.74		24.3	

Table E.2 - continued

		ML1		ML2		ML3	
Absorption	**Units**	**M/E P**	**PP**	**M/E P**	**PP**	**M/E P**	**PP**
Pressure	bar	0.15		0.15		0.15	
Temperature	^{o}C	40		40		40	
Equilibrium CO_2 Loading	mol/mol	0.4		0.36		0.28	
Heat of Absorption	kJ/mol CO_2	123.0		156		152	
Solution Viscosity	cP	910		632		319	
Desoprtion							
Pressure	bar	1.2		1.2		1.2	
Temperature	^{o}C	109		86		94	
Equilibrium CO_2 Loading	mol/mol	< 0.01		< 0.01		< 0.01	
Heat of Desorption	kJ/mol CO_2	123.0		156		152	

M/E P: Measured/ Estimated Performance	PP: Projected Performance

Small improvements to the properties are possible during the course of this project.

E.3.1.2 *Description of sources of data in Table E.2*

Normal Boiling point – Experimentally obtained using Differential Scanning Calorimetry (Q20 TA instruments machine) by heating the RevILs at 5ºC/minute.

Normal freezing point – Solvents remained liquids at dry ice/acetone temperatures, (-78 °C).

Vapor pressure @ 15ºC – Estimated using a combination of Wilson-Jasperson Method[7] for critical point, and Ambrose-Walton Corresponding States Method[7] for accentric factor and vapor pressure.

<u>Working Solution</u>: Measurements are obtained for a 95-5% RevIL-water solutions, while the estimates are obtained by linear interpolation of the pure water and pure RevIL properties.

Specific gravity – Data obtained using a vibrating tube densitometer (Anton Paar DMA 38) at multiple points between 25ºC and 55ºC and extrapolated to 15ºC.

Specific heat capacity – Estimated using method of Ruzika and Domalski.[7]

Viscosity – Measured using a Rheosys Merlin II rotational cone and plate viscometer

Surface tension – Measured using Ramé-Mart Model 250 goniometer.

<u>Absorption</u>

Experiments were performed by sparging a water-saturated gas mixture of (CO_2:N_2 15:85) through our solvent-water mixtures maintained at 40 ºC for 75 minutes. The gas was pre-saturated with water using water bubblers maintained at 40 ºC.

Equilibrium CO_2 loading –Measured gravimetrically as weight gain upon CO_2 sparging.

Heat of absorption – Approximated to be same as heat of desorption (see below).

Solution viscosity - By a Rheosys Merlin II rotational cone and plate viscometer.

Desorption:

Pressure –Estimated by comparing to pressures of regeneration with MEA corrected for the lower regeneration temperatures with our RevILs.

Temperature – Experimentally obtained using Differential Scanning Calorimetry DSC (Q20 TA instruments machine). Preformed ionic liquid (~2mg) ramped up from -40 ºC 400 ºC at a rate of 5 ºC/minute with a convective nitrogen flow of 50 mL/min.

Equilibrium CO_2 loading – The samples were reversed by heating at the respective regeneration temperatures. Subsequent NMR and refractive index measurements showed that the amount of CO_2 in the reversed molecular liquid was below the detection limit (< 1%).

Heat of desorption - Measured by DSC.

Structure-property relationships

We have extensively studied a wide variety of silylamines with respect to structure-property relationships. In this section we summarize results for the three chosen silylamines in the absence of water.

Thermodynamics: The thermodynamics of the capture process can be described by:

The reaction equilibrium constant K which determines the extent of reaction. High K values at absorption temperatures and low K values at regeneration temperatures would be ideal for the entire carbon capture process. The silylamines in Table E.2 possess these properties.

1. The heat required to raise the ionic liquid to regeneration temperature is expressed by the following equation: $Q = mC_p\Delta T$. This quantity depends on (1) the mass and hence the absorption capacity, (2) the heat capacity, C_p, which is nearly same for all three MLs (2.1 KJ/kg-K), and (3) the regeneration temperature T_{reg} ($\Delta T = T_{reg} - 40$) which ranges from 81-104ºC for the three compounds used here.
2. The enthalpy of reaction ΔH_{rxn} which we expect to vary little for the three molecules (~110 KJ/mol of CO_2 as they follow the same reaction scheme (Scheme 1).

Capacity: All our RevILs contain single amine functionality. Hence the capacity (in mol CO_2/kg solvent) depends on the molecular weight and the extent of reaction. All three of our solvents showed complete conversion at room temperature and which goes down with increasing temperature.

Kinetics: For all our RevILs the amine reaction was found to be mass transfer limited. The actual reaction of the silylamine with CO_2 is almost instantaneous. Detailed analysis of this is given below.

Viscosity: Viscosities at complete conversion (at room temperature) decreased from 7600cP to 4000 cP as we increased the size of the substituent chain from ethyl to propyl in RevIL1 and RevIL2, respectively. The introduction of a methyl group in the alpha position of the amine functionality reduced the viscosity to 1900 cP. Viscosities under the operating conditions of the particular silylamine will depend on temperature, extent of conversion, and water content.

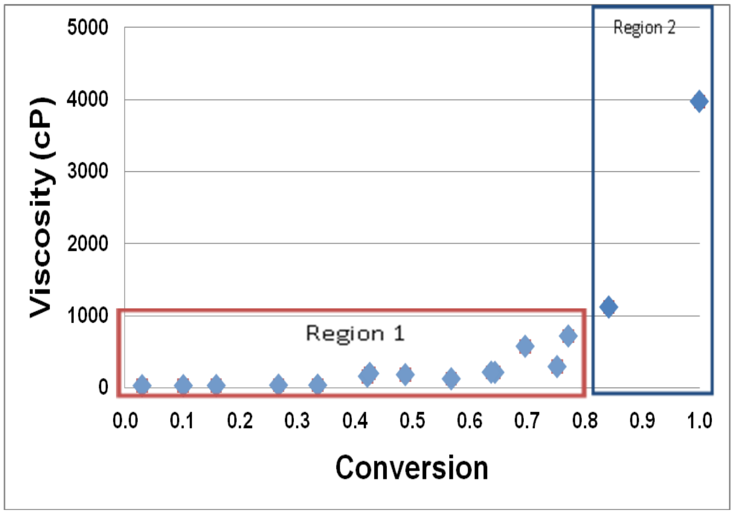

Figure E.2 - Effect of conversion on ionic liquid viscosity for RevIL2

Viscosity and extent of conversion: Figure E.2 above shows the viscosity as a function of conversion from ML2 to RevIL2 upon reacting with CO_2. Two regions are highlighted: region 1 (where viscosity varies slightly with conversion) and region 2 (where viscosity is highly dependent on conversion). The viscosity of the RevIL2 system remains relatively low up to 80% conversion; however, beyond 80% conversion small increments in conversion result in viscosity increase from 300cP to 4000cP (region 2). We shall use these results to our advantage to get a significant reduction in pumping costs as well as to minimize the water requirement with very small compromise in capacity. We expect similar behavior at a capture temperature of 40 ºC.

E.3.1.3 *Recyclability*

We have demonstrated recyclability by alternately reacting ML2 with CO_2 and subsequently releasing CO_2 from RevIL2 over 5 cycles. The procedure we use to demonstrate this is quite simple. We first expose ML2 to CO_2 through at 1 bar and room temperature to capture the CO_2. This is followed by heating the resulting RevIL2 to approximately 100ºC for 1 hour in order to release the CO_2. The capture and release behavior is shown over 5 cycles in Figure E.3. NMR spectra show no changes in structure or appearance of new peaks that would be indicative of possible degradation between the first and the fifth cycle.

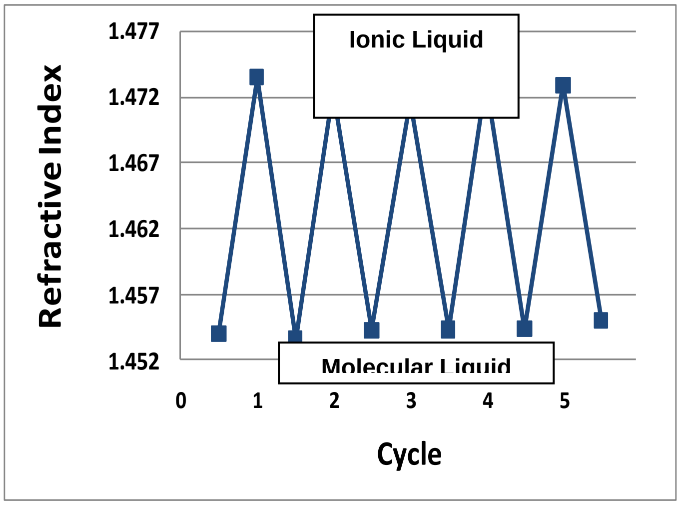

Figure E.3 - Recyclability of RevIL2 in CO_2 capture

E.3.1.4 *Interactions with other flue gas components (SO_2)*

We have demonstrated that our silylamines will reversibly react with SO_2.

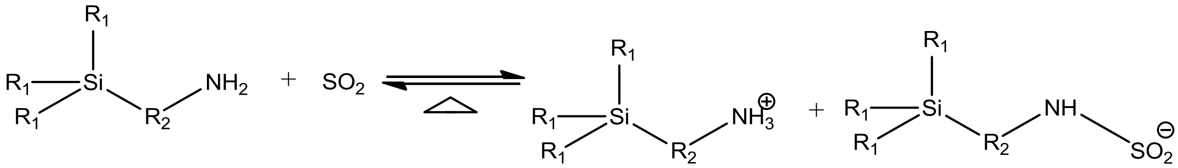

Figure E.4 - Reaction of silyl-amines with SO_2

Our experiments conducted with pure SO_2 at STP showed that our silylamines have similar absorption capacities for both SO_2 and CO_2. Infrared spectra of RevIL1 bubbled with SO_2 showed asymmetric and symmetric S=O stretches in the 1000-1300 cm^{-1} region, confirming the reaction. Therefore, we expect our silylated amines to capture both SO_2 and CO_2. Based on our data, release of the two would occur at different temperatures.

E.3.2 Proposed work I: Efficient solvent dispersion by ultrasonic atomizer

E.3.2.1 *Motivation*

A major adavantage of our silylamine compounds is the extremely short reaction times with CO_2, with reaction half lives less than a second (t_{rxn} ~ 1s). However, the total absorption time depends on three processes in series: (a) gas phase mass transfer from flue gas bulk to the solvent interface, (b) reaction kinetics and (c) CO_2 mass transfer through the ionic liquid skin into the bulk molecular liquid. The slowest of these dictates the absorption time. Although a detailed CFD (computational fluid dynamics) simulation would be required to model the dynamics of these processes accurately, a simple order of magnitude estimate can be easily obtained.

For CO_2, the gas-phase diffusivity D_{gas} is $\sim 16\ mm^2/s$ at STP while the diffusivity in the ionic liquid D_{IL} (estimated from Stokes-Einstein equation) is $3.1x10^{-6} mm^2/s$. The diffusion time scales can be related to diffusivity by ($t \sim \delta^2/D$), where δ is the characteristic diffusion path length. For a representative (target) droplet radius of r~20μm, the diffusion length in gas phase $\delta_{gas} \sim r$ [8], which gives $t_{diff,gas}$ ~25μs. Even if we consider a limiting case where the thickness of the ionic liquid layer is as small as the of vapor side interface $\delta_{IL} = \delta gas$, the diffusion time scale for CO_2 across ionic liquid layer will be $t_{diff,IL}$ ~ 131s, making the mass transfer of CO_2 in the IL the rate-limiting step. Also note that an *order of magnitude reduction in the size of the liquid layer will bring down the diffusion times by two orders of magnitude* (since $t \sim \delta^2/D$). Therefore, in this project we propose miniaturization of molecular liquid into micron size droplets to achieve faster absorption cycles. The three competing processes affecting the mass transfer in a liquid droplet are depicted in Figure E.5.

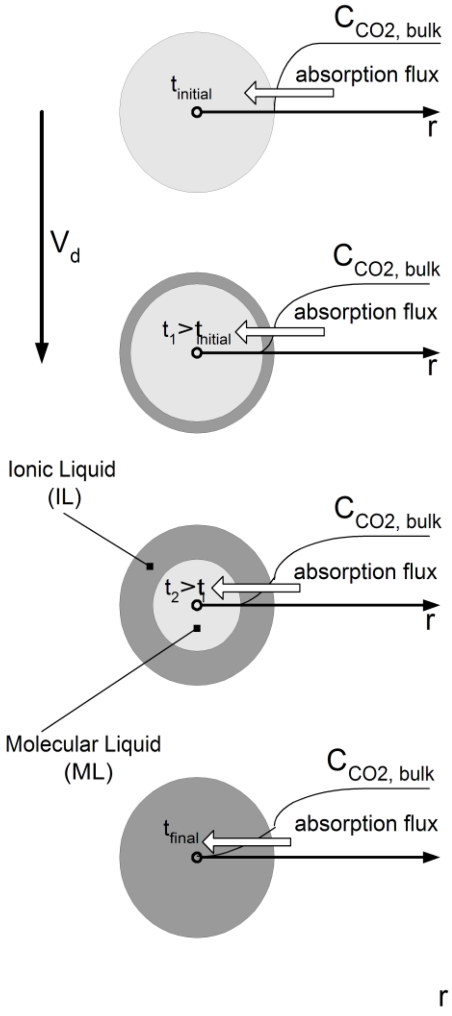

Figure E.5 - Mass transfer and reaction across a molecular liquid droplet

Supporting experimental evidence for the dependence of absorption times on the mass transfer between the gas and liquid phase can be seen in Figure E.6, which shows the extent of CO_2 capture for two modes of gas introduction into molecular liquid at room temperature for 1 minute with constant CO_2 flowrate of 200 ml/min . For the first case, the pure CO_2 is bubbled through a molecular liquid using an 18 gauge needle while for the second case CO_2 is introduced using a fritted glass tube providing much better mass transfer than a needle. It can be seen that the reaction extent was almost three times higher with better mass transfer.

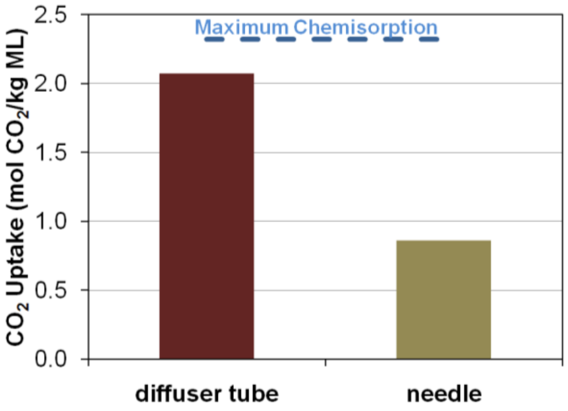

Figure E.6 - Effect of mass transfer on absorption times

The amine-CO_2 reaction is highly exothermic, which could elevate the system temperature and trigger the reverse reaction. Adequate heat transfer is essential to achieve high conversion. The time scales of heat dissipation depend on the thermal diffusivities in the gas phase ($\alpha_{gas} \sim 1.8x10^{-5} m^2/s$) and in the ionic liquid ($\alpha_{IL} \sim 7.4x10^{-8} m^2/s$) $t_{HT,total} \sim t_{HT,IL} + t_{HT,gas} \sim \delta_{IL}^2 / \alpha_{IL} + \delta_{BL}^2 / \alpha_{gas}$. For the target case of 20μm in radius droplets, $t_{HT,total} \sim 0.05s$ which is four orders of magnitude lower than the diffusion time scales. The calculation illustrates two key characteristics of the systems (1) *mass transfer in our systems is more limiting than the heat transfer*, thus allowing higher conversion rates without reversion, and (2) similar to mass transfer, the heat transfer time scales are proportional to square of the radius of the droplets, therefore *efficient dispersion of the solvent into an ultra-fine mist would also make the heat transfer highly efficient*.

E.3.2.2 *Atomizer*

To address the rate-determining mass transfer we propose to incorporate a novel ultrasonic atomization technique for converting our molecular precursors to fine droplets prior to CO_2 exposure. By enhancing the surface area available for CO_2 adsorption we decrease the characteristic time for gas phase heat and mass transfer processes, thus eliminating the mass transfer limitations in the gas phase. In addition, since the time scale for CO_2 transport into a droplet depends on the length scale, ultra-fine droplets will reduce the CO_2 diffusion times down to microseconds, thus removing the transport limitations in the liquid phase, as well.

Conventional fluid atomization techniques have severe limitations to their application in a CO_2 capture system: (1) they produce much larger than optimal droplets with diameter in hundreds of micrometers; (2) the size distribution of liquid droplets is broad and therefore puts severe constraints on design and operating conditions for the absorber with difficulty in fine-tuning for optimal mass transfer conditions; (3) the power required for fluid dispersion using conventional atomization techniques is large. The proposed ultrasonic atomization device overcomes all of the above practical limitations of conventional atomization devices.

The key enabling technology for the proposed CO_2 capture system is an array of ejectors capable of <u>*high-throughput*</u>, <u>*scalable*</u> generation of a mist of <u>*microscopic droplets*</u> of suitable size at <u>*low power input*</u>. It is based on the novel microelectromechanical systems (MEMS)-enabled ultrasonic atomization technology[9] that ejects fluid from micro-scale (3–50 μm) nozzles with incorporated electrodes for manipulation of electro-active fluids. Four aspects enable the superior ejection performance of this atomization technology: (1) ultrasonic frequency of operation, resulting in high throughput (high flow rate) atomization, (2) resonant operation enabling efficient power transfer from the transducer to the ejected liquid, resulting in minimum power input required for atomization, (3) acoustic wave focusing for localized delivery of mechanical (wave) energy bursts, resulting in peak pressure gradient right at the tip of the nozzle and hence enabling ejection of even very high viscosity liquids, and (4) a parallel format (arrayed device) with precisely-controlled (via MEMS fabrication) size of all ejecting nozzles, resulting in scalability of throughput and size uniformity of the mist.

This unique combination of features not only enables ejection of fluids that other droplet generators fundamentally cannot eject, but also brings about the critical operating advantages such as an increased power-efficiency of ejection (reduced power consumption), high throughput from a compact device (ejection of large liquid volumes by a single small-form-factor array), and linear scalability of technology (via adding identical nozzle arrays) to match a wide range of application requirements.

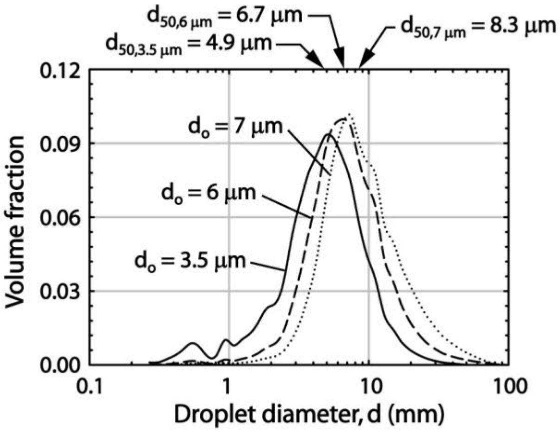

Figure E.7 - Aerosol size distributions for water using ejectors with varying orifice sizes measured by laser diffraction

In the course of the past seven years of focused research, we have demonstrated a number of key atomizer capabilities, which are relevant to the proposed effort and offer significant advantages over the conventional droplet formation techniques:

- Controlled ejection of droplets of uniform diameter between 5 and 50 μm, as governed by the operating frequency, fluid properties, and nozzle orifice size;[10] [11] (Figure E.7 above shows the unimodal size distribution of water droplets)
- High throughput due to ultrasonic frequency of operation up to 1.5 L/min (for 50 μm droplets at ~1.2 MHz frequency from a 400 active nozzle array in 1"x1" footprint), which is linearly scalable by increasing the number of nozzles and multiplexing; [12]
- Low power input for multi-nozzle array (sub-Watt level to power 400 nozzle devices) with diminishing extra-power-cost associated with adding new nozzles to the array;[13]
- Simple, scalable, low-cost batch microfabrication of ejector nozzle array in silicon;[10]
- High droplet ejection velocity of 5-25 m/s, controlled independently of the flow rate;[11]
- Capability to eject ionic conductors and dielectric fluids with the record large viscosities (0.7–3000 mN-s/m2) and significant variation in surface tensions (~25–73 mN/m);[14]
- Capability to operate in drop-on-demand (DOD) or continuous-jet-ejection mode
- Capability to charge droplets upon ejection to avoid post-ejection coalescence;[15,16]

- Device operation independent of orientation relative to the gravity field, with fast start-up and shut-down (~1 μsec) to respond to transient loads, and the ejector utilizes ultrasonic waves for droplet generation, resulting in ultrasonic cleaning (anti-clogging).

In the course of this project, we shall adopt and refine the ultrasonic atomizer for dispersion of our silyl-amines for efficient CO_2 capture. Our efforts will include an optimized atomizer design, aiming to minimize the specific power input (i.e., per unit flow rate of atomized liquid), and in-depth experimental characterization and modeling of the acoustics and fluid mechanics of device operation, targeting the necessary/desired flow rates (system throughput) and droplet size(s). Details about the device components and fabrication, atomizer design and operation, and description of the bench-scale apparatus for CO_2 capture with atomizer are discussed in MRC2.

E.3.2.3 *Preliminary results for CO_2 capture using atomizer*

A first generation prototype of the bench-scale device was constructed to demonstrate the higher efficiency of using the atomizer for solvent dispersion in CO_2 capture. We observed 90% conversion with use of atomizer, while only 14% conversion without it, clearly illustrating a significant advantage of using solvent atomization in improving the capture process efficiency. A detailed schematic of the device and the operating conditions are discussed in detail in MRC2.

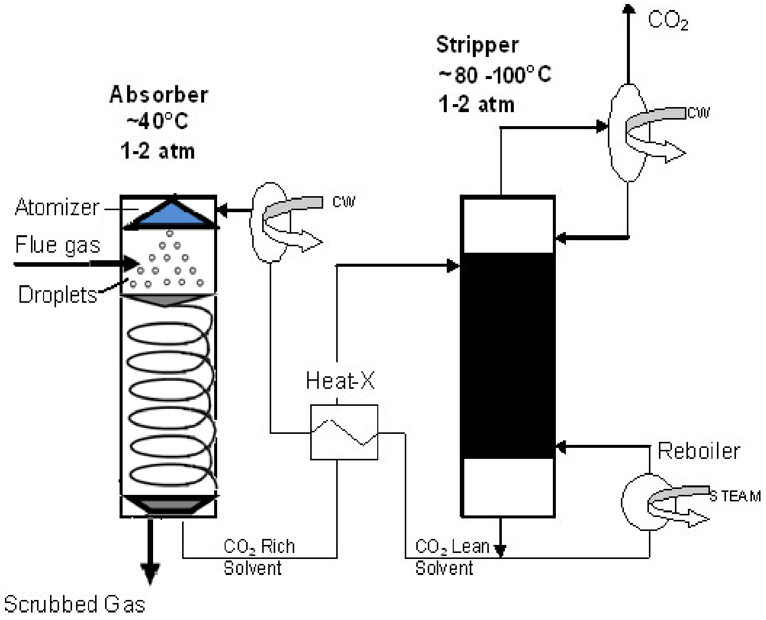

Figure E.8 - Block Diagram of CO_2 capture with Atomizer

E.3.2.4 *Block flow diagram*

A simple block diagram depicting the CO_2 absorption process from a flue gas stream using the atomizer technology is shown in Figure E.8. The atomizer disperses the molecular liquid droplets from the top of the absorption tower. Traditional absorption towers use a countercurrent operation of the solvent and the flue gas stream. However, in a tower equipped with atomizer, such an arrangement might lead to unsatisfactory conversion levels and solvent losses. To address this, we envision absorber geometries that will have a swirl flow of the flue gases within the capture chamber, into which the atomized ultra-fine solvent droplets will ejected from the top and carried to the bottom collection tray (for CO_2-saturated solvent) along an extended path with an optimally designed residence time to maximize the CO_2 capture efficiency per unit pumping power input. The helical shape of the chamber will allow optimum utilization of the available absorber volume. The molecular liquid droplets, once converted to ionic liquid at 40 ºC are collected at the bottom of the helical chamber while the scrubbed gas is vented out.

The CO_2 rich ionic liquid is then pumped to the stripping tower via a heat exchanger for molecular liquid regeneration. The regeneration temperatures (as reported in state-point data table) will depend of the particular choice of RevIL. These temperatures are lower than 120 ºC used for conventional MEA processes. Once regenerated the hot lean solvent is cooled by transferring heat to the counter flowing ionic liquid and a cooler unit and subsequently reintroduced in the absorber for the next CO_2 capture cycle.

E.3.3 Proposed work II: Bulk/commercial scale synthesis of the MLs/RevILs:

For CO_2 capture, a 500 MW power plant requires ~350 tons of initial solvent loading with additional 180 tons of solvent annually for make-up.[17] With nearly 8000 power plants in the U.S. alone,[18] the market for CO_2 capture solvents is of the order of several million metric tons. Therefore we shall show that the proposed solvent is relatively inexpensive and can be efficiently produced in bulk quantities. We are working with Evonik (formerly Degussa), who have extensive experience in research, scale-up, and manufacture of silyl compounds. We will work with Evonik on process scale-up in order to develop an inexpensive, reliable, and environmentally benign industrial process. This is described in greater detail in MRC2.

E.3.4 Proposed work III: Stability of MLs/RevILs and determination of important industrial parameters

The stability of our RevILs against corrosion and degradation is important for determining their applicability in the actual CO_2 capture process. A systematic stability study is essential for determining (a) equipment construction materials and solvent additives, (b) recyclability of the solvent over multiple cycles (c) potential environmental, health and safety concerns and (d) the overall economics of the process. ConocoPhillips, one of our industrial partners in this project, has many years of experience in corrosion and degradation testing in the oil and gas industry and will provide both expertise and facilities in this area. The company will also help in the evaluation of key performance parameters such as absorption kinetics, process recyclability, and spray contactors. The range of tests and analyses to be performed during this collaborative effort is listed in the Statement of Process Objectives.

E.3.5 Advantages of the technology

Table E.3 - Comparison of pure RevILs post CO_2 capture with MEA

	RevIL1	**RevIL2**	**RevIL3**	**MEA**	**30 % MEA aq. solution**
Reaction time for complete conversion at R.T., 1 bar CO_2 at 200 ml/min	2 min	2 min	2 min	10 hours	15 minutes
Regeneration temperature	104	95	81	120	120

The work proposed integrates reversible silylamine ionic liquids and the ultrasonic atomization technology, to achieve synergistically the target of 90% CO_2 capture with less than 35% increase in the cost by the year 2020. As shown in Table E.3, our RevILs demonstrate much more promising properties than pure MEA and 30% MEA aqueous solution. In the absence of water our silylamines show much faster kinetics and lower regeneration temperatures. In addition, the lower regeneration temperatures of our RevILs also ensure that lower energy inputs are required for CO_2 release*, thus enabling a more efficient usage of the existing steam in the power plant*. Due to faster kinetics, the *absorber residence time* for our RevILs will be significantly *shorter* than that for MEA.

The residence times will further improve due to the enhanced mass transfer from the atomizer. The ML systems proposed herein exhibit less reactive sites susceptible to undergo degradative chemistries, thus minimizing make-up and waste streams.

The atomizer unit proposed is a highly efficient (from input power prospective) and a cost-effective alternative to the conventional solvent dispersion systems, especially when used for producing essentially monodisperse mist of ultra-fine (<50 μm in diameter) droplets. The ultrasonic atomizer is a resonant device that exploits operation at judiciously matched resonant frequencies of the array of liquid horns and the piezoelectric transducer to enable low-power operation. In our most recent experiments, at a power consumption of *only 85 mW*, stable ejection of 10 μm water droplets with an estimated ejection flow rate of 100 mL/min was achieved while maintaining the transducer temperature below 30°C. An incremental increase of the array size driven by a single piezoelectric transducer comes at a significantly diminishing cost (a fraction of a percent) of additional power input, due to improved power utilization with an increase in the array size. The device also has a self-pumping capability by the flexing piezoelectric transducer, thus requiring *no additional pumping costs* for continuous operation.

The reduced energy penalty for solvent regeneration, decreased water usage, shorter residence times with efficient heat and mass transfer, and minimal solvent makeup needs contribute in *significantly bringing down the process costs* for CO_2 capture compared to current technology.

E.3.6 Anticipated technical challenges

Our group is a unique collaboration between three academic faculties with expertise in chemistry, chemical engineering, and mechanical engineering. Our two industrial partners have great strengths in silicon-based chemical synthesis and global energy solutions, making us highly capable of successfully addressing technical challenges during the course of the project. Below we list some of the challenges that we currently anticipate with the respective remedial strategies.

E.3.6.1 *Droplet coalescence and collection*

In-flight coalescence is a common problem encountered with dispersed solvents, and directing the mist of droplets towards the collection tray is also challenging. We have shown that putting a net charge of the same sign on the droplets can easily prevent coalescence, while a small opposite sign charge on the collection tray will help direct the drops towards the tray. This can be conveniently achieved in the ultrasonic atomizer, at very low bias DC potentials (V_{ext}) or even in purely AC mode of the piezoelectric transducer's operation (V_{PZT}) through the intrinsic coupling of electric and mechanic fields, by using a locally arranged set of electrodes in the vicinity of the nozzle array surface. [16]

E.3.6.2 *Device design and optimum integration of silyl-amine RevILs and atomizer for CO_2 capture*

Our preliminary experiments have shown that the two technologies can be successfully integrated. One challenge could be device design to ensure the desired conversion levels. We shall use extensive heat and mass transfer calculations to guide our device design. In addition, we shall explore absorber geometries with helical chambers with co-current solvent and flue gas streams.

E.3.6.3 *Stability of RevILs*

Our RevILs will be less susceptible to degradation than MEA because they contain less reactive sites. For instance, the absence of hydroxyl groups is expected to minimize or eliminate oxidations and intra-cyclization reactions which are observed in the case of MEA as a major source of parasitic side reactions. We will use the ConocoPhillips expertise for developing solvent additives that will improve the solvent stability.

E.3.6.4 *Availability of RevILs in bulk quantities*

The RevILs proposed here are not now commercially available. Our collaboration with Evonik will help us in optimizing the reaction pathways for bulk manufacture of the silylamines. Yields, cost, and environmental impact will be of prime importance.

E.3.7 Environmental, health and safety

The EH&S assessment will address two distinct areas of the technologies being developed in the proposal, per se the atomization process and the silylamine solvents.

(1) Atomization unit: Ultrasonic atomizers use standard electronic components (signal generators and RF power amplifier), which are extensively used in industrial practice and operated via well-established standard operating procedures. The driving voltage amplitude is modest (under 200V peak-to-peak after amplification) and transducer heating never exceeds 100°C, which is monitored using thermocouples. The personnel in the power plant are expected to be familiar, equipped and trained to safely handle such voltage levels safely. In addition, ~20 µm atomized droplets can potentially increase irritation by inhalation (entering respiratory tracks up to the bronchial tree). Large scale

process involving atomized droplets are established and will be used as a basis to develop a risk assessment and safety operative protocol for the atomizer unit. For example, engineering controls that would provide a secondary filter of the particles prior to any accidental release could be installed to prevent aerosolized RevILs being present in the working atmosphere.

(2) Silylamine solvents: A preliminary assessment of the proposed silylamines highlighted that these materials may be flammable and irritants. The silylamines proposed are novel solvents; as a result, there is little to no information to realistically estimate their level of flammability and health concerns (rating from 0-4) at this time. TWe propose to compile the data to establish MSDS (Material Safety Data Sheets) for our solvents. These MSDS will be used to develop a rigorous and realistic EHS assessment of large scale operations involving these systems. The proposed silylamine RevILs have less reactive sites susceptible to undergo degradative chemistries than monoethanolamine (current technology), therefore preventing the formation of large degradation by-products stream. As a result, we anticipate the waste streams resulting from solvent's purification and make-up streams to be minimized. In addition, RevILs have low water solubility (less than 0.3wt%), limiting aqueous-contaminated streams. In compliance with current federal regulations, the EH&S assessments and safety handling procedures of the final process will be established in collaboration with Georgia Tech's Department of Environmental Health and Safety team, ConocoPhillips and Evonik. An existing relationship exists with ConocoPhillips and letters of support from Georgia Tech EH&S and Evonik are included in the Appendices.

E.4 MRC2. Technical approach and understanding

E.4.1 Capture agents

E.4.1.1 *Current preparation of silylated amines*

The amines being investigated are currently synthesized by reaction of trialkylsilanes with allyl amine (or in the case of ML3, a substituted allyl amine) using a catalytic amount of platinum-divinyldisiloxane in refluxing toluene.[19] For ML3, before hydrosilylation we must make the 3-amino-1 butene hydrochloride salt through a Gabriel synthesis from 3-chloro-1-butene.[20] This hydrochloride salt requires neutralization prior to hydrosilylation, therefore increasing the number of steps from commercially available materials in the formation of ML3. Due to the expense of platinum catalysts, which would require further functionalization to recycle, and the multistep reactions required for the formation of ML3 precursor, we have developed a common method for the scalable preparation of all three MLs proposed.

E.4.1.2 *Scale-up synthesis of silylated amines*

We propose an environmentally-conscious synthesis for the multi-scale manufacturing of silylated amines. The synthesis requires the formation of silylpropylchlorides from inexpensive trialkylsilanes (triethyl and tripropylsilane) and readily available allyl chloride and methallyl chloride, followed by a simple amination to yield the target silylamines. The silylalkylchlorides can be obtained in quantitative yields from trialkylsilanes with both substituted and unsubstituted allyl chlorides.[21] Through scaling the amine syntheses to volumes on the order of hundreds of milliliters, a blueprint can be developed for future scaling to industrial volumes. We propose to use Aspen

HYSYS to calculate costs associated with the bulk manufacture of our proposed amine solvent.

The process chosen for scale up involves a much more benign and facile two-step reaction sequence. Figure E.9 shows the proposed synthesis of the intermediate (trialkylsilyl)propylchlorides through a hydrosilylation reaction run under neat conditions with an inexpensive copper acetate catalyst. Copper(I) salts have also been shown to have very limited solubility in most solvents, theoretically allowing for complete catalyst recycle, which will be investigated in our bench-scale formation of the silylatedpropylchlorides.

Amination of alkyl chlorides is a classic substitution reaction (Figure E.10).[22] We propose the amination of silylated propylchlorides by reaction with excess liquid ammonia, followed by a mildly basic aqueous wash to provide the desired silylamines. The reaction of the chlorides in excess liquid ammonia provides an opportunity for recycling the remaining amount of ammonia through evaporation and recondensation. We have noted the hydrophobicity of the target RevILs, thus providing an facile extraction from the aqueous wash required (unpublished results in our laboratory).

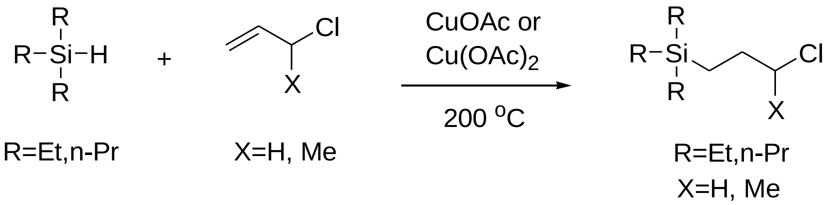

Figure E.9 - Hydrosilylation to desired silylpropylchlorides

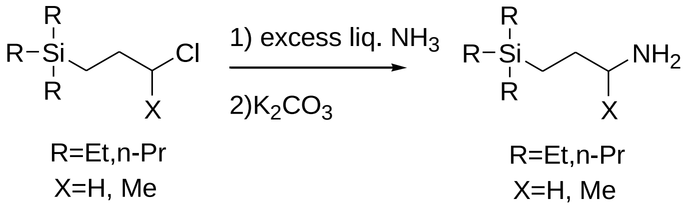

Figure E.10 - Amination of the silylpropylchloride to yield target silylamines

E.4.1.3 *Synthesis of (trialkylsilyl)propylchlorides*

Following a literature procedure, either triethylsilane or tripropylsilane will be mixed in optimized concentrations with allyl chloride or methallyl chloride and subsequently added to dry Cu(OAc) or Cu(OAc)$_2$ in a pressurizable glass tube at -40 ^{o}C through the use of a polyethylene glycol chiller.[21] The tube will be sealed and heated to 200 ^{o}C for an optimal amount of time and then cooled back down to room temperature. The resulting mixture of reactants and heterogeneous catalyst will be filtered and the solution will then be analyzed by LC, GC and ^{1}HNMR for product purity. Any remaining starting materials will be distilled from the product chlorides. Complete characterization through GC, ^{1}HNMR, ^{13}CNMR, MS, and elemental analysis of the chloride products will be conducted. Variables that will be taken into consideration for optimization of the formation of (3-chloropropyl)triethylsilane, (3-chloropropyl)tripropylsilane, and (3-chlorobutyl)triethylsilane will be reaction temperature, catalyst loading, reaction time, and starting material concentration. The optimized reaction conditions will then, with consultation with our research partner, Evonik, be used to scale the reaction to the order of 100 mL batches, which can be used as a model to get more information for commercial-scale production.

E.4.1.4 *Synthesis of (trialkylsilyl)propylamines*

The amination reaction will be conducted by reacting isolated and purified chlorides mentioned above with excess liquid ammonia. These reactions will be done by first condensing ammonia gas through a dry ice condenser into a reaction flask at -40^{o}C. The liquid chloride starting materials will then be added with efficient stirring. The product, once isolated, will be characterized by ^{1}HNMR, ^{13}CNMR, LC, MS, and elemental analysis. We shall consider reaction time, temperature, and ammonia concentration in order to scale the reactions to 100 mL batches.

The synthetic reaction conducted at 100 mL quantities will provide (1) materials for carbon capture and release for the bench-scale experiments, and (2) critical information for the development of synthesis scale-up to the tonnage quantities required for broad use in CO_2 capture facilities. In collaboration with Evonik and Environmental Health and Safety at Georgia Tech, we propose to demonstrate the viability of an industrial scale up procedure for the formation of our three target reversible CO_2 capturing silylamines. Additional proposed experimental details and timelines are included in the Standard Operating Procedures (SOPO) in MRC4.

E.4.2 Atomizer device and operation

Concurrently to the ML silylated amine studies, the CO_2 capture atomization unit will be designed, built and implemented for CO_2 capture in the laboratory. The CO_2 absorption tower design comprises two components: (1) the absorption tower and (2) the atomization device and ancillary equipment. The details are described below.

E.4.2.1 *Components*

The atomizer concept described in MRC1 is realized by (1) creating an array of resonant fluid cavities, (2) making each cavity focus acoustic waves when driven at appropriate resonant frequencies, and (3) selecting a piezoelectric transducer material and geometry for the most efficient operation in the desired frequency range. This conceptual framework has been used to design the droplet generator.[9] A representative device comprises of a fluid reservoir that is formed between a piezoelectric transducer and an array of liquid horn structures (nozzles) in the cover plate. Two power wires on the piezoelectric transducer connect to an external signal amplifier to power the device. A thermocouple is attached to monitor temperature of the piezoelectric transducer as well as the nozzle plate. A small stainless steel line fits into the side of the rubber spacer and is connected to an external device syringe pump to provide a feed for the molecular liquid. To protect the device, silicone gaskets are used on the top and bottom of the sandwich structure to provide a flexible cushion for device assembly and packaging. The device is held together by a custom stainless steel clamp and compression (sealing) of the package device is controlled by four peripherally located bolts. A sketch of the device (without the surrounding stainless steel clamp) is shown in Figure E.11.

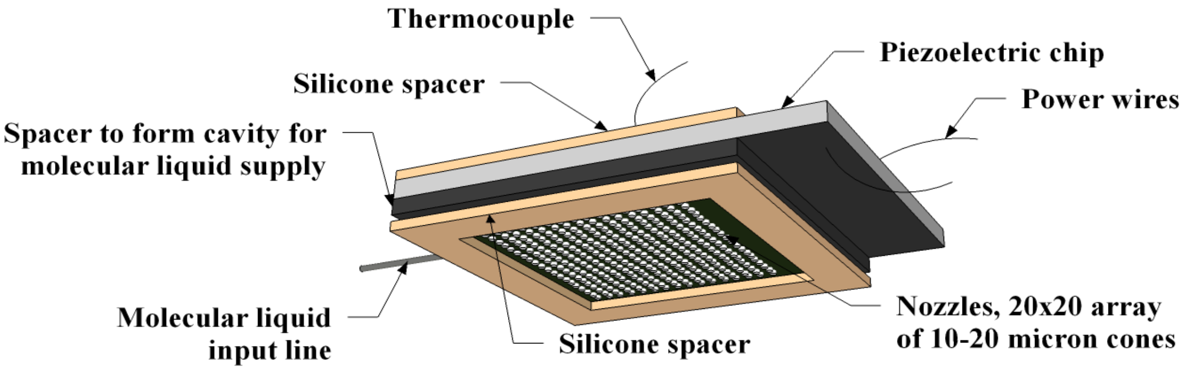

Figure E.11 - Schematic of the atomizer device highlighting integral components

There are three pieces of equipment required to operate the atomizer. The 300 MHz synthetic function generator (Model DS 345) is manufactured by Stanford Research Systems. The function generator provides control of the frequency and amplitude of the driving signal, as well as the number of pulses and pulse frequency (period) when operating at less than 100% duty cycle. Signal gain was set using an ULTRA Series RF power amplifier. To monitor the sinusoidal wave generated, a Tektronix TPS 2014 oscilloscope is used.

E.4.2.2 *Atomizer operation*

The atomizer generates liquid droplets by utilizing cavity resonances in the 1–3 MHz range along with the acoustic wave focusing properties of pyramidal liquid horns formed by a silicon wet etching process. The liquid horn structure, cavity size, and the speed of sound within the ejection fluid dictate the device resonances and thus the operating frequencies of the device.[10,13] Inexpensive and commonly available lead zirconate titanate (PZT-8) ceramic is used for the piezoelectric transducer. When the piezoelectric transducer is driven at the fundamental cavity resonant frequency or any of the higher cavity modes, a standing acoustic wave develops, and constructive interference in the pyramidal nozzles focuses the wave so that the peak pressure gradient occurs near the tip of the nozzles.

Selective operation of the atomizer can be in either drop-on-demand (DOD) or continuous-jet-ejection mode.[11,12] These different modes adapt to the requirements of specific tasks such as droplet-gas contact time, solvent consumption, etc. Regardless mode, the produced droplets/jets are highly uniform in size, which is an important consideration for achieving efficient and reproducible performance of any system relying on the "quality" of fluid dispersion.

Putting a net charge of the same sign is often beneficial in aerosol formation avoid in-flight coalescence of generated droplets in the dispersed phase. We do this in the atomizer, at very low bias DC potentials or even in purely AC mode of the piezoelectric transducer's operation through the intrinsic coupling of electric and mechanic fields in the ultrasonic atomizer, by using a locally arranged set of electrodes in the vicinity of the nozzle array surface.[16]

The atomizer is a resonant device that enables low-power operation, a critically-important consideration. An incremental increase of the active number of nozzles (array size) driven by a single piezoelectric transducer comes at a significantly diminishing cost (a fraction of a percent) of an additional power input due to improved power utilization with an increase in the array size.

E.4.2.3 *Absorption tower*

The tower, constructed of Plexiglas to verify ejection of molecular liquid and monitor experiment progress, will stand one meter tall and contain a collection tray on the bottom and the atomizer device mounted to the top. The atomizer device will be mounted to a Plexiglas disk attached to a custom clamp to allow for adjustment of the effective tower height. Beside the atomizer, a baffle will be mounted to direct the flow of the atomized molecular liquid as well as the flue gas to a mixing zone below the baffle. The atomizer will sit on one side of the baffle while the flue gas injection port will sit on the other. The design and placement of the baffle will be optimized using CFD simulations and supporting experiments in order to direct the atomized molecular liquid downward while allowing sufficient mixing. The tower will be completely sealed, to prevent escape of atomized molecular liquid. The device is shown below in Figure E.12

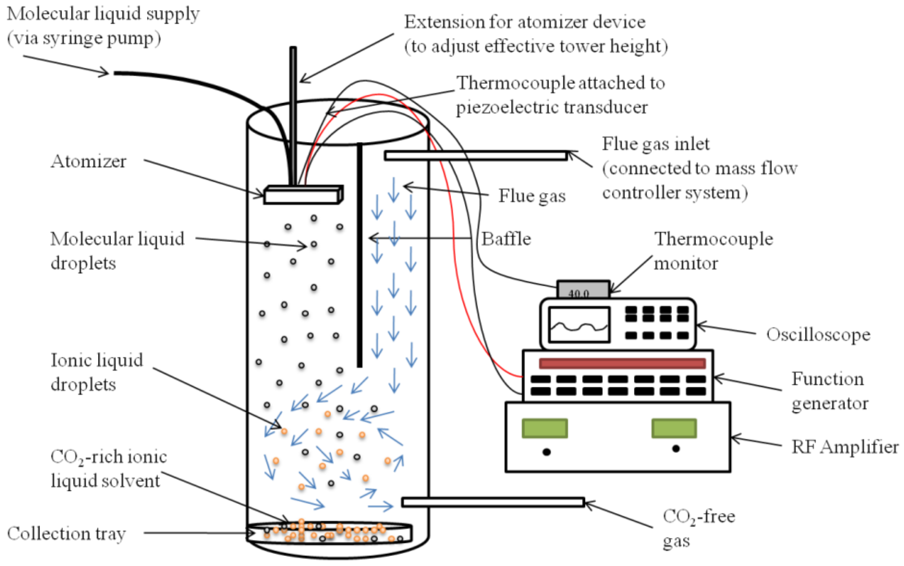

Figure E.12 - Schematic of atomizer, absorption tower and ancillary equipment

E.4.2.4 *Overall operation*

The ML is fed to the atomizer device as described above. The driving voltage signal is sent from the function generator, which produces a sinusoidal wave at a specified frequency and amplitude. The signal is amplified by the RF power amplifier and sent to the piezoelectric transducer (the voltage signal on the piezoelectric is in-situ monitored via an oscilloscope). The frequency used is the resonance frequency of the fluid filled device and the amplitude used is the minimum that provides sufficient ejection (to minimize power requirements). Prior to performing CO$_2$ capture experiments, the ML atomization process will be experimentally characterized for power input required for ML ejectability, nozzle aperture size and operating frequencies as a function of ML properties. These results will be used in the CO$_2$ capture process as well as further power requirement (using ANYSYS) and fluid flow modeling (using FLUENT). Once the atomization properties have successfully been set, the molecular liquid will be atomized into the column with the simulated flue gas that enters and flows downward on the opposite side of the baffle. The simulated flue gas is to be created using mass flow controllers and gas cylinders. Studies in Budget Period (BP) 1 will use simple simulations of 13%CO_2/N_2. BP2 will involve utilizing a more realistic gas mixture at also includes H_2O and SO_x. As the atomized molecular liquid and flue gas meet at the bottom of the baffle, a mixing zone will be created. The molecular liquid droplets absorb the CO_2 in the stream and fall to the collection tray at the bottom of the tower as RevIL. As the experiment progresses, the product gases will be monitored with a residual gas analyzer. After the runtime has expired, the collection tray will be removed and the ionic liquid formed will be analyzed.

E.4.3 Analysis and Data Integrity

E.4.3.1 *Post-experimental analysis*

To quantify the extent of conversion of the molecular liquid to the reversible ionic liquid, a sample of the formed RevIL will be taken from the bottom of the tower. Using a Reichert Arias 500 Abbe-style refractometer, the sample refractive index will be measured and used to calculate conversion of the molecular liquid to the ionic liquid and ultimately CO_2 capture. Additionally, the collected RevIL and regenerated ML will be analyzed by NMR, LC and GCMS to detect the possible formation of degradation products. Successful atomization of ML in the CO_2 absorption column with measurable conversion to RevIL will indicate success at the go/no-go decision point.

The reversible ionic liquid collected from the bottom of the absorption tower will also be analyzed to measure viscosity and study desorption. Viscosity plays an important part in determining the operating costs and as shown in MRC1, we can have sufficiently low viscosities (300cP) with fairly high conversion levels (80%). Desorption temperatures will be studied using a TGA. Potential loss of the ML as a result of elevated temperatures for desorption will be determined.

To eliminate variability as a function of the sampling location, ionic liquid samples will be collected from multiple locations at the bottom of the tower. This will allow for an accurate value of conversion to be calculated as well as any deviation or error that may be present. Calculation of standard deviation of the sample conversion will further allow us to optimize the system and achieve a uniformly converted ionic liquid for desorption and subsequent regeneration. At the end of BP1, a single ML/RevIL will be identified for further experimentation and analysis for commercial-scale CO_2 capture simulation.

E.4.3.2 *Variables*

Tower height and experiment duration will be varied to determine the optimal time of flight and contact time with CO_2 for the ejected droplets. Smaller droplets will lead to greater gas-to-solvent contact area, shorter diffusion paths, slower rate of fall (greater residence time), which yield higher CO_2 uptake. Increased CO_2 uptake for greater conversion of ML to RevIL will give an increase in viscosity. This would impose a pumping power overhead on the overall energy efficiency of the system. The optimum level of CO_2 capture and ML-to-RevIL conversion during the solvent transport are important design variables which we shall optimize.

In the course of this program, we shall also adopt and refine the ultrasonic atomizer for unique requirements of dispersing the molecular liquids. Our efforts will include an optimized atomizer design, aiming to minimize the specific power input (i.e., per unit flow rate of atomized liquid), and in-depth experimental characterization and modeling of the acoustics and fluid mechanics of device operation, targeting the necessary/desired flow rates (system throughput) and droplet size(s). The device performance will be tested with simulated flue gas, and the system-level results will be used to further enhance the ultrasonic atomizer design and performance. The effect of flue gas flow direction (co-, counter- or cross-current) and flow rate will be determined for optimal mass transfer in conjunction with atomizer parameters.

To establish a complete absorption / desorption capture system it will also be necessary to define the variables that influence the desorption process. The effect of desorption temperature and heating rate will be examined to achieve complete reversal of the ionic liquid to the molecular liquid and minimal solvent losses.

To perform these tasks we shall use the state-of-the-art simulation and experimental tools and manufacturing processes we have already used and described in the previous sections of the proposal, and will develop new tools and techniques, as necessary.

By altering the dimensions of the absorption tower, we can observe the effect of scale-up for our process. At bench-scale our lab can supply a flue gas for simulation with the composition and temperature of power plant flue gas after desulfurization.

E.4.4 Environmental health and safety

We have a long standing collaboration with the department of Environmental Health and Safety of the Georgia Institute of Technology. We will continue our collaboration to anticipate and evaluate the hazards of our proposed process at the bench-scale and as we progress towards the commercial process. We propose to approach the hazard assessment for the scale up of the carbon dioxide capture plant in a similar fashion to the way we have been doing for the laboratory bench-scale model. At this stage, we already have established chemical hazard assessments of all reactants and standard operating procedures (SOP) for the synthesis of the RevILs system 1, 2 and 3 and for operating the bench-scale atomizer model. In the final assessment, we will identify the hazards of all the reactants (including catalysts), products and by products/wastes. This would include chemical hazards and physical hazards such as flammability, heat, or cryogenic hazards. Also, we will consider the final disposition of all the products, wanted and unwanted, and determine how they will be dealt with, such as collect to recycle, or dispose of per local, state and federal regulations.

Additional proposed experimental details, activities and timelines are included in the Standard Operating Procedures (SOPO) in MRC4.

E.4.5 Scale-up and Simulation

E.4.5.1 *A. Analysis of ML/RevIL corrosion and degradation behavior*

Determining the corrosive behavior of liquids to be used in CO_2 capture is important for three reasons: selection of unit operation materials of construction, handing considerations and determination of degradation pathways. Many chemical degradation pathways are promoted by the presence of metal ions in the solvent that are a result of corrosion of the processing equipment by the solvent. ConocoPhillips, who are well-equipped and experienced in corrosion testing, will be aiding in the corrosion testing and interpretation. Once the corrosion properties have been analyzed, the degradation pathways will be investigated for the ML and resulting RevIL from CO_2 capture. Analysis of the ML/RevIL after cycling will be performed by FTIR, LC-MS, GC-MS and NMR. After identification of any degradation products has occurred, we shall seek to delineate potential degradation pathways, again consulting our partners ConocoPhillips and Evonik. Model reactions will also be performed to test the hypotheses. These may be implemented into the synthesis of the ML or as an additive step later.

E.4.5.2 *Establish critical parameters for pilot scale phase*

We shall work on design of a large scale system suitable for scale-up, including development of a design strategy for (1) integration of many atomization units into a large scale array with suitable solvent delivery and distribution system and (2) collection of ionic liquid, regeneration and return to the atomization unit to close the loop. This will require choosing the design and sizing of heat exchanger components and coupling with external heater/chiller system (optimally using being the utilities already available in a coal-fired power plant) for efficient heat supply/rejection to the capture system.

To transition to large scale demonstration, we shall address the issues of costs and manufacturability of components. Our baseline strategy is to use silicon micromachining to fabricate the nozzle arrays. Since these nozzle arrays are made using a standard 2-mask batch process, it is scalable to production of large quantities at reasonably low cost. The cost estimates have been prepared in consultation with the microfabrication service companies (Micralyne and MEMSCAP) and suggests a cost of 6-8 cents per nozzle is readily achievable.

E.4.5.3 *Modeling*

The atomization process will be analyzed for optimized power inputs using ANSYS and fluid flow of the droplets using computational fluid dynamics (CFD/ FLUENT software). Additionally, we will use the combination of simple analytical models and CFD simulations to evaluate and optimize the heat and mass transfer in the ML-CO_2-RevIL system. We have significant experience with such analytical tools, including validation on laboratory systems, with applications to a wide range of reaction-transport systems, including adsorption CO_2 capture and catalysis.[23] The goal of these simulations will be to design an optimal system configuration and develop operating guidelines that result in highest heat and mass transfer rates to/from solvents in order to reach near-intrinsic kinetics of CO_2 absorption and desorption during solvent regeneration, while minimizing the parasitic losses due to pumping power and heat rejection to the environment.

The results obtained from experiment and modeling of the atomization and CO_2 capture process along with EH&S analysis will be integrated into the final process simulation of a commercial-scale CO_2 capture system using Aspen HYSYS. The end result of the project will be a system simulated for CO_2 capture with information available for process costs and power needs. With the results obtained in this project, the proposed technology will be ready for scale-up to pilot scale in a future project.

E.5 References

(1) Blasucci, V.; Dilek, C.; Huttenhower, H.; John, E.; Llopis-Mestre, V.; Pollet, P.; Eckert, C. A.; Liotta, C. L. *Chemical Communications* **2009**, 116.

(2) Blasucci, V. M.; Hart, R.; Pollet, P.; Liotta, C. L.; Eckert, C. A. *Fluid Phase Equilibria* **2010**, *294*, 1.

(3) Blasucci, V.; Hart, R.; Mestre, V. L.; Hahne, D. J.; Burlager, M.; Huttenhower, H.; Thio, B. J. R.; Pollet, P.; Liotta, C. L.; Eckert, C. A. *Fuel* **2010**, *89*, 1315.

(4) Hart, R.; Pollet, P.; Hahne, D. J.; John, E.; Llopis-Mestre, V.; Blasucci, V.; Huttenhower, H.; Leitner, W.; Eckert, C. A.; Liotta, C. L. *Tetrahedron* **2010**, *66*, 1082.

(5) Shirota, H.; Edward W. Castner, J. *Journal of Physical Chemistry B* **2005**, *109*, 21576Crosthwaite, J. M.; Muldoon, M. J.; Dixon, J. K.; Anderson, J. L.; Brennecke, J. F. *Journal of Chemical Thermodynamics* **2005**, *37*, 559Chuit, C.; Corriu, R. J. P.; Reye, C.; Young, J. C. *Chemical Reviews* **1993**, *94*, 1371.

(6) Yeh, J. T.; Pennline, H. W.; Resnik, K. P. *Energy & Fuels* **2001**, *15*, 274.

(7) Poling, B. E. *The properties of gases and liquids*; 5th ed. ed.; McGraw-Hill: New York :, 2001.

(8) Eckert, E. R. G.; Drake, R. M. *Analysis of Heat and Mass Transfer*; McGraw Hill, New York.

(9) Fedorov, A. G.; Degertekin, F. L. USA, 2007Fedorov, A. G.; Degertekin, F. L. USA, 2009Degertekin, F. L.; Fedorov, A. G. USA, 2007.

(10) Meacham, J. M.; Ejimofor, C.; Kumar, S.; Degertekin, F. L.; Fedorov, A. G. *Review of Scientific Instruments* **2004**, *75*, 1347.

(11) Meacham, J. M.; Varady, M. J.; Degertekin, F. L.; Fedorov, A. G. *Physics of Fluids* **2005**, *17*.

(12) Forbes, T. P.; Degertekin, F. L.; Fedorov, A. G. *Review of Scientific Instruments* **2007**, *78*.

(13) Meacham, J. M.; Varady, M. J.; Esposito, D.; Degertekin, F. L.; Fedorov, A. G. *Atomization and Sprays* **2008**, *18*, 163.

(14) Meacham, J. M.; O'Rourke, A.; Yang, Y.; Fedorov, A. G.; Degertekin, F. L.; Rosen, D. W. *Journal of Manufacturing Science and Engineering-Transactions of the Asme* **2010**, *132*.

(15) Aderogba, S.; Meacham, J. M.; Degertekin, F. L.; Fedorov, A. G.; Fernandez, F. M. *Applied Physics Letters* **2005**, *86*.

(16) Forbes, T. P.; Dixon, R. B.; Muddiman, D. C.; Degertekin, F. L.; Fedorov, A. G. *Journal of the American Society for Mass Spectrometry* **2009**, *20*, 1684Forbes, T. P.; Degertekin, F. L.; Fedorov, A. G. *Journal of the American Society for Mass Spectrometry* **2010**, *21*, 501.

(17) DOE/NETL-2010/1397, 2010.

(18) Development, C. f. G. In *Science Daily*, 2007; Vol. November 15.

(19) Marzinke, M.; MacMillan, J. H.; August, T. F.; Telepchak, M. J.; United Chemical Technologies, Inc.: United States, 2001.

(20) Wang, H.; Matsuhashi, H.; Doan, B. D.; Goodman, S. N.; Ouyang, X.; Clark, W. M. J.; Tetrahedron, 2009; Vol. 65.

(21) Nguyen, B. T.; Dow Corning: United States, 2004.

(22) Shreve, R. N.; Burtsfield, D. R. *Journal of Industrial and Engineering Chemistry* **1941**, *33*, 218.

(23) Damm, D. L.; Fedorov, A.; Industrial & Engineering Chemistry Research, 2008; Vol. 47 Damm, D. L.; Fedorov, A.; Industrial & Engineering Chemistry Research, 2009; Vol. 48Fedorov, A.; Viskanta, R.; International Journal of Heat and Mass Transfer, 1999; Vol. 42Fedorov, A.; Viskanta, R.; Thermal Science and Engineering, 1999; Vol. 5Fedorov, A.; Viskanta, R.; Chemical Engineering Communications, 1999; Vol. 171Kaisare, N. S.; Lee, J. H.; Fedorov, A., *AIChE Journal*, Vol. 51 (8), pp. 2254-2264.; AIChE Journal, 2005; Vol. 51Kaisare, N. S.; Lee, J. H.; Fedorov, A.; Industrial & Engineering Chemistry Research, 2005; Vol. 44Kim, Y. J.; Joshi, Y.; Fedorov, A.; Journal of Mechanical Science and Technology, 2008; Vol. 22.

APPENDIX F - DOW ELASTOMERS, ELECTRICAL AND TELECOMMUNICATIONS: CHEMISTRY OPTIONS FOR ADVANCED TELECOMMUNICATIONS

F.1 Introduction

This proposal was submitted to Dow as an expansion of the project investigating the thermal degradation and stabilization of PVC presented in Chapter 4. The proposal was recently accepted and research is now in progress. Preparing the proposal involved extensive discussion with Dow, literature research on polyethylene processing, and original thinking to formulate the research plan.

F.2 Abstract

This proposal uses model compounds and polymer studies to build a fundamental understanding of chemical reactions and transformations that occur in polyethylene (PE) in the presence of peroxides, scorch retardants, antioxidants, and other relevant additives. The work will involve theoretical and experimental mechanistic model compound studies of the decomposition of peroxides in the presence of other additives, including both scorch retardants and antioxidants. The goal will be to understand the different reactions that can ultimately affect key crosslinking properties of peroxide-containing PE, including scorch retardance, acid-catalyzed decomposition of peroxides, and possible oxidation of stabilizing additives. The improved understanding of transformations occurring during crosslinking under relevant conditions can lead to better methods for mitigating deleterious effects.

F.3 Proposal

F.3.1 Background

High (>69 kV) and medium (5-69 kV) voltage cables for the underground transmission of power rely on a thick shell of cross-linked polyethylene (XLPE) to provide electrical insulation for the copper conductor. Dow's Electrical and Telecommunications Business provides formulated polyethylene pellets to cable manufacturers to be extruded and crosslinked in the power cable manufacturing process. The most common crosslinker included in PE formulations is dicumyl peroxide (DCP, Figure F.1). At elevated temperatures, the peroxide decomposes to give a radical, which can initiate crosslinking of the polymer.

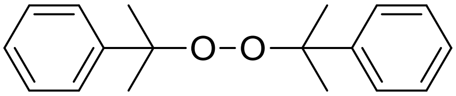

Figure F.1 – Dicumyl peroxide

It is important that PE formulations maintain stability through the extrusion process (at temperatures around 140°C), crosslinking only when desired in the subsequent continuous vulcanization (CV) step – where the average temperature is about 180°C. Premature crosslinking during extrusion (scorch) can lead to non-uniformity in the power cable insulation, which can cause harmful effects when attempting reliable power transmission. The manufacturing process proceeds in the following manner (Figure F.2):

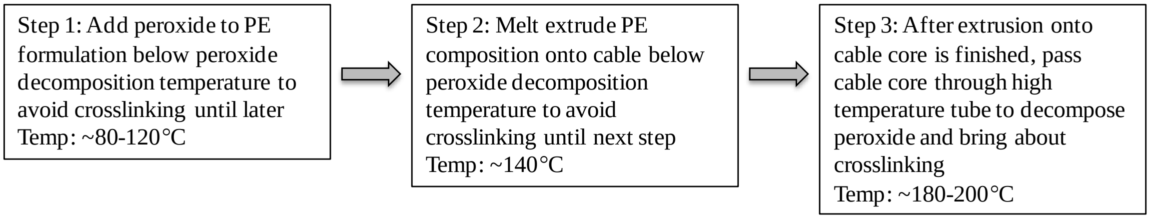

Step 1: Add peroxide to PE formulation below peroxide decomposition temperature to avoid crosslinking until later
Temp: ~80-120°C

Step 2: Melt extrude PE composition onto cable below peroxide decomposition temperature to avoid crosslinking until next step
Temp: ~140°C

Step 3: After extrusion onto cable core is finished, pass cable core through high temperature tube to decompose peroxide and bring about crosslinking
Temp: ~180-200°C

Figure F.2. Generalized PE cable manufacturing steps

Stabilizers are used to scavenge any decomposed dicumyl peroxide radicals that form before the crosslinking step. A typical PE formulation consists of 97-98 wt% polyethylene, 1-2 wt% peroxide, and 0-1wt% of stabilizing additives (i.e. scorch retardants, crosslinking boosters, and antioxidants). One antioxidant investigated and used by Dow is the thioester Cyanox STDP (Figure F.3, below). Dow has found that the PE scorch time is significantly increased by using this thioester with a special imbibing process (confidential, developed by Dow). The scorch time of a peroxide-containing polymeric composition is measured using a moving die rheometer that records torque as a function of time at elevated temperature. The increase in torque (modulus) over time is attributed to crosslinking of the PE. The scorch time is measured at a point defined as TS1 – the time for 1 Inch-Pound increase in torque over the minimum value (which corresponds to the modulus of uncrosslinked PE). A higher TS1 indicates a greater resistance to scorching. As shown in Table F.1, using the special imbibing procedure, including the Cyanox STDP brings about a 132 minute normalized scorch time improvement compared to a PE formulation without the thioester.

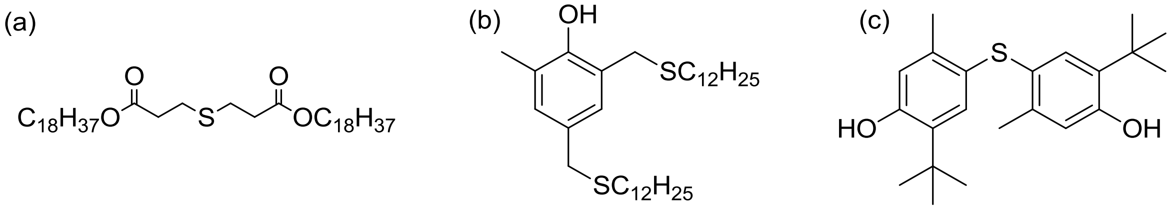

Figure F.3. (a) Cyanox STDP; (b) Irganox 1726; (c) TBM6.

Table F.1 - TS1 Results with Cyanox STDP

PE formulation: 98.00 wt% polyethylene, 1.70 wt% dicumyl peroxide, 0.20 wt% Cyanox STDP	Compounding Procedure	Imbibing Procedure (102°C, 12 hours)
Ultimate crosslinking level MH-ML[2] (dN-m)	3.9	3.0
Scorch time TS1 @ 140°C (minutes)	36	180
Normalized scorch improvement (minutes)*	1	132

*versus formulation at same MH-ML with only peroxide and PE

F.3.2 Proposed research

The current Dow hypothesis to explain these experimental observations is that "*during the special imbibing process, the thioester antioxidant is undergoing free radical oxidation to one or more sulfur-based acids that are active in reducing crosslinking at 140°C, but not competitive with free radical crosslinking at 180°C.*"

The purpose of this proposal is to present postulates and experiments aimed at answering three research questions on this hypothesis:

1. What is the detailed mechanism leading to the very large increase in TS1 in the special imbibing process?
2. What is the detailed mechanism of the acid-catalyzed peroxide decomposition?
3. What are the free-radical mechanisms of reaction between the peroxide and coagent?

Other questions to consider addressing, if and as appropriate, are as follows:

1. Can an ideal acid or acid precursor be directly utilized without need for special process?

---

[2] ML = minimum torque; related to viscosity of uncrosslinked polymer; MH = maximum torque, indicative of degree of crosslinking, TS1 = time to reach (ML + 1 inch-Pound) of torque; indicative of resistance to premature crosslinking (scorch)

2. Which acids are ideal?
3. Can blocked acids be used to avoid shelf life issues?
4. Can acids be identified that decompose prior to 180°C?
5. Would Lewis acids also be effective, in addition to Brønsted acids?
6. Peroxide structure effect?
7. Does TAIC, present in a key Dow formulation, play an important role in stabilizing the post-imbibing mixture so that it has sufficient storage stability to avoid loss of peroxide at room temperature?

To probe the mechanism behind Research Questions 1 and 2 and attempt to model conditions under which the scorch time can be improved, we have developed the following postulate on which experimental scenarios will be presented:

The dialkyl sulfide species (or a sulfur derivative of said species) acts as a sacrificial scavenger that reacts with decomposition products (radical decomposition) of the peroxide, thus hindering the cross-linking at lower temperatures. We will attempt to identify if this effect is attributed to the presence of a radical scavenger, a reduced amount of peroxide in the final mixture, or the presence of less-reactive cross-linking species in the final mixture.

From this hypothesis, we have developed four experimentation scenarios to model reaction conditions:

1. Identify the mechanism and kinetics of peroxide decomposition under the special imbibing conditions.
2. Identify the mechanism and kinetics of consumption of the sulfur species.

3. Screen various sulfur functionalities and known radical scavengers to monitor the influence of the sulfur species on peroxide decomposition.
4. Screen impurities of mixture components to monitor effects on system.

F.3.3 Scenario #1 – Thermal decomposition of the radical initiator

For polymer processing, an ideal radical initiator is one that is relatively stable under ambient conditions, but can be decomposed at the processing temperature. With the processing procedures described above, it is also critical to have an initiator that is relatively stable at elevated temperature to minimize premature crosslinking (<140oC for adding peroxide and melt extruding PE composition). The first hypothesis we will test is whether the imbibing process is actually initiating a measurable amount of dicumyl peroxide decomposition, and how the decomposition products could affect the system. A common quantitative metric for radical initiators is the temperature at which half of the initiator degrades over a period of 10 hours (10 h $t_{1/2}$). Literature has reported that dicumyl peroxide in benzene has a 10 hour $t_{1/2}$ temperature at 115^{o}C.[1] From this datum, we are working under the assumption that a portion of peroxide is decomposing[3] during the extended imbibing process. If this is true, then the actual peroxide composition in the mixture during the cross-linking phase is unknown, in addition to forming a mixture of compounds that could influence the chemistry. The overarching purpose of these experiments is to identify the chemical components associated with the decomposition of DCP and postulate how they are impacting the scorch time and ultimate cross-linking level. Possible decomposition pathways are shown in Figure F.4.

---

[3] Decomposition is assumed to be a combination of thermally initiated radical formation and acid decomposition (possibly from water in the air). The experimentation described herein will test this hypothesis.

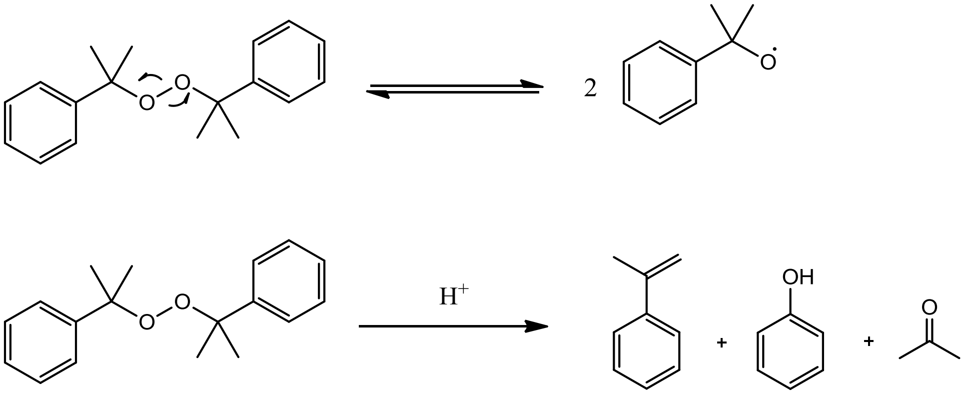

Figure F.4 – Possible decomposition pathways of dicumyl peroxide

F.3.3.1 *Experimental*

The general procedure for these experiments will involve dicumyl peroxide dissolved in an alkane solvent (ex. heptane, dodecane) with the following modifications:

1. Presence of air (open to the atmosphere).
2. Under an inert atmosphere (nitrogen, argon, etc.).
3. Under a dry air atmosphere to analyze in the presence of oxygen and absence of water.

We believe it's important to analyze the decomposition of DCP in a hydrocarbon solution, at suitably high temperatures (ranging from approximately 140°C to 180°C) to gain an initial understanding of how the peroxide behaves in the imbibing conditions and subsequent extrusion and CV conditions. In Scenario #2, we introduce the idea of an active sulfur species and will monitor its reactivity in the system.

All of the experiments in this section can be monitored via a variety of analytical methods (Gas Chromatography – Mass Spectrometry / GC-MS, Liquid Chromatography – Mass Spectrometry / LC-MS, High-Performance Liquid Chromatography / HPLC, ^{1}H

NMR, and ^{13}C NMR). The results of these experiments will suggest further experiments that can be conducted, depending on what (if any) active species are found in the resulting mixtures. These experiments will also be run in tangent with Scenario #2, where we are hypothesizing that the sulfur compound mixture is contributing to the increasing scorch time, possibly by catalyzing acidic decomposition.

F.3.4 Scenario #2 –Active sulfoxides in mixture – thermal eliminations

Prior work conducted at Dow laboratories has indicated the increase in TS1 was enhanced in the presence of Cyanox STDP and Irganox 1726 (Figure F.3) while incorporation of TBM6 resulted in little additional benefit. The differences in structure indicate the dialkyl thio-ethers (Cyanox and Irganox) are moieties that contribute to the enhanced scorch time. Oxidation of the dialkyl sulfide (through reaction with the peroxide or its decomposition products) would generate a sulfoxide in the mixture. It is well known that sulfoxides can undergo thermal β-elimination[2] where acidic protons alpha to a carbonyl functionality are available (retro-Michael addition), as would be the case for the sulfoxide analogues of Cyanox and Irganox (but not TBM6). Though this mechanism proceeds under basic conditions, it has been reported that sulfoxides are highly prone to these reactions, even occurring under thermal conditions. In this scenario, the presence of water at elevated temperatures may be driving such a reaction, though STDP was found to have relatively high thermal stability via TGA experiments.

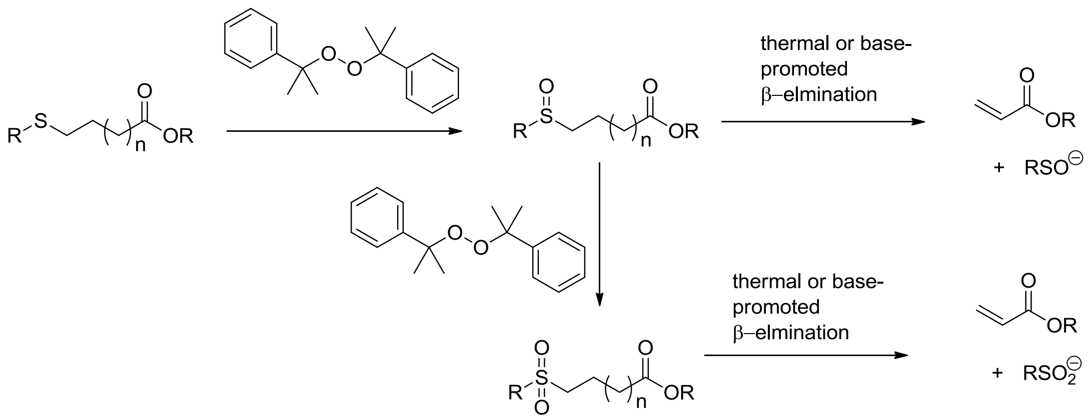

Figure F.5 - **β-elimination of sulfoxides**[2]

F.3.4.1 *Experimental* –

To examine the impact of sulfur species in the mixture, we propose the following experiments:

1. Repeating the experiments outlined in Scenario 1, but in the presence of different sulfur-based functionalities. Broadly, these will encompass dialkyl sulfides, sulfoxides, sulfones, and sulfolenes.

2. Within each class of sulfur compounds, examine various substitution patterns. For example, a good diagnostic would be to run two reactions with different dialkyl sulfides, where one compound contains β-protons and a separate compound that does not (to prevent β-elimination).

3. As in Scenario 1, these types of experiments can be monitored via a variety of analytical methods (Gas Chromatography – Mass Spectrometry / GC-MS, Liquid Chromatography – Mass Spectrometry / LC-MS, High-Performance Liquid Chromatography / HPLC, ^{1}H NMR, and ^{13}C NMR) with the following goals:

   - Clarifying the types of side-reactions that are occurring during the imbibing procedure.

- Seeing what types of sulfur compounds contribute to the increased scorch times.
- Manipulating the mixture stoichiometry to further enhance and optimize scorch times for these blends.

F.3.5 Scenario #3: Acid Catalyzed Decomposition of Peroxide

Non-free radical acid catalyzed decomposition of the dicumyl peroxide can cause its consumption and detract from its ability to cause crosslinking as shown in Figure 6.[3]

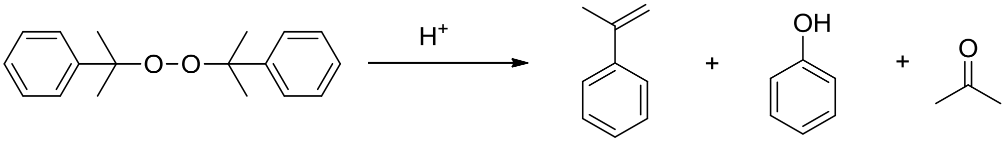

Figure F.6 - Acid catalyzed decomposition of dicumyl peroxide

It is proposed that the acid source could come from the repeated oxidation of the Cyanox STDP. A scheme of the formation of the peroxidolytic antioxidants by the oxidation of thiodipropionate ester was found in literature.[4]

We propose that the dicumyl peroxide could also be consumed simply by oxidation of the Cyanox STDP thioester as shown in Figure 8. The sulfone produced could be further oxidized to the sulfonic acid derivative as shown in the last step.

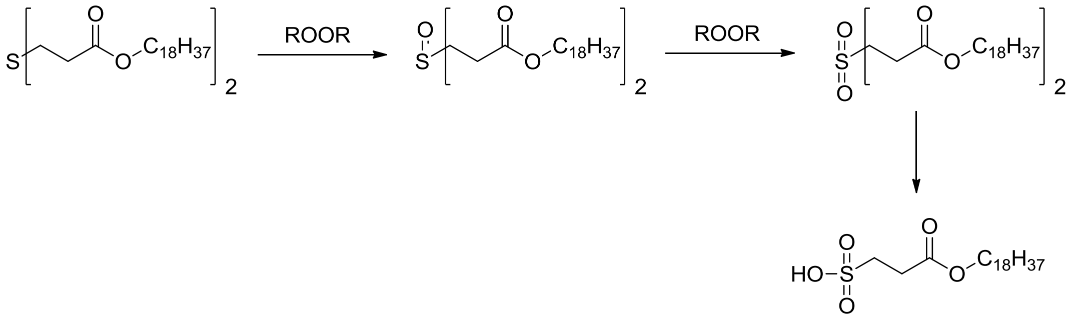

Figure 8 – Oxidation/Hydrolysis of Cyanox STDP[5]

To investigate the mechanism and gain an understanding of the proposed routes of dicumyl peroxide consumption, we propose the following experiments:

1. Investigate the oxidation of Cyanox STDP in the presence of dicumyl peroxide as a function of temperature.

2. Study the oxidation of the sulfoxide derivative of Cyanox STDP to determine the relative rates of formation of both the sulfoxide and subsequently oxidized sulfone.

3. Study the hydrolysis of sulfones to form the corresponding acid, in particular the hydrolysis of a sulfone similar to Cyanox STDP.

In addition, we plan to also investigate the possibility of disulfides being formed in the mixture during the imbibing process. From prior experimentation at Dow, we know that the increased scorch time was observed only in the presence of oxygen. Though this observation may be linked to water concentration in the atmosphere (which will be investigated through our experiments outlined in Scenario #1), we believe oxygen may be promoting the formation of disulfide linkages if any thiols are present in the mixture. Literature reports have shown that even in the presence of small amounts of base, thiols will oxidize in the presence of atmospheric oxygen via radical reaction (Figure F.7).[6] If such a mechanism is occurring during the imbibing process, then the active mixture will be a mixed system of peroxide and disulfides, which may aid in the inhibition of premature crosslinking, thus increasing TS1.

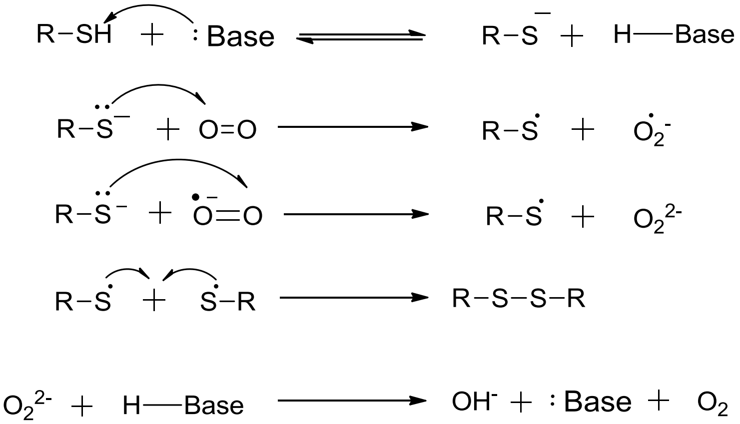

Figure F.7 - Base catalyzed formation of disulfide linkage from thiol in the presence of oxygen

F.3.5.1 *Experimental* –

We propose preparing mixtures of DCP and thiols in an alkane solvent to model the formation of disulfide linkages in the system. Questions to be answered include:

1. Are disulfides formed in the presence of oxygen?
2. Are they influencing the decomposition of DCP during the imbibing procedure?
3. Could disulfides be employed as a less-reactive alternative to peroxides in these mixtures?

We propose the following experiments relating to Research Question 2:

- Investigate modifying the thioester structure of Cyanox STDP to see its relative effect on the crosslinking at both 140°C and 180°C.

- Use model compounds such as hexane and dodecane to study crosslinking on a laboratory scale that is less challenging to analyze.

- Investigate the acid catalyzed decomposition of dicumyl peroxide in the presence of an alkyl sulfonic acid at both 140°C and 180°C (to be started after receiving summary of Dow work that is in progress).

F.3.6 Scenario #4 –Impurity Effects in Dicumyl Peroxide

We propose that impurities present in dicumyl peroxide could contribute to the oxidation of a thioether additive. Dow has reported that the dicumyl peroxide used in testing contains the impurities cumene, benzyl alcohol, and acetophenone. In the presence of oxygen, cumene can rapidly form its peroxide derivative as shown in Figure F.8. This peroxide formed is then capable of oxidizing any thioether additive to its sulfone and further sulfoxide forms. Sulfonic acid can be produced from the sulfoxide form as shown in Figure 10. The sulfonic acid is then potentially capable of consuming some of the dicumyl peroxide via the previously-mentioned acid catalyzed decomposition mechanism. This oxidation pathway (Figure F.9) would explain experimental results from Dow that show that the enhanced TS1 time is observed only in air and not under nitrogen alone. The air would be required to supply the necessary oxygen to produce cumene hydroperoxide.

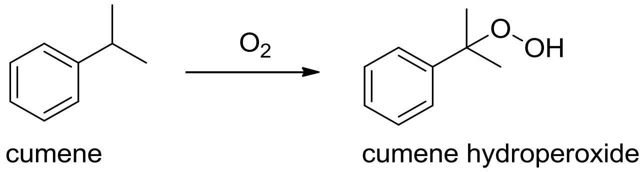

Figure F.8 - Formation of cumene hydroperoxide from cumene in the presence of oxygen

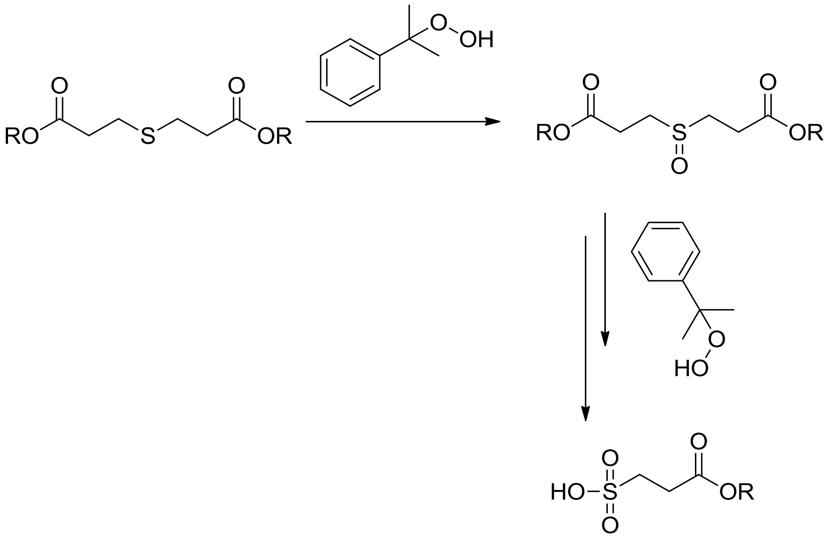

Figure F.9 - Formation of sulfonic acid by the oxidation of a thioether by cumene hydroperoxide

F.3.6.1 *Experimental* –

We have requested samples of the dicumyl peroxide and thioether used in the initial Dow studies. To investigate the hypothesis we propose the following studies:

- Analyze the impurities of the dicumyl peroxide and the thioether (GC/MS, NMR).

Intentionally form cumene hydroperoxide from cumene and investigate its ability to oxidize the thioether at 102°C and 140°C as opposed to dicumyl peroxide (GC/MS).

- Repeat the special imbibing procedure with and without the thioether and analyze the products formed (GC/MS).

- Study the imbibing procedure under air, dry air, and nitrogen to discern any role of oxygen and water.

- Determine whether or not it is feasible for traces of cumene to initiate such reactions (estimated ratio of cumene to STDP in these systems is about 0.0008).

F.4 References

(1) Brandrup, J.; Immergut, E. H.; Grulke, E. A. *Polymer Handbook*; 4th Edition ed.; John Wiley: New York, 1999.

(2) Katritzky, A. R.; Taylor, R. J. K. *Comprehensive Organic Functional Group Transformations II*; Elsevier, 2005.

(3) Dluzneski, P. R. *Rubber Chemistry and Technology* **2001**, *74*, 451.

(4) Grassie, N.; Scott, G. *Polymer Degradation and Stabilization*; Cambridge University Press: New York, 1985.

(5) Gilbert, V. E. E. *Sulfonation and Related Reactions*; Wiley: New York, 1965.

(6) Patai, S.; Wiley: New York, 1974; Vol. II.

VITA

Jackson Switzer was born in June 1986. Raised in Gulfport, MS, he attended Gulfport High School and was actively involved in the Boy Scouts of America and Saint James Catholic Church. After graduating from high school in 2004, Jackson chose to pursue undergraduate study in chemistry at the University of Alabama. While at the University, he was involved in the Computer-Based Honors Program and conducted research under Dr. David Dixon. He completed internships at the Naval Research Laboratory as well as the National Oceanographic and Atmospheric Administration. After graduating summa cum laude in 2008, he moved to Washington D.C. to study at the National Defense Intelligence College and work for the Department of Defense. Upon completion of his master’s degree in strategic intelligence in Washington, he began doctoral study at the Georgia Institute of Technology in chemical engineering. During that time, he has conducted research as a member of the Eckert-Liotta research group. He will continue his career at Albemarle Corporation as a chemical engineer in Baton Rouge, LA in July 2013.